TISSUE-SPECIFIC REQUIREMENTS FOR PROTECTION AGAINST ENDOGENOUS FORMALDEHYDE



Holly Russell

Linacre College

This dissertation is submitted for the degree of Doctor of Philosophy

April 2025

DECLARATION

This dissertation is the result of my own work and includes nothing, which is the outcome of work done in collaboration except where specifically indicated in the text. It has not been previously submitted, in part or whole, to any university of institution for any degree, diploma, or other qualification.

In accordance with the guidelines, this thesis does not exceed 50,000 words.

Signed: 

Date: 30/04/25

Holly Russell

University of Oxford

ABSTRACT

Formaldehyde is an endogenous genotoxin which can drive organ deterioration in humans. In mice, deficiency in the main formaldehyde-detoxifying enzyme, ADH5, combined with inactivation of specific DNA repair pathways mimics known human disorders. In particular, co-depletion of ADH5 and transcription-coupled repair (TCR; *Adh5*$^{-/-}$*Csb*$^{-/-}$) causes deterioration of non-replicative tissues such as the brain, largely recapitulating human Cockayne Syndrome (CS). In contrast, *Adh5*$^{-/-}$ mice lacking replication-coupled Fanconi Anaemia (FA) repair (*Adh5*$^{-/-}$ *Fancd2*$^{-/-}$) lose proliferative haematopoietic cells and develop severe anaemia, akin to FA patients. Using these models, we sought to examine whether endogenous formaldehyde and TCR- or FA-deficiency compromises other non-dividing or proliferative tissues, such as quiescent haematopoietic stem cells (HSCs) or rapidly-dividing gut epithelium. Additionally, we wished to assess the contribution of systemic formaldehyde detoxification to peripheral organ homeostasis.

Somatic mutation profiling of HSCs from *Adh5*$^{-/-}$*Csb*$^{-/-}$ mice revealed that TCR conducts mutagenic repair of formaldehyde-induced damage in these cells. However, loss of TCR did not compromise HSCs function indicating TCR as dispensable in this context. Instead, *Adh5*$^{-/-}$*Csb*$^{-/-}$ mice developed anaemia due to defects in erythroid progenitors, uncovering a previously unappreciated role of TCR in safeguarding erythroid differentiation.

Surprisingly, we found that ADH5/FANCD2-deficiency did not affect gut epithelium, with the small intestine showing no overt phenotype and no evidence of apoptosis or stress-induced proliferation. This indicates that gut epithelial cells, despite being highly sensitive to ionizing radiation, have unique resistance to formaldehyde-induced damage.

Finally, development of a novel *Adh5* allele allowed us to restore ADH5 expression specifically in the haematopoietic cells of otherwise ADH5-deficient mice. Systemic formaldehyde clearance, reactivated in those animals, reduced kidney and brain degeneration in CS mice but did not prevent liver deterioration in the FA model. This indicates that whilst the liver produces large amounts intrinsically, a significant proportion of formaldehyde in the brain and kidney can be

detoxified by systemic circulation. This has exciting implications for the use of blood-borne formaldehyde scavengers to treat human disease.

ACKNOWLEDGEMENTS

I would first like to thank KJ for giving me the opportunity to work in his lab and trusting me with this truly exciting project. I am grateful for his sharp scientific insights and challenging discussions which have pushed me to think critically about my work and be confident when discussing my ideas.

I would also like to thank my second supervisor, Ewa Gogola, who has been fundamental in my scientific progression. From my first day in the lab, all the way until my final week, Ewa has been teaching me how to be a good scientist: from lab techniques to efficient time management, to navigating collaborations. Many of my good qualities as a scientist come from observing Ewa; I cannot overstate my gratitude towards her for the time that she has invested into seeing me succeed.

I would also like to thank Ewa for her initial work in validating the *Adh5* switch mouse alongside Lee Mulderrig, who's work generating and phenotyping the *Adh5*$^{-/-}$*Csb*$^{-/-}$ model was also the foundation for my project. I am grateful to Lee for continuing to engage with me (and my constant emails) even after having left the Patel lab, showing his selfless dedication to scientific discovery. I am also thankful to Alex Frick and Juan Garaycoechea who were responsible for creation of the *Adh5* 'switch' allele.

I would also like to thank my collaborators: Owen Sansom's lab, in particular Rachel Ridgeway, who taught me how to dissect the mouse GI tract and engaged with me for its analysis; Colin Nixon and the CRUK histology service who performed the embeddings and stainings of the GI tract; Dick Jaarsma and Harry Macdonald for their work on the immunofluorescence and analysis of the CSB/ADH5-deficient brains.

I would like to thank all the members of the Patel lab for being so generous with their time. Thank you to Ashley Kamimae-Lanning and Felix Dingler for teaching me how to work with mice, and

how to wrangle a flow cytometer into submission at 4 AM in the morning. Thank you to them also for the contributions they have made to the work in this thesis: thank you to Felix for helping me generate the *Adh5*$^{-/-}$*Csb*$^{-/-}$ mutation signature, and to Ashley for her work on the foetal liver analysis. Thank you also to Christopher Millington for helping me measure the formaldehyde adducts in *Adh5*$^{sw/-}$ tissues, along with my summer students: Isaac Kam and Gretl Chan. I am immensely grateful for Jill Brown, who's skill with Western blots is unparalleled, and is demonstrated in Chapter 4. I am also grateful for her pastoral support: for propping me up on hard days and giving excellent hugs.

Thank you to the rest of the lab for all their advice, support, and camaraderie: Samuel Jones, Maddie Foster-Smith, Oliver Beaven, Xinran Huang, Caroline Scott and Kleitos Papadopoulos. The Patel lab is such a supportive environment, and every member is unique and wonderful in their own way. It has been my absolute pleasure to work with them.

I'd also like to thank the WIMM Flow Cytometry Facility staff: Paul Sopp, Sally-Ann Clark, Kevin Clark and Craigh Waugh for all their advice on flow cytometry and help with cell sorting. Additionally, I am grateful to the animal technicians at the JR-BMS, Kyle Clapton-Matheson and Roo Bhasin, who oversaw my mouse strains.

Finally, I would like to thank my friends and family, both near and far, for all their support through these four years. Thank you to Aniq Ahsan and Katie Beard for being my rocks in Oxford, and to Lizzy, Charlie, and Alex for always giving me a reason to come back to Maidenhead. To my sisters, Maddie, and Freya, for their support and the laughs we share. To my parents, for always encouraging me to pursue my interests and for giving me a wonderful home; I am immensely privileged to have them as my inspirations.

I would like to dedicate this thesis to my grandparents: David and Jenny Buck. Although as Cambridge graduates they might have felt obligated to disapprove of my choice of University, I know they would have been fascinated by this work. I hope they would have been proud to see it completed.

CONTENTS

1 INTRODUCTION 1

1.1 DNA DAMAGE DRIVES CANCER AND AGEING 1

1.1.1 Fanconi Anaemia 6

1.1.2 Cockayne syndrome and Transcription-Coupled Repair (TCR) 10

1.2 DNA REPAIR REQUIREMENTS IN DIVIDING VS NON-DIVIDING TISSUES – GAPS IN KNOWLEDGE 16

1.2.1 Unexplored roles of Fanconi anaemia repair in the gut 16

1.2.2 DNA repair in quiescent haematopoietic stem cells 18

1.3 ENDOGENOUS SOURCES OF DNA DAMAGE 20

1.4 FORMALDEHYDE AS AN ENDOGENOUS SOURCE OF DNA DAMAGE 23

1.4.1 Tier 1 – aldehyde detoxification 24

1.4.2 Models of Tier 1 deficiency 25

1.4.3 Models of combined Tier 1 and Tier 2 deficiency 27

1.5 THE SOURCE OF ENDOGENOUS FORMALDEHYDE 31

1.6 AIMS 32

2 METHODS 34

2.1 MOUSE STRAINS 34

2.1.1 $Adh5^{-/-}$ $Csb^{-/-}$ mice and controls for Chapter 3/4 34

2.1.2 $Adh5^{sw}$ allele generation 34

2.1.3 $Adh5^{sw/-}$$Csb^{-/-}$ Vav1-iCre mice and controls for Chapter 5 35

2.1.4 $Adh5^{sw/-}$$Fancd2^{-/-}$ Vav1-Cre mice and controls for Chapter 6 35

2.1.5 Competitive transplant donors and recipients 36

2.2 ANIMAL EXPERIMENTS 36

2.2.1 Animal Husbandry 36

2.2.2 Genotyping 36

2.2.3 Kaplan-Meier 36

2.2.4 Cerebellar ataxia scoring *37*

2.2.5 Grip strength measurements *37*

2.2.6 Blood sampling *37*

2.2.7 Methanol treatment *37*

2.2.8 Bone marrow transplantation *38*

2.2.9 Timed matings *39*

2.3 MOUSE TISSUE PROCESSING AND ANALYSIS 39

2.3.1 Serum biochemistry *39*

2.3.2 Total blood count *39*

2.3.3 Organ weighing *39*

2.3.4 Liver and kidney histology *40*

2.3.5 Brain immunofluorescence *40*

2.3.6 GI tract dissection *40*

2.3.7 Intestine immunohistochemistry *41*

2.3.8 Formaldehyde adducts measurement *43*

2.3.9 ADH5 western blot *44*

2.4 FLOW CYTOMETRY AND CELL SORTING 45

2.4.1 HSC cell sorting and culture immunophenotyping *45*

2.4.2 CFSE analysis *45*

2.4.3 Cell cycle analysis *46*

2.4.4 Chimerism analysis *47*

2.4.5 Haematopoietic immunophenotyping *48*

2.4.6 E13.5 embryo immunophenotyping *51*

2.5 EX VIVO 53

2.5.1 HSC culture *53*

2.5.2 Single cell quiescence analysis *53*

2.5.3 HSC formaldehyde sensitivity assay *53*

2.5.4 Bone marrow clonal expansion for sequencing *54*

2.6 LIBRARY PREPARATION AND SEQUENCING 55

3 THE MUTATIONAL SIGNATURE OF FORMALDEHYDE EXPOSURE AND TRANSCRIPTION-COUPLED REPAIR DEFICIENCY IN HAEMATOPOIETIC STEM CELLS 56

3.1 FORMALDEHYDE INDUCES TRANSCRIPTION-STRAND-BIASED MUTATIONS VIA MUTAGENIC TCR 60

3.2 DISCUSSION 64

3.3 LIMITATIONS 66

4 INVESTIGATING THE SOURCE OF ANAEMIA IN *ADH5*$^{-/-}$*CSB*$^{-/-}$ MICE 68

4.1 CREATION OF AN *EX VIVO* QUIESCENT SYSTEM TO EXAMINE HSC FIDELITY 69

4.2 TCR DEFICIENCY DOES NOT INCREASE HSC SENSITIVITY TO FORMALDEHYDE *EX VIVO* 77

4.3 METHANOL-TREATED *ADH5*$^{-/-}$*CSB*$^{-/-}$ MICE HAVE FUNCTIONAL HSCS 80

4.4 AGED *ADH5*$^{-/-}$*CSB*$^{-/-}$ MICE HAVE NORMAL HSC PROPORTIONS DESPITE ANAEMIA 85

4.5 DISCUSSION 88

4.5.1 How do quiescent HSCs repair formaldehyde damage? *88*

4.5.2 The role of formaldehyde damage and TCR in erythroid differentiation *90*

5 TISSUES ARE PROTECTED FROM FORMALDEHYDE BY HAEMATOPOIETIC DETOXIFICATION IN COCKAYNE SYNDROME MICE 93

5.1 THE *ADH5* 'SWITCH' ALLELE RESTORES ADH5 EXPRESSION IN HAEMATOPOIETIC CELLS IN THE PRESENCE OF *VAV1-ICRE* 94

5.2 SYSTEMIC DETOXIFICATION OF FORMALDEHYDE REDUCES CS-ASSOCIATED KIDNEY DAMAGE AND CACHEXIA 97

5.3 SYSTEMIC DETOXIFICATION OF FORMALDEHYDE REDUCES BRAIN DAMAGE AND DELAYS NEURODEGENERATION IN CS MICE 102

5.4 DISCUSSION 105

5.4.1 What is the source of formaldehyde in Adh5$^{-/-}$*Csb*$^{-/-}$ *mice?* *105*

5.4.2 Improving systemic clearance of formaldehyde - implications *108*

5.4.3 The contribution of residual immune cells to formaldehyde detoxification *109*

6 SYSTEMIC FORMALDEHYDE DETOXIFICATION DOES NOT RESCUE PERIPHERAL TISSUE DAMAGE IN FANCONI ANAEMIA MICE 112

6.1 RESTORING ADH5 EXPRESSION IN BLOOD PARTIALLY RESCUES DEVELOPMENTAL DEFECTS IN ADH5/FANCD2-DEFICIENT MICE 114

6.2 *ADH5$^{SW/-}$FANCD2$^{-/-}$ VAV1-ICRE* MICE LOSE HSCS PRENATALLY BUT MAINTAIN BLOOD PRODUCTION FOR UP TO 1 YEAR 117

6.3 SYSTEMIC CLEARANCE OF FORMALDEHYDE DOES NOT PREVENT LIVER AND KIDNEY DETERIORATION IN ADH5/FANCD2-DEFICIENT MICE 119

6.4 ADH5/FANCD2-DEFICIENT MICE HAVE NORMAL INTESTINAL EPITHELIUM 125

6.5 DISCUSSION 131

6.5.1 Cell-intrinsic formaldehyde detoxification is required for HSCs protection from the point of emergence *131*

6.5.2 Haematopoietic formaldehyde detoxification is insufficient to prevent liver and kidney deterioration in ADH5/FANCD2-deficient mice *133*

6.5.3 ADH5/FANCD2 deficiency increases nuclear ploidy and causes liver dysfunction *135*

6.5.4 The ADH5/FANCD2-deficient gut is uniquely protected against formaldehyde damage *138*

7 CONCLUDING REMARKS 142

8 REFERENCES 147

1 INTRODUCTION

1.1 DNA damage drives cancer and ageing

Cancer and age-related diseases pose significant challenge to the health and social care systems in the developed world. The World Health Organisation reports that cancer caused 9.7 million deaths worldwide in 2022, and population growth estimates predict that this number will increase to 35 million annually by 2050 (Bray et al., 2024). Other age-related diseases, such as cardiovascular diseases, diabetes, and chronic respiratory diseases (COPD) raise this to 41 million people annually – 74% of all deaths worldwide (Institute for Health Metrics and Evaluation, 2024). As well as lifespan, age-related diseases affect healthspan – the length of time for which an individual remains healthy. In 2019, average life expectancy was 73 years, but the average healthy life expectancy (HALE) only 64 years (World Health Organisation, 2024). Diseases which contribute substantially to this discrepancy include age-related cardiovascular disease and neurodegenerative diseases such as dementia (GBD 2016 DALYs and HALE Collaborators, 2017). Whilst global life expectancy has accelerated from 2000 to 2019, HALE has not increased at the same rate, leading to an ageing population with a substantial disease burden (World Health Organisation, 2024). It is therefore imperative to understand the mechanisms of ageing and cancer to ameliorate their rising global mortality and extend healthy lifespan.

Cancer is defined by the National Cancer Institute as "a disease in which some of the body's cells grow uncontrollably and spread to other parts of the body (National Cancer Institute, 2007). Conversely, ageing is defined as the "progressive loss of physiological integrity, leading to impaired function and increased vulnerability" (López-Otín et al., 2013). Despite obvious differences, the two processes are interconnected: ageing itself is one of the major risk factors for most cancers (Laconi et al., 2020). Indeed, stochastic changes that accumulate with age are often drivers of malignant disease, with DNA damage being a prime example (Vijg, 2014; Yousefzadeh et al., 2021).

A key ramification of DNA damage is genomic instability which can arise through: (1) errors during DNA replication, (2) DNA breakage leading to loss or rearrangement of genetic information, or (3) error-prone repair (Tubbs & Nussenzweig, 2017). This in turn can lead to inactivation of tumour suppressor genes or amplification of oncogenes - the first events in oncogenic transformation. Knudson's 'two-hit hypothesis' proposes that neoplastic initiation requires the mutation of two tumour suppressor genes (Knudson, 1971). This theory has been validated both *in vitro* and *in vivo.* Kinzler and Vogelstein described that mutations in either 'gatekeeper' genes controlling cell growth (*P53, Rb, VHL* or *APC*) or 'caretaker' genes which encode fundamental DNA repair and/or damage recognition genes is required for full neoplastic transformation (Kinzler & Vogelstein, 1998). Later during cancer progression, defects in DNA repair enable cancer cells to accumulate mutations that confer their aggressive phenotype and shape cancer evolution (Jeggo et al., 2016; Ye et al., 2009; J. Zhou et al., 2020).

To counteract genomic instability and prevent neoplastic transformation, cells with persistent activation of the DNA damage response can be, depending on the cellular context, driven into differentiation, cell death (apoptosis) or senescence (Blackford & Jackson, 2017; Sherman et al., 2011). These outcomes prevent the propagation of mutations but compromise the regenerative and functional capability of cells and contribute to the ageing process. Numerous studies have shown that DNA damage accumulates with age across various tissues and cell types (Rübe et al., 2011; Soares et al., 2014; Vlachogiannis et al., 2023). In haematopoietic stem cells (HSCs), DNA

damage accumulation impairs their ability to replenish downstream cells, particularly lymphoid lineages, as shown by Flach and colleagues, who found that aged HSCs exhibit persistent DNA damage response activation, elevated replication stress, and defective lineage repopulation (Flach et al., 2014). In the aged human prefrontal cortex, increased DNA damage at gene promoters has been shown to correlate with reduced gene expression (T. Lu et al., 2004). The affected regions included genes critical for survival, memory, and learning, highlighting another mechanism through which DNA damage can contribute to the functional age-related decline. DNA damage can also induce cellular senescence – a pathophysiological state of irreversible cell cycle arrest. Di Leonardo et al., (1994) showed that DNA damage triggers senescence through P53-mediated G1 checkpoint activation. A later study revealed that the aberrant induction of senescence (through *p63* disruption) in mice leads to rapid development of aged-related phenotypes (alopecia, skin defects, spine curvature, glomerular thickening), and a shortened lifespan, demonstrating that senescence can directly contribute to ageing (Keyes et al., 2005)

One of the strongest lines of evidence for the role of DNA damage in cancer and ageing comes from genetic studies of human diseases of DNA repair deficiency. For instance, inactivating germline mutations in homologous recombination repair factors, *BRCA1* and *BRCA2,* result in dramatically increased risk of breast and ovarian cancers in women (Antoniou et al., 2003). Deficiencies in another DNA repair pathway - mismatch repair (MMR) (due to mutations in *MLH1, MSH2, MSH6* or *PMS2*) - predispose to endometrial and colorectal cancers, while lack of global genome nucleotide excision repair (GG-NER) causes sunlight sensitivity and a 10,000-fold increased risk of skin cancers (Black, 2016; Møller et al., 2017). Meanwhile, mutations in Werner Helicase (WRN) or transcription coupled nucleotide excision repair (TC-NER) factors cause rapid-ageing syndromes (progerias). Patients affected by these mutations show premature signs of physiological ageing including neurodegeneration, alopecia, cataracts, osteoporosis, hearing loss and multi-organ functional decline leading to dramatically shortened lifespan (Karikkineth et al., 2017; Oshima et al., 2017).

Different DNA repair deficiencies can therefore cause a spectrum of ageing or cancer-prone phenotypes affecting various tissues. In some cases, this is dictated by the specific type of DNA damage cells are exposed to, which in turn necessitates particular DNA repair activities. For instance, skin cells rely on NER to repair UV-induced DNA damage, whilst organs with high oxidative metabolism such as the brain might rely more heavily on pathways to resolve oxidative damage, such as base excision repair (BER) (D. Clarke & Sokoloff, 1999). Indeed, though complete BER-deficiency appears incompatible with life in humans, decreased expression of several BER factors has been associated with neurodegenerative diseases (Jacob et al., 2013; Lillenes et al., 2016; C. Shao et al., 2008; Weissman et al., 2007).

Other cellular contexts such as replication-status can also influence the phenotype caused by DNA repair deficiencies. Highly replicative cells (such as blood and gut progenitors) have been shown to accrue DNA mutations from replication errors, increasing the likelihood of oncogenic mutations (Blokzijl et al., 2016; Osorio et al., 2018; Spisak et al., 2024). Meanwhile, it has been proposed that DNA damage in post-mitotic cells such as neurons induces senescence more readily than in proliferating cells, promoting degenerative rather than cancer-prone phenotypes (Fujimaki et al., 2019; Sah et al., 2021). A prime example of the differing ramifications of DNA damage depending on cell context is the distinct phenotypes which occur in humans which lack either replication-coupled Fanconi anaemia repair (FA) or transcription-coupled nucleotide excision repair (TC-NER).

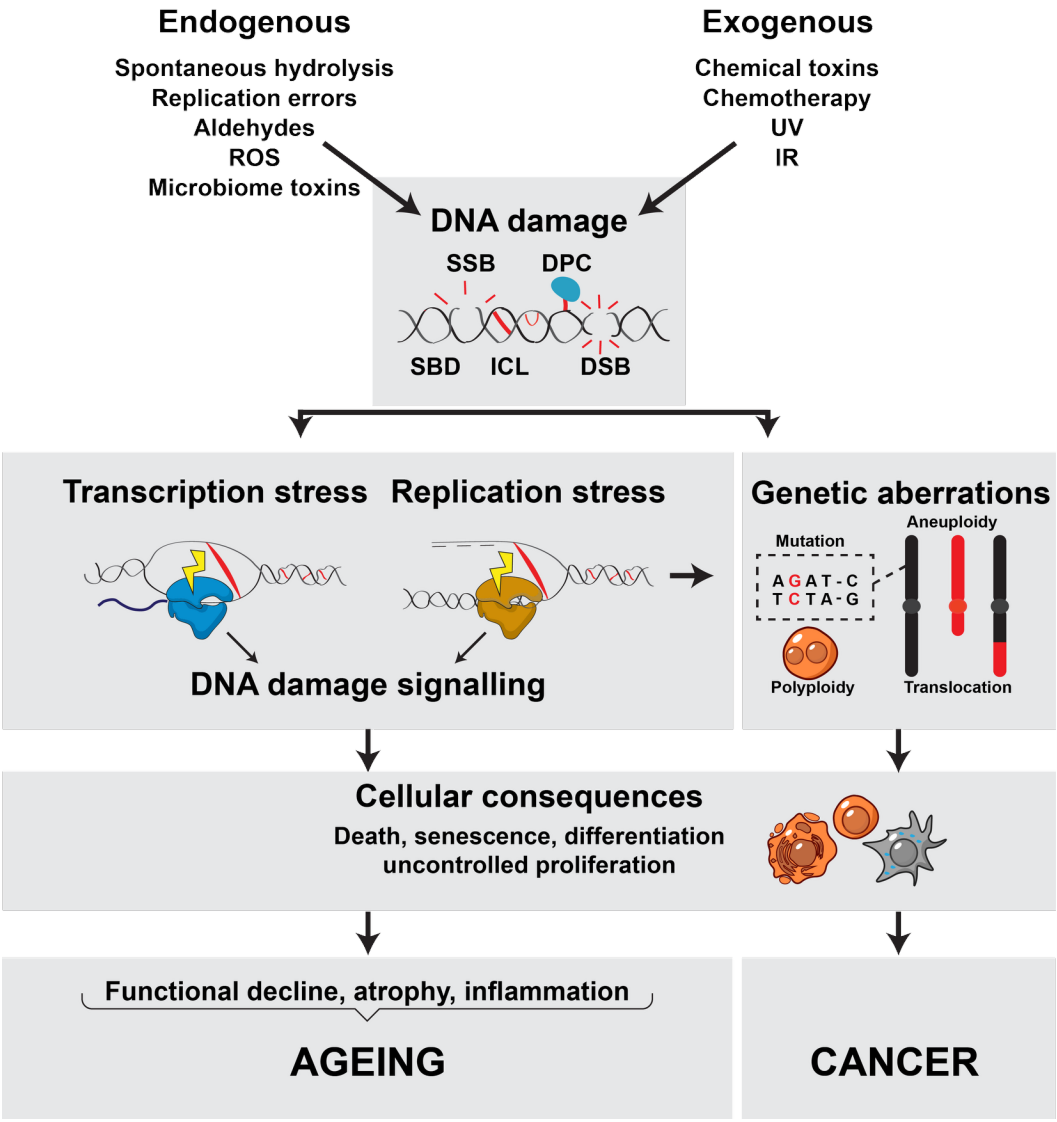

Figure 1.1. DNA damage drives ageing and cancer.

Model illustrating how exogenous and endogenous sources induce different forms of DNA damage, such as single base damage (SBD), single base substitutions (SBS), DNA-protein crosslinks (DPC), interstrand crosslinks, and double strand breaks (DSB). DNA damage can lead to transcription stress, replication stress, and genetic aberrations, which can alter cell fate and drive cancer and ageing. ROS, Reactive Oxygen Species. UV, Ultraviolet. IR, Ionising Radiation. Partially created in BioRender. Russell, H. (2026) https://BioRender.com/x8j92uu

1.1.1 Fanconi Anaemia

The Fanconi anaemia pathway is a replication-coupled DNA repair pathway activated by stalling of converging replication forks at an interstrand DNA-crosslink (ICL) (Ceccaldi et al., 2016) (Fig. 1.2). This is recognised by the FANCM-complex, which recruits the Fanconi anaemia core complex consisting of 14 proteins which cooperate alongside the Ataxia Telangiectasia and RAD3-related protein (ATR) and Ataxia Telangiectasia Mutated (ATM) to stabilise the FANCD2-FANCI dimer (FANCD2-I complex), which slides and clamps around the ssDNA-dsDNA junction prior to the crosslink (Alcón et al., 2020, 2024; Kupculak et al., 2023). Activated FANCD2-I utilises the nuclease scaffold protein (SLX4) to recruit nucleotide-excision repair endonucleases (XPF-ERCC1, MUS81-EME1, SLX1) which incise one parental DNA strand. The 5'-3' exonuclease, SNM1A, loads onto this nicked region and further digests the incised DNA strand past the crosslink to unhook it (Wang et al., 2011). Following this, translesion synthesis polymerases perform lesion bypass of the opposing parental strand and extend the complementary nascent DNA. This generates a DNA duplex with an unhooked monoadduct which can be removed by NER (Moldovan & D'Andrea, 2009). This intact DNA duplex also acts as a template for homologous recombination (facilitated by BRCA1/2, RAD51 and other HR factors) to repair the incised parental strand (Ceccaldi et al., 2016) (Fig. 1.2). Aside from repairing ICLs, the Fanconi anaemia pathway is also implicated in protecting stalled replication forks from collapse, fork restart after repair, regulating chromosome segregation in cytokinesis, and resolution of DNA-RNA hybrids generated from collisions of transcription and replication (García-Rubio et al., 2015; Naim & Rosselli, 2009; Schwab et al., 2015).

Germline, homozygous mutations of the Fanconi anaemia genes in humans leads to an inherited bone marrow failure syndrome, known as Fanconi Anaemia (FA). Patients with this disease often present with developmental birth defects in the upper limbs (35%), renal (20%), skeletal (25%), gonadal (25% of males) and ocular (20%) systems, have short stature (40%) and hyperpigmentation of the skin (40%) (Shimamura & Alter, 2010; Tischkowitz & Hodgson, 2003). However, the most common and characteristic symptoms of Fanconi anaemia are aplastic

anaemia due to bone marrow failure, and cancer predisposition. Patients typically develop bone marrow failure by age 7 which necessitates bone marrow transplantation (Shimamura & Alter, 2010). Those surviving transplant remain predisposed to both haematologic and solid cancers, with a cancer-free survival of 29 years, which is also their median lifespan (Shimamura & Alter, 2010). FA patients have a 50-fold increased risk of cancers, with a 700-fold and 600-fold increased risk of leukaemia or head and neck squamous cell carcinomas (HNSCCs) specifically. Aside from leukaemia and HNSCCs, liver, brain, vulvar and Wilms renal tumours are the most common cancers in FA patients (Alter et al., 2007; Rosenberg et al., 2003).

The defects that occur in FA are inherently linked to the role of the Fanconi's anaemia pathway in conserving DNA replication. Perturbed replication can affect early development and lead to congenital abnormalities such as those seen in FA patients (Kerzendorfer et al., 2013; Zeman & Cimprich, 2014). Similarly, the haematopoietic system is highly proliferative, both during embryogenesis, when haematopoietic stem cells (HSCs) rapidly divide to populate the bone marrow, and in adulthood, when the blood is constantly replenished by proliferative haematopoietic progenitors (Mikkola & Orkin, 2006). The early-onset bone marrow failure in FA patients is indicative of an inability of these cells to proliferate and repopulate downstream progenitors. Indeed, FANCA-deficient HSC and progenitor cells have a significant competitive disadvantage compared to gene-therapy-corrected cells in the bone marrow of human FA patients, highlighting their impeded replication (Lasaga et al., 2023). The cancer predisposition in FA patients also underscores a replication-coupled defect. Neoplastic transformation is inherently tied to replication, as cell proliferation facilitates the accumulation of mutations and provides opportunities for oncogenic clones to gain selective advantage (Greaves & Maley, 2012). In FA, the combination of genomic instability with high selective pressure of a failing bone marrow can amplify this process. Li et al., demonstrated this experimentally, with FANCC-deficient mouse bone marrow cells acquiring significant cytogenetic abnormalities only after *ex vivo* proliferation, directly linking replication stress to chromosomal instability in FA (X. Li et al., 2005). Transplantation of these cultured cells into bone marrow-ablated wild-type mice led to clonal

abnormalities and acute myeloid leukaemia, demonstrating that genome instability drives leukemogenesis in FA-deficiency. Together, the phenotypes of FA exemplify the requirement for the Fanconi anaemia pathway in conserving replicating cells, preventing their dysfunction and oncogenic transformation.

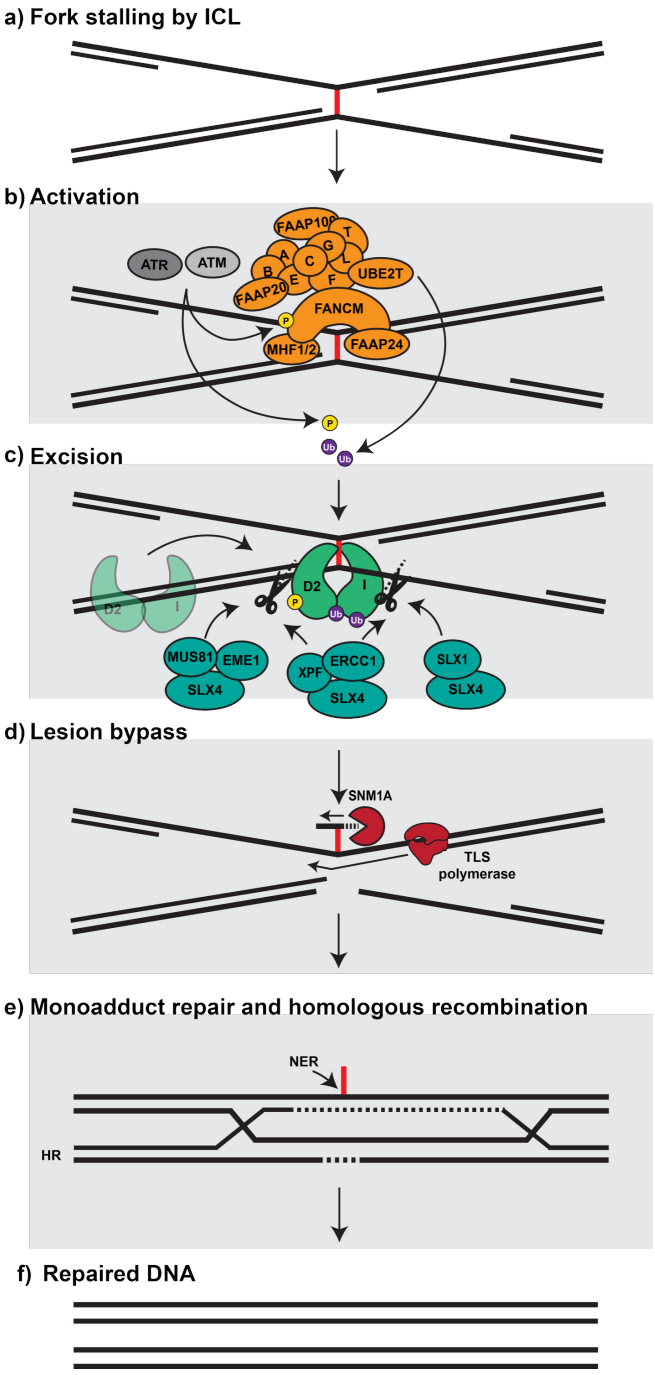

Figure 1.2. The Fanconi Anaemia pathway.

a) Converging replication fork progression is blocked by an interstrand crosslink

b) recruitment of FANCM, which in turn (1) recruits other components of the FA core complex (orange) and (2) activates ATR and ATM (grey) which promote phosphorylation and further activation of the FA core complex, and phosphorylation of FANCD2. The activated FA core complex monoubiquitylates the FANCD2-FANCI heterodimer (green).

c) FANCD2-FANCI slides and clamps around the ICL at the dsDNA-ssDNA junction. Clamping is stimulated by DNA binding. Ubiquitination of FANCD2 by UBE2T stabilises the clamp. FANCD2-FANCI recruits SLX4 in complex with specific endonucleases (dark green) which incise either side of one DNA strand.

d) SNM1A exonuclease digests the remaining crosslinked oligo, leaving an unhooked crosslink on one strand which can be bypassed by translesion synthesis polymerases, generating an intact duplex.

e) The unhooked crosslink on the TLS-repaired duplex is thought to be removed by NER. Homologous recombination repairs the remaining double strand break, using the intact DNA duplex as a template.

1.1.2 Cockayne syndrome and Transcription-Coupled Repair (TCR)

Transcription-coupled nucleotide excision repair (TC-NER) is a repair pathway which is activated in response to stalling of transcribing RNA polymerase II (RNAPII) on damaged template DNA (Fig. 1.3) (Nieto Moreno et al., 2023). When RNAPII encounters a simple DNA modification, such as single base adduct, it can be pushed to bypass it by Cockayne Syndrome group B protein (CSB), which is transiently bound to the complex and promotes its forward translocase activity (Xu et al., 2017). However, if RNAPII encounters a lesion which blocks its translocation, such as bulky UV-induced cyclobutane pyrimidine dimers, interstrand crosslinks, or DNA-protein crosslinks, the complex stalls, causing CSB to become more tightly bound and stimulating TC-NER initiation (Brueckner et al., 2007; Damsma et al., 2007). During this, CSB recruits the $CRL4^{CSA}$ E3 ubiquitin ligase complex via its substrate recognition substrate, Cockayne Syndrome group A (CSA) (Henning et al., 1995). CSA then recruits elongation factor 1 (ELOF1) which cooperate to recruit the UV stimulated scaffold protein (UVSSA) and direct CRL^{CSA}-mediated ubiquitylation of RNAPII on K1268 of its largest subunit, RBP1 (Geijer et al., 2021; van der Weegen et al., 2021). This ubiquitylation promotes the removal of stalled RNAPII from the damage site. CSA and UVSSA also bind serine/threonine kinase 19 (STK19) and cooperate to recruit and position the transcription factor IIH (TFIIH) complex which mediates further repair (Heuvel et al., 2024; Mevissen et al., 2024). Alternatively, lesion sensing and recruitment of TFIIH can also occur through direct recognition of DNA lesions by xeroderma pigmentosum C (XPC) or xerodermapigmentosum E (XPE) (Nieto Moreno et al., 2023). This process is known as global genome nucleotide excision repair (GG-NER) and does not require transcription activity.

Once TFIIH is recruited (either by GG-NER or TC-NER factors), it unwinds the DNA using the helicase xeroderma pigmentosum D (XPD) (Mathieu et al., 2013). This exposes the DNA for binding of XPA and RPA, which stabilize the repair bubble and position and stimulate the endonucleases xeroderma pigmentosum G (XPG) and ERCC1-XPF which excise the lesion (de Laat et al., 1998). Following this, DNA polymerases (delta, epsilon, or kappa) and ligases (DNA ligase 1 or XRC11-DNA ligase 3) fill and seal the single strand gap (Ogi et al., 2010; Paul-Konietzko et al., 2015).

Interestingly, humans with loss-of-function mutations in NER genes exhibit different clinical manifestations depending on the branch of NER that is compromised. Mutations in GG-NER (*XPC, XPE*) or canonical NER genes (*XPA, XPB, XPD, XPG, XPV*) cause the disease Xeroderma Pigmentosum (XP) – a sunlight sensitivity condition with high predisposition to skin cancer (Black, 2016). Conversely, deficiency in specifically TC-NER genes (*CSA, CSB*) causes Cockayne Syndrome (CS) – a rapid ageing condition involving neurodegeneration, growth failure, progressive microcephaly, and sun sensitivity (but not skin cancer) (Karikkineth et al., 2017). The difference between these syndromes indicates that GG-NER is primarily required for repair of UV-induced damage and prevention of neoplastic mutations, whilst TC-NER has additional roles in preventing tissue deterioration. Sequencing techniques have shown that, unlike in XP-deficient cells, CS cells do not have an increased mutagenic burden after UV exposure (Reid-Bayliss et al., 2016). This may underlie the lack of cancer phenotype in CS compared to XP, with CS patients experiencing mutagenesis at normal levels, and thus not living long enough for cancers to develop. It has also been suggested that lack of TC-NER, and the inability to resolve transcriptional stress, is more toxic to cells than the lack of GG-NER and leads to apoptosis or senescence rather than tolerance and mutation (Y. Lu et al., 2001).

Several groups have postulated that it is these specific roles for CSA and CSB in resolving transcriptional stress that underpin the unique neurodegenerative phenotype of CS (Balajee et al., 1997; Dianov et al., 1997; Gregersen & Svejstrup, 2018; Tufegdžić Vidaković et al., 2020; Vélez-Cruz et al., 2013; Wang et al., 2014). Normally, transcription-stalling lesions trigger global

transcriptional shutdown through CSA/CSB-mediated ubiquitylation of RNAPII at RBP1-K1268, promoting its removal from the DNA to allow access of canonical NER factors. Study has shown that cells lacking CSA or CSB cannot ubiquitylate and remove stalled RNAPII from the lesion, preventing repair and transcription resumption (Meer et al., 2024; Nakazawa et al., 2020). However, contrasting observations by Tufegdžić Vidaković et al. suggests that lacking CSA/CSB instead causes persistent ubiquitylation and degradation of RNAPII and inability to re-initiate transcription regardless of lesion repair (Tufegdžić Vidaković et al., 2020). In both cases, it is argued that it is the DNA damage-induced transcriptional shutdown – either due to persistent stalling of RNAPII, or its degradation – that causes the unique CS phenotype.

Prevention of RNAPII ubiquitylation and degradation through mutation of RPB-K1268 has been shown to cause persistent stalling, and delayed recovery of RNA synthesis after UV irradiation akin to in CS cells (Nakazawa et al., 2020; Tufegdžić Vidaković et al., 2020). Conversely, UVSSA-deficient cells cannot recruit TFIIH to displace RNAPII, but can still degrade the RNAPII complex (Kokic et al., 2024). Patients with UVSSA mutations show mild sunlight sensitivity but do not exhibit the severe organ degeneration characteristic of CS (Nakazawa et al., 2012). This observation suggests that it is the prolonged RNAPII arrest, rather than persistent degradation, which underlies the transcriptional dysregulation and severe phenotype of CS. Nonetheless, it will be important to resolve the reason for the discrepancy in RNAPII degradation observed between studies of CS cells, which may point to the presence of context-specific pathways regulating the transcriptional response to DNA damage.

Several recent studies have shown that CSA and CSB also play important roles in repairing transcription-stalling DNA-protein crosslinks (DPCs), independently of canonical NER (Carnie et al., 2024; Oka et al., 2024; van Sluis et al., 2024). Consistent with this, CSA/CSB-deficient cells are sensitive to the DPC-inducing agent 5-aza-deoxycytidine, but cells deficient in canonical NER proteins are not (Carnie et al., 2024). It is conceivable that the unique roles for CSA and CSB in resoving DPCs might also contribute to the CS-specific phenotype. Though, in both, TC-NER and transcription-coupled DPC repair (referred to together as ‘TCR’), mutations in

CSA/CSB cause perturbation of the RNAPII pool and transcriptional dysregulation, indicated by loss of actively transcribing RNAPII, or lack of RNA synthesis recovery following DNA damage (Carnie et al., 2024; Tufegdžić Vidaković et al., 2020). It is therefore likely that both DPCs and other, NER-invoking, transcription-stalling lesions are responsible for transcriptional stress and tissue deterioration which occurs in CS.

Interestingly, functional deterioration in CS appears biased towards less proliferative tissues. In contrast to FA, which causes defects in replicating cells either during development or homeostasis, loss of TCR manifests as a progressive degenerative syndrome which mainly affects either post-mitotic or quiescent tissues after embryogenesis (Fig. 1.4) (Karikkineth et al., 2017). The brain is one such tissue; neurogenesis peaks at 3-5 months post-gestation, with most brain cells becoming post-mitotic shortly after birth (Ackerman, 1992; Anda et al., 2016). CS patients develop neurodegeneration following this post-mitotic shift, characterised by progressive microcephaly and intellectual decline with age, correlating with white matter demyelination and brain atrophy (Laugel, 1993). Patients display cognitive and motor defects as a result, with most unable to speak beyond single words, and many unable to walk or perform fine motor functions (Nance & Berry, 1992). Stunted growth and loss of fat mass (cachectic dwarfism) is also reported in most CS cases. Over time, other differentiated organ systems, such as the kidney, auditory and optic tissues also degenerate, with CS patients often developing cataracts and ocular atrophy, and a retrospective study reporting renal failure in 69.2% of deceased patients (Kubota et al., 2015). Average lifespan for CS patients is 12.5 years; respiratory ailments such as pneumonia are the primary cause of death, though liver and kidney failure, cardiac arrest and seizure complications have also been reported as cause of death in some of the patients (Nance & Berry, 1992; Natale, 2011). Combined, these features represent a multi-organ, progressive decline in largely non-dividing tissues which occurs when transcription-coupled repair of DNA damage is compromised.

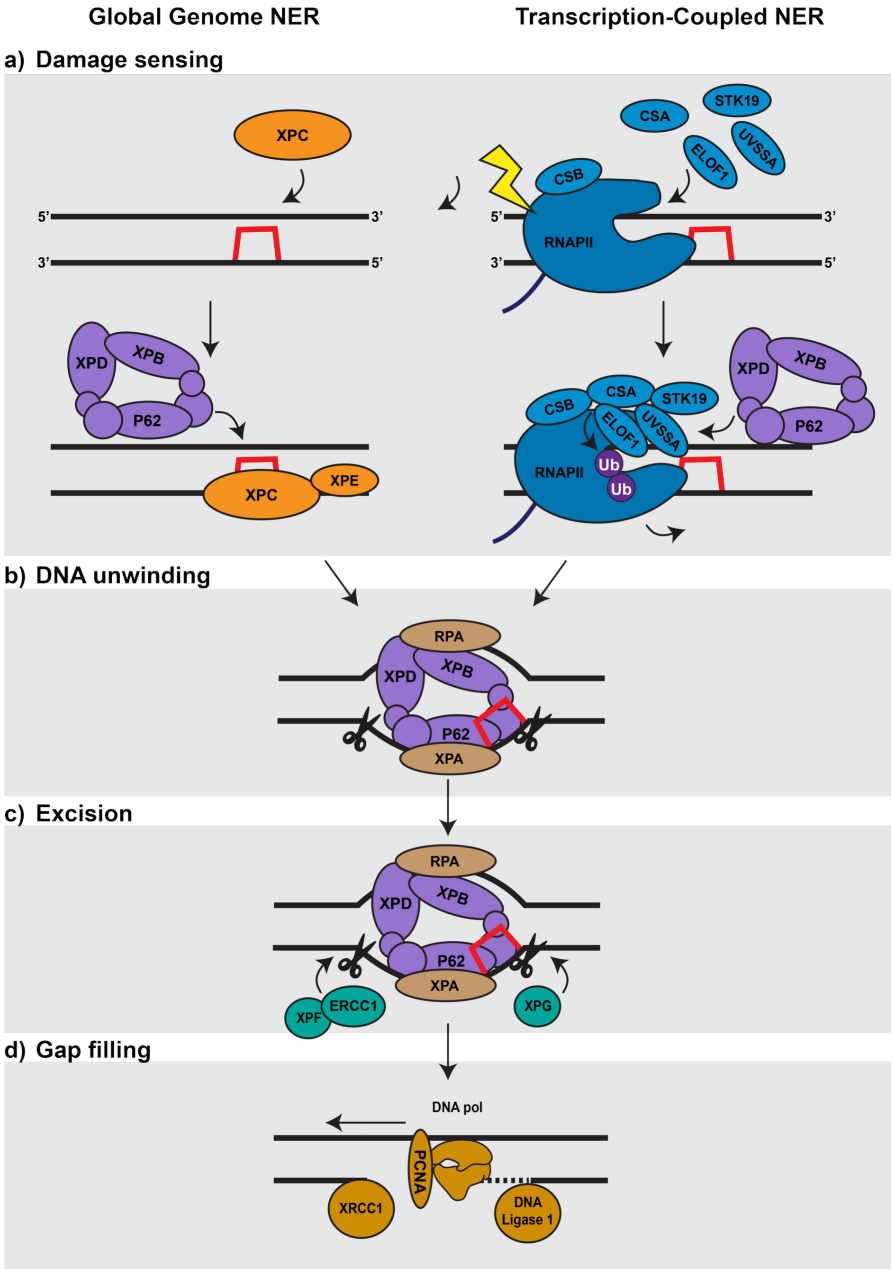

Figure 1.3. Nucleotide Excision Repair.

a) Sensing of helix-distorting DNA lesions can occur through recognition by XPC and XPE. XPC acts as a platform for recruitment of the TFIIH complex (which includes XPD, XPB and P62). Alternatively, lesions in the transcribed regions can be detected by stalling of RNAPII, which activates CSB. CSB recruits CSA and ELOF1 which cooperate to recruit UVSSA and ubiquitylate RNAPII to promote its removal from DNA. STK19 binds RNAPII, CSA and UVSSA and helps position TFIIH which is recruited by UVSSA through interaction with the P62 subunit.

b) TFIIH unwinds DNA surrounding the lesion using the XPD helicase, facilitating binding of RPA and XPA which stabilize the bubble.

c) Endonucleases XPF-ERCC1 and XPG bind unwound DNA and excise it on either side of the lesion.

d) DNA polymerase fills in the resulting single-strand gap in cooperation with PCNA, using the intact strand as a template. DNA ligase 1 and XRCC1 seal the gap.

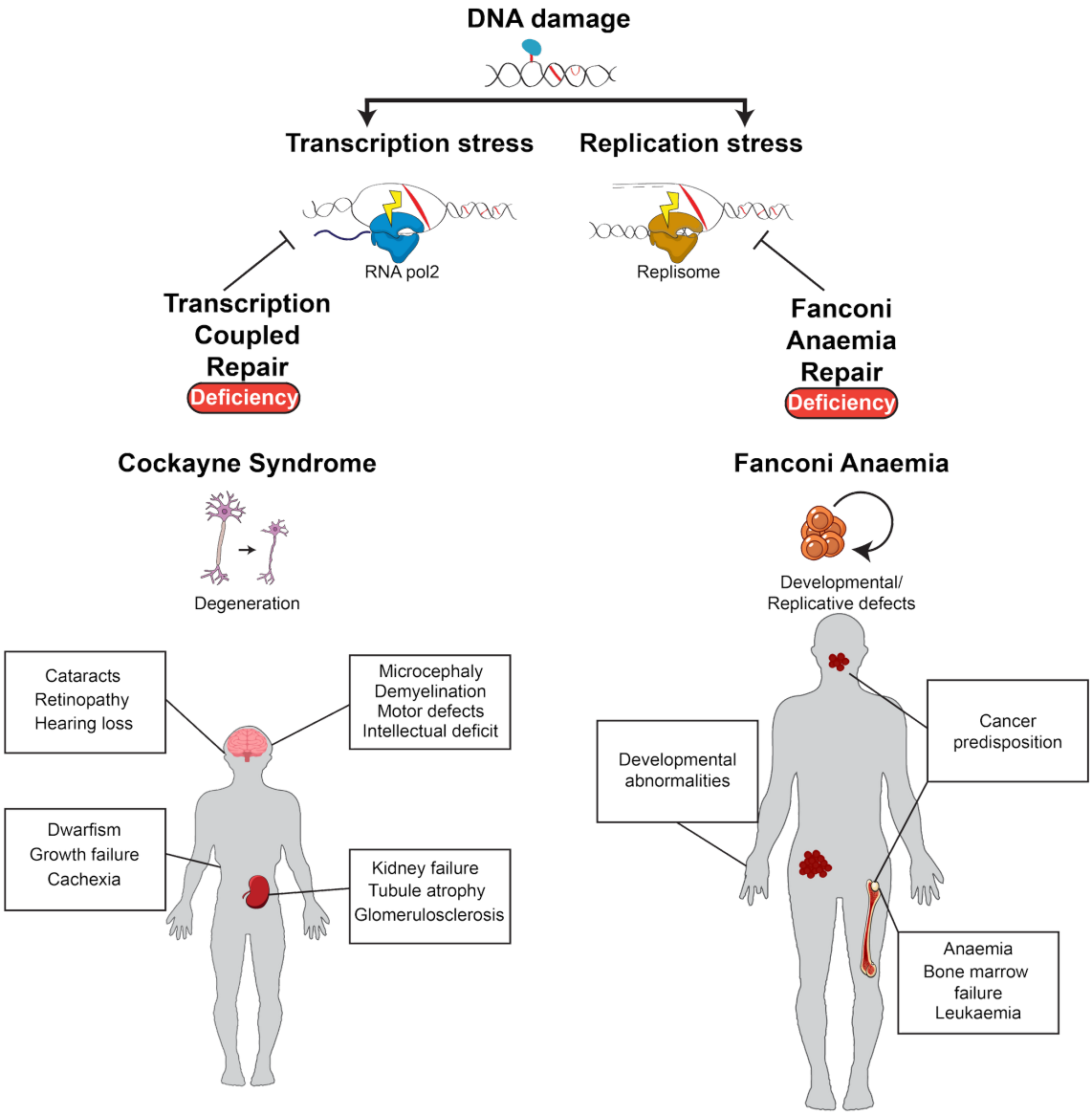

Figure 1.4. Phenotypes of Fanconi anaemia and Cockayne Syndrome.

DNA damage can cause transcription or replication stress which can be resolved by TCR or FA repair, respectively. Deficiency in TCR in humans causes the degenerative disease Cockayne Syndrome, whilst FA repair deficiency causes Fanconi Anaemia which affects developing and highly replicative tissues, and leads to cancer predisposition. Partially created in BioRender. Russell, H. (2026) https://BioRender.com/x8j92uu

1.2 DNA repair requirements in dividing vs non-dividing tissues – gaps in knowledge

The distinct phenotypes caused by lack of FA repair vs TCR exemplify the different requirements for repair based on the cellular context. Tissues can be subjected to different forms of DNA damage from different sources depending on their metabolic status and anatomical location. However, the choice of the repair pathway, and the ramifications of repair deficiency, can also depend on cell proliferative capacity. Indeed, whilst many DNA repair pathways are downregulated or absent in post-mitotic or quiescent cells, TC-NER remains active, and is essential for the survival of quiescent B lymphocytes in response to UV damage (Hsu et al., 2007; Sandoval et al., 1996). Similarly, whilst neurons have reduced GG-NER activity and lack replicative repair owing to their post-mitotic status, they retain TCR and show preferential repair of cyclopyrimidine dimers in transcribed regions, suggesting a reliance on this pathway to maintain transcriptional fidelity (Nouspikel & Hanawalt, 2000). This reliance on TCR in less proliferative cells may account for the distinct degeneration of post-mitotic, or less replicative, tissues in CS, as opposed to the defect in highly proliferative haematopoietic cells which occurs in FA (Fig. 1.4). However, there remain some intriguing gaps in knowledge on the role of TCR and FA repair in some tissues.

1.2.1 Unexplored roles of Fanconi anaemia repair in the gut

The intestinal tract is one of the most proliferative tissues in the body, with its epithelial lining renewing every 3-4 days in humans (Reynolds et al., 2014). Like the haematopoietic system, this tissue relies on a pool of stem and progenitor cells to constantly replenish downstream cells, in this case the gut epithelium. This regeneration is driven by transient amplifying cells near the midline of the intestinal crypts, which are replaced by cycling intestinal stem cells (ISCs), expressing leucine-rich repeat-containing G protein-coupled receptor 5 (LGR5) at the crypt base (Barker, 2014). However, unlike the haematopoietic system, which is significantly impaired in the absence of FA repair, the intestinal system does not appear to be as affected in FA patients.

This is surprising, given that the gut is a highly proliferative tissue which is subjected to a plethora of DNA damaging agents. For instance, indolamines, *bacteroides fragilis* toxin (bft) or typhoid toxin, which induce double and single strand DNA breaks, can be produced from the gut commensal bacteria *Morganella morganii, Bacteroides fragilis* and members of the *Salmonella enterica* subspecies (Cao et al., 2022; Dejea et al., 2018a; Lopez Chiloeches et al., 2024). Other microbiome bacteria such as *Escherichia coli*, *Klebsiella pneumoniae*, *Citrobacter koseri*, and *Enterobacter aerogenes* can also produce colibactin which can alkylate DNA to induce interstand or intrastrand crosslinks (Auvray et al., 2021; Putze et al., 2009; Thakur et al., 2019; M. R. Wilson et al., 2019). Studies have shown that these bacteria are enriched in the guts of patients with inflammatory bowel disease and colorectal cancer, demonstrating their pathogenic potential (Cao et al., 2022; Dejea et al., 2018b; He et al., 2019). Simultaneously, other DNA damaging agents such as reactive oxygen species (ROS) can be produced from metabolic and immune processes in the gut epithelium. Intestinal epithelial cells utilise oxidative metabolism which can generate ROS as a by-product, whilst also secreting ROS as a signalling molecule in response to commensal bacteria (Nath et al., 2022; Rath & Haller, 2022). Both ROS and reactive nitrogen species (RON) can also be released as antimicrobial peptides as part of the immune response to pathogens (Enocksson et al., 2004; Schöneich, 2005; Singer et al., 1996). These chemicals are capable of inducing various forms of DNA damage including single and double strand breaks, base modifications and interstrand crosslinks (Imlay et al., 1988; Rozelle et al., 2021; Valverde et al., 2018).

The repair of DNA damage is clearly important in the gut, as exemplified by the consequences of dysfunctional repair. For instance, MMR is imperative to resolve mismatches generated from base-adducts, and germline deficiencies in this pathway lead to an 40 - 80% lifetime risk of colorectal cancer compared to just 5% in the general population (Bonadona et al., 2011). Hereditary defects in BER, which resolves base damage from ROS or RON, also cause a substantially increased risk of colorectal cancers (Cleary et al., 2009; Jones et al., 2002). However, the importance of interstrand crosslink repair (through the FA pathway) in the gut has not been

intensively studied. Interstrand crosslinks are potent replication-stalling lesions which can be induced by microbiome toxins, ROS and other metabolic by-products (Breton et al., 2011; Rozelle et al., 2021; Vare et al., 2012). It is logical that inability to repair these lesions would impede intestinal proliferation and compromise gut architecture. However, descriptions of gastro-intestinal aberrations in FA are limited to developmental defects of gut anatomy rather than affecting intestinal epithelium homeostasis (Fanconi Cancer Foundation, 2023). While this could be simply due to the lack of extensive studies of the GI tract in FA patients, it is tempting to speculate that gut epithelium could be somehow protected against physiological sources of replication-stalling lesions, or have a unique capacity to counteract this type of damage.

1.2.2 DNA repair in quiescent haematopoietic stem cells

The importance of replication-coupled repair in HSCs is well described. The FA pathway is essential to protect HSC proliferation during embryogenesis, and it is during this window that haematopoiesis is thought to be compromised in Fanconi's anaemia (Domenech et al., 2018; Kamimae-Lanning et al., 2013; Kovuru et al., 2024; Suzuki et al., 2017; Tulpule et al., 2010; Yoon et al., 2016). However, in steady-state (i.e non-stressed, homeostatic) conditions, HSCs are only highly proliferative during this limited timespan. Following embryogenesis, HSCs become largely quiescent, with long-term repopulating HSCs (LT-HSCs) predicted to divide less than once per year in humans (Boyle et al., 2023). These quiescent HSCs are at the pinnacle of the haematopoietic hierarchy, defined by their ability to self-renew, and their capacity to produce all downstream haematopoietic lineages. HSCs give rise to shorter lived, but highly proliferative, multipotent progenitor cells which cannot self-renew, but are responsible for replenishing committed progenitors of either myeloid or lymphoid lineages. These committed progenitors then repopulate their downstream lineages, with myeloid progenitors giving rise to erythrocytes, granulocytes, macrophages and megakaryocytes, whilst lymphoid progenitors replenish B-, T- and natural killer cells (Bryder et al., 2006).

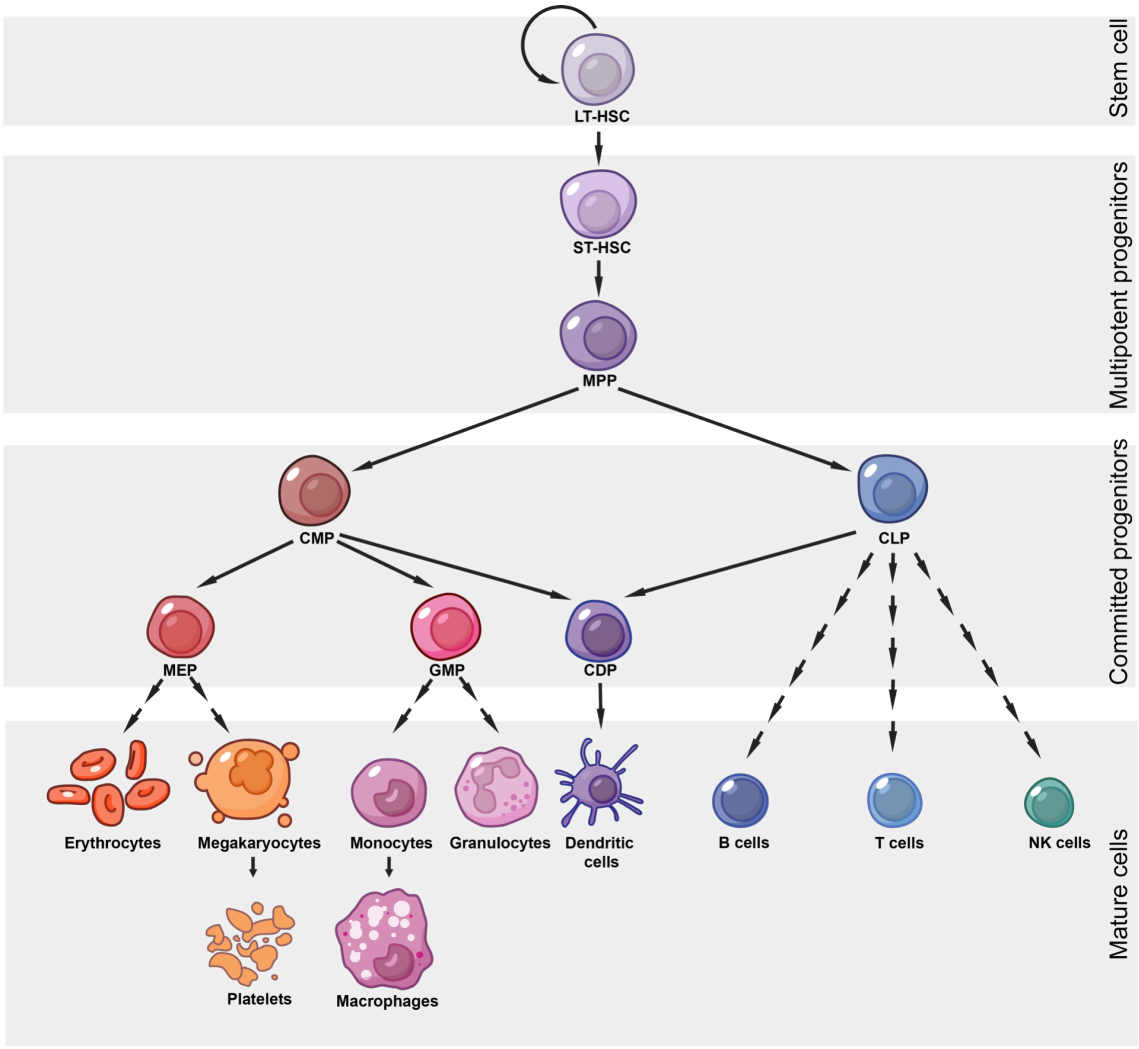

Figure 1.5. Haematopoiesis

Simplified schematic of the haematopoietic tree adapted from Garaycoechea, 2014, and Bryder et al, 2006. Long-term haematopoietic stem cells (LT-HSCs) are capable of self-renewal and can produce short-term HSCs, which retain multipotency but have low self-renewal. ST-HSCs produce short-lived, proliferative multipotent progenitors (MPPs), which replenish committed progenitors of myeloid (common myeloid progenitor, CMP) or lymphoid (common lymphoid progenitor, CLP) lineages. CMPs give rise to myeloid-erythroid progenitors (MEPs which produce other committed progenitors (simplified by multiple arrows) which replenish erythrocytes or platelet-producing megakaryocytes. CMPs also give rise to granulocyte-macrophage progenitors (GMPs), which produce monocytes (immature macrophages) and granulocytes. Both CMPs and CLPs are thought to give rise to common dendritic progenitors (CDPs), which replenish dendritic cells. CLPs also give rise to B-, T- and natural killer (NK) cells through a series of differentiation stages (simplified by multiple arrows).

Despite their dormancy, it has been shown that DNA damage accrues in HSCs with age, leading to accumulation of mutations which can drive malignancy (Beerman et al., 2014; Beerman, 2017; Corces-Zimmerman et al., 2014; Jamieson et al., 2004). It has been proposed that quiescent HSCs may act as a 'reservoir' for DNA damage, with single and double strand breaks shown to accumulate in quiescence and only being repaired upon re-entry into cell cycle (Beerman et al., 2014). It is questionable whether this would occur with all forms of DNA damage, however. The accumulation of too many of potentially transcription- or replication-stalling lesions during quiescence would likely impair transcriptional homeostasis or cause replication stress upon cell cycle re-entry. Indeed, deficiency in several non-replication-coupled repair pathways – non homologous end joining (NHEJ), telomere maintenance pathway (mediated by mTR), or canonical NER – does not deplete steady-state HSCs in mice but leads to a significant functional defect when HSCs are forced to divide to repopulate downstream progeny (Rossi et al., 2007). This might indicate that a certain level of quiescence-associated DNA repair is required for proper HSC maintenance, to facilitate cell cycle re-entry during periods of stress. The contribution of TCR to this repair has not been studied, though sequencing of haematopoietic stem and progenitor cells identified mutational bias on the transcribed strand, which may indicate the activity of transcription-coupled repair and its mutagenic potential in this context (Osorio et al., 2018). Further studies are required to better understand the potential role for TCR in protection of quiescent HSCs from DNA damage, and its contribution to age-related decline.

1.3 Endogenous sources of DNA damage

It is well-established that DNA repair is fundamental to prevent premature ageing, mutagenesis, and cancer (reviewed by T. L. Clarke & Mostoslavsky, 2022). But what are the sources of this damage? In the case of some syndromes, such as Xeroderma Pigmentosum, the source is obvious; UV light catalyses the formation of bulky pyrimidine dimers in skin cells which impede replication and transcription in the absence of repair (van Steeg & Kraemer, 1999). However, the

potential sources of DNA damage which compromise the internal organs, such as in FA and CS, are less well defined.

DNA damage, such as deamination of cytosines to uracil due to limited chemical stability of the DNA molecule, can occur spontaneously, or can be induced by specific enzymes such as activation-induced deaminase (AID) during immunoglobulin diversification, or apolipoprotein B m-RNA-editing catalytic polpeptide-like 3 (APOBEC3), during retroviral infections (Lindahl, 1993; Swanton et al., 2015). Though part of the natural immune response, the expression of these DNA-damaging enzymes is dysregulated in some cancers and contributes to their genomic instability (Alexandrov et al., 2013; Burns et al., 2013). Errors can also be incorporated into DNA during replication. It is estimated that around 100,000 – 1,000,000 polymerase errors occur per cell division (Kunkel, 2009; McCulloch & Kunkel, 2008; Preston et al., 2010). Most of these errors are not replication- or transcription- stalling, however, and are rapidly repaired through proofreading and MMR (Preston et al., 2010).

More toxic DNA lesions can be formed by reactive by-products of metabolism. For instance, reactive oxygen species (ROS) are produced from mitochondrial electron chain transport, as a by-product of lipid peroxidation, and from phagocytic immune cells (de Almeida et al., 2022). Oxidation of guanine by ROS forms 8-oxo-guanine, which can mispair with adenine to cause G>T mutations post-replication (K. C. Cheng et al., 1992, p. 88; Hahm et al., 2022; Shibutani et al., 1991). ROS is thought to be one of the most common sources of endogenous DNA damage and is one of the best characterised endogenous drivers of ageing and mutagenesis (reviewed by de Almeida et al., 2022).

Some of the DNA damage in FA might be attributed to ROS. FA-repair-deficient cells exhibit slower growth in high oxygen tension (Schindler & Hoehn, 1988) and have increased chromosomal aberrations, indicating this repair is important in resolving oxidative lesions (Joenje et al., 1981). Further evidence for the involvement of ROS in FA comes from mouse models of this disease. Mice deficient in FA repair do not recapitulate the human syndrome, with some

models showing no abnormal phenotypes (FANCG mutants) (Koomen et al., 2002; Y. Yang et al., 2001) and other models (FANCA, FANCC mutants) exhibiting defects in haematopoietic colony formation or increased sensitivity to irradiation *ex vivo*, but not *in vivo* (Noll et al., 2002; Whitney et al., 1996). Growth retardation and cataract development has been observed in some FANCA, FANCC- and FANCD2-deficient mouse models (Chen et al., 1996; Houghtaling et al., 2003; Wong et al., 2003), and an increased cancer incidence has also been documented in FANCA, FANCF, FANCM and FANCD2-deficient mice (Bakker et al., 2009, 2012; Houghtaling et al., 2003; Wong et al., 2003). FANCD2-deficient mice also have a mild reduction in HSC proportion (Parmar et al., 2010), however none of these mouse models exhibit the characteristic bone marrow failure and spontaneous aplastic anaemia which is characteristic of human FA, indicating either an increased capacity to tolerate DNA damage, or a reduced level of endogenous damage in mice. Increasing the burden of DNA damage in FANCC-deficient mice through mutation of a ROS-metaboliser, superoxide dismutase 1 (SOD1), does unveil some additional FA phenotype. *Sod1*$^{-/-}$*Fancc*$^{-/-}$ mice have reduced red blood cell counts, bone marrow hypocellularity, and reduced ability of haematopoietic progenitors to form colonies *ex vivo* (Hadjur et al., 2001). This suggests that endogenous ROS can indeed damage DNA and at least partially contribute to the haematopoietic failure which occurs in FA. However, *Sod1*$^{-/-}$*Fancc*$^{-/-}$ mice still exhibit normal levels of HSCs and do not develop bone marrow failure, suggesting that additional forms of DNA damage are required to fully recapitulate the human disease (Hadjur et al., 2001).

ROS has also been proposed as a source of DNA damage which drives the CS phenotype. Cells deficient in CSB are more sensitive to oxidative damage, suggesting a role for TCR in repair of oxidative lesions (Ranes et al., 2016). Like with FA, mice lacking CSA or CSB do not recapitulate the CS phenotype. These mice are indistinguishable from wild-type controls and exhibit some of the CS-like traits (hearing loss, reduced RNAPII recovery, mild cancer predisposition) only when exposed to exogenous damaging agents such as cisplatin or UV (van der Horst et al., 1997; Van Der Horst et al., 2002). Additional knockout of 8-oxoG DNA glycosylase 1 (OGG1), which removes ROS-induced 8-oxo-guanine lesions, does increase the level of 8-oxo-G in CSB-

deficient mice compared to singly OGG1-deficient mice, indicating a role for TCR in oxidative lesion repair (Trapp et al., 2007). However, *Csb*$^{-/-}$*Ogg1*$^{-/-}$ mice do not show additional CS phenotypes, suggesting that, like in FA, ROS can increase the burden of DNA damage, but does not fully drive the disease.

1.4 Formaldehyde as an endogenous source of DNA damage

Seminal work from the Patel lab has identified simple aldehydes as potent endogenous genotoxins which drive both FA and CS in mice and can cause bone marrow failure in humans (Dingler et al., 2020; Langevin et al., 2011; Mulderrig et al., 2021; Pontel et al., 2015). Aldehydes, in particular acetaldehyde and formaldehyde, the simplest in class, are highly reactive molecules which can be introduced into the body from exogenous sources. For instance, ethanol in alcoholic drinks or methanol derived from pectin-containing fruits are metabolised to acetaldehyde or formaldehyde, respectively, by the enzyme ADH in the liver (Pocker & Li, 1991; Zakhari, 2006). More importantly, these aldehydes are also produced endogenously from innate cellular processes such as one-carbon metabolism, histone demethylation or DNA demethylation (Loenarz & Schofield, 2008; Shi et al., 2004a; Walport et al., 2012).

Both acetaldehyde and formaldehyde are highly reactive and capable of adducting or forming crosslinks between DNA, proteins, and RNA (Cheng et al., 2003; Hodskinson et al., 2020; Wang et al., 2000). It is this potent crosslinking ability that makes formaldehyde a useful reagent for tissue preservation or in biochemical pulldown assays such as Chromatin ImmunoPrecipitation (ChIP) (Hoffman et al., 2015; Tayri-Wilk et al., 2020), but also what makes aldehydes so genotoxic. Acetaldehyde- and formaldehyde-induced damage can impede replication and transcription and cause widespread damage to several tissues in the body if not dealt with promptly (Anandarajan et al., 2020; Dingler et al., 2020; Langevin et al., 2011; Mulderrig et al., 2021; Oka et al., 2024; Pontel et al., 2015).

1.4.1 Tier 1 – aldehyde detoxification

To prevent these chemicals from reacting and impeding fundamental processes, aldehydes are rapidly removed by aldehyde dehydrogenase 2 (ALDH2) and alcohol dehydrogenase 5 (ADH5). ALDH2 is a mitochondrial enzyme that converts acetaldehyde into acetate, and formaldehyde into formate (Jacobson & Bernofsky, 1974; Uotila & Koivusalo, 1974). Inactivating mutations in this enzyme are common in the East Asian population (29-52% of Japanese, Chinese and Korean population) (Eng et al., 2007), and are causative of a syndrome known as 'asian flush', wherein affected individuals experience nausea, facial flushing and tachycardia upon alcohol consumption due to histamine release in response to acetaldehyde accumulation (Harada et al., 1981).

In a mechanism distinct from ALDH2, ADH5 locates to cytoplasm and detoxifies primarily formaldehyde through combined action with glutathione, which reacts spontaneously with free formaldehyde to form S-hydroxymethylglutathione. ADH5 reacts with this compound to produce formate (using S-formylglutathione hydrolase) and replenish free GSH for further formaldehyde scavenging (Sanghani et al., 2000). These two mechanisms of aldehyde detoxification are referred to by our lab as the 'first tier' of protection against genotoxic aldehydes (Fig. 1.5).

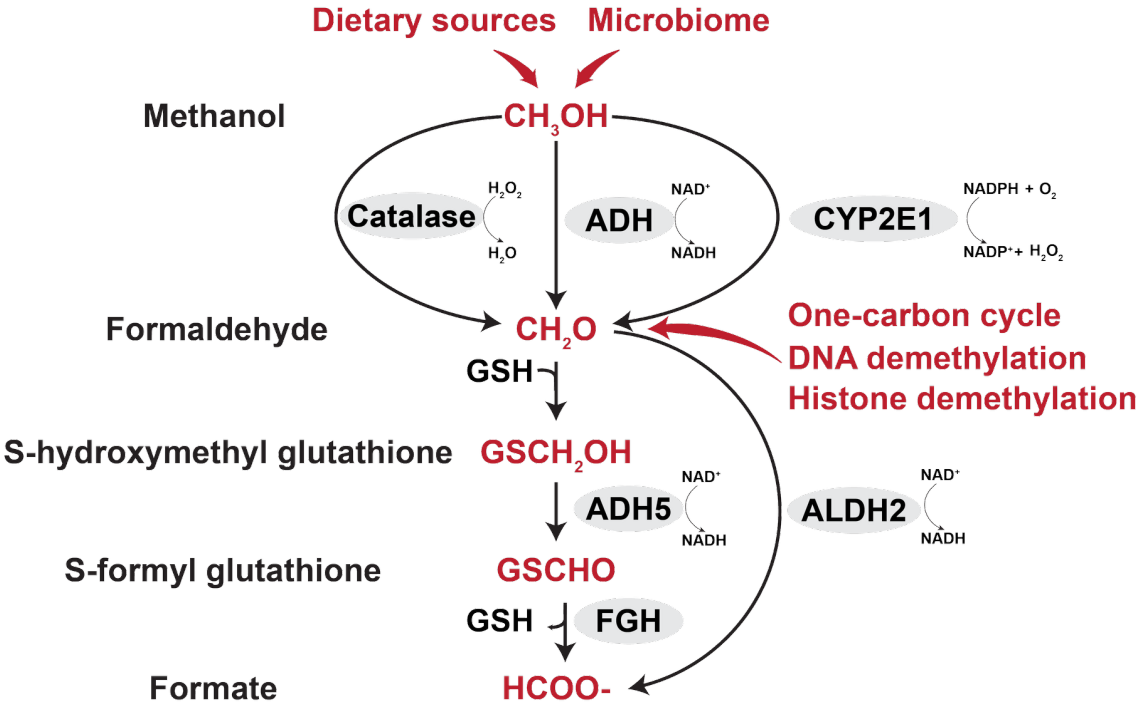

Figure 1.6. Formaldehyde sources and detoxification

Methanol from dietary sources or derived from the microbiome is primarily oxidised to formaldehyde by alcohol dehydrogenase (ADH), but catalases and cytochrome P450 monooxygenases such as CYP2E1 can also perform some catabolism (Dorokhov et al., 2015). Formaldehyde can also dissociate from metabolites of the one carbon cycle or be released during enzymatic DNA or histone demethylation. Glutathione (GSH) spontaneously reacts with formaldehyde to form S-hydroxymethyl glutathione, which is then oxidized to S-formyl glutathione by alcohol dehydrogenase 5 (ADH5). S-formylglutathione hydrolase (FGH) hydrolyzes S-formylglutathione to formate, recycling free GSH for further formaldehyde detoxification. Formaldehyde can also be directly oxidized to formate by alcohol dehydrogenase 2 (ALDH2) (Reingruber & Pontel, 2018).

1.4.2 Models of Tier 1 deficiency

The combined inactivation of ADH5 and ALDH2 leads to disastrous consequences in both mice and humans. Humans with concomitant *ADH5* and *ALDH2* mutations present with aplastic Anaemia, Mental retardation, and Dwarfism syndrome (AmeD) (Dingler et al., 2020; Oka et al., 2020), which shares phenotypes with both FA and CS, indicating that deficiency in aldehyde detoxification may lead to levels of endogenous DNA damage capable to overwhelm repair systems. Generation of a mouse model of tier one deficiency by our lab and the Ogi group confirmed that the AmeD phenotype is largely driven by formaldehyde (Dingler et al., 2020; Oka et al., 2020). ADH5 knockout combined with homozygosity for *Aldh2 rs671* (an Asian flush

patient allele with weak catabolic activity) causes HSPC exhaustion, anaemia, cachexia, kyphosis, shrunken organs and mortality within 4-weeks of birth, recapitulating many phenotypes of AmeD (Oka et al., 2020). Meanwhile, fully tier-1-deficient mice (*Aldh2*$^{-/-}$*Adh5*$^{-/-}$; Dingler et al., 2020) mice exhibit perinatal lethality, growth retardation, microcephaly, predisposition to leukaemia, and reduced HSCs resulting in anaemia and immune cell deficiencies. Importantly, treatment of *Adh5*$^{-/-}$ deficient mice with methanol, a metabolic precursor of formaldehyde, recapitulated the DNA damage and haematological phenotype of *Aldh2*$^{-/-}$*Adh5*$^{-/-}$, inferring formaldehyde as the primary endogenous genotoxin in this context. This notion was also supported by the mass spectrometric measurement of acetaldehyde and formaldehyde-induced modifications to DNA, which showed marked increase in formaldehyde-but not acetaldehyde-DNA adducts in *Aldh2*$^{-/-}$ *Adh5*$^{-/-}$ mice compared to single-knockout controls, suggesting a combined action of both enzymes in formaldehyde detoxification. Moreover, HSPCs in these mice had increased rates of sister-chromatid exchanges, indicating vigorous activation of DNA repair in response to formaldehyde damage. Clonal expansion and sequencing of *Aldh2*$^{-/-}$*Adh5*$^{-/-}$ HSPCs revealed a unique, formaldehyde-driven mutational signature with similarities to cancer-associated mutational signatures (Alexandrov et al., 2020) SBS25, SBS40, and SBS3, as well as to SBS5 which has been shown to accumulate with age (so called “clock-like” signature) (Alexandrov et al., 2013). Interestingly, these mice also showed a transcriptional bias in T-to-A and T-to-G transversions, providing evidence that endogenous formaldehyde might also trigger activation of TCR.

To summarise, mice and humans have a high endogenous burden of formaldehyde which requires enzymatic detoxification. Inability to detoxify formaldehyde through concomitant loss of ALDH2 and ADH5 leads to increased DNA damage, development of CS- and FA-like symptoms, and accumulation of specific DNA mutations in the haemopoietic system and likely also in other tissues. Together, these results implicate the requirement for both FA repair and TCR in resolving formaldehyde damage, and show this damage is a potent endogenous driver of disease.

1.4.3 Models of combined Tier 1 and Tier 2 deficiency

More direct evidence for the role of aldehydes as endogenous genotoxins in FA and CS comes from our mouse models of combined deficiency in tier one enzymes and DNA repair systems, which we define as the 'second tier' of protection against aldehydes (Fig. 1.5). Mice deficient in either TCR or FA repair do not show the characteristic phenotypes of the human syndromes, unless they are also deficient in aldehyde detoxification (Mulderrig et al., 2021; Pontel et al., 2015).

1.4.3.1 *Aldh2*$^{-/-}$*Fancd2*$^{-/-}$ and *Adh5*$^{-/-}$*Fancd2*$^{-/-}$ mice recapitulate Fanconi Anaemia

The contribution of endogenous aldehydes to FA was first revealed through the generation of a mouse with combined deficiency in ALDH2 and FANCD2 (Langevin et al., 2011). These mice require maternal ALDH2 expression to survive embryogenesis, are born at sub-mendelian ratios and have developmental defects. Mice surviving the perinatal window develop lymphoblastic leukaemia and/or aplastic anaemia with age. Flow cytometry analysis of the bone marrow showed that the HSC pool in *Aldh2*$^{-/-}$*Fancd2*$^{-/-}$ mice is markedly reduced (by 600-fold), display increased levels of phosphorylated histone H2AX (γH2AX) indicative of double strand break formation, and has a functional defect in the ability to repopulate host bone marrow after transplantation. This was the first demonstration that acetaldehyde is a physiological genotoxin and an endogenous mutagen that generates ICLs (a long-standing question in the FA field). We later expanded on this work by generating the *Adh5*$^{-/-}$*Fancd2*$^{-/-}$ mouse, which shows similar developmental and haematopoietic defects, but much more severely (Pontel et al., 2015). These mice develop bone marrow failure and leukaemia much earlier, with a median survival of just 33 days (compared to 145 days for *Aldh2*$^{-/-}$*Fancd2*$^{-/-}$ mice). *Adh5*$^{-/-}$*Fancd2*$^{-/-}$ mice also develop liver and kidney defects, characterised by increased karyomegaly in both tissues, elevated γH2AX signalling and functional decline. These additional phenotypes and the shortened lifespan of *Adh5*$^{-/-}$*Fancd2*$^{-/-}$ mice suggest that ADH5 is the primary formaldehyde detoxifier essential for haematopoietic fidelity and protection of other tissues, and that formaldehyde is either more toxic compared to acetaldehyde, or produced at higher concentrations. Interestingly however, unlike

Aldh2$^{-/-}$*Fancd2*$^{-/-}$, *Adh5*$^{-/-}$*Fancd2*$^{-/-}$ mice could be produced from ADH5-deficient mothers, suggesting ADH5 might act more cell-intrinsically, whereas ALDH2 can act in a cell-extrinsic manner to protect against aldehydes (Langevin et al., 2011; Pontel et al., 2015). Together, these mice represent a robust model of Fanconi anaemia driven by a physiological genotoxin and show the importance of FA repair in protecting multiple tissues from formaldehyde damage.

1.4.3.2 *Adh5*$^{-/-}$*Csb*$^{-/-}$ mice recapitulate Cockayne Syndrome

Our observations in FA mice led us to speculate whether other DNA repair pathways were required to protect against formaldehyde. Given formaldehyde's ability to induce ICLs and DPCs which stall transcription, it was conceivable that TCR might be required to resolve formaldehyde damage in transcribed regions of the genome, especially in non-dividing cells which can't utilise replication-coupled repair. Indeed, crossing ADH5 deficient-mice with animals bearing inactivating mutation in the *CSB* gene (Horst et al., 1997) (referred to henceforth as *Csb*$^{-/-}$) generated *Adh5*$^{-/-}$*Csb*$^{-/-}$ mice which almost completely phenocopied human Cockayne Syndrome (Mulderrig et al., 2021). *Adh5*$^{-/-}$*Csb*$^{-/-}$ mice were born at sub-mendelian ratios, showed reduced growth and inability to generate fat-mass (cachetic dwarfism) which progressed with age – a characteristic symptom of CS. RNA sequencing of the kidneys of these mice revealed increased expression of the hormone growth/differentiation factor 15 (GDF-15) downstream of P53 activation. This hormone is a known appetite suppressor (Mullican et al., 2017) which can be induced by DNA damage, likely as part of an evolutionarily conserved response to the ingestion of toxins, to prevent further poisoning by acting on the brain to inhibit feeding behaviour. Elevated levels of GDF-15 are found in patients undergoing chemotherapy (Di Pastena et al., 2024), who are known to exhibit reduced appetite (Boltong & Keast, 2012), as well as in pregnant females experiencing morning sickness (Fejzo et al., 2024). In the *Adh5*$^{-/-}$*Csb*$^{-/-}$ mice, blocking this response with anti-GDF-15 antibodies alleviated their progressive wasting (cachexia) (Mulderrig et al., 2021).

Adh5$^{-/-}$*Csb*$^{-/-}$ mice eventually succumb to kidney failure ~1.5 years of age as confirmed by high levels of serum urea (a waste product normally filtered by the kidney) and histological

identification of interstitial tubule nephritis and focal tubule loss. These mice also exhibit progressive neurodegeneration, with increased infiltration of inflammatory microglia in the cerebellum and onset of cerebellar ataxia by 9 months of age. Interestingly, *Adh5*$^{-/-}$*Csb*$^{-/-}$ mice also develop anaemia at >40-weeks of age, hinting at a role for TCR in preserving haematopoiesis. Moreover, a recent study by Zayoud et al. (2024) revealed that CS patients also exhibit reduced red blood cell counts and lower haemoglobin levels. The source of anaemia in CS – namely the identity of haematopoietic cells that are either depleted or dysfunctional and therefore halt red blood cell production – has not been studied. It is plausible that, similarly to non-dividing nephrons and neurons, quiescent HSCs might rely more heavily on TCR repair and, when damaged, may be unable to re-enter cell-cycle and efficiently replenish downstream progenitors.

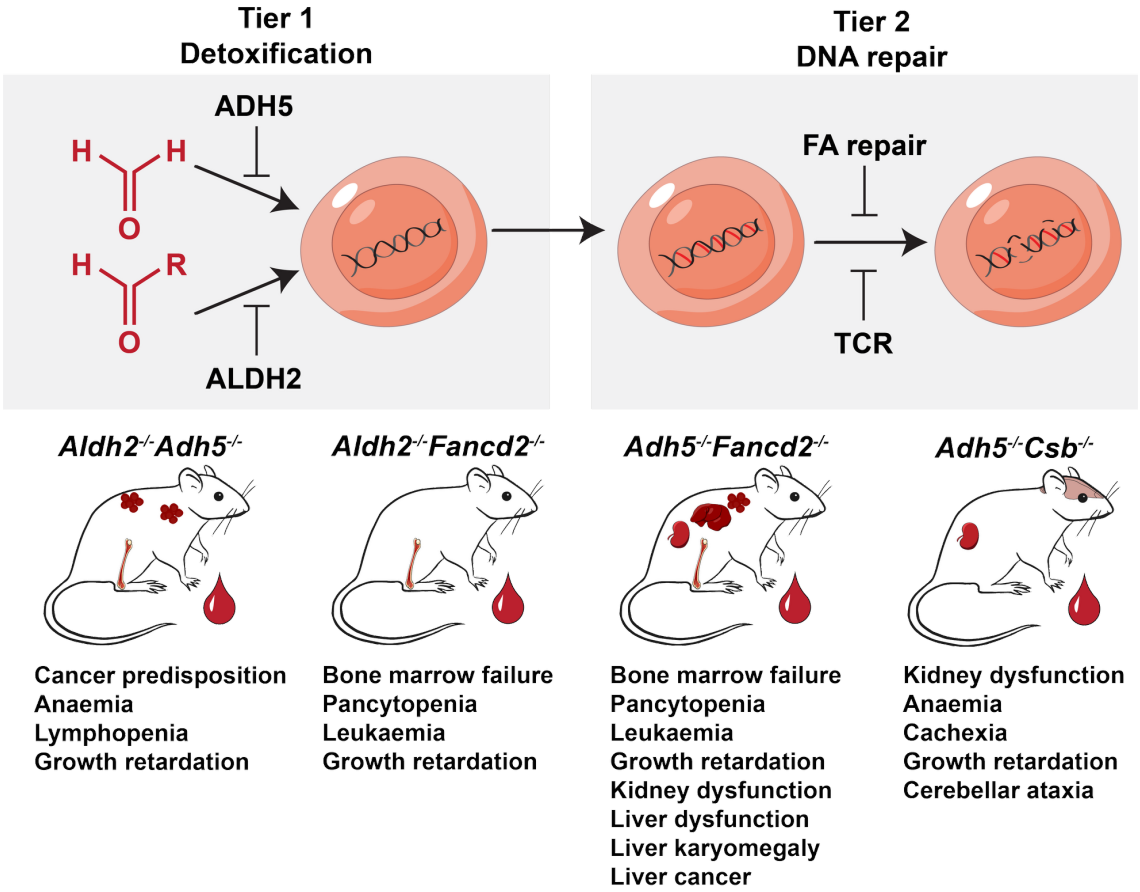

Figure 1.7. Two-tier protection against genotoxic aldehydes and relevant mouse models.

Top panel: model of the two tiers of protection against endogenously produced aldehydes. ADH5 detoxifies formaldehyde and ALDH2 detoxifies acetaldehyde and formaldehyde. These enzymes are the 'first tier' of protection. If accumulating aldehydes overwhelm the first tier, they can induce toxic DNA damage. The deleterious consequences of such damage are prevented by the second tier of protection – DNA repair by the Fanconi Anaemia pathway (FA repair), involving FANCD2, and Transcription-Coupled Repair (TCR), involving CSB. This model was proposed based on observations made in mouse models with inactivating mutations in genes involved in protection against formaldehyde (bottom panel). These animal models allowed for further characterisation of pathological phenotypes associated with endogenous aldehydes.

1.5 The Source of Endogenous Formaldehyde

Adh5$^{-/-}$*Fancd2*$^{-/-}$ and *Adh5*$^{-/-}$*Csb*$^{-/-}$ mice represent two distinct models of rapid ageing of either proliferative or quiescent/post-mitotic tissues induced by deficiency in replication-coupled or transcription-coupled repair of endogenous formaldehyde (Fig. 1.5). These models offer insights into the mechanisms of ageing in different tissues (brain, kidneys, liver, developing blood) and their different requirements for repair. However, two questions remain: (1) how are other tissues protected against formaldehyde and what is their reliance on DNA repair mechanisms? (2) What is the source of formaldehyde in those tissues?

Numerous studies have shown that formaldehyde can be produced from both histone and DNA demethylation during epigenetic remodelling. In human cells, the *Alkb1* homologues ABH2/3 remove methyl groups from single-stranded adenines or cytosines and release them as free formaldehyde (Falnes et al., 2002; Trewick et al., 2002). Meanwhile, oxidative demethylation of histone lysines by lysine-specific-histone demethylase (LSD1) or Jumonji-C-demethylases also generates formaldehyde during activation or repression of genes (Hopkinson et al., 2010; Shi et al., 2004b; Tsukada et al., 2006). Formaldehyde is also produced from oxidative degradation of components of the one carbon cycle, a process essential for nucleotide and amino acid synthesis (Burgos-Barragan et al., 2017). Metabolism of folate derivatives in this cycle can generate formaldehyde at high enough concentration to kill FA repair-deficient cells.

Formaldehyde-producing epigenetic events occur in many cells, though the contribution of different tissues to overall formaldehyde burden has not been studied. The liver may contribute largely to the body's formaldehyde burden, as this organ performs the majority of folate metabolism (Steinberg, 1984; Steinberg et al., 1979). However, the organs which deteriorate in two-tier deficient models also include the kidney and brain (Mulderrig et al., 2021; Pontel et al., 2015), indicating these organs also encounter a significant load of formaldehyde. One possibility is that the blood may act as a disseminator of this toxic chemical by circulating formaldehyde produced in the liver to other organs such as the brain and kidney. Serum levels of formaldehyde

have been measured between 10-100 uM (Heck et al., 1985; Luo et al., 2001; Martos & Pawliszyn, 1998), and blood formaldehyde detoxification is clearly important to protect haematopoietic cells, as evidenced by the severe haematopoietic defect in *Adh5*$^{-/-}$*Fancd2*$^{-/-}$ mice (Pontel et al., 2015). Might the inability of the blood to detoxify formaldehyde in two-tier deficient models contribute to the formaldehyde burden and solid-tissue deterioration observed these mice? If so, could rescuing systemic formaldehyde detoxification alleviate organ defects in two-tier deficient mice? Understanding the contribution of blood formaldehyde, and its detoxification, to the damage which occurs in two-tier-deficient tissues, would help narrow down the source of this endogenous genotoxin. Additionally, identifying if formaldehyde is a blood-circulating genotoxin would have profound implications for treatments to alleviate organ damage in Cockayne Syndrome and Fanconi's Anaemia, and possibly other conditions.

1.6 Aims

Formaldehyde is an endogenous genotoxin which drives ageing and cancer in many tissues. The requirement for FA repair and TCR to resolve formaldehyde damage in proliferating or non-dividing tissues has been demonstrated. However, the role of FA repair in the protection of highly proliferative intestinal epithelium, or the role of TCR in quiescent HSCs is unknown. Additionally, the contribution of blood formaldehyde to peripheral tissue degeneration, and the extent of protection that systemic detoxification provides to those tissues, has not been elucidated. Thus, in my doctoral studies, I aimed to:

1) **Examine the role of TCR in repairing formaldehyde damage in haematopoietic cells.** In Chapter 3, I examine this through whole-genome sequencing of ADH5/CSB-deficient mouse HSPCs to identify if loss of TCR alters the mutational signature compared to *Adh5*$^{-/-}$ controls, which would indicate TCR is active in HSPCs. I then investigate if this loss of TCR affects HSC function in Chapter 4, first by culturing *Adh5*$^{-/-}$*Csb*$^{-/-}$ HSCs *ex-vivo* and assessing their sensitivity to formaldehyde. Finally, I use comprehensive flow cytometric

immunophenotyping of haematopoietic cells to identify the source of the anaemia in *Adh5*$^{-/-}$*Csb*$^{-/-}$ mice and determine if it stems from HSC dysfunction.

2) **Understand the contribution of systemic detoxification to the protection of peripheral organs from formaldehyde damage.** To do this, I validate and utilise a novel mouse model in which all the tissues are lacking ADH5 expression except for the haemopoietic system. In Chapters 5 and 6, I cross this model into either a FANCD2-deficient or CSB-deficient background, respectively, and study whether rescuing haematopoietic formaldehyde detoxification alleviates the organ deterioration in these two models of human disease.
3) **Study the requirement for FA repair of formaldehyde-induced DNA damage in other proliferative tissues**. In Chapter 6, I utilise the FANCD2/ADH5-deficient mouse model with rescued haematopoietic ADH5 expression to study the GI tract without the confounding effect of juvenile bone marrow failure that occurs in constitutive ADH5/FANCD2-deficient mice.

2 METHODS

2.1 Mouse strains

2.1.1 *Adh5*$^{-/-}$ *Csb*$^{-/-}$ mice and controls for Chapter 3/4

The generation of *Adh5*$^{-/-}$*Csb*$^{-/-}$ mice has been described previously in our lab. In short, the *Ercc6tm1Gvh* (*Csb*^{m}, MGI 1932102,C57BL/6) mouse (henceforth referred to as *Csb*$^{-}$) was a kind gift from G.T. van der Horst, Errol Friedberg and Jan Hoeijmakers (Horst et al., 1997). This mouse was crossed with the previously described *Adh5*^{tm1stam} mouse (L. Liu et al., 2004) (MGI 3033711, C57BL/6, henceforth referred to as *Adh5*$^{-}$) which was a kind gift from Dr L. Liu at UCSF. Resultant mice were intercrossed to generate *Adh5*$^{+/-}$*Csb*$^{-/-}$ mice, which were bred together in the final cross to produce either *Adh5*$^{-/-}$*Csb*$^{-/-}$, *Adh5*$^{+/+}$*Csb*$^{-/-}$ or *Adh5*$^{-/+}$*Csb*$^{-/-}$ mice. *Adh5*$^{-/-}$ controls were generated from intercrossing *Adh5*^{tm1dstam} mice. WT controls (C57BL/6JOlaHsdOxuni) were purchased from Biomedical Services, University of Oxford.

2.1.2 *Adh5*^{sw} allele generation

Adh5$^{sw/+}$ mice were created by targeting C57BL/6N embryonic stem cells with a vector containing exon 3 of ADH5 in reverse orientation, flanked by modified Lox66 and Lox71 sites, as described by Lang and Zhutz (2002), with a neomycin resistance cassette on the 3' end. The whole construct was flanked by FRT sites and homology arms for targeting into the ADH5 locus. ES cell clones were selected with neomycin and validated with PCR, before being injected into blastocysts. Resultant chimeric mice were crossed with the FLP-expressing mice, which induces germline removal of the neomycin cassette in resultant pups, which were *Adh5*$^{sw/+}$. These were intercrossed and resultant *Adh5*$^{sw/sw}$ mice maintained through interbreeding. This work was completed by Alex Frick, Juan Garaycoechea and Lee Mulderrig, and is further described in Dr Mulderrig's thesis.

2.1.3 *Adh5$^{sw/-}$Csb$^{-/-}$ Vav1-iCre* mice and controls for Chapter 5

Adh5$^{sw/+}$ mice were crossed with *Adh5$^{+/-}$Csb$^{-/-}$* mice (from Chapter 3/4) to generate *Adh5$^{sw/+}$Csb$^{-/-}$* mice. *Adh5$^{sw/+}$Csb$^{-/-}$* mice were bred with *Adh5$^{sw/+}$* to produce *Adh5$^{sw/sw}$Csb$^{+/-}$* mice which were maintained as a parental strain through intercrossing with littermates and periodic backcrossing. *Adh5$^{+/-}$Csb$^{-/-}$* mice (from Chapter 3/4) were also crossed with *Vav1-iCre*:*Het* C57B6L mice (RRID:IMSR_JAX:008610) (heteryzygous allele henceforth referred to as just '*Vav1-iCre'*) to produce *Adh5$^{+/-}$Csb$^{+/-}$Vav1-iCre* mice. *Adh5$^{+/-}$Csb$^{+/-}$Vav1-iCre* mice were crossed again with *Adh5$^{-/+}$Csb$^{-/-}$* to generate *Adh5$^{-/-}$Csb$^{+/-}$ Vav1-iCre* mice which were maintained as parental breeders through intercrossing with littermates and periodic backcrossing. To produce experimental mice, *Adh5$^{sw/sw}$Csb$^{+/-}$* mice were bred with *Adh5$^{-/-}$Csb$^{+/-}$ Vav1-iCre* mice. *Csb$^{+/-}$* mice do not show haploinsufficiency, so *Adh5$^{sw/-}$Csb$^{+/-}$* or Adh5$^{sw/-}$*Csb$^{+/-}$ Vav1-iCre* mice were experimentally grouped with *Adh5$^{sw/-}$Csb$^{+/+}$* or *Adh5$^{sw/-}$Csb$^{+/+}$Vav1-iCre* mice respectively and referred to together as *Adh5$^{sw/-}$* or *Adh5$^{sw/-}$Vav1-iCre* henceforth. *Csb$^{-/-}$* controls were produced from intercrossing *Adh5$^{+/+}$Csb$^{-/-}$* mice (from Chapter 4).

2.1.4 *Adh5$^{sw/-}$Fancd2$^{-/-}$ Vav1-Cre* mice and controls for Chapter 6

C57BL/6 *Adh5$^{sw/sw}$* mice were crossed with 129sv *Fancd2$^{-/-}$* (MGI 2673422) mice and backcrossed for 10 generations to generate 129sv *Adh5$^{sw/+}$Fancd2$^{+/-}$* mice. *Adh5$^{sw/+}$Fancd2$^{+/-}$* mice were intercrossed to generate *Adh5$^{sw/sw}$Fancd$^{+/-}$* mice which were maintained as male breeders through crossing with littermates. Female breeders were produced by crossing the *Adh5^{tm1d}* allele (MGI 6390884, henceforth referred to as *Adh5^{-}*) into C57BL/6 *Fancd2$^{-/-}$* mice to generate *Adh5$^{-/-}$ Fancd2$^{+/-}$* which were intercrossed with *Vav1-iCre* C57BL/6 (RRID:IMSR_JAX:008610). Resultant *Adh5$^{-/-}$Fancd2$^{+/-}$ Vav1-iCre* or *Adh5$^{+/-}$Fancd2$^{+/-}$ Vav1-iCre* mice were maintained as parental breeders through intercrossing with littermates and periodic backcrossing. Experimental mice were generated from breeding 129sv *Adh5$^{sw/sw}$Fancd2$^{+/-}$* males with C57BL/6 *Adh5$^{-/-}$ Fancd2$^{+/-}$ Vav1-iCre* or *Adh5$^{+/-}$Fancd2$^{+/-}$ Vav1-iCre* females. ADH5 and FANCD2 do not exhibit haploinsufficiency in mice, so *Adh5$^{sw/-}$Fancd2$^{+/-}$* or *Adh5$^{sw/-}$Fancd2$^{+/-}$ Vav1-iCre* mice were experimentally grouped with *Adh5$^{sw/-}$Fancd2$^{+/+}$* or *Adh5$^{sw/-}$Fancd2$^{+/+}$ Vav1-iCre* mice and

referred to as *Adh5$^{sw/-}$* or *Adh5$^{sw/-}$Vav1-iCre* henceforth. Similarly, *Adh5$^{sw/+}$Fancd2$^{+/+}$, Adh5$^{sw/+}$Fancd2$^{+/+}$ Vav1-iCre, Adh5$^{sw/+}$Fancd2$^{+/-}$,* and *Adh5$^{sw/+}$Fancd2$^{+/-}$ Vav1-iCre* mice were simplified as "WT" for experiments. *Adh5$^{sw/+}$Fancd$^{-/-}$* or *Adh5$^{sw/+}$Fancd$^{-/-}$ Vav1-iCre* mice were simplified as *Fancd2$^{-/-}$*.

2.1.5 Competitive transplant donors and recipients

Wild-type, CD45.1-expressing B6SJL (B6.SJL-Ptprca Pepcb/BoyJ) and CD45.2-expressing C57BL/6 mice were purchased from Biomedical Services, University of Oxford. CD45.1/2-expressing mice were obtained by breeding B6SJL mice with C57BL/6 mice.

2.2 Animal experiments

2.2.1 Animal Husbandry

All animal experiments in this study had the approval of the MRC Weatherall Institute of Molecular Medicine animal welfare and ethical review body and the UK Home Office under the Animal (Scientific Procedures) Act 1986 License PFC07716E (from 1st March 2021 – 25th September 2023) or PP2564045 (from 20th September 2023 – 19th September 2028). Mice were kept in individually ventilated cages with environmental enrichment (tunnel, nesting material) at 19-23 °C with light from 7:00 am to 7:00 pm and fed SAFE A03 diet (SAFE®) *ad libetum*.

2.2.2 Genotyping

An ear biopsy was taken from mice by 2-3 weeks after birth and sent to Transnetyx who performed genotyping via real-time PCR with specific probes designed for each gene (Transnetyx, Cordova, TN).

2.2.3 Kaplan-Meier

Mice were weighed and health checked for pale paws, hunching, ascites, masses, or signs of discomfort (grimacing, lethargy) twice weekly. Mice with >10% loss from maximum weight were weighed/checked daily and provided moist food on the cage floor until recovery. Mice were culled

upon identification of a mass, lethargy, grimacing, hunching, ascites, or >10% weight loss accompanied by pale paws or underconditioning (as defined by Ullman-Culleré & Foltz, 1999) which was not within 24 hours after blood sampling. Mice were culled if they had already lost 10% of their maximum weight and continued to lose weight over 5 days which surpassed 15% below their maximum without recovery. Mice were also culled if they lost more than 8% of their maximum weight within 24 hours.

2.2.4 Cerebellar ataxia scoring

Cerebellar ataxia scoring was performed as previously described (Guyenet et al., 2010) every 3 months after 8 weeks of age. Scoring was performed by the same person for all tests and the scorer was blinded to mouse genotype.

2.2.5 Grip strength measurements

Maximum grip strength of the front limbs was measured every 3 months from 8 weeks of age, using a grip strength meter (Bioseb, France) and taking the average of three measurements.

2.2.6 Blood sampling

10% of blood volume (calculated by body weight (kg) x 58.5 (mL) x 0.1) was collected from the tail vein either monthly (for transplant recipient mice in Chapter 4 or mice in Chapter 6) or every three months (for mice in Chapter 5) from 8-weeks of age. Terminal blood was collected by cardiac puncture under anaesthesia using a heparinised syringe. Blood was collected into K_3EDTA MiniCollect tubes (Greiner Bio-one) for complete blood counting or flow cytometry analysis. For serum biochemistry, blood was collected into Microvette 100 CAT-gel or 500 CAT-gel tubes (SARSTEDT), centrifuged at 10,000 x g for 5 minutes, supernatant collected and snap-frozen on dry ice.

2.2.7 Methanol treatment

Mice were injected once per week intraperitoneally with 10 mL/kg of 20% (v/v) methanol in Ringer's solution (Millipore, 115525), equating to a dose of 1.5 g/kg body weight. Mice on

methanol treatment were weighed 3-times weekly or weighed daily and provided moist food on the cage floor if weight loss surpassed 10% from maximum body weight. At the end of treatment (4-7 weeks), blood was collected terminally via cardiac puncture.

2.2.8 Bone marrow transplantation

2.2.8.1 Chapter 4 *ex vivo* HSCs

Immunophenotypic HSCs from 8-12-week-old, wild-type, CD45.1-expressing BSJL mice were FACs sorted (as per Wilkinson et al., 2019), 200 HSCs per well, into a round-bottom 96-well plate containing 200 uL of quiescent media (described below) and incubated at 37 °C in a tissue culture incubator set to 1% oxygen. After 7 days the entire culture in media was taken and mixed with 1 million whole bone marrow cells extracted from the hindlegs of 8-12 week-old CD45.1/2-expressing BSJL/C57BL/6 competitor mice and counted using a Nucleocounter NC-3000 (chemometec) with solution 13 (chemometec, 910-3013). For comparison, 200 immunophenotypic HSCs were freshly sorted on the same day into 200 μL Ham's F-12 Nutrient Mix liquid media and mixed with 1 million competitor bone marrow cells in the same manner. Donor/competitor mixes were transplanted via tail vein injection using a 27-guage needle into wild-type, CD45.2-expressing, C57BL/6 recipient mice which had been irradiated with two X-ray doses of 500 rads each from a caesium source. Following this, 100 uL blood was sampled from the recipient tail veins every month, over a period of 5 months, for flow cytometry analysis of donor chimerism.

2.2.8.2 Chapter 4 methanol treated mouse bone marrow

Following 6 weeks of methanol treatment, bone marrow was flushed with PBS from the femurs and tibiae of CD45.2-expressing donor mice and an aliquot counted using a Nucleocounter NC-3000 (chemometec) with solution 13 (chemometec, 910-3013). 200,000 whole bone marrow cells from the CD45.2-expressing, methanol-treated donor mice were transplanted alongside 200,000 bone marrow cells from wild-type, untreated, CD45.1/CD45.2-expressing B6SJL/C57BL/6 competitors into irradiated CD45.1-expressing B6SJL recipients (irradiated with 2 doses 450

rads). 100 μL of blood was sampled from the recipient tail veins every four weeks, over a period of four months, for flow cytometry analysis of donor chimerism.

2.2.9 Timed matings

129sv *Adh5*$^{sw/+}$*Fancd2*$^{+/-}$ males were pooled with two C57BL/6 *Adh5*$^{-/-}$*Fancd2*$^{+/-}$ *Vav1-iCre* or *Adh5*$^{+/-}$*Fancd2*$^{+/-}$ *Vav1-iCre* females. Females were checked for a vaginal plug the next morning and the time noted as E0.5.

2.3 Mouse tissue processing and analysis

2.3.1 Serum biochemistry

Serum biochemical analysis was performed by MRC Metabolic Diseases Unit Mouse Biochemistry Laboratory [MC_UU_00014/5]. Analysis of serum urea, creatinine, aspartate aminotransferase, alanine aminotransferase, bilirubin and albumin done using a Siemens Healthineers Dimension EXL200 analyser. GDF15 was measured via in-house MSD electrochemiluminescence immunoassay using Bio-Techne R&D Systems DuoSet antibodies and standard.

2.3.2 Total blood count

Blood was analysed in a scil VetABC Plus+ blood counter (Horiba).

2.3.3 Organ weighing

Organs were dried and weighed within 3 hours of animal death except for in chapter 5 where brain and kidneys were weighed after *in vivo* perfusion-fixation and 24-hour post-fixation with 4% paraformaldehyde (PFA) in PBS (v/v). Weights were measured on a Secura 0.1 mg analytical balance (Sartorius, SECURA124-1S).

2.3.4 Liver and kidney histology

Liver and kidneys were fixed for 24 hours in 4% paraformaldehyde, then washed three times in PBS and stored in 70% ethanol (v/v) in PBS until processing by Barts Cancer Institute pathology services. Tissues were embedded in paraffin wax, 4 μm sections mounted on slides, and stained with haematoxylin and eosin. Images were taken on a Zeiss Axioscan 7 (Zeiss).

2.3.5 Brain immunofluorescence

Mice were anaesthetised with pentobarbital and transcardially perfused with 20 mL PBS followed by 20 mL 4% PFA in PBS (v/v). The brain was carefully dissected from the skull and post-fixed for 24 hours in 4% PFA in PBS (v/v), then transferred to 70% ethanol in PBS (v/v) and sent to Dick Jaarsma and Harry Macdonald (Department of Neuroscience, Erasmus MC) for embedding, staining and analysis. Brains were embedded in gelatin blocks and 50 μm sections taken with a freezing microtome, then incubated, free floating with rabbit anti-GFAP (DAKO, 1:5000), rat anti-Mac2 (Cedarlane, 8942AP, 1:2000) or mouse anti-p62/SQSTM1 (Abcam, 56416, 1:2000). Sections were washed and incubated with 1:200 dilutions of FITC-, cyanine 3 (Cy3)-, and Cy5-conjugated secondary antibodies raised in donkey (Jackson ImmunoResearch, West Grove, PA). Sections were imaged with a Zeiss (Oberkochen, Germany) LSM 510 confocal laser scanning microscope using 40x/1.3 and 63x/1.4 oil-immersion objectives. Quantification was based on analysis of at least 3 sections per mouse with areas randomly selected. For P62, density of cells per area was measured. For GFAP quantification sections were imaged with 5x objective and optical densities of rectangular 200x250 μm areas determined using MetaMorph 4.6 image analysis software.

2.3.6 GI tract dissection

Stomach, small intestine (SI), caecum and large intestine (LI) were dissected and flushed with PBS using a syringe. Organs were cut lengthwise (and SI cut into 3-4 strips) and pinned flat with lumen facing outwards onto 50 cm petri dishes half-filled with dried paraffin wax (ThermoScientific, W11/4) containing 10% mineral oil (Sigma, M8410). 10% neutral buffered

formalin (CellPath, BAF-6000-08A) was added to the plate and organs fixed for 24 hours. Intestines were then rolled with lumen facing inwards (SI rolled towards stomach end, LI rolled towards distal end), pinned and transferred to 70% ethanol in PBS (v/v) along with caecum and stomach.

2.3.7 Intestine immunohistochemistry

Embedding, histology and immunohistochemistry of GI tract was performed in collaboration with the Sansom group and histology service at the Cancer Research UK Scotland Institute. The tissue was trimmed, placed into a histology tissue processing cassette and processed on a Epredia Excelsior tissue processor. Tissue was processed using an overnight processing cycle where tissue passed through 5 changes of graded industrial denatured alcohol (Genta, UN1307), 3 changes of xylene (Genta, UN1170) and 3 changes of histology wax (CellPath, GCA-0400-00A). Following processing tissue was orientated in a tissue mould and embedded in histology wax to produce a formalin fixed paraffin embedded (FFPE) tissue block. All alcian blue (AB), haematoxylin and eosin (H&E), immunohistochemistry (IHC) and in-situ hybridisation (ISH) staining was performed on 4 μm FFPE sections which had been ovened at 60ºC for 2 hours.

2.3.7.1 Ki67 and Lysozyme immunofluorescence

The following antibodies were stained on a Leica Bond Rx autostainer Ki67 (32064, Cell Signaling Technology) and Lysozyme (Agilent, A0099). All FFPE sections underwent on-board dewaxing (Leica, AR9222,) and epitope retrieval using appropriate epitope retrieval solution. Sections for Ki67 staining underwent epitope retrieval using ER2 solution (Leica, AR9640) for 20 minutes at 95°C and sections for Lysozyme staining were retrieved using enzyme 1 solution (Leica, AR9551) for 5 minutes at 37°C. Sections were rinsed with Leica wash buffer (Leica, AR9590) before peroxidase block was performed using an Intense R kit (Leica, DS9263,) for 5 minutes. Sections were rinsed with wash buffer and then primary antibody applied at an optimal dilution (Ki67, 1:1000; Lysozyme, 1:200). The sections were rinsed with wash buffer and had rabbit envision (Agilent, K4003,) applied for 30 minutes. The sections were rinsed with wash

buffer and visualised using DAB from the Intense R kit. The sections were counter-stained with haematoxylin using the intense R kit.

2.3.7.2 Cleaved PARP immunofluorescence

Cleaved Parp (cPARP) (Abcam, ab32064) staining was performed on an Agilent AutostainerLink48. The sections were loaded into an Agilent pre-treatment module to be dewaxed and undergo HIER using high pH target retrieval solution (Agilent, K8004,) where sections were heated to 97ºC for 20 minutes. After HIER sections were washed thoroughly with flex wash buffer (Agilent, K8007,) prior to being loaded onto the Agilent AutostainerLink48. The sections underwent peroxidase blocking (Agilent, S2023,) for 5 minutes and rinsed with flex wash buffer then cPARP antibody was applied at 1/1000 dilution for 30 minutes. Following this the sections were rinsed with flex wash buffer before application of rabbit envision to all sections for 30 minutes. Flex wash buffer rinsing took place before applying liquid DAB (Agilent, K3468) for 10 minutes. After staining sections were washed in tap water and counterstained with haematoxylin z (CellPath, RBA-4201-00A).

2.3.7.3 RNAscope

ISH detection for, *Olfm4* (311838) or *Clusterin* (427898) RNA was performed using RNAScope 2.5 LSx (Brown) detection kit (Bio-Techne, 322700) on a Leica Bond Rx autostainer strictly according to manufacturer's instructions.

2.3.7.4 Alcian blue staining

Staining for Alcian Blue (AB) was performed manually on FFPE sections that were dewaxed and rehydrated through xylene and a graded ethanol series before washing in water. Rehydrated slides were stained for 10 minutes in Alcian Blue solution (0.1 g/L in 3% acetic acid) before rinsing in tap water and then counterstained with Eosin for 30 seconds. To complete the AB staining sections were rinsed in tap water, dehydrated through graded ethanol's and placed in xylene. The stained sections were coverslipped in xylene using DPX mountant (CellPath, SEA-1300-00A)

To complete AB, H&E, IHC and ISH staining sections were rinsed in tap water, dehydrated through graded ethanol's and placed in xylene. The stained sections were coverslipped in xylene using DPX mountant (CellPath, SEA-1300-00A,).

2.3.8 Formaldehyde adducts measurement

Organs were washed once in PBS, snap frozen and stored at -80°C until processing. For GI tract adduct measurements, the faeces/stomach contents were flushed out with PBS before freezing. All centrifugation steps were performed at 21,300 x g for 3 minutes at 4 °C. 10-20 mg of tissue was homogenised (4 minutes in Qiagen/Retsch tissue lyzer at 30 HZ) in 700 µL Cell Lysis Solution (Qiagen, 158113) with 4 µL Proteinase K (Qiagen, 158146) and two 7 mm stainless steel metal balls (Qiagen, 69997), then incubated in a ThermoMixer at 37°C for 30 minutes at 900 rpm. 4 µL of RNAse A (Qiagen, 19101) was then added and samples were incubated at 37°C for 1 hour on a ThermoMixer at 900 rpm before being transferred to tubes containing 700 µL of Protein Precipitation Solution (Qiagen, 158126). Samples were vortexed and centrifuged and supernatant separated into tubes containing 700 µL pre-chilled isopropanol (Merck, 67-63-0) for DNA precipitation at 4°C. Samples were mixed by inversion, incubated 5 minutes and then centrifuged and supernatant discarded. Tubes were left open on a paper towel for 5 minutes to allow isopropanol evaporation, then 600 µL of 70% ethanol (v/v in PBS) was added to wash the pellet. Samples were centrifuged and supernatant removed, then left to dry before incubation for 48 hours at 37°C in 500 µL of 50mM $NaCBNBD_3$ in 200mM NaOAc at pH 5.2. After 48 hours DNA was re-precipitated by addition of 900 µL of isopropanol followed by centrifugation and removal of the supernatant. Tubes were left open to dry for 5 minutes before addition of 900 µL 70% ethanol (v/v in PBS), inversion and centrifugation. Ethanol was removed, tubes left to dry 5 minutes and DNA dissolved in 80 µL of PBS. DNA was quantified by nanodrop, then 5 ug added to an enzyme mix containing 2 U shrimp alkaline phosphatase (New England Biolabs, M0371), 3.8 U phosphodiesterase I (Sigma, P3243), 10 U DNase I (Roche, 4716728001) in 1x DNase digestion buffer made up to 100 uL with ultrapure water. Internal standards for 15N-N2-Me-dG and 15N-

dA. were added to each digest. A standard curve was generated using 5 ug of non-reduced DNA from wild-type mouse 32D cells with the addition of 2′-deoxyadenosine (dA) and N2-Me-dG added at various concentrations (0.24 - 100 fmol for N2-MedG, 8.5 - 272 nmol for dA plus a control without either). Digestion was performed overnight at 37 °C (18 hours minimum) and samples vortexed, filtered through a 1000 MWCO Vivacon® 500 column (Sartorius, VN01H32) and centrifuged at 16,000 x g at 12°C for 20 minutes. Tubes were then turned 180 degrees in the centrifuge and centrifuged again to increase flowthrough. Finally, samples were transferred to a mass spectrometry vial (Waters, 186000385c) and analyzed on a TSQ Altis™ Triple Quadrupole Mass Spectrometer with a DIONEX UltiMate 3000 RS Autosampler.

2.3.9 ADH5 western blot

10-15 mg of snap frozen tissue was homogenized in 100-500 µL (volume varies depending on size of tissue piece) RIPA buffer (ThermoFisher, 89900) containing 5mM $MgCl_2$, 5mM N-Ethylmaleimide (NEM) and 25 unit/mL Benzonase (Millipore). A 7 mm metal ball was added to the tubes and disruption performed by shaking in a tissue lyzer at 30 Hz for 4 minutes at 4 °C. Solution was incubated for 30 minutes on ice, then cleared by centrifuging at 21,300 x g for 25 minutes at 4 °C and collecting the supernatant. Protein concentration was measured using a Pierce™ BCA Protein Assay Kit (ThermoFisher, 23225) with 0 – 20 µg/mL standards according to manufacturer's instructions and read on a CLARIOstar plus microplate reader (BMG labtech) at 562 nm absorbance. Samples were then diluted to 1.5 – 5 µg/mL and re-measured and protein aliquoted (30 ug for spleen, bone marrow and kidney, 50 µg for brain, 15 µg for liver), mixed with 1x SDS loading buffer, denatured by incubation at 70 °C in a ThermoMixer, then loaded into Bolt™ 4-12% Bis-Tris Plus Gels in 1x NuPAGE™ MOPS SDS Running Buffer (Invitrogen, NP0001) and run at 140 V for 75 minutes. Following this, samples were transferred onto a 0.45 µm PVDF Transfer Membrane (ThermoFisher, 88518) for 4 hours at 35V at 4 °C, then blocked 30 minutes with 5% milk (Millipore, 70166) in Tris-buffered saline with 0.05% Tween-20 (TBST) (Sigma-Aldrich, P1379), then cut and blotted for 2 hours with 1:1000 of in-house rabbit

anti-ADH5 antibody which has been previously described (Pontel et al., 2015). For loading control, the membrane was cut and blotted with 1:25,000 anti-mouse vinculin (Sigma, 05-386) in 1% milk in TBST for bone marrow, spleen, liver and kidney or 1:10,000 anti-mouse beta-catenin for brain (BD, 610153). The membrane was then washed three times in TBST and incubated 1 hour with secondary antibody (1:5000 swine anti-rabbit (DAKO, P0217)) or 1:1000 goat anti-mouse (Invitrogen, 31432). Secondary antibody was removed with three 5-minute TBST washes and blots were visualised with Western ECL substrate (Bio-rad, 1705061) on a Chemidoc imaging system (Bio-rad).

2.4 Flow cytometry and cell sorting

2.4.1 HSC cell sorting and culture immunophenotyping

c-Kit enrichment, HSC sorting and *ex-vivo* culture immunophenotyping was performed according to the protocol by Wilkinson et al., (2020) using all reagents as stated. Sorting was done on a FACSARIA Fusion, immunophenotyping on a BD Fortessa X-20.

2.4.2 CFSE analysis

CellTrace™ CFSE (Invitrogen, C34554) was diluted to 5 mM in dimethyl-sulfoxide and 1 µL added to 1 mL of HSC cultures (sorted prior and maintained for 21 days as per standard protocol) in 6-well plates, then incubated 20 minutes at room temperature. Following this, cells were washed with 5 mLs of Ham's F-12 Nutrient Mix liquid media (Gibco, 11765–054) containing 10% fetal bovine serum (FBS), centrifuged 400 x g for 5 minutes, supernatant aspirated and cells resuspended in 1 mL of either low or high cytokine media (described below) and transferred to a 37 °C incubator set to either 1% or 5% oxygen concentration and incubated for 4 days (with ~80% of media replaced at 2 days). Following this, cultures were centrifuged at 450 x g for 5 minutes, resuspended in PBS containing 0.5 ng/mL propidium iodide, (Biolegend, 421301), and analysed on a BD LSR Fortessa.

2.4.3 Cell cycle analysis

HSC cultures (sorted prior and maintained for 21 days as per standard protocol) in 6-well plates were centrifuged at 450 x g for 5 minutes, supernatant removed and resuspended in 1 mL of either high or low cytokine cultures (described below) and 1% or 5% oxygen concentration and incubated for 3 days. Cultures were then disrupted by pipetting and half the volume taken and stained with 1 μL of fluorophore-conjugated antibody mix (c-Kit-APC-Cy7, Sca1-PECy7, CD201-APC, TER119-FITC, CD8a-FITC, CD4-FITC, CD127-FITC, CD45R-FITC, LY6G-FITC in PBS) per 50 μL sample. After 30 minutes incubation at 4°C, suspension was washed in PBS (containing 2% FBS), centrifuged for 5 minutes, resuspended in 100 μL of 1x Cytofix/Cytoperm buffer (BD Biosciences, 554714) and incubated 30 mins at 4°C. Following this, cells were washed with 400 μL, then 1000 μL, of 1x Perm/Wash buffer (BD Biosciences Cat #554714), centrifuged for 5 minutes at 1000 x g, supernatant discarded and resuspended in 50 μL of anti Ki67-PE or anti-IgG-PE (as isotype control) antibody diluted 1:50 in PBS/FCS, then incubated overnight on an IKA LOOPSTER at 4°C. Following this, antibody was washed off with 1 mL of 1x Perm/wash buffer, the sample centrifuged for 5 minutes at 1000 x g and resuspended in 50 μL of Hoechst 33342 (Invitrogen, H3570, 1 ng/μL in 1x Perm/Wash buffer). After 1 hour incubation at 4°C, Hoechst was diluted with 100 μL 1x Perm/Wash buffer and solution analysed on a BD Fortessa X20 using excess cells stained singly with fluorophore-conjugated antibodies to calculate compensation matrix.

Cell cycle analysis staining panel

Epitope	Fluorophore	Dilution	Manufacturer	Catalog no.
CD4	FITC	1:1000	BioLegend	130308
CD8a	FITC	1:1000	BD Biosciences	553031
CD127	FITC	1:1000	eBioscience	11-1271-85
CD45R	FITC	1:1000	BD Biosciences	553088
Ly6G	FITC	1:1000	eBioscience	11-5931-85
TER119	FITC	1:1000	BioLegend	116206
CD201	APC	1:1000	eBioscience	17-2012-82
c-Kit	APC/Cy7	1:400	BioLegend	105825
Sca1	PE/Cy7	1:400	eBioscience	25-5981-82
Ki67 Or IgG	PE	1:400	BD Biosciences	556027

2.4.4 Chimerism analysis

100 µL of blood was incubated in 1 ml haemolytic buffer (155 mM NH_4Cl, 10 mM $KHCO_3$, 0.1 mM EDTA) for ten minutes, washed twice in PBS/FCS and stained with fluorophore-conjugated antibodies against CD45 and mature cell markers (CD4-FITC, CD8a-FITC, B220-PerCPCy5.5, MAC1-PE, Gr-1-PE, TER119-PE/Cy7, CD45.1-BV421, CD45.2-APC). Stained cells were washed in PBS/FCS, stained for live/dead cells with 0.5 g/ml 7-Aminoactinomycin D (7-AAD) and analysed on a BD Fortessa X20 using Ultracomp beads (Invitrogen, 01-2222-42) stained singly with fluorophore-conjugated antibodies to calculate compensation matrix. A minimum of 10,000 live, TER119- single cell events were recorded.

Blood chimerism staining panel

Epitope	Fluorophore	Dilution	Manufacturer	Catalog no.
CD4	FITC	1:500	BioLegend	130308
CD8a	FITC	1:500	BD Biosciences	553031
B220	PerCPCy5.5	1:143	BioLegend	103236
MAC1	PE	1:500	BD Biosciences	553311
GR-1	PE	1:500	BioLegend	108407
TER119	PE/Cy7	1:200	BD Biosciences	557853
CD45.1	BV421	1:143	BioLegend	110732
CD45.2	APC	1:143	BioLegend	109814

2.4.5 Haematopoietic immunophenotyping

All steps were performed on ice and centrifugation steps were performed at 300 x g and 4 °C unless otherwise stated. Hindlegs, pelvis, spine (where applicable), spleen (where applicable) were dissected into PBS. Where applicable, 100 µL blood was collected via cardiac puncture. Femurs, tibiae, and pelvic bones were flushed with PBS (containing 2% FCS) using a 27G needle. For FANCD2/ADH5-deficient mice, bone marrow was also extracted from the spine by grinding in PBS/FCS with a mortar and pestle and homogenising with a 16G needle. Bone marrow (or spleen where applicable) was strained through a 70 µm filter, centrifuged, and washed in PBS/FCS. Bone marrow, spleen, or blood cells were incubated for 10 minutes in haemolytic buffer (155 mM NH_4Cl, 10 mM $KHCO_3$, 0.1 mM EDTA) then washed with PBS/FCS and counted using a Nucleocounter NC-3000 (chemometec) with solution 13 (chemometec, 910-3013). 10 million bone marrow cells (or the entire bone marrow for *Adh5*$^{sw/-}$*Fancd*$^{-/-}$ mice) were incubated for 90 minutes with fluorophore-conjugated antibodies against extracellular markers of lineage (FITC-conjugated CD4, CD8, B220, CD11b, CD11c, CD3e, CD41, FcER1, LY-6G, TER-119), progenitor (CD117-APCe780, Sca1-PEcy7, CD34-AlexaFluor700, CD135-PE, CD127-BV605,

CD16/32-APC) and stem (CD150-BV785, CD48-BV421) cells. Where applicable, 5 million bone marrow, spleen or blood cells were stained for 15 minutes with fluorophore-conjugated antibodies against mature cell markers (CD4-BV421, CD8-BV786, LY-6G-FITC, CD11b-BV711, B220-APC, TER-119 PEcy7, CD3e BV605, IgM-APCe780, CD71-PE). Stained cells were washed in PBS/FCS, stained for live/dead cells with 0.5 mg/mL 7-AAD and analysed on a BD Fortessa X20 using Ultracomp beads (Invitrogen, 01-2222-42) stained singly with fluorophore-conjugated antibodies to calculate compensation matrix. A minimum of 500,000 bone marrow or 250,000 blood/spleen events were recorded.

Stem and Progenitor staining panel

Epitope	Fluorophore	Dilution	Manufacturer	Catalog no.
CD4	FITC	1:440	BioLegend	130308
CD8a	FITC	1:440	BD Biosciences	553031
B220	FITC	1:440	BD Biosciences	553088
MAC1/CD11b	FITC	1:440	BD Biosciences	553310
CD11c	FITC	1:440	eBioscience	11-0114-85
CD3e	FITC	1:440	eBioscience	35-0031-U500
CD41	FITC	1:440	BD Bioscience	553848
FCεR1	FITC	1:440	eBioscience	11-5898-85
Ly-6G	FITC	1:440	eBioscience	11-5931-85
TER119	FITC	1:440	BioLegend	116206
c-Kit	APCeF780	1:1600	eBioscience	47-1171-82
Sca-1	PE/Cy7	1:200	eBioscience	25-5981-82
CD150	BV795	1:200	BioLegend	115937
CD48	BV421	1:100	BioLegend	103428
CD135/Flt3	PE	1:200	eBioscience	12-1351-82
CD34	AF700	1:10	eBioscience	17-0161-82
CD127	BV605	1:200	BioLegend	135025

Mature cell staining panel

Epitope	Fluorophore	Dilution	Manufacturer	Catalog no.
CD4	BV421	1:200	BD Biosciences	740024
CD8a	BV786	1:200	BD Biosciences	563332
GR1/Ly-6G	FITC	1:200	eBioscience	553127
B220	APC	1:200	BD Biosiences	553092
CD3e	BV605	1:200	BD Biosciences	563004
TER119	PE/Cy7	1:200	BD Biosiences	557853
IgM	APC/e780	1:200	eBioscience	47-5790-82
CD71	PE	1:200	eBioscience	12-0711-82
MAC1/CD11b	BV711	1:200	BD Biosciences	563168

2.4.6 E13.5 embryo immunophenotyping

All steps until analysis were performed on ice unless otherwise stated. At E13.5, the embryos were dissected from the uterine horn of females and foetal liver extracted into IMDM. Foetal livers were homogenised by disruption with a p1000 pipette (Gilson) and strained through a 40 μm strainer (Falcon, 352235). Live cells were counted using a Nucleocounter NC-3000 (chemometec) with solution 13 (chemometec, 910-3013). 10 million live cells were blocked for 10 minutes with 100 μL of 5% rat serum in PBS (v/v) (Jackson Immunoresearch, AB_2337141) for 15 minutes, then stained with 200 μL of fluorophore-conjugated antibody mix (CD3e-FITC, CD4-FITC, CD5-FITC, CD8a-FITC, CD11c-FITC, B220-FITC, FCeRIα-FITC, GR1-FITC, TER-119-FITC, Mac-1-BV605, c-Kit-PerCP-Cy5.5, Sca1-PECy7, CD150-PE, CD41-BV421, CD48-BV421 in PBS + 1% bovine serum albumin (BSA) (w/v)) for 15 minutes at room temperature. Following this, samples were centrifuged at 300 x g for 5 minutes and pellet

resuspended in 300 µL of 1% BSA in PBS containing 0.5 mg/mL 7-AAD. Samples were analysed on a BD Fortessa X-20 using excess foetal liver cells stained singly with fluorophore-conjugated antibodies to calculate compensation matrix. This work was done in collaboration with Ashley Kamimae-Lanning.

Foetal liver staining panel

Epitope	Fluorophore	Dilution	Manufacturer	Catalog no.
CD4	FITC	1:400	BioLegend	130308
CD8a	FITC	1:400	BD Biosciences	553031
B220	FITC	1:400	BD Biosciences	553088
MAC1/CD11b	FITC	1:400	BD Biosciences	553310
CD11c	FITC	1:400	eBioscience	11-0114-85
CD3e	FITC	1:400	eBioscience	35-0031-U500
CD41	FITC	1:400	BD Bioscience	553848
FCεR1	FITC	1:400	eBioscience	11-5898-85
Ly-6G	FITC	1:400	eBioscience	11-5931-85
TER119	FITC	1:400	BioLegend	116206
c-Kit	PerCP/Cy5.5	1:200	BioLegend	105824
Sca-1	PE/Cy7	1:200	eBioscience	25-5981-82
CD150	PE	1:200	BioLegend	115914
CD48	BV421	1:200	BioLegend	103428
CD41	BV421	1:200	BioLegend	133911

2.5 Ex vivo

2.5.1 HSC culture

HSC were grown in Ham's F-12 Nutrient Mix liquid media (Gibco, 11765–054) containing 1 mg/mL 87–90%-hydrolyzed polyvinyl alcohol (PVA) (Sigma, P8136), 1X Insulin-Transferrin-Selenium-ethanolamine (ITS-X) (Gibco, Cat# 51500–056), 1X Penicillin-Streptomycin-Glutamine (P/S/G) (Gibco Cat# 10378–016), 10 mM HEPES (Gibco, 15630–080) and supplemented with Stem Cell Factor (SCF) (Peprotech, AF-315–14) and Thrombopoietin (TPO) (Peprotech, AF-315–14). Standard, proliferating culture contained SCF and TPO at 10 ng/μL and 100 ng/μL respectively. For quiescent culture SCF concentration was 1.5 ng/mL and TPO at 1 ng/mL.

2.5.2 Single cell quiescence analysis

Single HSCs were sorted into 200 μL of high or low cytokine media in a round bottom 96-well plate (COSTAR, 3799) and incubated 7 days at 1% or 5% oxygen. After 7 days, the number of cells per well was counted using a light microscope at 20X magnification. Cells with faded, undefined surface membranes were excluded as dead. Following this, 80% of media was removed via pipetting from the side of the well, replaced by high cytokine media and all cultures moved to 5% oxygen and incubated for 15 days with media replaced every 2-3 days. Following this, the culture was collected, stained (according to Wilkinson et., al 2019 protocol) and immunophenotyped on a BD Fortessa.

2.5.3 HSC formaldehyde sensitivity assay

50 HSCs were sorted into 200 μL of high or low cytokine media in a round bottom 96-well plate (COSTAR, 3799) and incubated at 5% or 1% oxygen concentration. 24 hours after plating, cells were counted using a light microscope at 20X magnification. Cells with faded, undefined surface membranes were excluded as dead. This cell count was used as a baseline pre-treatment measurement. 5.3 M formaldehyde (ThermoScientific, 28906) was serially diluted in media to

make 5X concentrated stocks of 0, 150, 300 and 450 μM formaldehyde. 25 μL of stock was added to wells containing 200 μL of media to make final concentrations. Cultures were incubated for 48 hours at 1% or 5% oxygen and then re-counted using a light microscope at 20X magnification. Images of wells for counting validation were taken using an EVOS™ XL Core Imaging System (ThermoFisher, AMEX1000). Dead cells were identified by faded, undefined surface membranes and were excluded from the count. Post-treatment cell counts were divided by pre-treatment counts per well, and then this was normalised to the untreated growth to determine percentage growth of each well compared to untreated.

2.5.4 Bone marrow clonal expansion for sequencing

Bone marrow was flushed from mouse hindlegs in PBS/FCS, strained through a 70 μm filter (Greiner, 542070) and counted using a Nucleocounter NC-3000 (chemometec) with solution 13 (chemometec, 910-3013). Bone marrow was diluted to 1 x 10^6 cells/mL, 2 x 10^5 cells/mL or 5 x 10^4 cells/mL in IMDM, then 1 volume of diluted cells added to 10 volumes of Methocult GF M3434 (Stem Cell Technologies, 03434) semisolid medium, vortexed vigorously and left 10 minutes to settle. 1.1 mL of this was added to 35 mm tissue culture dishes (Corning, 430165) and incubated in a 37 °C tissue culture at 20% O_2 concentration and 5% CO_2. After 2 weeks, isolated colonies were identified with a light microscope and transferred to 120 uL of X-Vivo 20 (Lonza, 04-448Q) supplemented with 10 ng/mL IL-3, 10 ng/mL IL-6, 50 ng/mL SCF and 50 ng/mL TPO (Peprotech, 213-13, 216-16, AF-315–14, AF-315–14) and 5% (v/v) BIT9500 (Stem Cell Technologies, 09500). After another week, DNA was extracted from outgrown colonies using a Quick-gDNA microprep kit (Zymo Research, D3021) according to the manufacturer's instructions. DNA was extracted from a matched brain sample for each mouse for use as a reference genome.

2.6 Library Preparation and Sequencing

DNA was quantified using an AccuBlue High Sensitivity dsDNA Quantitation Kit (Biotium, 31006) according to manufacturer's instructions with fluorescence measured on a CLARIOstar plus microplate reader (BMG labtech). Libraries were prepared using an NEBNext Ultra II FS DNA Library Preparation kit and Multiplex Oligos for Illumina (96 Unique Dual Index Primer Pairs) (New England Biolabs, E6177, E6440S) according to the manufacturer's recommendation. Libraries were size selected for a peak ~ 400 bp using SPRIselect beads (Beckman Coulter, B23317) and size validated with an Agilent Bioanalyzer 2100 and D1000 screen tape system according to manufacturer's instructions (Agilent, 5067-5583, 86). Libraries were quantified by qPCR on a QuantStudio 3 using the Kapa library quantification kit for Illumina (Roche, KK4824). Libraries were sequenced by Novogene on a NovaSeq X Plus (Illumina) with 150 bp paired end reads. Raw sequence data was converted to BAM format using BWA and the Genome Analysis Toolkit (GATK) for data pre-processing and somatic variant discovery according to best practice (Van der Auwera et al., 2013). For base quality score recalibration, the Sanger Mouse Genome Project database of single-nucleotide polymorphisms and indels was used, and samples aligned against the Illumina mm10 reference genome. Mutect2 was used to identify bone marrow somatic variants compared to the reference matched brain sample. Mutect2 passing variants were then filtered to those with > = 8 coverage depth and variant allele frequency > = 0.3 to restrict analysis to high confidence variants.

3 The Mutational Signature of Formaldehyde Exposure and Transcription-Coupled Repair Deficiency in Haematopoietic Stem Cells

Haematopoietic stem cells (HSCs) remain largely quiescent in adulthood, but evidence suggest that they still accumulate DNA damage in a time-dependent manner (Beerman et al., 2014). This damage can compromise their ability to re-enter cell cycle and self-renew or produce downstream blood progenitors (Rossi et al., 2007). How DNA damage is repaired in quiescent HSCs, or whether it even is repaired, has not been fully elucidated, nor has the role of TCR generally in haemopoietic cells. Understanding how haematopoietic cells accumulate damage is important to understand how pre-leukemic mutations, which are thought to mainly occur in HSCs, arise (Jamieson et al., 2004). Additionally, DNA damage can drive clonal haematopoiesis, wherein HSCs acquire mutations which impart a competitive advantage and leads to over-representation of blood cells derived from one HSC clone. This condition is present in >10-20% of adults >70 years old, and predisposes to the development of leukaemia, and cardiovascular disease (Genovese et al., 2014; Jaiswal et al., 2014; Xie et al., 2014). The processes that drive this

mutation accrual, as well as the contributions of different DNA repair pathways and endogenous mutagens, are not fully understood.

Quiescent cells cannot utilize replication-coupled means of repair, and it is speculated that they rely more heavily on non-replication-coupled means, such as TCR, gg-NER or NHEJ (Enoiu et al., 2012; Mohrin et al., 2010; Williams et al., 2012, 2013). Indeed, several studies have shown that TCR remains active in quiescence and lack of this repair pathway sensitizes quiescent cells to DNA damage (Hsu et al., 2007; Sandoval et al., 1996). The activity of TCR in HSCs has been hinted at by whole-genome sequencing of single-cell-derived colonies. In this process, the somatic mutations that a cell acquires over time can be identified by isolation of single cells, expansion of these cells into clonal liquid cultures, and deep sequencing (Fig. 3.1A). Mutational profiles are then obtained by comparing clone-specific sequences with a germline reference (e.g., by sequencing DNA from non-proliferative tissues such as brain cortex) or another appropriate control (e.g., for *in vitro* studies of cells exposed to mutagens reference sequences are typically extracted from untreated controls). The single base substitutions that are subsequently identified can be categorized by mutation type (typically ascribed to the pyrimidine: C>A, C>G, C>T, T>A, T>C or T>G) and the surrounding trinucleotide context (e.g., if the mutation occurs at A**T**A, A**T**G, A**T**C etc.). Recurrent features give rise to 'mutational signatures' which can be then assigned to action of a specific mutagen(s) and/or mutagenic processes that operate in the cells and leave characteristic genomic 'scars'.

Interestingly, somatic SBS mutations in human HSPCs have been found to exhibit a transcriptional strand bias, with C>T substitutions in gene bodies occurring more on the transcribed (vs untranscribed) strand (Osorio et al., 2018). This presence of a transcriptional strand bias hints that TCR is active in HSPCs. Bulky DNA-protein crosslinks or interstrand crosslinks may stall RNAPII and induce repair regardless of the strand on which the lesions reside. However, lesions contained to one strand, such as UV-induced lesions or intrastrand crosslinks are only recognised and repaired by TCR if they are on the transcribed strand (Mellon et al., 1987;

Selby et al., 2023; Svejstrup, 2002). If these lesions are faithfully repaired, whilst untranscribed lesions are ignored, this would lead to more lesions on the untranscribed strand. Misincorporation of a base opposite these lesions during replication would cause this base change to be more prevalent on the transcribed strand (Fig. 3.1C). Conversely, if TCR repairs a transcribed lesion mutagenically, leading to a substitution, this could also induce a bias towards certain base changes on the transcribed strand (Fig. 3.1D). The bias of different base changes towards either strand may vary depending on the type of lesion, and whether its repair by TCR is mutagenic, but the presence of this bias indicates that a transcription-coupled process contributes to the mutagenic landscape of HSCs.

In our previous work, we have shown that endogenous formaldehyde induces a specific mutational signature with a transcriptional strand bias: bone marrow clonal expansion and sequencing revealed that *Aldh2*$^{-/-}$*Adh5*$^{-/-}$ mice have high mutational burden (approx. 3x more SBS mutations compared to WT) with increased propensity for T>A or T>G substitutions on the transcribed strand (Dingler et al., 2020). This work confirmed that formaldehyde is a metabolic mutagen which causes significant damage to the genomes of HSPCs and induces mutations with similarity to cancer-derived mutational signatures (Alexandrov et al., 2020) (SBS25, SBS40, SBS5, SBS3), suggesting endogenous formaldehyde might contribute to neoplastic mutation accrual.

The transcription bias in *Aldh2*$^{-/-}$*Adh5*$^{-/-}$ HSPC mutations could point to increased demand for TCR in those cells. Alternatively, the transcriptional bias in this context could be explained by the increased exposure of the transcribed or untranscribed strand to cellular formaldehyde (Fig. 3.1E). In the latter case, the strand-bias would be caused by strand-specific exposure to mutagen rather than strand-specific DNA repair process. Therefore, to conclusively ascertain whether TCR is indeed responsible for the transcription bias associated with formaldehyde, one must assess the effect of TCR deficiency in this context. Thus, I set out to determine the mutational signature of mouse HSPCs which lack both formaldehyde detoxification (via ADH5 deficiency) and TCR (via CSB deficiency). If loss of CSB shifts the transcriptional bias of mutations in ADH5-deficient

HSPCs, this would show that TCR acts on formaldehyde lesions in haematopoietic cells and reveal a previously undescribed role for TCR in this tissue.

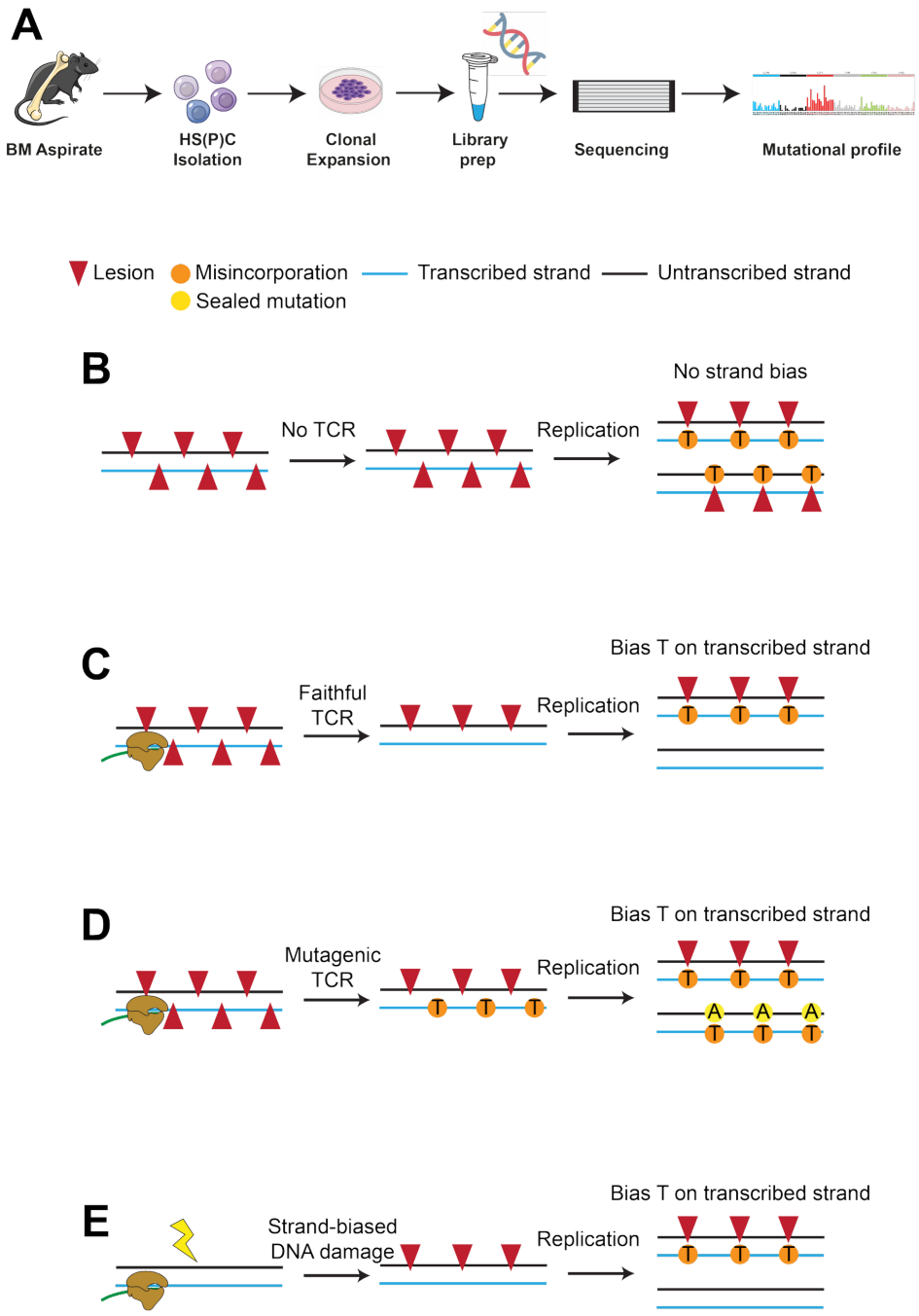

Figure 3.1 HSPC somatic mutation discovery and interpretations

Model of **A)** the method for discovery of somatic mutations in mouse bone marrow used by Dingler et al., (2020) and in this study. Bone marrow was taken from male, 40-week-old C57B6JL mice and plated at single cell dilutions on methocult 3434 media which encourages expansion of haematopoietic stem and progenitor cells. DNA was extracted from expanded colonies and prepped for sequencing. HSPC colonies were compared to a brain germline reference to obtain somatic mutations and generate a mutation profile.

B-E) DNA damage can evoke transcriptionally biased mutations which are detected by sequencing. **B)** If there is no transcriptionally biased DNA damage or repair, then lesions (red triangles) which induce misincorporations (orange circles) in the next replication cycle will occur with equal likelihood in the transcribed (blue) or untranscribed (black) strand. **C)** If TCR is active and repairs lesions faithfully on the transcribed strand, this will lead to a bias towards unrepaired lesions on the untranscribed strand, which can induce misincorporations (a T in this example) on the new transcribed strand during replication. This would lead to a bias towards T substitutions on the transcribed strand. **D)** If TCR repairs mutagenically, this could induce misincorporations (T in this example) on the transcribed strand whilst the untranscribed strand retains unrepaired lesions. In the next replication, mutations on the transcribed strand will be sealed (in this case A incorporated on the new untranscribed strand opposite the initially misincorporated T). Meanwhile lesions on the old untranscribed strand will induce misincorporations (in this example T) on the new transcribed strand during replication. In this example, this would lead to a bias in substitutions where the T is on the transcribed strand. **E)** If TCR is not active, but there is a bias towards DNA damage on one strand (in this example, the untranscribed strand), this would induce more lesions on this strand, which induce misincorporations (in this case T) on the new transcribed strand during replication.

3.1 Formaldehyde induces transcription-strand-biased mutations via mutagenic TCR

In previous work from our lab, we sequenced and identified mutations in clonally expanded bone marrow HSPC colonies from 40-week-old, C57B6L WT, *Aldh2*$^{-/-}$, *Adh5*$^{-/-}$ and *Aldh2*$^{-/-}$*Adh5*$^{-/-}$ mice (Dingler et al., 2020). To allow comparison, I aged C57B6L *Csb*$^{-/-}$ and *Adh5*$^{-/-}$*Csb*$^{-/-}$ mice to 40-weeks and performed bone marrow extraction, *ex vivo* expansion, genomic DNA extraction from colonies, library preparation, sequencing and data processing using an identical protocol as in our previous work. DNA extracted from the brains of these mice was used to generate germline reference. For simplicity, and due to the limited number of large substitutions and insertions in these samples, analysis was restricted to single base substitutions (SBS).

Analysis of SBS types and their trinucleotide context revealed the mutational landscape of *Adh5*$^{-/-}$*Csb*$^{-/-}$ HSPCs (Fig. 3.2). By cosine similarity, the composite mutational spectrum resembled most the SBS1 and SBS40 signatures. SBS1 is a ‘clock-like’ mutation signature which correlates with age (Nik-Zainal et al., 2012), whilst SBS40 is a cancer-associated signature of unknown aetiology which is also age-associated (Alexandrov et al., 2020). Together, this might hint that endogenous formaldehyde and TCR deficiency exerts similar mutagenic effects to physiological ageing, and some cancers.

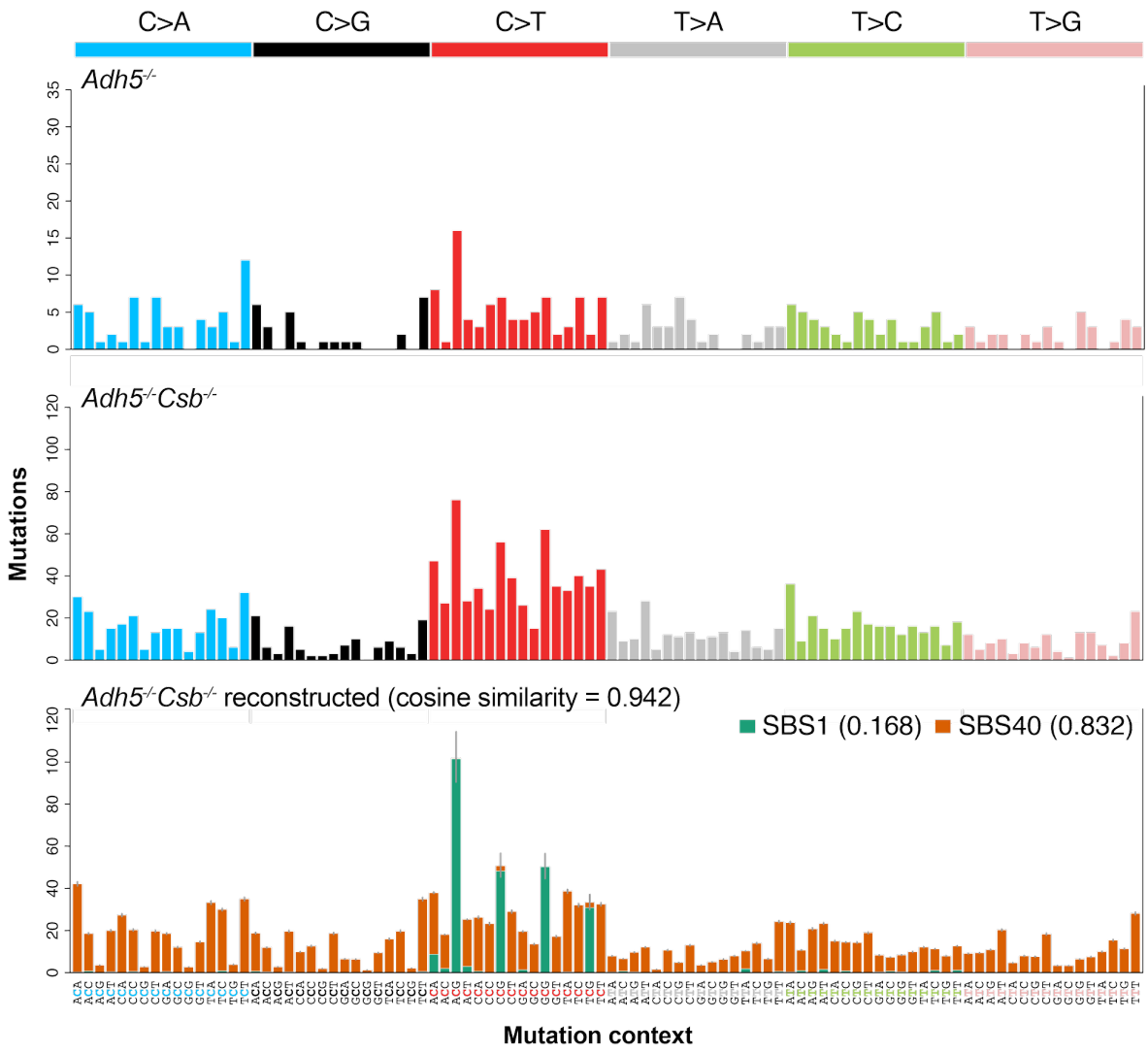

Figure 3.2 The mutation spectrum of *Adh5*$^{-/-}$*Csb*$^{-/-}$ HSPCs
Somatic single base substitution mutations (SBS) in male, 40w old mouse HSPCs detected by clonally expanding the bone marrow and sequencing HSPC colonies compared to a germline brain reference. Mutational landscape of the number of different types of SBS detected (ascribed to the pyrimidine) in *Adh5*$^{-/-}$ or *Adh5*$^{-/-}$*Csb*$^{-/-}$ mouse colonies and the trinucleotide context at which they occur (X axis). *Adh5*$^{-/-}$ (n = 2) or *Adh5*$^{-/-}$*Csb*$^{-/-}$ (n = 8). Note the different y-axis scale for the *Adh5*$^{-/-}$ and *Adh5*$^{-/-}$*Csb*$^{-/-}$ spectra.

Examining the overall numbers of SBS mutations revealed a difference in the burden of mutations between mouse genotypes (Fig. 3.3A). *Csb*$^{-/-}$ and *Adh5*$^{-/-}$ HSPCs had ~140 mutations per genome, whilst WT and *Adh5*$^{-/-}$*Csb*$^{-/-}$ mice had 99 and 120 SBS mutations per genome respectively. Separating these mutations by type of transversion revealed that *Csb*$^{-/-}$ mice had significantly increased numbers of C>T and T>C mutations but reduced level of T>G substitutions compared to WT (Fig. 3.3B). This result suggests that, depending on the context, TCR can protect against potentially mutagenic damage, or it can itself be a source of mutations.

The mutagenic activity of TCR became more apparent in the context of high exposure to endogenous formaldehyde. ADH5-deficient HSPCs had increased rates of mutations compared to WT, particularly C>A, C>G, T>A and T>C substitutions (Fig. 3.3B). Though this increase fell shy of statistical significance ($P \sim 0.1$), it suggests that endogenous formaldehyde increases mutational rate in HSPCs. Concomitant deficiency in TCR reduced levels of these mutations, with *Adh5*$^{-/-}$*Csb*$^{-/-}$ HSPCs showing a modest, but significant, reduction in C>A, C>G and T>C substitutions compared to *Adh5*$^{-/-}$ (Fig. 3.3B). This suggests that mutagenic TCR is responsible for the increased mutational burden induced by endogenous formaldehyde.

The notion that TCR is involved in active repair of formaldehyde damage was further evidenced by the shift in transcriptional strand bias that occurred in *Adh5*$^{-/-}$*Csb*$^{-/-}$ HSPCs compared to *Adh5*$^{-/-}$. In *Adh5*$^{-/-}$ HSPCs, mutations were evenly distributed between the transcribed and untranscribed strands (Fig. 3.3C). However, in *Adh5*$^{-/-}$*Csb*$^{-/-}$ HSPCs, mutations at A:T base pairs were significantly more likely to occur when the thymine was on the transcribed strand (Fig. 3.3C). The PCR amplification in the sequencing preparation masks which base the actual mutation occurred on (i.e., whether CSB-deficiency causes more mutations on the transcribed thymine, or less mutations on the untranscribed adenine). However, the fact that lacking CSB shifts the transcriptional strand bias shows that TCR is active and exerts an effect on mutagenesis in ADH5-deficient HSPCs.

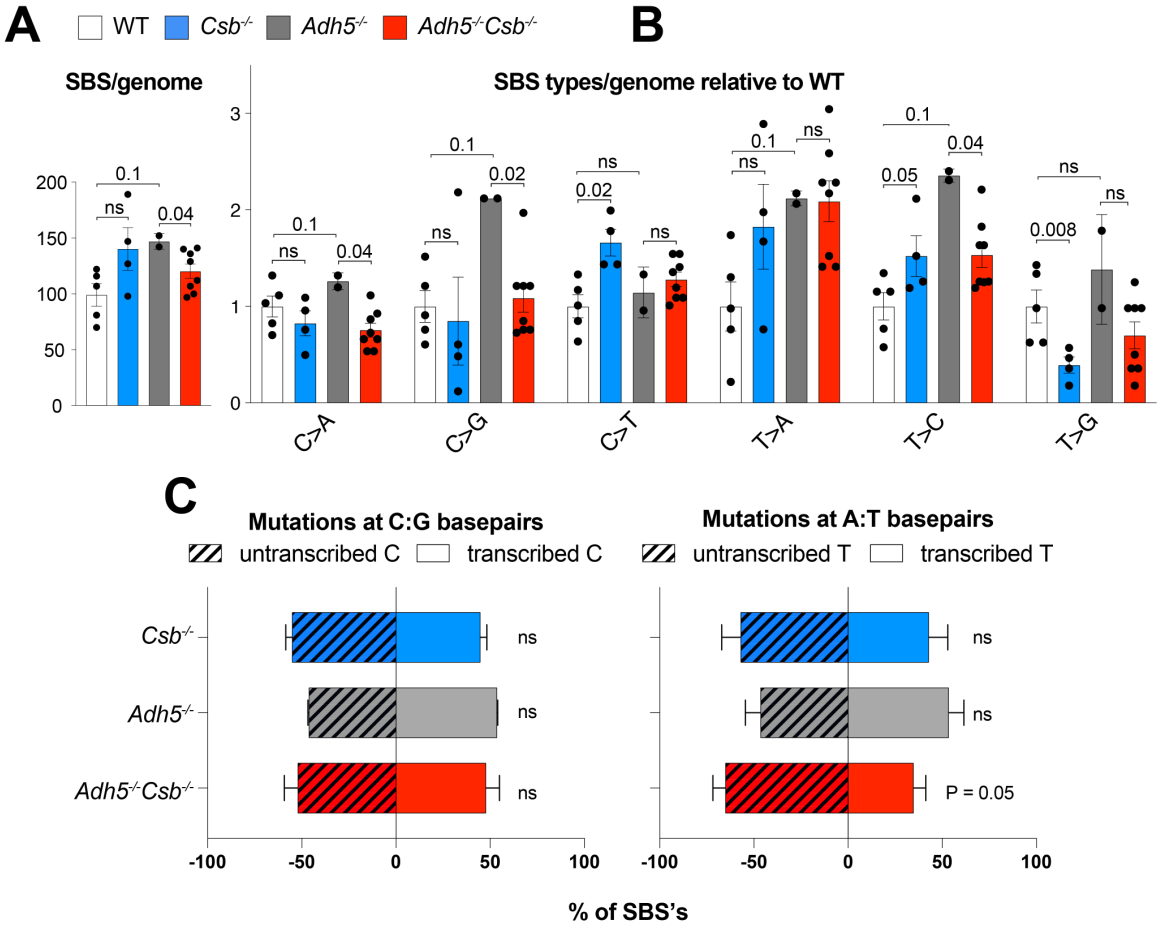

Figure 3.3 CSB deficiency alters the mutational landscape of mouse HSPCs

Somatic single base substitution mutations (SBS) in male, 40w old mouse HSPCs detected by clonally expanding the bone marrow and sequencing HSPC colonies compared to a germline brain reference **A)** Average number of SBS mutations per genome **B)** Average number SBS's per genome normalised to WT segregated into each type of substitution. **C)** Average percentage of SBS mutations at C:G or A:T base pairs which occur when the pyrimidine is on the untranscribed vs transcribed strand. For all figures, error bars indicate standard error of the mean. P value calculated via Mann-Whitney U (B, C), or paired T test comparing percentage of mutations with pyrimidine on transcribed vs untranscribed strand (D). ns = P value > 0.1. Each dot denotes data obtained from one colony. WT (n = 5), *Csb*$^{-/-}$ (n = 4), *Adh5*$^{-/-}$ (n = 2) or *Adh5*$^{-/-}$*Csb*$^{-/-}$ (n = 8).

3.2 Discussion

My data has shown that TCR contributes to the mutational landscape of mouse HSPCs, indicating that this repair pathway is active and can drive the mutational process in those cells.

Profiling of somatic mutations in *Csb*$^{-/-}$ vs WT HSPCs indicated that TCR suppresses C>T and T>C substitutions but promotes T>G mutations (Fig. 3.3B). This suggests that in some contexts, TCR can be mutagenic. This mutagenic effect of TCR becomes even more apparent in mice with a high formaldehyde burden (Fig. 3.3B), with TCR activity in ADH5-deficient mice significantly increasing the levels of C>A, C>G and T>C mutations. The notion that TCR can be mutagenic is supported by several published reports. Work in bacteria and yeast has shown that inactivation of TCR reduces the level of mutations induced by oxidative or UV damage (Carvajal-Garcia et al., n.d.; Kozmin & Jinks-Robertson, 2013). This mutagenic effect was recently modelled in mammalian cells by Anderson et al., (2024), who sequenced DEN-induced mouse liver tumours, and analyzed the strand bias and segregation of mutations through the lineage of daughter cells. This analysis led them to propose the NER translesion resynthesis-induced mutagenesis (TRIM) model, wherein lesions on opposite strands of a transcribed region induce mutagenesis during TCR. In this model, TCR repairs a transcribed strand lesion by excising it, then filling in the gap by replicating across the other lesion on the opposing strand using translesion synthesis. This error prone resynthesis would induce mutation on the new segment of the transcribed strand. In the next cell division, the remaining lesion on the untranscribed strand would be replicated using translesion synthesis, inducing the same mutation on the new transcribed strand. This would lead to two daughter cells inheriting the same mutation (Fig. 3.4). Deep sequencing by Anderson and colleagues revealed that such inherited pattern of mutations can indeed be detected. My work is in line with this model, and directly shows that TCR can be mutagenic in non-transformed mammalian cells.

My work also indicates that this mutagenic TCR occurs in response to endogenous formaldehyde damage. HSPCs lacking formaldehyde detoxification (via ADH5-deficiency) had elevated

mutation levels compared to WT, confirming that formaldehyde is a potent mutagen in these cells (Fig. 3.3A-B). Concomitant loss of TCR (via CSB deficiency) significantly reduced these mutations. This suggests that endogenous formaldehyde induces DNA damage in HSPCs that necessitates mutagenic TCR for repair – perhaps through the proposed NER-TRIM (Anderson et al., 2024). This NER-TRIM may occur due to increased propensity for formaldehyde to form lesions in transcribed regions. Formaldehyde reacts with nucleotides to form hydroxy-methyl-adducts which can persist on DNA and serve as precursors of DNA-DNA or DNA-protein crosslinks (unpublished data). During transcription, unwinding of dsDNA within the RNAPII complex may increase the propensity for DPC formation with transcriptome proteins, or crosslink formation between proximal ssDNA regions, thus increasing the load of formaldehyde-DNA lesions specifically in active gene bodies. If these lesions occurred in proximity on opposing strands, this could potentially induce NER-TRIM (Fig. 3.4). Alternatively, opposing formaldehyde lesions may form with equal likelihood in active gene bodies vs non-coding regions, but are only detected and repaired by NER-TRIM in transcribed regions, owing to the transcription-coupled nature of this repair.

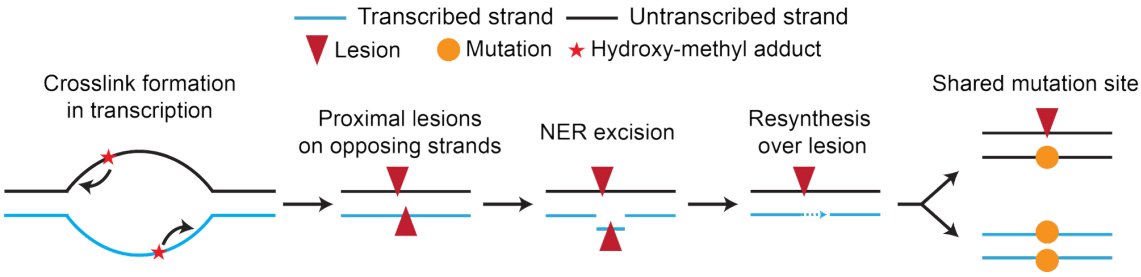

Figure 3.4 Model: Formaldehyde induces mutations via mutagenic TCR

Hypothesis for how formaldehyde induces mutations in HSPCs. Formaldehyde forms hydroxy-methyl adducts in DNA which can form crosslinks with nearby amines. Proximity of protein or DNA amines during transcription may increase the likelihood of multiple formaldehyde-induced DNA lesions in a transcribed region. Opposing lesions on both strands would induce NER-TRIM, wherein TC-NER excises the lesion on the transcribed strand and uses the damaged un-transcribed strand as a template for gap filling. This necessitates translesion synthesis to bypass the remaining lesion, which induces a mutation in the repaired transcribed strand. The remaining lesion on the untranscribed strand generates the same mutation on the new transcribed strand during the next round of replication.

Regardless, my work shows that transcription-coupled repair is active in HSPCs, both in the steady state, and in response to endogenous formaldehyde damage. The next question to address is whether this active repair is biologically important to preserve cell fidelity. Counterintuitively, transcription-coupled repair of formaldehyde damage seems to induce mutations in HSPCs. However, this mutagenic repair may be the 'greater of two evils' required to avoid more toxic ramifications of unrepaired lesions, such as persistent transcription or replication stalling. Determining the biological effect of TCR deficiency on formaldehyde-damaged HSPCs requires further study of the phenotype of *Adh5*$^{-/-}$*Csb*$^{-/-}$ haematopoietic cells, which I pursue in Chapter 4.

3.3 Limitations

It is worth noting that the method of bone marrow clonal expansion used here enriches for both haematopoietic stem cell (HSC) and haematopoietic progenitor cell colonies which are then sequenced for mutation discovery. Thus, we cannot conclude that TCR activity is specific to quiescent HSCs, as the observed mutations may have accrued during DNA repair in proliferative progenitors. Specifically showing the impact of TCR deficiency on quiescent HSCs requires isolation of this distinct population, for instance through immunophenotyping and single cell sorting – a technique which is employed in Chapter 4. This single cell sorting could be employed in future to examine somatic mutations in specifically TCR-deficient HSCs using ultra-deep sequencing as per the method developed by Lee Six et al. (2018).

Additionally, this work would benefit from increased statistical power. Though the reduction in mutation rates in *Adh5*$^{-/-}$*Csb*$^{-/-}$ vs *Adh5*$^{-/-}$ HSPCs is statistically significant (P value < 0.05), the increased mutational rate in *Adh5*$^{-/-}$ vs WT HSPCs is not (P value ~ 0.1). This is likely owing to 1) the low number of replicates, particularly for *Adh5*$^{-/-}$ colonies (2 *Adh5*$^{-/-}$ colonies sequenced vs 8 for *Adh5*$^{-/-}$*Csb*$^{-/-}$ mice) and 2) the limited effect size. To be certain of the conclusions made, additional *Adh5*$^{-/-}$ colonies should be sequenced to gain more statistical power – this work is in progress. The effect size could be enhanced by increasing the burden of mutations through greater exposure to formaldehyde. For instance, examining TCR deficiency in *Aldh2*$^{-/-}$*Adh5*$^{-/-}$ HSPCs,

which have >2-times more SBS mutations than *Adh5*$^{-/-}$ mice (Dingler et al., 2020), would be one way to address this. Indeed, it would be interesting to examine whether the transcription-strand-biased T>A and T>G mutations which occur in *Aldh2*$^{-/-}$*Adh5*$^{-/-}$ HSPCs are lost when TCR is removed.

4 INVESTIGATING THE SOURCE OF ANAEMIA IN *ADH5*$^{-/-}$*CSB*$^{-/-}$ MICE

My observations in Chapter 4 suggest that TCR is active in haematopoietic stem and progenitor cells and promotes mutagenic repair of endogenous formaldehyde damage. However, it is unclear how important this TCR is for preserving haematopoietic cells. A role for TCR in haematopoietic cells has yet to be described, but we have previously observed perturbations in the blood of *Adh5*$^{-/-}$*Csb*$^{-/-}$ mice indicative of a function for this repair pathway (Mulderrig et al., 2021). These mice develop normocytic anaemia with age (Fig. 4.1). We first speculated this was a result of impaired release of the erythropoietin (EPO), a hormone produced in the kidneys which stimulates red blood cell production (Shih et al., 2018). *Adh5*$^{-/-}$*Csb*$^{-/-}$ mice develop kidney failure (indicated by high serum creatinine or urea) which might impact this release (Fig. 4.1). However, serum biochemistry of anaemic *Adh5*$^{-/-}$*Csb*$^{-/-}$ mice shows an increase of EPO (compared to WT) in conjunction with the reduction in red blood cells (Fig. 4.1). This indicates that the anaemia is a result of dysfunction in the haematopoietic process, as opposed to its extrinsic stimulation.

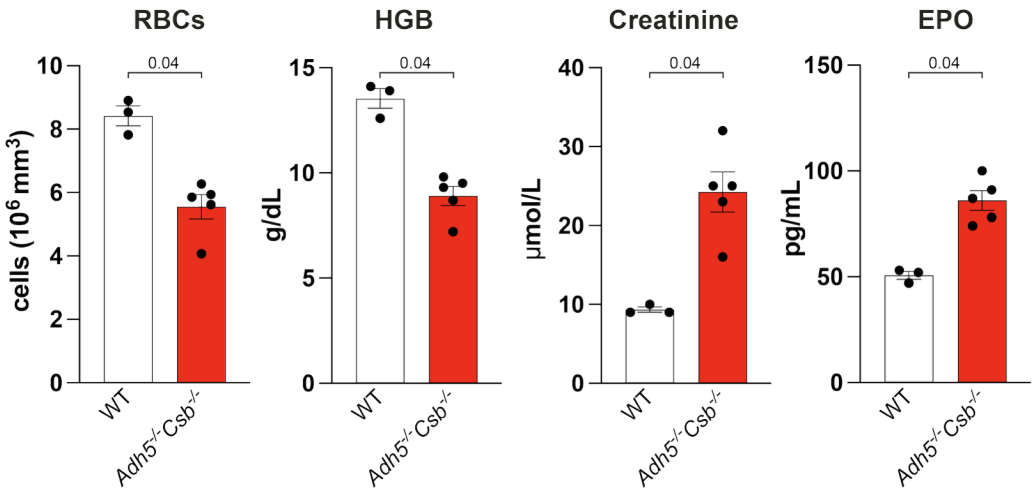

Figure 4.1. Aged *Adh5$^{-/-}$Csb$^{-/-}$* mice are anaemic but produce erythropoietin despite kidney damage.

Red blood cell (RBC), haemoglobin (HGB), creatinine and erythropoietin (EPO) levels in 8-week-old WT and 71-105 week old *Adh5$^{-/-}$Csb$^{-/-}$* mice. Dots denote individual mice (n = 3, 5), columns represent average values. Error bars indicate standard error of the mean. P value calculated by Mann-Whitney U test.

The defects previously observed in *Adh5$^{-/-}$Csb$^{-/-}$* mice impact primarily non-replicative tissues – brain, liver and kidney (Mulderrig et al., 2021). Such tissues are unable to utilise replication-coupled means, such as the Fanconi's anaemia pathway, to repair formaldehyde damage. It is therefore plausible that they would rely more heavily on the non-replicative transcription-coupled repair. The haematopoietic system is highly replicative, with red blood cells and erythroblasts constantly replaced by proliferative progenitors (A. Wilson et al., 2008). However, these progenitors are renewed periodically by HSCs, which reside primarily in quiescence in adults, only exiting dormancy once every 40 weeks in humans (Boyle et al., 2023). Given TCR's importance in other non-replicative tissues, we speculated that the source of the *Adh5$^{-/-}$Csb$^{-/-}$* anaemia may be dysfunction in these quiescent HSCs. I sought to test this through detailed examination of the haematopoietic cells in *Adh5$^{-/-}$Csb$^{-/-}$* mice.

4.1 Creation of an *ex vivo* quiescent system to examine HSC fidelity

I first sought to create an *ex vivo* culture system to examine the dynamics of quiescent HSCs following formaldehyde damage. Work by Wilkinson et al. (2020) has established a robust culture system for the expansion of mouse HSCs at low oxygen concentration (5%), using polyvinyl alcohol (PVA)-containing media and a high concentration of stem cell growth-promoting cytokines – stem cell factor (SCF) and thrombopoietin (TPO). These cytokines act to promote HSC self-renewal and proliferation of functional mouse HSCs (~200-900-fold over 28 days) which can repopulate the bone marrow of lethally irradiated mice – the gold standard test for HSC functionality. In its base form, this system was unsuitable for my purposes, as the HSCs are maintained in constant proliferation, in contrast to the quiescent state in which unperturbed HSCs

reside *in vivo*. However, work from Kobayashi et al., (2020) showed that HSCs can be maintained in quiescence through the inclusion of fatty acids in the media, reduction of oxygen concentration to 1%, and, crucially, the reduction of SCF and TPO concentrations to 1.5-5ng/mL and 0.1-4 ng/mL respectively (>10-100-fold less than the Wilkinson et.al method). Based on these insights, I endeavoured to modify Wilkinson et al's PVA-based culture to a favour quiescence, through lowering cytokine and oxygen concentrations (Fig. 4.2). I chose not to add fatty acids to the media in order keep conditions as close to the proliferative culture as possible and allow comparison between the two with minimal confounding variables.

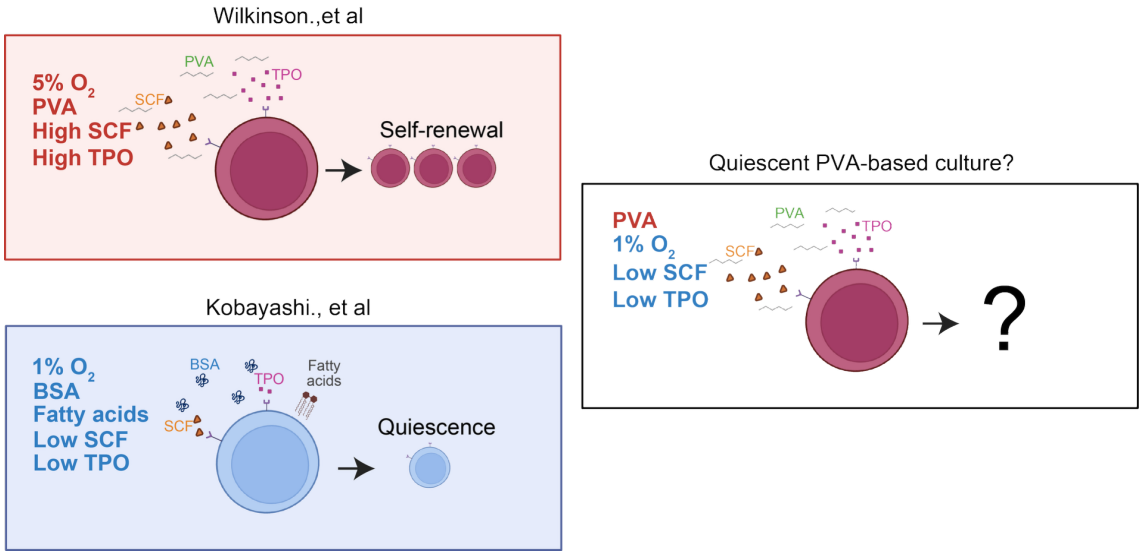

Figure 4.2. Development of a quiescent PVA-based culture.

Summary of the culture conditions described by Wilkinson et al., (2019), red box, proliferating mouse HSC cultures, and by Kobayashi et al., (2020), blue box, maintenance of mouse HSCs in quiescence. White box indicates new culture conditions developed for PVA-based culture of quiescent mouse HSCs. Partially created in BioRender. Russell, H. (2026) https://BioRender.com/x8j92uu

I began by taking immunophenotypic HSCs which had been sorted and cultured for 21 days using Wilkinson et al's method. I moved these HSCs into combinations of high (10 ng/mL SCF, 100 ng/mL TPO) or low (1.5 ng/ml SCF, 1 ng/ml TPO) cytokines and 1% or 5% oxygen concentration. Prior to this, the cultures were incubated with carboxyfluorescein succinimidyl ester (CFSE), a cell-permeable fluorescent dye which binds, and is retained on, intracellular proteins (Lyons & Parish, 1994). Each subsequent cell division halves the amount of CFSE within its progeny,

allowing the number of divisions to be determined by flow cytometric analysis of fluorescence. Fig. 4.3.A-C shows the representative fluorescent traces and respective number of divisions for each culture condition. Cytokine concentration had the largest effect on number of divisions, with 39-49% of $Cyto_{low}$ cells having divided less than 4 times, as opposed to only 3-4% of cells in high cytokine cultures (Fig. 4.3A, C). Lower oxygen concentration also marginally increased the percentage of cells with < 4 divisions (10% difference between 5% oxygen and 1% oxygen) (Fig. 4.3C).

It is unsurprising that lowering the concentration of growth-promoting ligands would reduce growth. However, a reduction in the number of divisions does not delineate quiescence. To truly test this, I performed cell cycle analysis using intracellular staining with a stochiometric DNA-stain, Hoechst, and anti-Ki67 antibodies (Fig. 4.3D). In this well-established method, quiescent cells arrested in G_0 can be identified by the absence of Ki67 (a proliferative marker present in G1/S/G2/M) (Gerdes et al., 1984) and incorporation of the DNA stain consistent with two copies of the genome. The Wilkinson et al. HSC culture is a mixed population comprised mainly of haematopoietic stem and progenitor cells (30-50%), committed progenitors, and some differentiated cells such as megakaryocytes (Wilkinson et al., 2019). To ensure quiescence was occurring in specifically haematopoietic stem cells, I co-stained with antibodies against immunophenotypic HSC markers (Lineage- c-Kit+ Sca1+ CD150+ CD201+) (Rix et al., 2022). Encouragingly, 75-89% of HSCs in the $Cyto_{low}$ cultures resided in G_0, in contrast to only 24-29% of HSCs in high cytokine conditions (Fig. 4.3D). In $Cyto_{low}$ cultures, a 5% oxygen concentration appeared to increase the number of cells in G0, but at the price of lower viability (data not shown). I therefore decided to proceed with low cytokine and 1% oxygen concentration for further validation.

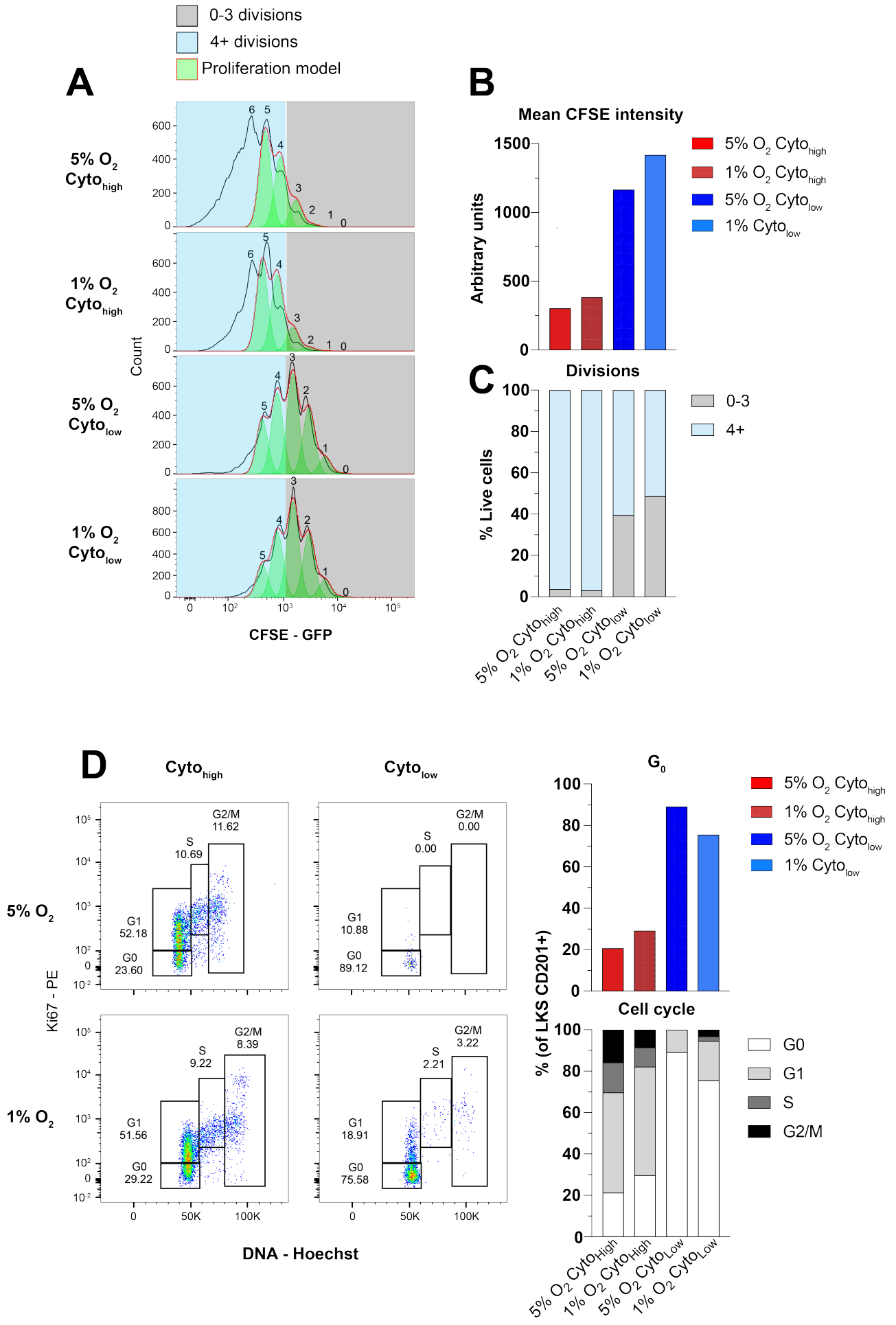
A
0-3 divisions
4+ divisions
Proliferation model
5% O2 Cytohigh
1% O2 Cytohigh
5% O2 Cytolow
1% O2 Cytolow
Count
CFSE - GFP
B
Mean CFSE intensity
Arbitrary units
5% O2 Cytohigh
1% O2 Cytohigh
5% O2 Cytolow
1% Cytolow
C
Divisions
% Live cells
0-3
4+
D
Cytohigh
Cytolow
Ki67 - PE
DNA - Hoechst
G1 52.18
G0 23.60
S 10.69
G2/M 11.62
G1 10.88
G0 89.12
S 0.00
G2/M 0.00
G1 51.56
G0 29.22
S 9.22
G2/M 8.39
G1 18.91
G0 75.58
S 2.21
G2/M 3.22
G0
% (of LKS CD201+)
Cell cycle
G1
S
G2/M

Figure 4.3. Low cytokine concentrations in mouse HSC cultures reduce cell division and increases proportion of cells in G_0.

Flow cytometry analysis of WT mouse HSCs incubated for 20 minutes with CFSE, which is retained on intracellular proteins. CFSE fluorescent halves with each cell division. After CFSE incubation, HSCs were cultured for 6 days in 1% or 5% oxygen tension with low or high TPO and SCF concentrations ($Cyto_{low}$ / $Cyto_{high}$). **A)** Plots of CFSE fluorescence in whole cultures (gated on single, live cells). Green indicates proliferation model generated by FlowJo used as a guideline for manual gating of divisions (0-6) based on halving of cell CFSE fluorescence per cell division. **B)** Average CFSE fluorescence intensity for each culture (higher intensity indicates less divisions). **C)** Percentage of live cells with 0-3 or >4 divisions based on CFSE intensity. **D)** Cell cycle status of HSCs gated for single cells and for HSC immunophenotypic markers (Lin- c-Kit+ Sca1+ CD150+ CD201+). The G0 population was defined as the diploid population negative for Ki67 expression, gated using an isotopic control (sample with IgG-PE antibody added instead of anti-Ki67-PE).

Quiescence, as opposed to senescence, is defined as "the reversible state of a cell in which it does not divide but retains the ability to re-enter cell proliferation" (Marescal & Cheeseman, 2020). It was important to ensure culture conditions preserved functionality of the HSCs – their ability to exit cell cycle arrest and produce all downstream blood lineages. To first test this, I sorted single HSCs into high or low cytokine conditions, maintained for seven days. Following this, as an additional validation of cell cycle arrest, I counted the number of wells where division of the single cell had occurred (Fig. 4.4A). During this, dead or apoptotic cells could also be recognised by eye by undefined, faded, or blebbed cell membranes. In support of my flow cytometric findings, over 60% of single HSCs sorted into low cytokine/oxygen culture remained undivided. Conversely, all the $Cyto_{high}$, 5% O_2 single cells had divided or died (Fig. 4.4B). Next, I tested the ability of the cells to exit cell cycle arrest by moving them back into high cytokine/oxygen concentrations for 15 days and performing flow cytometric analysis. In this period, 40% of formerly quiescent single cells divided to produce live progeny (>5 propidium iodide negative cells) (Fig. 4.4C). This proportion likely reflects the generally low survival rate of single cells in culture rather than toxicity of the quiescent culture specifically. Indeed, only 47% of the single cells sorted and cultured continuously in high cytokine/oxygen retained >5 live cells per well (Fig. 4.4C).

Within each well, the proportions of different haematopoietic cells could be determined using flow cytometry for established immunophenotypic markers. Cells negative for differentiated

lineage markers (CD4, CD8, CD127, CD45R, Ly6G, TER119) indicate the stem, multipotent progenitor and committed progenitor populations. Within this population, HSCs and multipotent progenitors can be identified by c-Kit and Sca1 expression, with HSCs also expressing CD201 and CD150. It was important to assess these proportions to determine if culture conditions maintain HSC self-renewal or bias towards differentiation into progenitors. I found the proportions of lineage negative and LKS cells were similar between expanding and quiescent cultures (Fig. 3.4D). Interestingly, the proportion of phenotypic HSCs (LKS CD150+ CD201+) was on average 10-fold higher for wells that had initially been in quiescent culture vs those continuously in high cytokine/oxygen conditions. This suggests that the quiescent state may favour the survival of self-renewing HSCs, whilst constant proliferation might bias HSCs towards asymmetric division or differentiation.

My data thus far has shown that sorting mouse HSCs into PVA-based culture with low SCF, TPO and oxygen concentration favours reversible cell cycle arrest. When moved back into high cytokine/oxygen conditions, these HSCs were capable of self-renewal and differentiation into early progenitors. However, their ability to produce all blood lineages including committed progenitors and mature cells was not yet clear. The gold standard measurement for this, and for HSC functionality, is the competitive repopulation assay (Szilvassy et al., 1990). In this assay, donor cells are transplanted into bone marrow-ablated mice along with competitor bone marrow from another mouse. The two populations compete to repopulate the haematopoietic compartment of the recipient mouse. Monthly blood samples are collected from recipient mice over 4 months, and the proportion of blood produced from donor vs competitor can be measured to give an indication of the capability and competitivity of the donor cells. To perform this assay, I sorted HSCs from CD45.1-expressing mice and maintained them in quiescent culture for 7 days before transplanting into lethally irradiated, CD45.2-expressing recipients alongside whole bone marrow from CD45.1/2-expressing competitor mice. Freshly harvested HSCs were transplanted in the same manner for comparison (Fig. 4.4E). Fig. 4.4F-G shows that HSCs cultured in quiescence are capable of long term, multi-lineage haematopoietic reconstitution. Though non-significant,

repopulation capacity of quiescently cultured HSCs was slightly lower compared to freshly sorted HSCs. This could be a result of delayed exit from quiescence, or a slight toxicity of culture conditions providing a disadvantage to cultured vs fresh cells. Nonetheless, this data provides confidence that the quiescent culture method preserves HSC functionality.

To conclude, by adapting Wilkinson et al's PVA-based culture method, I created an *ex vivo* system to maintain functional HSCs in reversible quiescence which I could then use to directly examine the effects of formaldehyde on quiescent HSCs.

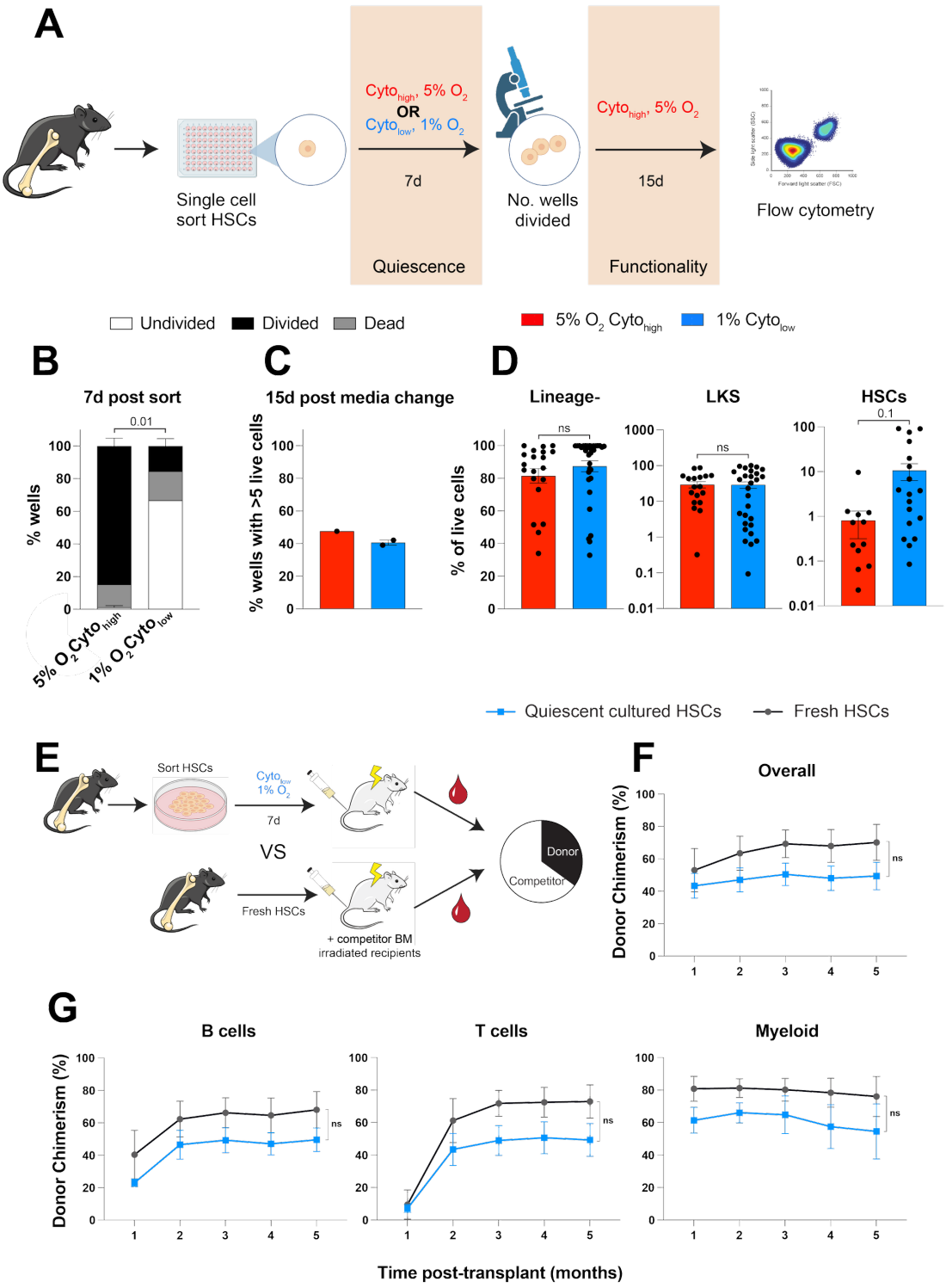

Figure 4.4. Mouse HSC cultures maintained in quiescence retain the ability to re-enter cell cycle and repopulate downstream lineages.

Schematic of methodology for testing quiescence and functionality of single-cell-sorted mouse HSCs. **B)** Average percentage of wells with sorted single cells which had divided, died or not divided after 7 days in high cytokine/oxygen or low cytokine/oxygen culture. Biological replicates (number of mice from which 50 single cells were sorted) = 2. P value from Welch's t-test of percentage undivided. **C-D)** Flow cytometric analysis of HSC cultures 15 days after being moved into high cytokine/oxygen culture gated on live, single cells and immunophenotypic

markers. **C)** Average percentage of wells with >5 live cells after moving to high cytokine/oxygen culture. 50 HSCs per mouse were single-cell sorted into individual wells. Each dot indicates the percentage of the 50 wells containing >5 live cells at the end of the experiment, derived from a single mouse. **D)** Immunophenotyping of each well. Dots indicate individual wells. LKS = Lineage- c-Kit+ Sca1+, HSCs = Lin- c-Kit+ Sca1+ CD150+ CD201+. Error bars denote standard error of the mean. P values from unpaired T-test. Ns = P > 0.1. **E)** Schematic of competitive transplantation experiment to test functionality of mouse HSCs cultured in quiescence compared to freshly sorted HSCs. **F, G)** Percentage of donor-derived cells in the peripheral blood of lethally irradiated recipients which received 200 cultured HSCs (N = 5) or 200 freshly sorted HSCs (N = 4), alongside 1 million whole bone marrow cells from competitor. Chimerism was quantified by flow cytometry of peripheral blood using antibodies against immunophenotypic markers of B cells, T cells and myeloid cells, and CD45 variants expressed by donor (CD45.1), recipient (CD45.2) or competitor (CD45.1 and CD45.2) mouse. Error bars indicate standard error of the mean. P value calculated by two-way ANOVA. ns = P > 0.1. Figures A, E partially created in BioRender. Russell, H. (2026) https://BioRender.com/x8j92uu

4.2 TCR deficiency does not increase HSC sensitivity to formaldehyde *ex vivo*

Using my quiescent culture system, I set out to examine the effect of formaldehyde and lack of transcription-coupled repair on mouse HSCs. The ability to tune cells in this culture to either quiescence or proliferation using growth factors provided insight on the importance of transcription-coupled repair of formaldehyde in quiescence vs proliferation. I sorted 50 HSCs per well from *Adh5*$^{-/-}$ or *Adh5*$^{-/-}$*Csb*$^{-/-}$ mice into quiescent or expanding culture. 24 hours after sorting, I counted the cells by eye to gain a pre-treatment baseline, then treated the cells for 48 hours with 0-120μM of formaldehyde and recounted, excluding visibly dead cells (Fig. 4.5A). Strikingly, proliferating HSCs were far more sensitive to formaldehyde than those in quiescent culture (Fig. 3.5D), though additional biological repeats for the proliferating culture are required to fully validate this (HSCs from 1 mouse per genotype harvested for proliferating culture). Nonetheless, the reduced sensitivity of the quiescent culture is consistent with the concept of quiescence as a DNA damage-resistant state (Alekseenko et al., 2018; Becker et al., 2024). Cells entering cell cycle continuously are more likely to both expose unwound DNA to damaging agents, such as formaldehyde, as well as encounter DNA damage lesions during replication which leads to cell cycle arrest and/or death. Despite this, non-replicating cells might still encounter DNA lesions during transcription, and the importance of repair of such lesions in HSCs is unknown. I found

that *Adh5*$^{-/-}$*Csb*$^{-/-}$ HSCs lacking TCR had similar sensitivity to *Adh5*$^{-/-}$ HSCs in both expansion and quiescence, suggesting a limited role for the repair pathway in this context (Fig. 5.3D).

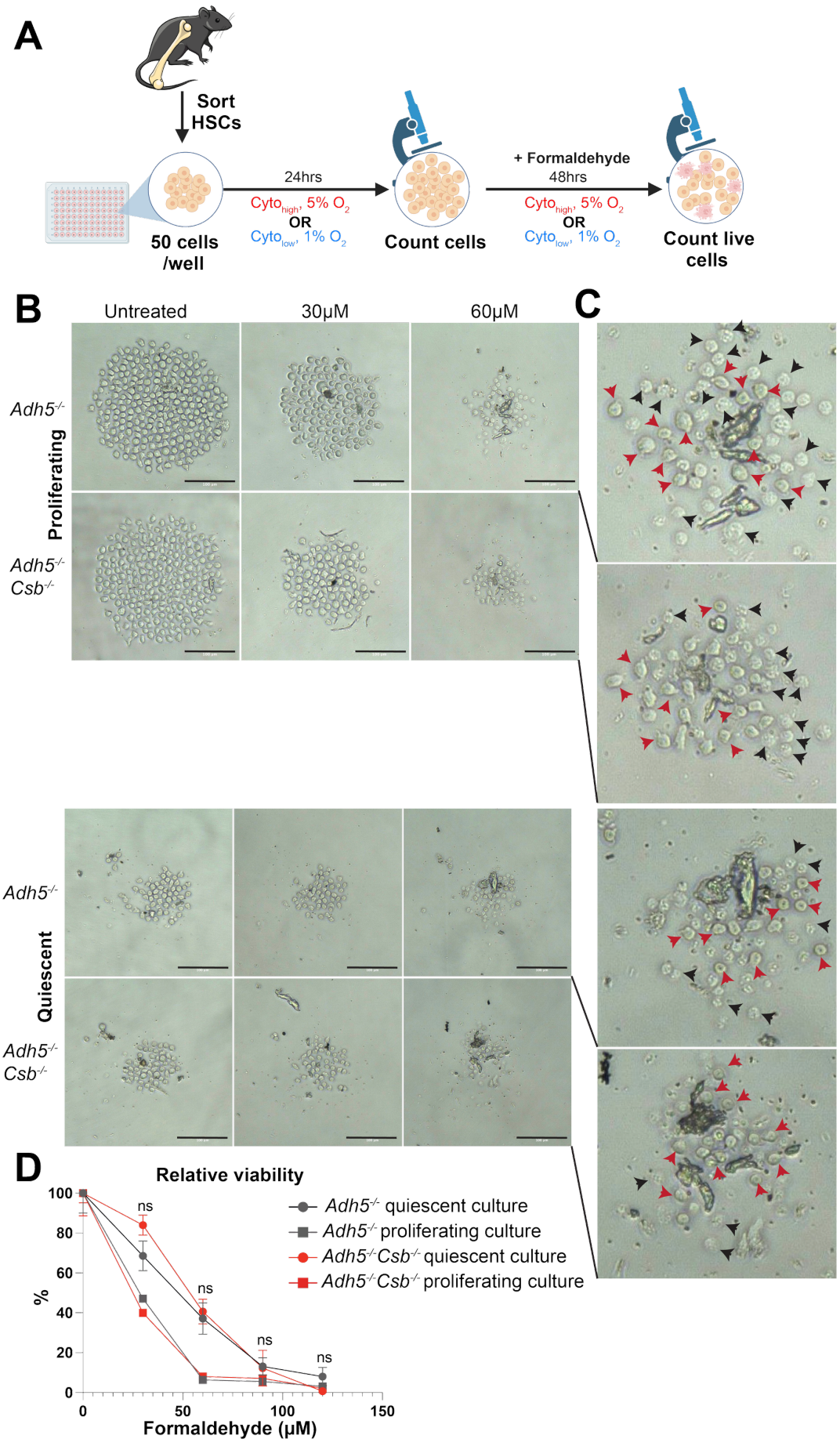
A
Sort HSCs
50 cells /well
24hrs
Cyto high, 5% O2
OR
Cyto low, 1% O2
Count cells
+ Formaldehyde
48hrs
Cyto high, 5% O2
OR
Cyto low, 1% O2
Count live cells
B
Untreated
30μM
60μM
Adh5-/-
Proliferating
Adh5-/- Csb-/-
C
Adh5-/-
Quiescent
Adh5-/- Csb-/-
D
Relative viability
Adh5-/- quiescent culture
Adh5-/- proliferating culture
Adh5-/-Csb-/- quiescent culture
Adh5-/-Csb-/- proliferating culture
%
ns
Formaldehyde (μM)

Figure 4.5 CSB-deficiency does not increase *Adh5*$^{-/-}$ mouse HSC sensitivity to formaldehyde in quiescence or proliferation.

A) Overview of the formaldehyde sensitivity assay in mouse HSCs maintained under quiescent or proliferative conditions. Created in BioRender. Russell, H. (2026) https://BioRender.com/x8j92uu **B)** Example images of HSC cultures (from 8–12-week-old female mice) 48 hours after formaldehyde treatment. Scale bar, 100 μm. **C)** Zoomed images of cultures treated with 60 μM formaldehyde. Arrows indicate examples of cells counted as live (red) or excluded as dead (black). **D)** Mean normalised growth of HSC cultures after formaldehyde treatment. Growth calculated as change in cell number per well compared to pre-treatment, then normalised as % of the growth of untreated wells. Error bars indicate standard error of the mean. P value calculated by Mann-Whitney U test comparing *Adh5*$^{-/-}$ and *Adh5*$^{-/-}$*Csb*$^{-/-}$ for each culture condition and formaldehyde concentration. ns = P value > 0.1. N = 3 mice (quiescent cultures) or 1 mouse (proliferating cultures).

My *ex vivo* sensitivity assay in *Adh5*$^{-/-}$*Csb*$^{-/-}$ HSCs suggest TCR plays a limited role in protecting quiescent HSCs from damage. However, the true sensitivity of the quiescent HSCs to formaldehyde may not have been revealed in this assay, as cells remained in quiescence throughout. Unrepaired formaldehyde lesions could have accrued in the *Adh5*$^{-/-}$*Csb*$^{-/-}$ HSCs, but the ramifications of such lesions may not be seen until the cell cycle is re-entered and replication stalled. Additionally, it is unclear from this assay whether the cells counted by eye: A) remain HSCs and B) are actually viable. Immunophenotyping of these cells for HSC markers, as well as live/dead stains would be a better way to determine HSC presence and viability. To truly test the HSCs, they must be put in a system which demands their activation and proliferation, allowing the consequences of accumulated DNA damage to manifest, and be measured. It is for this reason that I chose to pursue this research in a more dynamic and applicable system – that of the mouse itself.

4.3 Methanol-treated *Adh5*$^{-/-}$*Csb*$^{-/-}$ mice have functional HSCs

We know that *Adh5*$^{-/-}$*Csb*$^{-/-}$ mice develop anaemia (Fig. 4.1), but upstream analysis of the blood progenitors has never been done to identify its source. I hypothesised that it originates from the HSCs, which may rely more heavily on transcription-coupled repair owing to their quiescent state. Damage to the HSCs could manifest in a deficiency in their numbers, or in the number of progenitor cells they can produce. To assess this, I performed comprehensive flow cytometric

analysis of all the blood lineages using established staining and gating strategies to detect haematopoietic populations (Fig. 4.6A, C) (Akashi et al., 2000; Kondo et al., 1997; Mayle et al., 2013; L. Yang et al., 2005). I first performed this in mice which had been injected for 6 weeks with methanol – a precursor to formaldehyde which is converted in the body (Pocker & Li, 1991). The aim of this was to increase the level of formaldehyde damage, exacerbating and expediting any blood phenotype. However, these mice showed no reduction in HSCs (short term ST-HSCs or long-term LT-HSCs), multipotent progenitors (MPPs), common lymphoid progenitors (CLPs), megakaryocyte erythroid progenitors (MEPs), common myeloid progenitors (CMPs) or granulocyte macrophage progenitors (GMPs) compared to their controls (Fig. 4.6A-C).

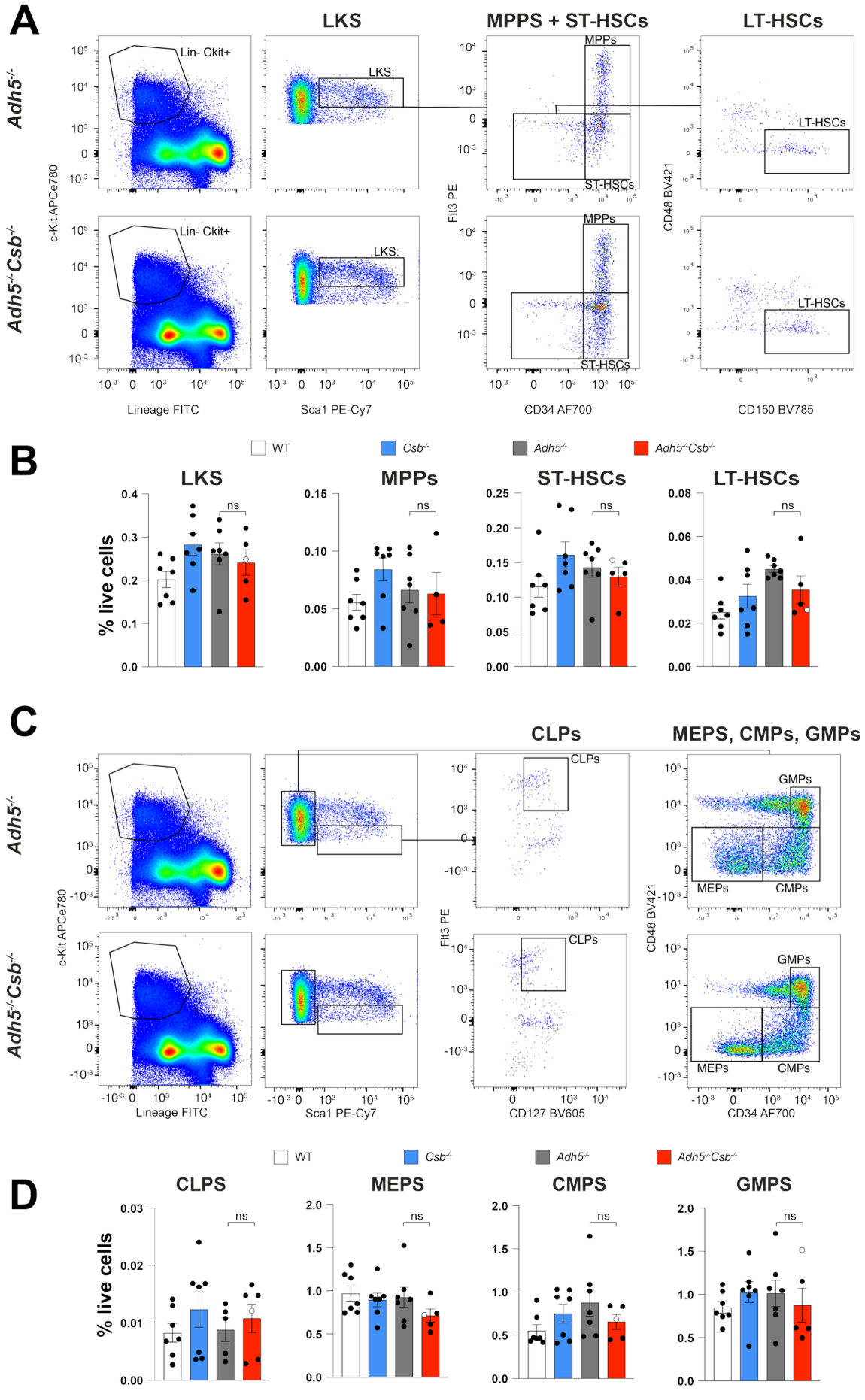
A
LKS
MPPS + ST-HSCs
LT-HSCs
Adh5-/-
Adh5-/-Csb-/-
Lin- Ckit+
LKS:
MPPs
ST-HSCs
LT-HSCs
c-Kit APCe780
Flt3 PE
CD48 BV421
Lineage FITC
Sca1 PE-Cy7
CD34 AF700
CD150 BV785
B
WT
Csb-/-
Adh5-/-
Adh5-/-Csb-/-
LKS
MPPs
ST-HSCs
LT-HSCs
% live cells
ns
C
CLPs
MEPS, CMPs, GMPs
CLPs
GMPs
MEPs
CMPs
CD127 BV605
D
CLPS
MEPS
CMPS
GMPS

Figure 4.6. Methanol-treated *Adh5$^{-/-}$Csb$^{-/-}$* mice do not have reduced HSCs or blood progenitors.

Flow cytometry of bone marrow HSCs and progenitors from 14-18-week-old female mice after intraperitoneal injection with 1.5 g/kg methanol, weekly, for 6 weeks. (A,C) Example flow cytometry plots and gating strategies for haematopoietic populations. Populations were gated after exclusion of cell debris and doublets/triplets by side and forward scatter and exclusion of dead cells by 7-AAD fluorescence (not included in figure). Following this, progenitor cells were selected as c-Kit+ and negative for lineage markers (CD4, CD8a, CD127, CD45R, Ly6G and TER119) (left-most plot for A, C). For A), LKS cells were identified as c-Kit^{high}Sca1+ and within this population ST-HSCs were further defined as CD34+Flt3-, and MPPS as CD34+Flt3+. LT-HSCs were gated within the CD34-Flt3- population as CD150+CD48-. For C), CLPs were gated within the progenitor population as c-Kit^{low}Sca1+ and further defined as CD127+Flt3+. Committed progenitors were defined within the progenitor population as c-Kit^{high}Sca1-, and further differentiated based on CD34 and CD48 expression (MEP = CD34-CD48-, CMPs = CD34+CD48-, GMPs = CD34+CD48+). (B, D) Average proportions of haematopoietic populations per mouse by genotype. Data is represented as the percentage of each cell-type within the overall population of live, single cells. At least 500,000 events were sampled per mouse. Error bars indicate standard error of the mean. P value calculated by Mann-Whitney U test, ns = P > 0.1. Each dot indicates one mouse. White dot indicates mouse which only received 4.4 weeks of treatment due to methanol toxicity. For WT, *Csb$^{-/-}$* and *Adh5$^{-/-}$*, n = 7. For *Adh5$^{-/-}$Csb$^{-/-}$*, n = 5 (except MPPs, where n = 4).

Despite their proportions being unchanged, the *Adh5$^{-/-}$Csb$^{-/-}$* HSCs could still have been functionally compromised. Like in my ex vivo experiments, damage to the HSCs may have accrued, but not had the chance to manifest. The best way to unveil a functional defect in HSCs is by forcing them to rapidly expand and repopulate the entire haematopoietic system. Thus, I extracted bone marrow from the methanol-treated mice and transplanted it into lethally irradiated recipients alongside competitor bone marrow (Fig. 4.7A). Fig. 4.7C shows that bone marrow from methanol-treated *Adh5$^{-/-}$Csb$^{-/-}$* mice was equally competent in repopulating recipient haematopoiesis compared to *Adh5$^{-/-}$* controls. Repopulation of all lineages persisted up to four months, wherein reconstitution is solely driven by long-term HSCs as opposed to short-lived progenitors. Bone marrow from methanol-treated ADH5 deficient mice (*Adh5$^{-/-}$* and *Adh5$^{-/-}$Csb$^{-/-}$*) did have a non-significantly lower repopulation capacity compared to methanol-treated WT and *Csb$^{-/-}$* bone marrow, suggesting that formaldehyde damage does functionally compromise HSCs, but lack of TCR did not exacerbate this (Fig. 4.7C). I therefore concluded that transcription coupled repair is not essential to protect HSCs from formaldehyde damage.

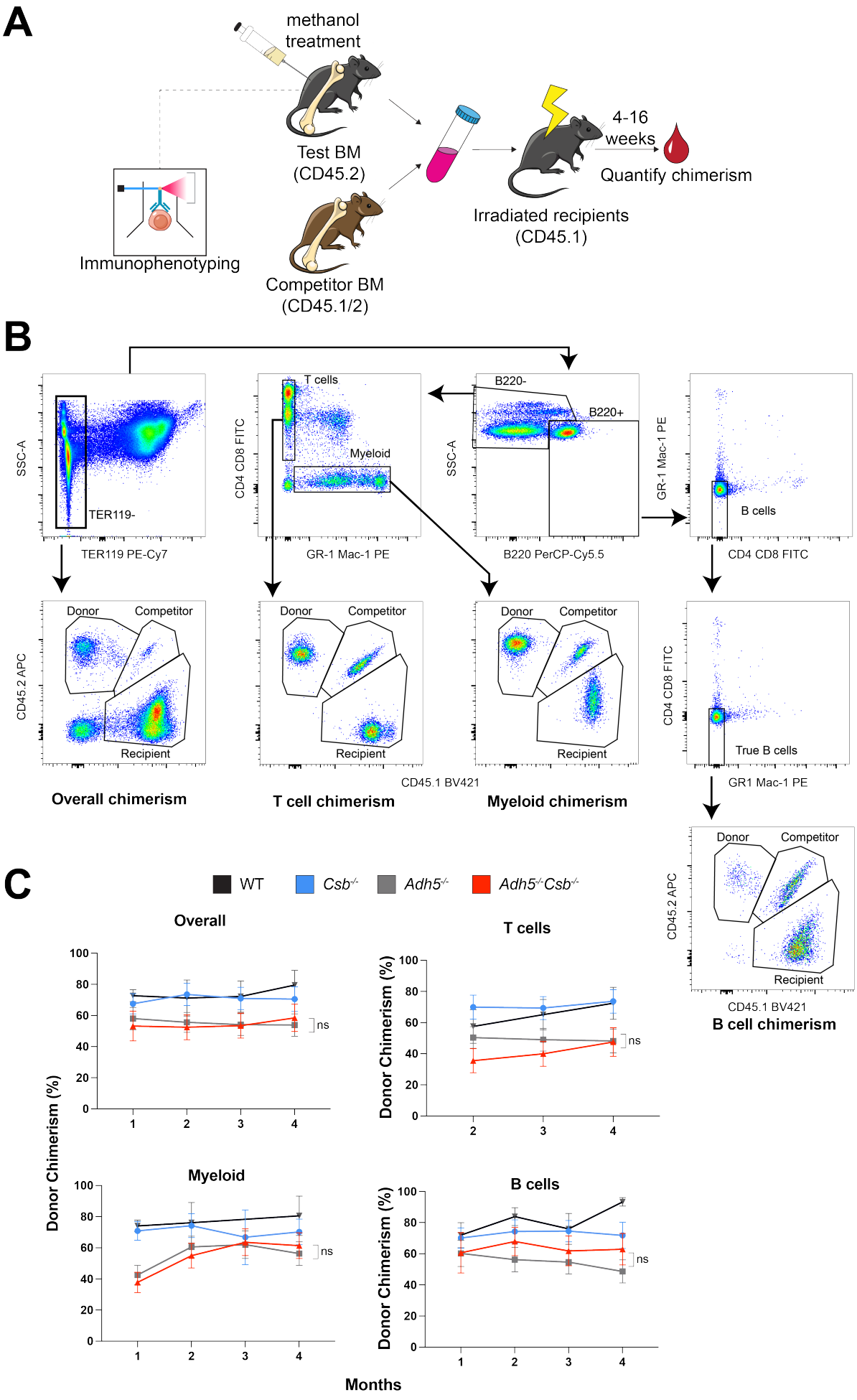
A
methanol treatment
Test BM (CD45.2)
Competitor BM (CD45.1/2)
Immunophenotyping
Irradiated recipients (CD45.1)
4-16 weeks
Quantify chimerism
B
SSC-A
TER119-
TER119 PE-Cy7
CD4 CD8 FITC
T cells
Myeloid
GR-1 Mac-1 PE
B220-
B220+
B220 PerCP-Cy5.5
GR-1 Mac-1 PE
B cells
CD4 CD8 FITC
CD45.2 APC
Donor
Competitor
Recipient
Overall chimerism
T cell chimerism
Myeloid chimerism
CD45.1 BV421
True B cells
GR1 Mac-1 PE
B cell chimerism
C
WT
Csb-/-
Adh5-/-
Adh5-/-Csb-/-
Overall
T cells
Myeloid
B cells
Donor Chimerism (%)
ns
Months

Figure 4.7. Methanol-treated *Adh5$^{-/-}$Csb$^{-/-}$* mice do not have compromised HSC function compared to *Adh5$^{-/-}$*.

A) Schematic of methodology of methanol exposure and competitive transplantation. Female mice were given intraperitoneal injections of 1.5 g/kg methanol weekly for 6 weeks before bone marrow (BM) was extracted and either immunophenotyped with flow cytometry or transplanted (200,000 cells) into lethally irradiated mice alongside equal amounts of competitor bone marrow. Peripheral blood chimerism was quantified every 4 weeks by flow cytometry. **B)** Flow cytometry gating strategy for analysis of donor chimerism in peripheral blood of mice transplanted with 1 million bone marrow cells from methanol treated, female, 14-18-week-old mice. Cells were first gated for single cells via forward and side scatter and dead cells excluded by 7-AAD fluorescence. **C)** Average percentage of live, donor-derived cells per recipient mouse. Error bars indicate standard error of the mean. P value calculated by mixed effects analysis. ns = P > 0.1. Donor mice were WT (n = 1), *Csb$^{-/-}$* (n = 4), *Adh5$^{-/-}$* (n = 5) or *Adh5$^{-/-}$Csb$^{-/-}$* (n = 3). Numbers of recipient mice which received WT, *Csb$^{-/-}$*, *Adh5$^{-/-}$* or *Adh5$^{-/-}$Csb$^{-/-}$* bone marrow were 5, 5, 15 and 10, respectively.

4.4 Aged *Adh5$^{-/-}$Csb$^{-/-}$* mice have normal HSC proportions despite anaemia

Adh5$^{-/-}$Csb$^{-/-}$ HSCs are not functionally compromised (Fig. 4.7C). This prompts the question of where the anaemia that occurs in the aged mice of this genotype originates (Fig. 4.1A). These mice develop normocytic and normochromic anaemia (reduced haemoglobin and red blood cell counts, with these cells retaining normal size and colour) (Mulderrig et al., 2021). To examine this, I returned to this aged model to identify at which point in the haematopoietic tree attrition begins. In agreement with my findings in the methanol-treated mice, 40-week-old *Adh5$^{-/-}$Csb$^{-/-}$* males showed no reduction in proportions of HSCs, multipotent progenitors or committed progenitors compared to controls (Fig. 4.8A, B). Despite their anaemia, these mice had wild-type-levels of megakaryocyte-erythroid progenitors (MEPs) (Fig. 4.8B), which supply pro-erythroblasts (Akashi et al., 2000; Debili et al., 1996). Restriction of erythroid cells must therefore occur either at the point of red blood cell enucleation, or during differentiation from pro-erythroblast to reticulocyte. In adult mice, maturation of pro-erythroblasts occurs primarily in the bone marrow but can also occur in the spleen during stress, known as extramedullary haematopoiesis (Chiu et al., 2015; Rivera-Torruco et al., 2024). Flow cytometric gating strategies using antibodies against CD71 and TER119 have been developed to identify the different stages of murine erythroid differentiation in these tissues (Koulnis et al., 2011), defined as ProE, EryA, EryB and EryC with increasing maturity (Fig. 4.8E). Using this strategy, I found that *Adh5$^{-/-}$Csb^{-}*

$^{-/-}$ mice had significantly reduced levels of bone marrow EryA, EryB and EryC cells compared to *Adh5*$^{-/-}$ mice (Fig. 4.8C, E). This reduction was even more substantial in the spleen, occurring at all four stages of differentiation including Pro-Erythroblasts. Together, this suggests that the anaemia in *Adh5*$^{-/-}$*Csb*$^{-/-}$ originates from a defect in the maturation of cells after the pro-erythroblast stage in bone marrow. Splenic haematopoiesis fails to compensate for this defect, perhaps due to increased levels of formaldehyde in the spleen, or a failure of pro-erythroblasts to migrate to this tissue. These findings reveal an importance of transcription-coupled repair of formaldehyde in erythroid differentiation and raise the question of why this repair is so important at this stage of haematopoiesis.

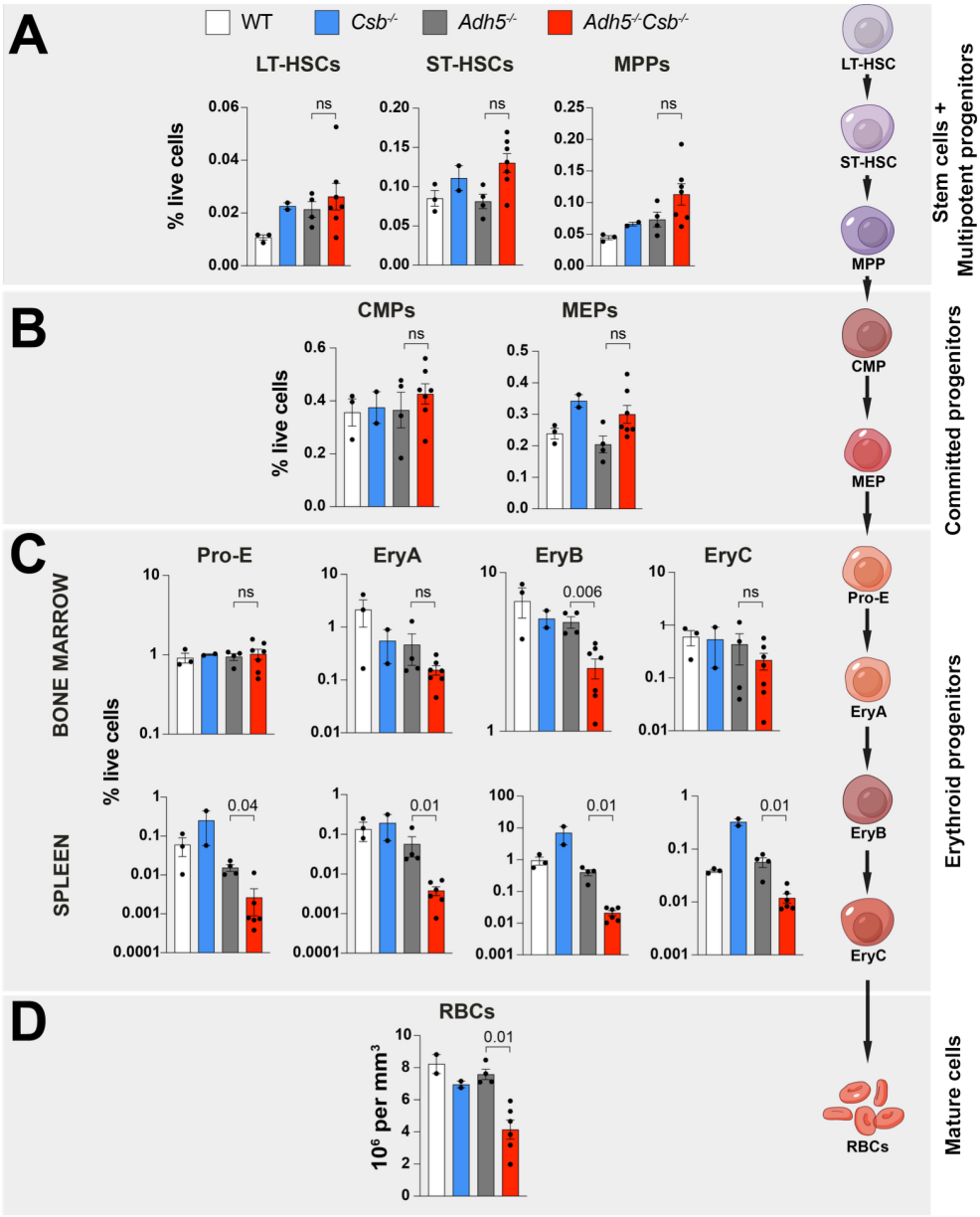
A
WT
Csb-/-
Adh5-/-
Adh5-/-Csb-/-
LT-HSCs
ST-HSCs
MPPs
% live cells
ns
LT-HSC
ST-HSC
MPP
Stem cells + Multipotent progenitors
B
CMPs
MEPs
CMP
MEP
Committed progenitors
C
BONE MARROW
SPLEEN
Pro-E
EryA
EryB
EryC
0.006
0.04
0.01
Erythroid progenitors
D
RBCs
10⁶ per mm³
RBCs
Mature cells

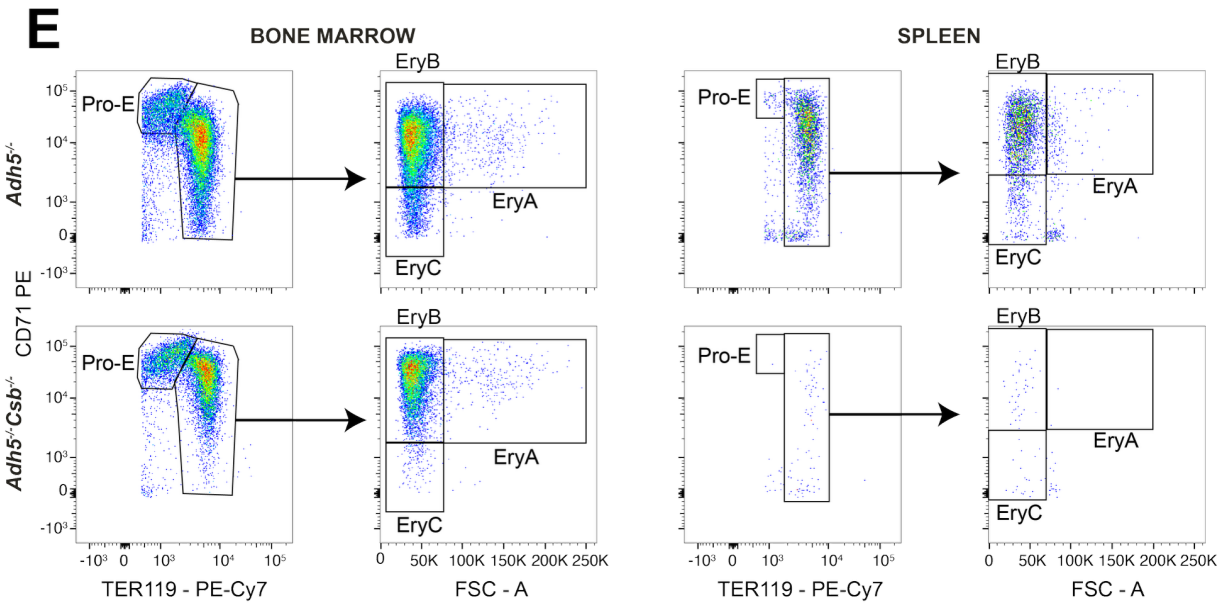
E
BONE MARROW
SPLEEN
Adh5-/-
Adh5-/-Csb-/-
CD71 PE
Pro-E
EryB
EryA
EryC
TER119 - PE-Cy7
FSC - A

Figure 4.8. Anaemia in aged *Adh5*$^{-/-}$*Csb*$^{-/-}$ mice is due to reduced erythroid progenitors.

A-C) Flow cytometry of bone marrow or spleen haematopoietic populations from 40-45-week old male mice. Populations were gated based on immunophenotypic markers as in Fig. 4.6. Data is represented as the percentage of each cell-type within the overall population of live, single cells. At least 250,000 events were sampled per mouse spleen/bone marrow. **D)** Red blood cell counts in mouse blood determined by Sc1Vet ABC plus+ cell counter. Error bars indicate standard error of the mean. P values calculated by Mann-Whitney U test. ns = P > 0.1. N = 3 (WT), 2 (*Csb*$^{-/-}$), 4 (*Adh5*$^{-/-}$), 7 (*Adh5*$^{-/-}$*Csb*$^{-/-}$). E) Flow cytometry gating strategy for Pro-E, EryA, EryB and EryC proportions after exclusion of cell debris and doublets/triplets by side and forward scatter and exclusion of dead cells by staining with 7-AAD.

4.5 Discussion

In this chapter, I created an *ex vivo* culture system wherein HSCs can be maintained in quiescence using low cytokine and low oxygen concentrations (Fig. 4.3-4). Crucially, this culture system does not compromise the function of these HSCs, which can be moved back into proliferation both *ex vivo* and after transplantation, wherein all downstream lineages can be repopulated (Fig. 4.4). This provides a system to move HSCs between proliferative states by changing cytokine concentrations, which could be useful for future studies of HSC cell cycle dynamics. Using this system, I examined the impact of TCR deficiency on HSC sensitivity to formaldehyde in proliferation vs quiescence. Interestingly, I found that TCR deficiency (via loss of CSB) did not increase the sensitivity of *Adh5*$^{-/-}$ HSCs to formaldehyde in either quiescence or proliferation, indicating there is a limited role for TCR in protecting these cells from formaldehyde damage (Fig. 4.5D). This finding was matched in my *in vivo* work, wherein *Adh5*$^{-/-}$*Csb*$^{-/-}$ mice showed no reduction in HSCs, nor defect in their function, compared to *Adh5*$^{-/-}$ mice, even after exogenous formaldehyde treatment via methanol injection (Fig. 4.6, 4.7, 4.8). Instead, I found that *Adh5*$^{-/-}$ *Csb*$^{-/-}$ mice have reduced numbers of erythroid progenitors leading to anaemia (Fig. 4.8C, D, E). This indicates that whilst TCR is dispensable for repairing formaldehyde damage in HSCs, this pathway has particular importance during erythroid maturation.

4.5.1 How do quiescent HSCs repair formaldehyde damage?

Given the quiescent state of HSCs in homeostasis (A. Wilson et al., 2008), one might assume they would rely more heavily on non-replication-coupled means of repair, such as TCR. Indeed, my

results in Chapter 3 showed that TCR is active in mouse haematopoietic stem and progenitor cells. However, lacking this repair pathway did not cause an HSC defect in *Adh5*$^{-/-}$*Csb*$^{-/-}$ mice exposed to endogenous or exogenous formaldehyde, suggesting that despite its activity, TCR is dispensable for repairing formaldehyde damage in *Adh5*$^{-/-}$ HSCs.

Following completion of my work, study by Oka et al., (2024) revealed that TCR does in fact preserve HSCs at higher levels of endogenous formaldehyde damage. This study examined haematopoiesis in mouse mutants of TCR and formaldehyde detoxification. Analogous to my findings, they showed that *Adh5*$^{-/-}$*Csb*$^{-/-}$ mice had normal levels of HSC and progenitor cells. However, concomitant deficiency in the secondary formaldehyde detoxifier, ALDH2, unveiled a haematopoietic defect. *Aldh2*$^{+/-}$*Adh5*$^{-/-}$*Csb*$^{-/-}$ mice had ~2-fold less HSCs, and substantially reduced progenitors compared to *Aldh2*$^{+/-}$*Adh5*$^{-/-}$ mice, indicating TCR deficiency precipitates loss of these cells in high formaldehyde conditions. The drastic difference in blood phenotype between *Adh5*$^{-/-}$*Csb*$^{-/-}$ and *Aldh2*$^{+/-}$*Adh5*$^{-/-}$*Csb*$^{-/-}$ mice highlights the importance of ALDH2 in HSC protection from formaldehyde. Only when detoxification is almost completely removed in HSCs is formaldehyde damage sufficient to require TCR. Perhaps at this level of endogenous formaldehyde other repair pathways are overwhelmed, necessitating TCR.

What might these other repair pathways be that can compensate for TCR deficiency at lower formaldehyde levels (i.e in *Adh5*$^{-/-}$*Csb*$^{-/-}$ mice)? Rossi et al. (2007) showed that deficiency in GG-NER and NHEJ causes a functional HSC defect. Perhaps it is these repair pathways which repair formaldehyde damage in *Adh5*$^{-/-}$ HSCs in the absence of TCR. Alternatively, repair of low-level formaldehyde damage may only occur minimally in quiescent HSCs. It has been proposed that quiescent HSCs act as a 'reservoir' for DNA damage (Beerman et al., 2014; Jan et al., 2012; Shlush et al., 2014). Studies have shown that HSCs accumulate strand breaks during ageing, which are only resolved upon re-entry into cell cycle (Beerman et al., 2014). Given the relatively low transcription rate of quiescent HSCs, it is conceivable that formaldehyde-induced lesions similarly remain unrepaired or minimally repaired until HSCs exit quiescence and repair them via replication-coupled mechanisms during proliferation.

Future work should aim to test these possibilities. For instance, my quiescent HSC culture system could be used to examine the expression of repair proteins in quiescent vs proliferating HSCs after formaldehyde treatment. Analysis of γH2AX foci could also be used in this HSC culture system to visualise DNA damage signalling after formaldehyde and identify DNA repair mutants which impact this signalling or prevent repair.

Finally, it would also be worth performing cell cycle analysis of *Adh5*$^{-/-}$*Csb*$^{-/-}$ mouse bone marrow to confirm that their HSCs are actually quiescent. In my work I have assumed that, as in steady-state HSCs, *Adh5*$^{-/-}$*Csb*$^{-/-}$ HSCs are quiescent *in vivo.* However, it is possible that the downstream erythroid progenitor depletion has pushed these *Adh5*$^{-/-}$*Csb*$^{-/-}$ HSCs into stress-induced haematopoiesis. This is a known phenomenon, wherein downstream damage, or depletion of cells, for instance through 5-FU treatment, pushes HSCs into cell cycle (S.-Y. Jeong et al., 2015; Randall & Weissman, 1997; Singh et al., 2020). This would allow these cells to utilise FA repair, and perhaps mask a phenotype of TCR-deficiency in *Adh5*$^{-/-}$*Csb*$^{-/-}$ HSCs. This analysis of the cell cycle status of *Adh5*$^{-/-}$*Csb*$^{-/-}$ HSCs should be performed and might reveal an intriguing role for stress-induced haematopoiesis in maintaining HSC genome fidelity.

Overall, my data indicate that TCR is not required to maintain HSC function in mice lacking the primary formaldehyde detoxifying enzyme, suggesting TCR plays a limited role in resolving formaldehyde-induced DNA damage in these cells. This could be due to compensation by other DNA repair pathways, or tolerance of quiescent HSCs to this damage until repair during S-phase. However, the findings of Oka et al. (2024) suggest that under higher levels of endogenous formaldehyde, TCR becomes essential, either due to the overwhelming of tolerance mechanisms or the saturation of alternative repair pathways.

4.5.2 The role of formaldehyde damage and TCR in erythroid differentiation

I found that the source of anaemia in *Adh5*$^{-/-}$*Csb*$^{-/-}$ mice was a reduction in the number of bone marrow and splenic erythroid progenitors. To understand why this might occur, we can examine

the unique properties of erythroid differentiation. During this process, global DNA demethylation occurs, decreasing by a third across all genomic loci within three divisions through both passive and active processes (Shearstone et al., 2011). One such process – the oxidative demethylation of DNA by AlkB – produces formaldehyde as a by-product (Falnes et al., 2002). At the same time, dramatic genomic reorganization occurs. Chromatin accessibility of specific regions reaches maximum, whilst transcription of alpha-globin surges, peaking at the basophilic-polychromatic stage (Jeziorska et al., 2022). This could produce a 'perfect storm', wherein formaldehyde produced from demethylation has access to adduct exposed DNA during chromatin reorganization and transcription. In the absence of ADH5 and CSB, this formaldehyde cannot be detoxified, nor its damage repaired, leading to persistent stalling of the transcriptional machinery during a period of intense transcriptional demand. This unresolved transcriptional stress could trigger P53 activation and cell death, causing the restriction of erythroid progenitors and mature red blood cells observed in *Adh5*$^{-/-}$*Csb*$^{-/-}$ mice (Fig. 4.9).

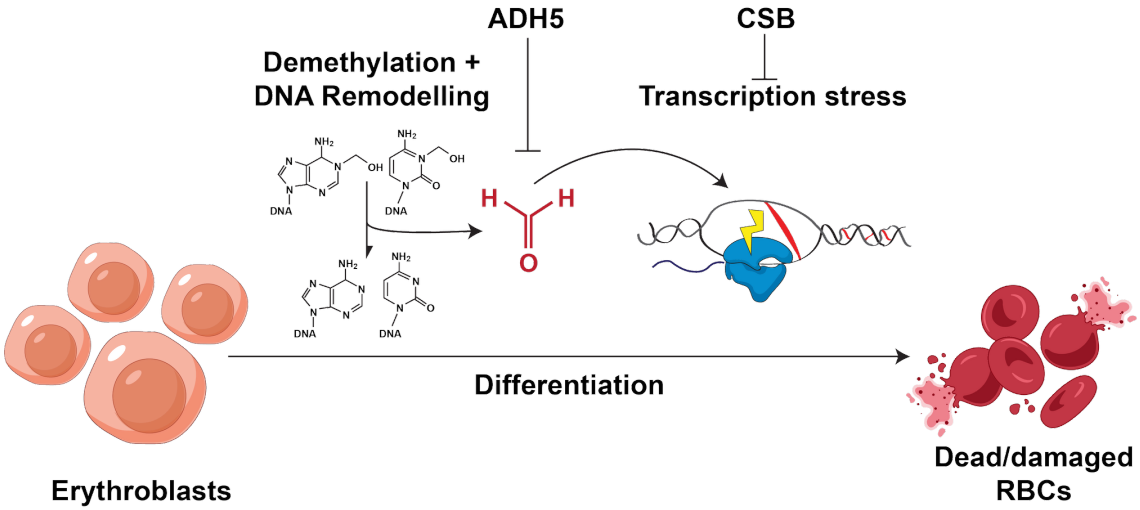

Figure 4.9. Model: Formaldehyde induces toxic transcription stress during erythroid differentiation.

Proposed mechanism for the erythroid depletion which occurs in *Adh5*$^{-/-}$*Csb*$^{-/-}$ mice. Erythroblasts undergo global DNA demethylation which can release formaldehyde during their differentiation to red blood cells. If not detoxified by ADH5, formaldehyde damages single stranded DNA during this period of high transcription and chromatin/DNA restructuring. In the absence of CSB this leads to transcription stress which cannot be resolved, resulting in cell death or dysfunction. Partially created in BioRender. Russell, H. (2026) https://BioRender.com/x8j92uu

Whilst an attractive hypothesis, this model requires significant validation. For instance, by assessing the fidelity of haemoglobin transcription in *Adh5*$^{-/-}$*Csb*$^{-/-}$ erythroid cells through nascent RNA RT-qPCR as by Tufegdžić Vidaković et al. (2020). To this end, I have used flow cytometry cell sorting to isolate ProE – EryC subsets from these mice for future RNA analysis.

This erythroid differentiation could also be studied *in vitro*, using the human umbilical cord blood-derived erythroid progenitor (HUDEP-2) cell line, which undergoes pro-erythroblastic to orthochromatic erythroid differentiation (Kurita et al., 2013). The dynamics of nascent transcription through differentiation can be assessed in *Adh5*$^{-/-}$*Csb*$^{-/-}$ mutants of this cell line through techniques such as TT-chem-seq to which can identify transcriptional stalling and stress (Gregersen et al., 2020). Creation of this mutant cell line is currently in progress. These experiments are outside of the scope of my PhD thesis but have the potential to generate exciting insights on the role of TCR in erythropoiesis.

5 TISSUES ARE PROTECTED FROM FORMALDEHYDE BY HAEMATOPOIETIC DETOXIFICATION IN COCKAYNE SYNDROME MICE

In my previous work I examined how combined deficiency in CSB and ADH5 impacts the haematopoietic system. I next sought to extend this question and ask what the effect of two-tier deficient haematopoiesis on the peripheral tissues is. Blood cells encounter most tissues in the body through systemic circulation (Huang et al., 2019). Blood can therefore disseminate systemic formaldehyde to distal tissues causing damage or, conversely, blood-derived detoxification may be important in alleviating tissue-intrinsic burden of formaldehyde. To understand the contribution of blood formaldehyde detoxification to peripheral tissue protection, the two must be decoupled.

To address this, we engineered an *Adh5* 'switch' allele, in which critical exon – exon 3 – has been inverted and flanked by modified *LoxP* sites (*Lox66* and *Lox71*), resulting in a dysfunctional, knockout-first allele. Action of the CRE recombinase restores exon 3 to a correct position, thus regenerating functional allele. After restoration, recombination cannot occur again, as CRE has only negligible affinity to the resulting *LoxP* sequences (Fig. 5.1A). By crossing the *Adh5* 'switch' allele with the published *Vav1-iCre* model, which drives 'improved' (optimised recombinant

activity) *Cre* (*iCre*) expression from the haematopoietic *Vav1* promoter (de Boer et al., 2003; Ogilvy et al., 1998, 1999; Shimshek et al., 2002), we can generate mice wherein ADH5 expression is rescued specifically in the haematopoietic cells. Using this strategy, I aimed to understand the impact of rescuing blood-mediated formaldehyde detoxification on other tissues. This would give insight into the source of formaldehyde in these tissues, and the protection that systemic detoxification provides.

5.1 The *Adh5* 'switch' allele restores ADH5 expression in haematopoietic cells in the presence of *Vav1-iCre*

First, we set out to validate the functionality and specificity of the *Adh5* 'switch' allele and *Vav1-iCre* in reactivating ADH5 in haemopoietic system. To do this, I performed western blotting to detect ADH5 protein in tissues from mice harbouring one *Adh5* 'switch' allele ($Adh5^{sw}$) and one non-functional *Adh5* allele ($Adh5^{tm1d}$ or $Adh5^{stam}$, referred to henceforth as $Adh5^{-}$). As expected, these mice had no detectable levels of ADH5 expression in haematopoietic (spleen, bone marrow) or peripheral (brain, kidney, liver) tissues. However, $Adh5^{sw/-}$ mice heterozygous for *Vav1-iCre* ($Adh5^{sw/-}$ *Vav1-iCre*) had restored ADH5 expression in haematopoietic tissues, with protein levels similar to those in $Adh5^{sw/+}$ mice (Fig. 5.1B).

Crucially, ADH5 expression was not restored in the peripheral tissues of $Adh5^{sw/-}$ *Vav1-iCre* mice (Fig. 5.1B). There was faint signal in the liver or kidney of one $Adh5^{sw/-}$ *Vav1-iCre* mouse (Fig. 5.1B, asterisks), however the intensity of this band was similar to the $Adh5^{sw/-}$ mice, which have no possibility of inadvertent Cre recombination. This indicates this may be background signal. Additionally, some of the ADH5 expression in $Adh5^{sw/-}$ *Vav1-iCre* kidneys or livers may have been from residual blood within these organs. Perfusion of these tissues with PBS before protein extraction could potentially avoid this issue – this work is in progress.

As means of further functional validation, I performed mass spectrometry analysis to quantify levels of a formaldehyde-DNA adduct – N^2-hydroxymethyl-deoxyguanosine – on genomic DNA. This modification is prevalent in the cells and is known to correlate with intracellular levels of

formaldehyde (Dingler et al., 2020). Genomic DNA from bone marrow, spleen, brain, kidney, or liver tissue was extracted and chemically reduced to stabilise the adduct to N^2-methyl-deoxyguanosine (N^2-MeG). N^2-MeG was then quantified using ultra-sensitive liquid chromatography-tandem mass spectrometry. Compared to *Adh5*$^{sw/+}$, *Adh5*$^{sw/-}$ mice had significantly elevated levels of N^2-MeG in the bone marrow and spleen, indicative of the high formaldehyde burden in these tissues due to absence of ADH5 (Fig. 5.1C). In the spleen, adduct levels were higher in males compared to females of this genotype – a phenomenon we have observed previously across several tissues including the brain, kidney and the liver. Of note, this sexual dimorphism disappears in *Aldh2*$^{-/-}$*Adh5*$^{-/-}$ mice, indicating it is due to differences in ALDH2 expression or detoxification capability in males vs females. Reassuringly, the adduct levels in *Adh5*$^{sw/-}$ *Vav1-iCre* mice were indistinguishable from *Adh5*$^{sw/+}$ mice, confirming that reactivated ADH5 is fully competent in detoxifying formaldehyde.

Remarkably, the levels of N^2-MeG in non-haematopoietic tissues of *Adh5*$^{sw/-}$ *Vav1-iCre* mice were also decreased when compared to *Adh5*$^{sw/-}$ controls, and this difference was especially pronounced in males (Fig. 5.1C). Indeed, adducts were down by 24% in the kidney tissue and approx. by 58% in the brains. There was a less prominent reduction in the liver (17%, n.s.). This suggests that blood-specific formaldehyde detoxification confers some level of protection to peripheral tissues, especially brain and kidney. This result prompted us to consider whether this systemic protection is sufficient to alleviate organ deterioration which occurs in two-tier deficient mice.

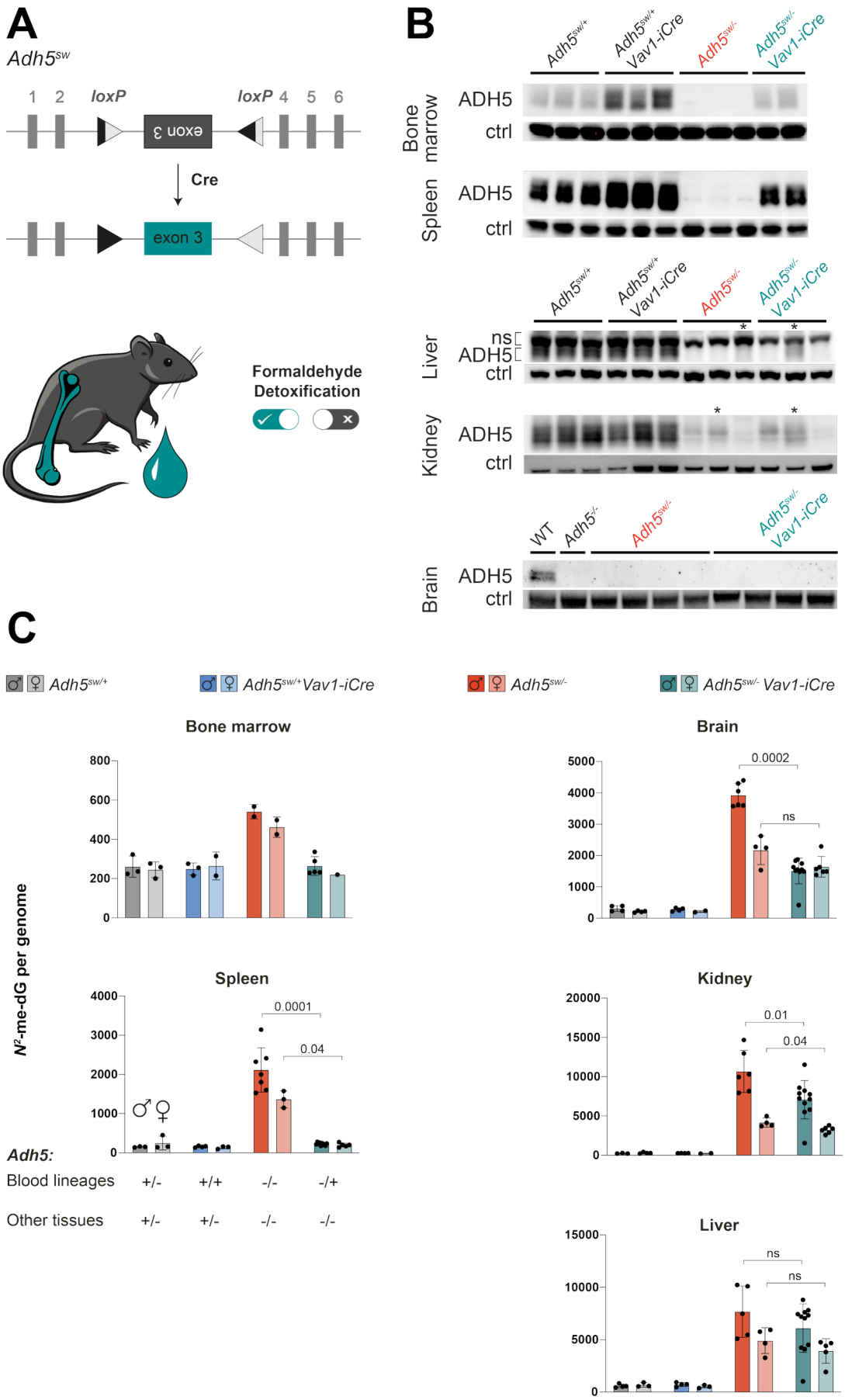
A
Adh5sw
1 2 loxP exon 3 loxP 4 5 6
Cre
exon 3
Formaldehyde Detoxification
B
Adh5sw/+
Adh5sw/+ Vav1-iCre
Adh5sw/-
Adh5sw/- Vav1-iCre
Bone marrow
ADH5
ctrl
Spleen
ADH5
ctrl
Liver
ns
ADH5
ctrl
Kidney
ADH5
ctrl
WT
Adh5-/-
Brain
ADH5
ctrl
C
Adh5sw/+
Adh5sw/+ Vav1-iCre
Adh5sw/-
Adh5sw/- Vav1-iCre
Bone marrow
Brain
0.0002
ns
Spleen
0.0001
0.04
Kidney
0.01
0.04
Liver
ns
ns
N2-me-dG per genome
Adh5:
Blood lineages +/- +/+ -/- -/+
Other tissues +/- +/- -/- -/-

Figure 5.1. Development and validation of the *Adh5* switch model.

A) Schematic of the *Adh5*^{sw} allele. Exon 3 of *Adh5* is in reverse orientation flanked by modified LoxP sites (Lox71 and Lox66). In the presence of CRE, exon 3 is inverted into the correct orientation. Recombination also modifies the LoxP sites to become Lox72 and WT LoxP which prevents further recombination. Combining the *Adh5*^{sw} allele with the published *Vav1-iCre* allele, which drives CRE expression only in haematopoietic lineages, allows rescue of ADH5 expression specifically in these cells. **B)** Western blot for ADH5 in mouse tissues. Loading control is either a non-specific band from anti-ADH5 blot (bone marrow, spleen), vinculin (liver, kidney) or β-catenin (brain). "ns" indicates non-specific band for liver. Asterisks indicate samples with potential background signal **C)** Average levels of N^2-methyldeoxyguanine per genome in the DNA of 6–15-week-old mouse tissues. Dots denote individual mice. Error bars indicate standard error of the mean. P value from Mann-Whittney U test. ns = P > 0.1.

5.2 Systemic detoxification of formaldehyde reduces CS-associated kidney damage and cachexia

Aged *Adh5*$^{-/-}$*Csb*$^{-/-}$ mice recapitulate phenotypes seen in patients with Cockayne syndrome, including progressive neurodegeneration, cachexia, kidney failure, and anaemia (Mulderrig et al., 2021). We wanted to understand if any of these phenotypes could be mitigated by the haematopoietic formaldehyde detoxification and to what extent.

To test this, I crossed the *Adh5* 'switch' allele into the CSB-deficient background to produce mice globally deficient in CSB and with ADH5 expression restored specifically in the haemopoietic system (*Adh5*$^{sw/-}$*Csb*$^{-/-}$ *Vav1-iCre*) (Fig. 5.2A). Homozygous expression of CRE is embryonic lethal (Joseph et al., 2013), thus all mice were hemizygous for the *Vav1-iCre* allele and bred as such ('*Vav1-iCre*' indicates heterozygous mouse). Both *Adh5*$^{sw/-}$*Csb*$^{-/-}$ *Vav1-iCre* and *Adh5*$^{sw/-}$*Csb*$^{-/-}$ control mice were born at sub-mendelian ratios, albeit *Adh5*$^{sw/-}$*Csb*$^{-/-}$ *Vav1-iCre* mice were more prevalent than *Adh5*$^{sw/-}$*Csb*$^{-/-}$ (6% vs 3% of pups) (Fig. 5.2A). This observation was an early indication that systemic detoxification of formaldehyde could confer some protection to Cockayne syndrome mice, at least in the perinatal window. Whether this was due to an increased protection *in utero* or an advantage in post-natal survival is unclear; pups which die shortly after birth are often cannibalised by the parents and are therefore difficult to detect. Additionally, *Adh5*$^{sw/-}$*Csb*$^{-/-}$ *Vav1-iCre* pups were significantly larger than their globally deficient counterparts

(Fig. 5.3A). This difference in size may have conferred a competitive advantage for breast milk access and improved survival.

Next, I set out to evaluate the phenotype of the newly-generated *Adh5*$^{sw/-}$*Csb*$^{-/-}$ *Vav1-iCre* mice. Most of the *Adh5*$^{-/-}$*Csb*$^{-/-}$ phenotypes precipitate with age, however our previous work has shown that some of the defects, particularly kidney failure and cachexia, can be additionally accelerated by repeated injections of methanol (an exogenous source of formaldehyde). We have observed that female *Adh5*$^{-/-}$ mice tolerate methanol treatment much better than males, therefore I subjected mutant and control females to weekly intraperitoneal injections of methanol for 5 weeks and evaluated kidney function (via serum biochemistry) at the end of the experiment. In parallel, male mice were allowed to age and were routinely monitored for signs of cerebellar ataxia (using behavioural tests) and kidney damage (serum biochemistry) (Fig. 5.2B).

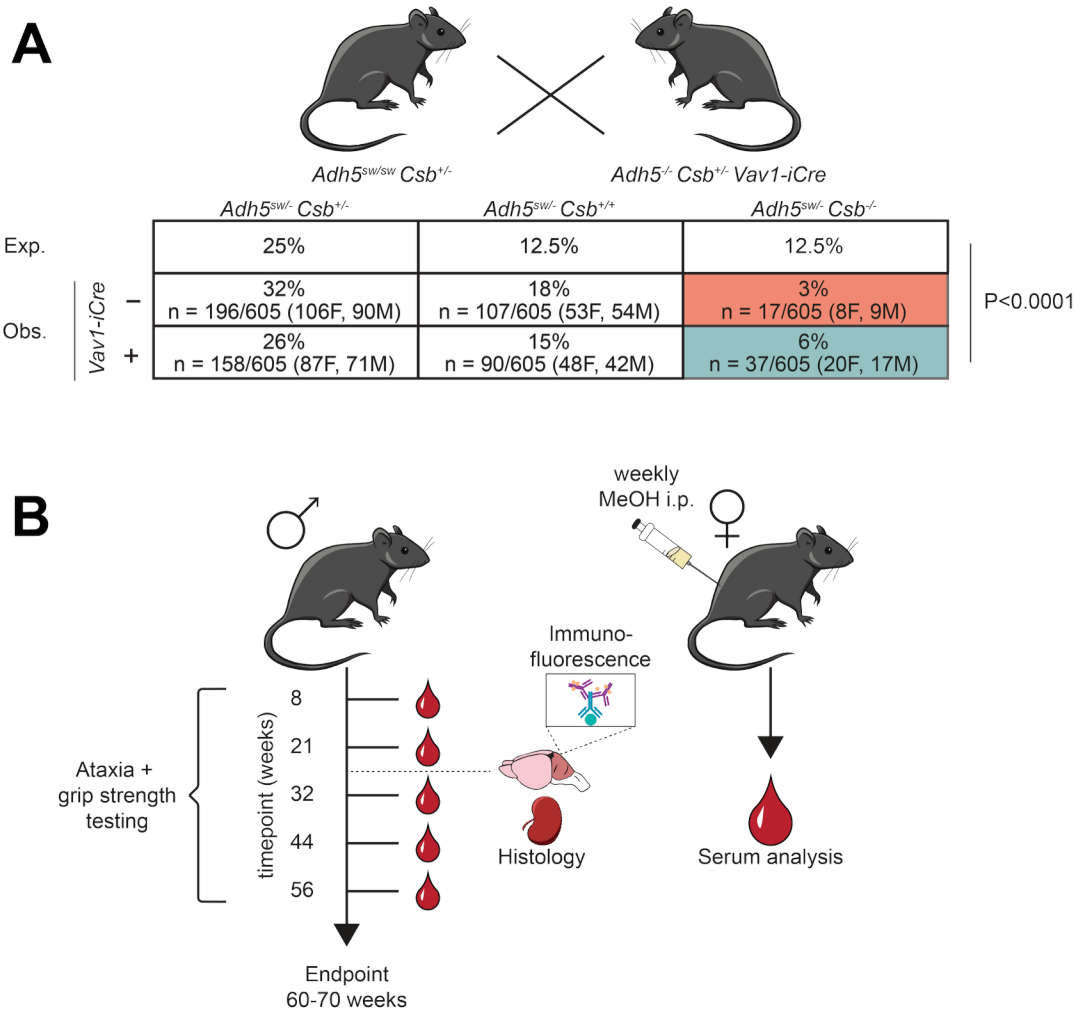

Figure 5.2. *Adh5$^{sw/-}$Csb$^{-/-}$ Vav1-iCre* mice - breeding strategy and experimental set-up.

A) Breeding crosses of *Adh5$^{sw/-}$ Csb$^{+/-}$* X *Adh5$^{-/-}$Csb$^{+/-}$ Vav1-iCre* mice in a C57BL/6 background with observed numbers of male (M) and female (F) pups genotyped 2-3 weeks after birth. ADH5/CSB-deficient mice are born at sub-mendelian ratios. P value calculated by Fisher's exact test. **B)** Experimental methodology for examining the phenotype of *Adh5$^{sw/-}$Csb$^{-/-}$ Vav1-iCre* mice. Males were aged and assessed for cerebellar ataxia, grip strength and serum markers of kidney dysfunction (urea, GDF15) every 3 months from 8 weeks of age. At 6 months of age a cohort was culled, and the kidneys and brain assessed by histologically. Remaining mice were aged and measurements continued up to 70 weeks before culling. Female mice were given intraperitoneal injections of 1.5 g/kg methanol once weekly for 4-7 weeks, culled and serum urea and GDF15 measured.

In agreement with previous work (Mulderrig et al., 2021), *Adh5*$^{sw/-}$*Csb*$^{-/-}$ males had normal life span but reduced body mass compared to controls (Fig. 5.3A). This phenotype was partially rescued in *Adh5*$^{sw/-}$*Csb*$^{-/-}$ *Vav1-iCre* mice which were on average 28% larger than their constitutive knockout counterparts (Fig. 5.3A). We have previously shown that the growth defect in *Adh5*$^{-/-}$ *Csb*$^{-/-}$ mice is largely mediated by the anorexic hormone, GDF15, produced by damaged kidney cells and possibly other tissues (Mulderrig et al., 2021). Thus, the partial rescue of body weight in *Adh5*$^{sw/-}$*Csb*$^{-/-}$ *Vav1-iCre* males could be a sign of reduced tissue damage. Indeed, the serum of *Adh5*$^{sw/-}$*Csb*$^{-/-}$ *Vav1-iCre* males had significantly decreased levels of urea – a marker of kidney dysfunction – as well as reduced levels of GDF15 (Fig. 3.3B, C). Moreover, *Adh5*$^{sw/-}$*Csb*$^{-/-}$ *Vav1-iCre* kidneys were significantly larger than in *Adh5*$^{sw/-}$*Csb*$^{-/-}$ males, and did not have the nodular, shrivelled appearance typically seen in the CS mice (Fig. 3.3D). Histological analysis at 6 months revealed cortical immune infiltration and tubular atrophy in *Adh5*$^{sw/-}$*Csb*$^{-/-}$ males consistent with interstitial nephritis (Fig. 5.3D). In contrast, *Adh5*$^{sw/-}$*Csb*$^{-/-}$ *Vav1-iCre* mice had only mild histological changes confirming that kidney damage is largely alleviated in this model.

This phenomenon was replicated in female mice exposed to methanol. *Adh5*$^{sw/-}$*Csb*$^{-/-}$ mice quickly lost weight following methanol treatment, had high levels of serum GDF15, and developed nodular kidneys reminiscent of aged *Adh5*$^{sw/-}$*Csb*$^{-/-}$ males (Fig. 5.3F, G). In contrast, *Adh5*$^{sw/-}$*Csb*$^{-/-}$ *Vav1-iCre* female mice continued to gain weight throughout the experiment, had reduced levels of serum GDF15, and their kidneys were seemingly normal in both size and appearance (Fig. 5.3F, G).

Together, these data show that rescuing systemic formaldehyde detoxification protects the kidney from both exogenous and endogenous formaldehyde, and this protection is sufficient to reduce cachexia and alleviate kidney failure in Cockayne syndrome mice.

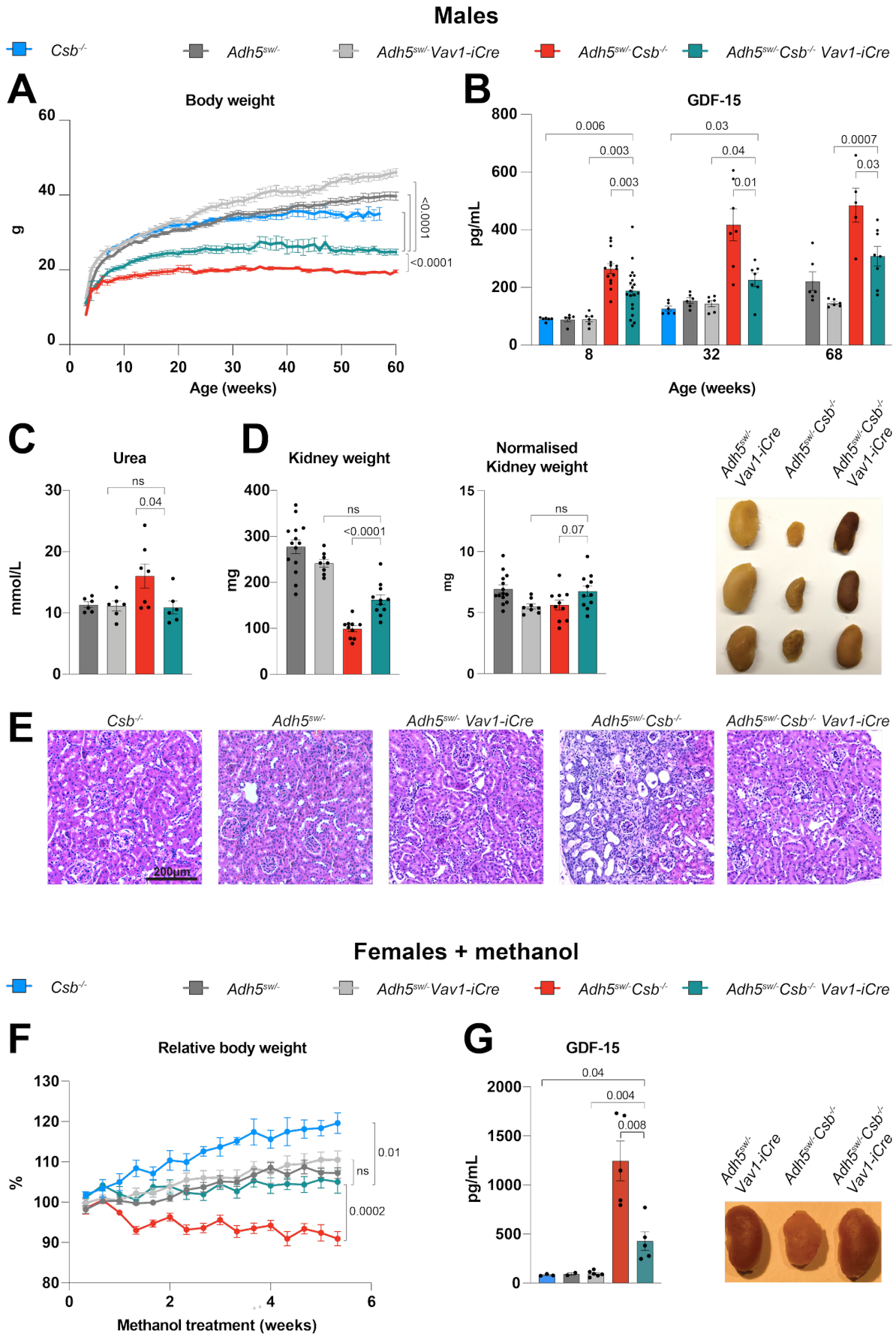
Males
Csb-/-
Adh5sw/-
Adh5sw/-Vav1-iCre
Adh5sw/-Csb-/-
Adh5sw/-Csb-/- Vav1-iCre
A
Body weight
g
Age (weeks)
<0.0001
<0.0001
B
GDF-15
pg/mL
Age (weeks)
0.006
0.003
0.003
0.03
0.04
0.01
0.0007
0.03
C
Urea
mmol/L
ns
0.04
D
Kidney weight
mg
ns
<0.0001
Normalised Kidney weight
mg
ns
0.07
E
200µm
Females + methanol
F
Relative body weight
%
Methanol treatment (weeks)
0.01
ns
0.0002
G
GDF-15
pg/mL
0.04
0.004
0.008

Figure 5.3. *Adh5$^{sw/-}$Csb$^{-/-}$ Vav1-iCre* mice have reduced kidney damage and cachexia compared to *Adh5$^{sw/-}$Csb$^{-/-}$*

Phenotypic analysis of mice. For all bar graphs (except kidney weights) dots denote individual mice/N values, error bars indicate standard error of the mean, and ns = P value > 0.1. **A)** Average body weights of male mice, P value from two-way ANOVA. N = 17, 43, 24, 24, 22 for *Csb$^{-/-}$, Adh5$^{sw/-}$*, *Adh5$^{sw/-}$ Vav1-iCre*, *Adh5$^{sw/-}$Csb$^{-/-}$* and *Adh5$^{sw/-}$Csb$^{-/-}$ Vav1-iCre* mice, respectively. **B)** Serum GDF-15 levels in male mice. P value from Mann-Whitney U test. **C)** Serum urea in 44-week old male mice, P value from Mann-Whitney U test. **D)** Kidney weights (raw or normalised to body weight) of 68-76-week old male mice (left panel) together with representative macroscopic images (right panel). Dots indicate single kidneys. P Value from Mann-Whitney U test. **E)** Representative sections from 6-month-old male mouse kidneys stained with haematoxylin and eosin. Scale bar, 200 μm. *Adh5$^{sw/-}$Csb$^{-/-}$* mice have increased infiltration of (likely immune) cells (purple nuclei) and focal tubule loss. **F)** Average relative body weight (normalised to pre-treatment weight) of female mice treated with weekly injections of 1.5 g/kg methanol (MeOH). N = 3, 9, 6, 5, 5 for *Csb$^{-/-}$, Adh5$^{sw/-}$*, *Adh5$^{sw/-}$ Vav1-iCre*, *Adh5$^{sw/-}$Csb$^{-/-}$* and *Adh5$^{sw/-}$Csb$^{-/-}$ Vav1-iCre* mice, respectively. **G)** Serum GDF15 levels and representative kidney images of 8–12-week-old female mice intraperitoneally injected with 1.5 g/kg methanol (MeOH) weekly for 5 weeks. P value calculated by two-way ANOVA (weights) or Mann-Whitney U test (GDF-15).

5.3 Systemic detoxification of formaldehyde reduces brain damage and delays neurodegeneration in CS mice

In addition to kidney damage, *Adh5$^{-/-}$Csb$^{-/-}$* mice develop cerebellar ataxia which can be measured using a series of phenotypic assessments indicative of neuromotor function (kyphosis score, hind limb clasping, gait analysis, ledge test and grip strength). We therefore studied aged *Adh5$^{sw/-}$Csb$^{-/-}$ Vav1-iCre* male mice in more detail and asked if systemic detoxification of formaldehyde can protect against neurodegenerative processes associated with CS.

Consistent with published data (Mulderrig et al., 2021) *Adh5$^{sw/-}$Csb$^{-/-}$* mice had reduced grip strength compared to genetic controls (Fig. 5.4C) and developed kyphosis by 21 weeks (data not shown, Fig. 5.4B). In contrast, *Adh5$^{sw/-}$Csb$^{-/-}$ Vav1-iCre* mice had a delayed onset of kyphosis (average of 26 weeks) and significantly improved grip strength compared to *Adh5$^{sw/-}$Csb$^{-/-}$* (Fig. 5.4C). This difference became more pronounced with age. Also, the severity of cerebellar ataxia was markedly reduced in *Adh5$^{sw/-}$Csb$^{-/-}$ Vav1-iCre* mice, which were visibly much better coordinated than *Adh5$^{sw/-}$Csb$^{-/-}$* (Fig. 5.4A) and maintained a 50% lower ataxia score throughout life (Fig. 5.4A,B).

To examine whether improved motor function was due to reduced brain damage, we performed immunofluorescent analysis of damage markers in the brains of 6-month-old mice (in collaboration with D. Jaarsma, Erasmus MC, Rotterdam, the Netherlands). Indeed, *Adh5*$^{sw/-}$*Csb*$^{-/-}$ *Vav1-iCre* mice had reduced neuroinflammation compared to *Adh5*$^{sw/-}$*Csb*$^{-/-}$, as evidenced by less infiltration of inflammatory MAC2-positive microglial cells in the brainstem (Fig. 5.4D). Similarly, the level of GFAP-expressing cells in the cerebellum and medulla oblongata was also reduced (Fig. 5.4D, E). GFAP expression denotes reactive astrocytes which form glial scars around damaged brain tissue (Liddelow & Barres, 2017), and their reduction indicates diminished neural injury in *Adh5*$^{sw/-}$*Csb*$^{-/-}$ *Vav1-iCre* mice. Finally, we found that levels of the DNA autophagy and neurodegeneration-associated marker, P62 (Bjørkøy et al., 2009; Jackson et al., 2017), was also significantly reduced in the cerebellum of *Adh5*$^{sw/-}$*Csb*$^{-/-}$ *Vav1-iCre* mice compared to *Adh5*$^{sw/-}$*Csb*$^{-/-}$ (Fig. 5.4E).

Altogether, these findings reveal that systemic detoxification of formaldehyde reduces the level of DNA damage, inflammation and scarring in the brains of CS mice, and delays neurodegeneration in these mice.

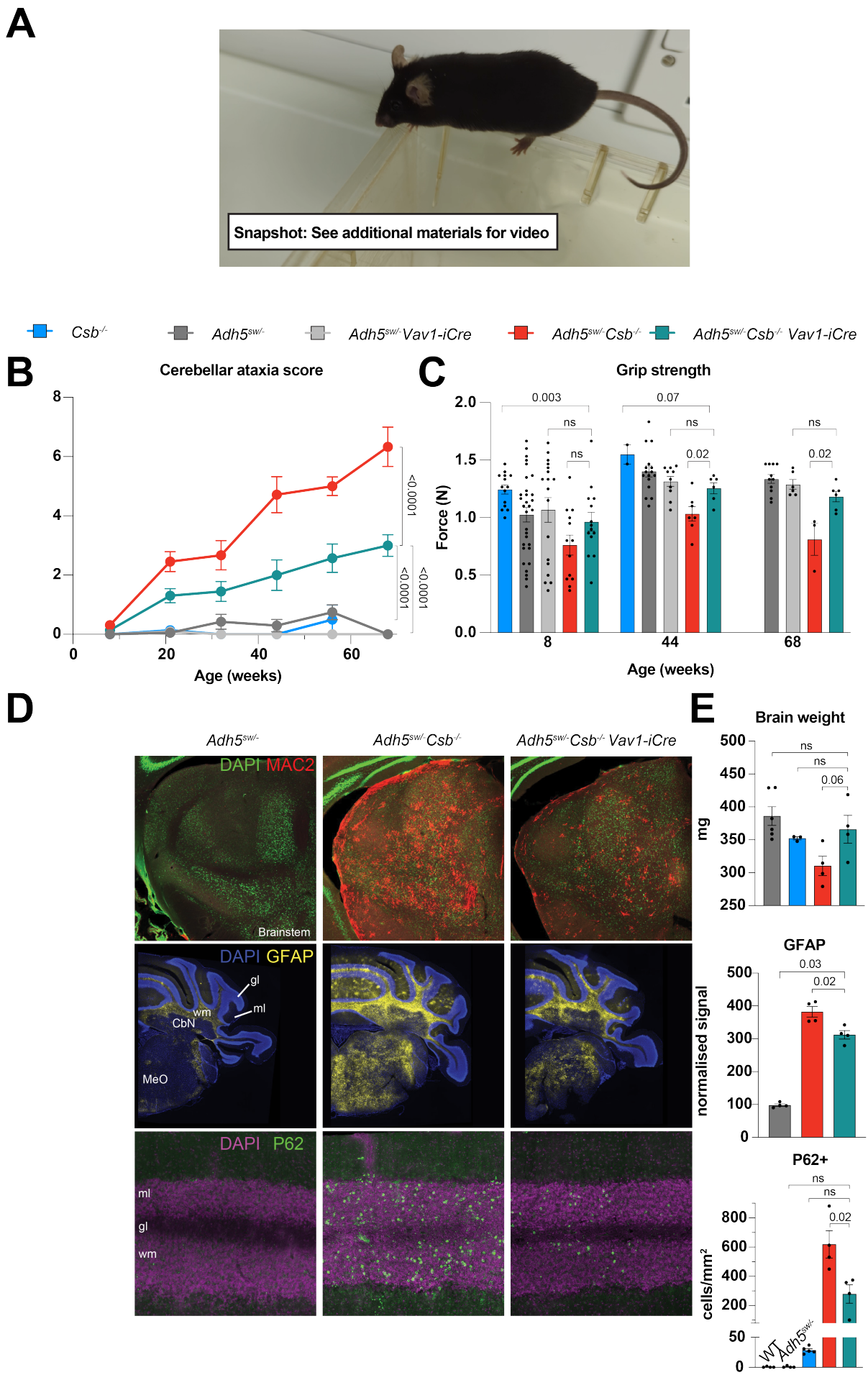
A
Snapshot: See additional materials for video
Csb-/-
Adh5sw/-
Adh5sw/-Vav1-iCre
Adh5sw/-Csb-/-
Adh5sw/-Csb-/- Vav1-iCre
B
Cerebellar ataxia score
Age (weeks)
<0.0001
<0.0001
C
Grip strength
Force (N)
Age (weeks)
0.003
ns
ns
0.07
ns
0.02
ns
0.02
D
Adh5sw/-
Adh5sw/-Csb-/-
Adh5sw/-Csb-/- Vav1-iCre
DAPI MAC2
Brainstem
DAPI GFAP
gl
ml
wm
CbN
MeO
DAPI P62
ml
gl
wm
E
Brain weight
mg
ns
ns
0.06
GFAP
normalised signal
0.03
0.02
P62+
cells/mm2
ns
ns
0.02
WT
Adh5sw/-

Figure 5.4. *Adh5$^{sw/-}$Csb$^{-/-}$ Vav1-iCre* mice have reduced neurodegeneration compared to *Adh5$^{sw/-}$Csb$^{-/-}$*.

A) Video of a 50-week-old male mice performing the ledge test as part of cerebellar ataxia scoring. **B)** Average cerebellar ataxia score (consists of scoring of gait, kyphosis, ledge test, and hindlimb clasping). Error bars indicate standard error of the mean. P value calculated by mixed effects analysis. N = 15 (*Csb$^{-/-}$*), 23 (*Adh5$^{sw/-}$*), 13 (*Adh5$^{sw/-}$ Vav1-iCre*), 11 (*Adh5$^{sw/-}$Csb$^{-/-}$*), 13 (*Adh5$^{sw/-}$Csb$^{-/-}$ Vav1-iCre*). **C)** Grip strength measurements in male mice. Error bars indicate standard error of the mean. Dots indicate individual mice and N values. P value calculated by Mann-Whitney U test. Ns = P > 0.1. **D)** Representative immunofluorescence images of brain tissue from 6-month-old male mice stained with DAPI, and anti-MAC2, anti-GFAP, or anti-P62 antibodies. MeO = medulla oblongata, CbN = cerebellum, wm = white matter, gl = granule layer, ml = molecular layer. **E-G)** Quantification of average brain weight and GFAP+ cells in the medulla oblongata or P62+ cells in granule layer of 6-month-old male mice. Error bars denote standard error of the mean. Dots indicate individual mice with at least 3 sections quantified and averaged per mouse for immunofluorescence. P value from Mann-Whittney U test. ns = P > 0.1. N = 4 (WT), 6 (*Adh5$^{sw/-}$*), 3 (*Csb$^{-/-}$*), 4 (*Adh5$^{sw/-}$Csb$^{-/-}$* and *Adh5$^{sw/-}$Csb$^{-/-}$ Vav1-iCre*).

5.4 Discussion

5.4.1 What is the source of formaldehyde in *Adh5$^{-/-}$Csb$^{-/-}$* mice?

My data show that ADH5 expressed by the haemopoietic system protects the kidney and brain against deleterious consequences of increased formaldehyde levels. However, the origin of the tissue-specific formaldehyde burden remains elusive. Is the blood scavenging formaldehyde produced within cells in distal tissues for systemic detoxification, or is the blood disseminating it to peripheral organs, causing damage to sites that would otherwise never experience high loads of formaldehyde? In other words, is the blood part of a problem, or a solution?

Formaldehyde is a volatile substance which can rapidly traverse cell membranes and disseminate through tissues (Hewlett, 2002). However, my measurement of formaldehyde-DNA adduct levels shows that it does not reach an equilibrium across the whole body, with some ADH5-deficient tissues, such the kidney, harbouring substantially more adducts per genome compared to others, e.g. the bone marrow (Fig. 5.1C). This indicates that there are tissue-intrinsic mechanisms that regulate local formaldehyde burden resulting in concentration gradient. This tissue-intrinsic formaldehyde burden could be influenced by various factors. These include the rate of cell division, which may dilute formaldehyde-adducted DNA, the amount of formaldehyde generated or removed by metabolism, exposure to dietary or environmental sources of formaldehyde, and

the interaction with other tissues, such as blood or immune cells, which might produce or remove formaldehyde.

For example, adduct levels of ADH5-deficient mice indicate the liver experiences substantial exposure to formaldehyde (>15X the bone marrow) (Fig. 5.1C). This organ performs the majority of the body's folate metabolism, a process which is known to release formaldehyde. Additionally, the liver serves as the primary site for methanol conversion to formaldehyde (Pocker & Li, 1991) and may also mediate the conversion of other dietary precursors, increasing its intrinsic load. Rescuing blood formaldehyde detoxification did not significantly lower the level of liver formaldehyde-DNA adducts (Fig. 5.1C), suggesting that most of the formaldehyde in this tissue is intrinsic, and systemic detoxification is not sufficient to remove it. Indeed, unpublished work from our lab has shown that mice with liver-specific knockout of ADH5 (*Adh5*$^{c/d}$ *Albumin-Cre*) have high levels of serum formaldehyde, similar to mice globally deficient for ADH5. This suggests that in fact a sizeable proportion of serum formaldehyde originates from the liver. Conversely, the kidney has an even higher level of formaldehyde adducts than the liver (Fig. 5.1C), but rescuing blood detoxification significantly reduced adducts in this tissue and rescued organ failure in ADH5/CSB-deficient mice. This suggests that either the blood more effectively removes kidney-intrinsic formaldehyde or that the primary source of formaldehyde in this tissue is blood-borne – perhaps disseminated from the liver.

Truly determining the contribution of tissue-intrinsic vs blood-borne formaldehyde to the total formaldehyde burden in different organs would require generation of additional, refined models where ADH5-deficiency is restricted to specific tissues. This could be done using existing tissue-specific *Cre* alleles such as *Nestin-Cre* or *Cdh16-Cre*, which direct CRE recombinase activity in neurons and kidney cells, respectively (Giusti et al., 2014; X. Shao et al., 2002). Additionally, there may be other tissues which are protected by systemic formaldehyde detoxification which have not been investigated. Measurement of formaldehyde adducts in other 'switched' vs constitutively ADH5-deficient tissues might reveal these additional dependencies.

These investigations, combined with my current work, would provide a comprehensive map of the tissues responsible for formaldehyde production, dissemination, or detoxification. However, the important question about the cellular sources of formaldehyde — specifically, which metabolic, (epi)genetic, or chemical processes within cells result in its release — still stands. Formaldehyde is released during the metabolism of folic acid derivatives (Burgos-Barragan et al., 2017); however, the blood concentration of folic acid is several orders of magnitude lower than recorded blood formaldehyde levels (Burgos-Barragan et al., 2017; Dingler et al., 2020), suggesting that the contribution of this pathway to the overall formaldehyde burden is limited. Likewise, DNA and histone demethylation generate formaldehyde as part of epigenetic regulation, but the contribution of these processes to the total formaldehyde levels is unclear (Hopkinson et al., 2010).

Efforts to reveal more cellular sources have proven challenging. The volatility and rapid reactivity of formaldehyde makes measuring endogenous formaldehyde and identifying the exact cellular source of production difficult. Though formaldehyde adducts are readily detectable in ADH5-deficient mice, the sensitivity of this assay is still insufficient to detect adducts in WT cell cultures (unpublished). *In vitro,* the phenotypes of two-tier deficiency are also significantly less prominent than *in vivo*, with most cellular models showing either absent or marginal growth defects (Wit et al., 2023) . This may be due to the dissemination of cellular formaldehyde into relatively large volumes of liquid tissue culture, diluting this chemical and its toxic effects. Additionally, there may be multiple, incremental sources of formaldehyde, as well as redundancies in formaldehyde detoxification pathways which make identifying sources through approaches such as loss-of-function genetic screens difficult. Multiple genetic screens to identify formaldehyde sources have indeed been attempted by our lab, but so far only one has been successful (Wit et al., 2023). In this approach, we took advantage of the fact that formaldehyde can provide a backup source of one-carbon units for nucleotide synthesis in the absence of serine (Burgos-Barragan et al., 2017). We have therefore generated a cell line with deficiency in serine metabolism (through SHMT1/2

ko), which became reliant on endogenous formaldehyde for survival. CRISPR/Cas9 screen in this cell line identified histone deacetylase HDAC3 as a suppressor of endogenous formaldehyde (Wit et al., 2023). The exact source of formaldehyde that HDAC3 suppresses remains unclear, however, and it can nevertheless account only for a small fraction of the cellular pool.

While my work has provided insights into the contribution of blood detoxification to formaldehyde burden, the challenge of pinpointing its cellular sources remains. The development of sensitive methods to detect formaldehyde (e.g., fluorescent probes) or its by-products (e.g., DNA/protein adducts) should further aid this area of research and help identify both the tissue-specific and cellular processes responsible for regulating endogenous formaldehyde.

5.4.2 Improving systemic clearance of formaldehyde - implications

Regardless of the origin of formaldehyde, my work shows that detoxifying it specifically in haematopoietic cells can significantly reduce organ damage and deterioration. This could potentially be beneficial for the treatment of diseases such as Cockayne syndrome and Fanconi anaemia, where endogenous formaldehyde likely acts as a driver (Mulderrig et al., 2021; Pontel et al., 2015). Additionally, formaldehyde as an endogenous mutagen contributes to the stochastic accumulation of DNA damage with time. Clearing this formaldehyde systemically might ameliorate degenerative process associated with physiological ageing. The possibility of alleviating symptoms by simply scavenging systemic formaldehyde represents a promising and relatively straightforward approach. Derivatives of simple compounds such as L-cysteine, which react with formaldehyde and significantly reduce its concentration in ADH5-deficient cells (Pietzke et al., 2020), could be potentially utilised for this purpose. In fact, such compounds – D-penicillamine and cysteamine - are already being used in the clinic for the treatment of arthritis, cystinuria and cystinosis (DeBerardinis et al., 2008; Kleta et al., 2004). The idea of extending their use to prevent formaldehyde-driven damage is worth exploring.

5.4.3 The contribution of residual immune cells to formaldehyde detoxification

While blood-mediated formaldehyde detoxification likely plays the major role in the organ protection, the contribution of residual immune cells should also be considered. The *Vav1* promoter is expressed in all descendants of haematopoietic stem cells, including lymphoid and myeloid immune cells (Ogilvy et al., 1999). Lineage tracing experiments in *Vav1-iCre* mice show *Vav1* promoter activity in lymphoid tissues such as thymus, spleen and Peyer's patches (de Boer et al., 2003). The kidneys of *Adh5*$^{-/-}$*Csb*$^{-/-}$ mice get heavily infiltrated with cells of lymphoid and myeloid origin (Mulderrig et al., 2021). It is plausible that these infiltrating immune cells, which are proficient for ADH5 in *Adh5*$^{sw/-}$*Csb*$^{-/-}$ *Vav1-iCre* mice, could contribute to formaldehyde detoxification. However, the fact that the kidneys of *Adh5*$^{sw/-}$*Csb*$^{-/-}$ *Vav1-iCre* mice have only very few of those cells argues against this possibility.

Immune infiltrates are also present in the brains of the *Adh5*$^{-/-}$*Csb*$^{-/-}$ mice in the form of MAC2-positive microglial cells (Fig. 5.4D). Microglia are mainly produced from the yolk sac at embryonic day 8 (E8) in mice, migrating to the brain where they persist and self-renew throughout life (Leavy, 2010). Since *Vav1* expression is first detected around embryonic day 11.5 (E11.5), ADH5 rescue by *Vav1-iCre* should be excluded from microglia. However, some debate exists on the presence of non-yolk sac-derived microglia originating post-E11.5 from haematopoietic progenitors (Swinnen et al., 2013; Xu et al., 2015). To address this, Fehrenbach et al. (2018) utilized a *Vav1-iCre* knockout system to disrupt microglial recruitment to the brain, specifically after yolk sac development. This depleted the number of brain microglia by 40%, suggesting that a significant proportion of microglia indeed originate from *Vav1*-expressing haematopoietic cells. It is therefore possible that some microglia in *Adh5*$^{sw/-}$*Csb*$^{-/-}$ *Vav1-iCre* mice express ADH5, contributing to a reduction in formaldehyde burden in the brain. However, the brains of *Adh5*$^{sw/-}$*Csb*$^{-/-}$ *Vav1-iCre* mice show reduced MAC2+ microglial staining compared to global knockouts (Fig. 5.4D). This indicates that their presence, and therefore their contribution to detoxification, is limited.

To truly determine the contribution of infiltrating cells to reducing formaldehyde burden, further assessment of the ADH5 expression in the tissues of *Adh5*$^{sw/-}$*Csb*$^{-/-}$ *Vav1-iCre* mice is required. My western blot assessments showed that, grossly, ADH5 is absent in both the brain and kidney of *Adh5*$^{sw/-}$ *Vav1-iCre* mice (Fig. 5.1B). However, this assay has limited sensitivity (Ghosh et al., 2014; Xiang et al., 2021). Ideally, we would employ spatial techniques such as RNA-scope or ADH5 immunohistochemistry to detect ADH5 expression in specific cell populations in histological sections. Immunohistochemistry of ADH5 in brain sections has been attempted, however existing anti-ADH5 antibodies suffer from non-specific binding (Burgos-Barragan, 2017). Non-specific ADH isoforms can be excluded from western blot analysis based on size, but this is not possible for immunohistochemical assays. Ongoing work is underway to utilise spatial techniques to check ADH5 expression in immune cells and exclude the possibility of rare rescue events in non-haematopoietic cells.

In summary, my research demonstrates the critical role of systemic clearance in protecting the kidney and brain from formaldehyde-induced damage. While the precise source of formaldehyde remains uncertain, studies suggest that both systemic and tissue-specific sources contribute to overall formaldehyde burden. The possibility to use systemic route to mitigate formaldehyde toxicity presents promising therapeutic opportunities to counteract formaldehyde-associated degeneration.

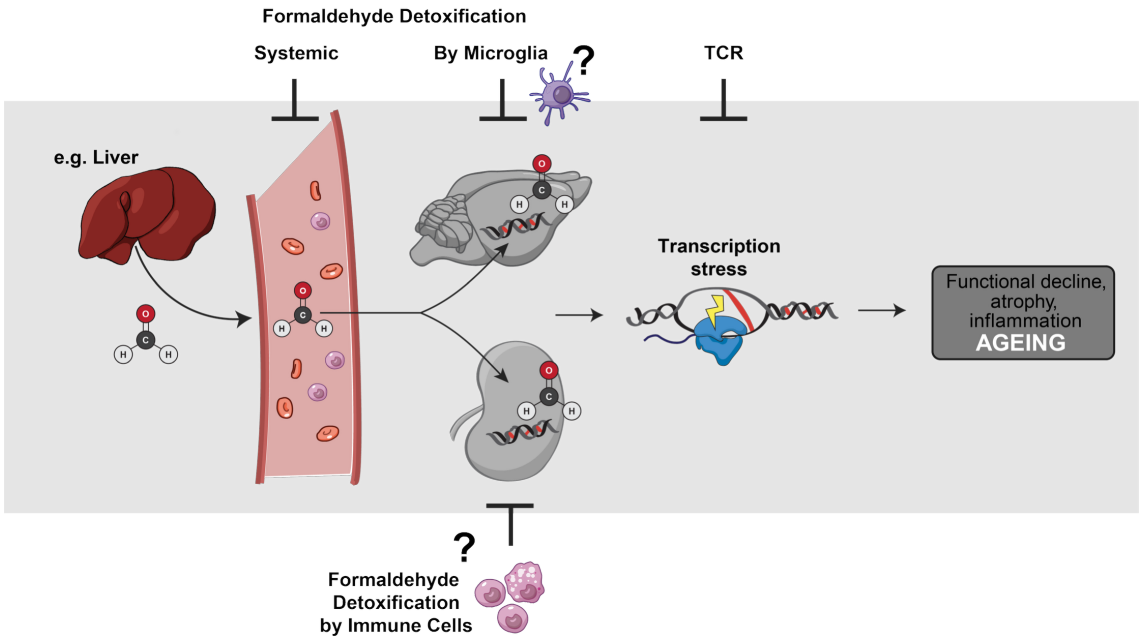

Figure 5.5. Model for the contribution of haematopoietic formaldehyde detoxification to brain and kidney protection.

Organs such as the liver produce formaldehyde during metabolism which diffuses into the systemic circulation and is carried to other organs such as the brain and kidney. Formaldehyde damages DNA and induces transcription stress which drives dysfunction and ageing of these tissues. Detoxification of formaldehyde by haematopoietic cells in the circulation and tissue-resident immune cells can reduce kidney and brain damage and deterioration. Partially created in BioRender. Russell, H. (2026) https://BioRender.com/x8j92uu.

6 SYSTEMIC FORMALDEHYDE DETOXIFICATION DOES NOT RESCUE PERIPHERAL TISSUE DAMAGE IN FANCONI ANAEMIA MICE

My analysis of *Adh5*$^{sw/-}$*Csb*$^{-/-}$ *Vav1-iCre* mice has shown that systemic detoxification protects the brain and kidney from formaldehyde-driven DNA damage. This prompts the question whether other organs are also protected this way. For instance, the liver is a key metabolic organ (Alamri, 2018) and a site of high rates of formaldehyde accumulation. Indeed, DNA from adult ADH5-deficient mouse livers contains approximately 10,000 formaldehyde adducts per genome – twice the amount found in ADH5-deficient brain tissue (Fig. 5.1C).

The liver has a unique dual blood supply system supported by the hepatic artery and the portal vein (Kan & Madoff, 2008). Like in the brain and kidney, could formaldehyde detoxification provided by the systemic circulation protect this organ? My measurement of formaldehyde-DNA adducts in ADH5 blood-rescue mice showed some reduction of formaldehyde burden in the liver, though this effect was only moderate and fell short of statistical significance (Fig. 5.1C). To robustly test whether systemic formaldehyde clearance protects liver cells from deterioration requires a model with a significant liver phenotype that could be then rescued. Aged (18 months) *Adh5*$^{-/-}$*Csb*$^{-/-}$ mice show only modest phenotype in the liver, including reduced serum albumin levels and a mild increase in nuclear ploidy indicative of a compromised synthetic function and presence of genotoxic stress, respectively (Mulderrig et al., 2021). On the other hand, *Adh5*$^{-/-}$

Fancd2$^{-/-}$ mice present with much more severe liver defect (Pontel et al., 2015). Hepatocytes accumulate high levels of DNA damage, and develop striking nuclear hyperpolyploidy, with ~20% of nuclei harbouring 16 copies of each chromosome by 4-6 weeks of age. This coincides with elevated levels of serum aspartate aminotransferase (AST) and alanine transaminase (ALT), markers of liver damage, and decreased albumin synthesis.

Importantly, the phenotype of *Adh5*$^{-/-}$*Fancd2*$^{-/-}$ mice extends beyond the liver as these animals develop defects in other tissues (*e.g.*, the kidney), distinct from those seen in *Adh5*$^{-/-}$*Csb*$^{-/-}$ (Mulderrig et al., 2021; Pontel et al., 2015). Restoring formaldehyde detoxification in the blood of *Adh5*$^{-/-}$*Fancd2*$^{-/-}$ model should therefore allow us to uncover additional roles for systemic clearance in protecting peripheral organs.

It is worth mentioning that we have previously attempted to address this question in published work by Pontel et al. (2015), where we found that rescuing haematopoietic ADH5 did not preserve *Adh5*$^{-/-}$*Fancd2*$^{-/-}$ liver cells. When *Adh5*$^{-/-}$*Fancd2*$^{-/-}$ mice were transplanted with wild-type bone marrow they still developed extensive hepatocellular ploidy and sustained elevated levels of AST and ALT. However, this approach had several limitations. First, due to the fragility of these mice and to avoid confounding DNA damage, transplantation had to be performed without conditioning – a process which normally uses irradiation or chemotherapy to ablate recipient bone marrow to allow donor cells to engraft (Zulu & Kenyon, 2018). This meant that only few mice (6 out of 33 transplanted) had undergone successful reconstitution, with the rest developing bone marrow failure due to lack of engraftment. Second, transplantation was performed in 3–4-week-old *Adh5*$^{-/-}$*Fancd2*$^{-/-}$ mice. At this stage, significant liver damage has already occurred, and therefore liver cells may have further deteriorated regardless of the haematopoietic rescue. Our current strategy – the use of the *Adh5* 'switch' allele in *Fancd2*-deficient background – should allow us to overcome these limitations, by avoiding the confounding effects of transplantation and by rescuing blood early during embryonic development.

Furthermore, the *Adh5*$^{sw/-}$*Fancd2*$^{-/-}$ *Vav1-iCre* model has the potential to reveal novel phenotypes associated with two-tier deficiency. We have previously shown that the Fanconi Anaemia repair pathway is crucial for repairing formaldehyde-driven damage in highly replicative HSCs and blood progenitors (Langevin et al., 2011; Pontel et al., 2015). In *Adh5*$^{-/-}$*Fancd2*$^{-/-}$ mice, loss of these cells halts blood production and drives bone marrow failure by 4-6 weeks of age. Like the haematopoietic system, the gastrointestinal tract is highly proliferative, uses a stem cell pool to regenerate progenitors which then replace the intestinal lining every 3-4 days (Reynolds et al., 2014). It is therefore very likely that, also in this context, replication-coupled repair of formaldehyde-induced DNA damage plays an important role in maintaining tissue homeostasis, but the impact of ADH5/FANCD2 deficiency on the GI tract has never been studied, mainly due to early deterioration of *Adh5*$^{-/-}$*Fancd2*$^{-/-}$ mice (Pontel et al., 2015). Similarly, the effect of hepatocellular hyperpolyploidy on liver function is not known, but the short lifespan of *Adh5*$^{-/-}$ *Fancd2*$^{-/-}$ mice limits the use of this model for further studies. While polyploidisation is a conserved physiological process in hepatocytes, it has also been linked to chronic liver disease and cancer (Donne et al., 2021; Duncan et al., 2010; Gentric et al., 2015; Kudryavtsev et al., 1993; Wang et al., 2017). It is therefore unclear whether polyploidisation, especially in the context of chronic DNA damage, is a pathogenic or protective mechanism. If *Adh5*$^{sw/-}$*Fancd2*$^{-/-}$ *Vav1-iCre* mice still show hyperpolyploidy in the liver, it would be interesting to assess the effect of this process on liver function as the mice age.

To summarise, restoring systemic clearance of formaldehyde will allow the study of long-latency phenotypes of *Adh5*$^{-/-}$*Fancd2*$^{-/-}$ deficiency and reveal new roles for the Fanconi's Anaemia pathway in protecting tissues from formaldehyde.

6.1 Restoring ADH5 expression in blood partially rescues developmental defects in ADH5/FANCD2-deficient mice

To generate *Adh5*$^{sw/-}$*Fancd2*$^{-/-}$ *Vav1-iCre* mice, we have crossed *Adh5*$^{sw/sw}$*Fancd2*$^{+/-}$ C57B6L mice with *Adh5*$^{-/-}$*Fancd2*$^{+/-}$ *Vav1-iCre S6129*/*sv* breeders (Fig. 6.1A). We and others have previously

observed that *Fancd2* knockout was much better tolerated on a mixed C57B6L x S6129/sv background than in pure C57BL mice, with homozygous mutants born at expected Mendelian ratios (Houghtaling et al., 2003; van de Vrugt et al., 2009). Additionally, *Adh5*$^{-/-}$ *Fancd2*$^{-/-}$ mice were not viable in the pure C57B6L background but born at sub-Mendelian ratios from C57B6L x S6129/sv crosses (Pontel et al., 2015). Consistent with this, only 2.4% of the genotyped F1 pups (2-3 weeks old) produced from our experimental cross were globally deficient in ADH5 and FANCD2 (*Adh5*$^{-/sw}$*Fancd2*$^{-/-}$) (Fig. 6.1A). *Adh5*$^{-/sw}$*Fancd2*$^{-/-}$ *Vav1-Cre* pups were born at improved frequency (4.3%) albeit still below the expected Mendelian ratios (Fig. 6.1A). Moreover, *Adh5*$^{sw/-}$*Fancd2*$^{-/-}$ *Vav1-iCre* mice were significantly larger than *Adh5*$^{sw/-}$*Fancd2*$^{-/-}$ post weaning (>5-weeks old) (Fig. 6.1B), but remained smaller than controls, indicating only partial rescue of the developmental defects associated with two-tier deficiency.

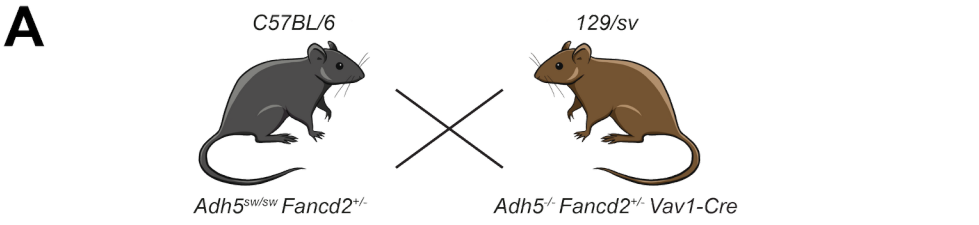

		Adh5sw/- Fancd2+/-	Adh5sw/- Fancd2+/+	Adh5sw/- Fancd2-/-	
	Exp.	25%	12.5%	12.5%	
	Obs.	31.7% n = 248/783 (129F 119M)	16.4% n = 128/783 (73F 55M)	2.4% n = 19/783 (12F 7M)	P<0.0001
Vav1-iCre	Obs.	30.1% n = 236/783 (111F 125M)	15.1% n = 118/783 (65F 53M)	4.3% n = 34/783 (16F 18M)	

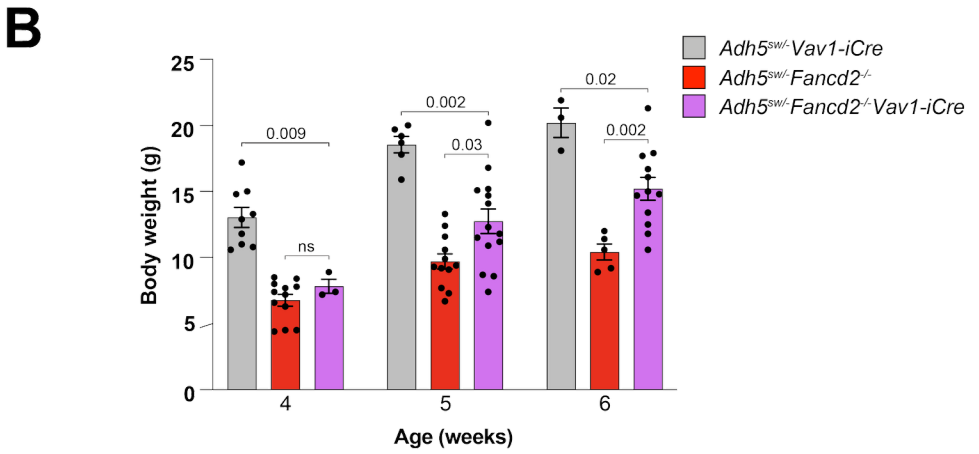

Figure 6.1 Restoring ADH5 expression in blood partially rescues developmental defects in ADH5/FANCD2-deficient mice.

A) Breeding crosses of *Adh5$^{sw/sw}$ Fancd2$^{+/-}$* and *Adh5$^{-/-}$Fancd2$^{+/-}$ Vav1-iCre* mice in a C57BL/6 x 129/sv background with observed numbers of male (M) and female (F) pups genotyped 2-3 weeks after birth. FANCD2/ADH5-deficient mice are born at sub-mendelian ratios. P value calculated by Fisher's exact test. **B)** Average body weight of juvenile mice. Dots denote individual mice. Error bars indicate standard error of the mean. P value calculated by Mann-Whitney U.

6.2 *Adh5$^{sw/-}$Fancd2$^{-/-}$ Vav1-iCre* mice lose HSCs prenatally but maintain blood production for up to 1 year

I first aimed to confirm that rescuing ADH5 expression by *Vav1-iCre* prevents the HSC loss and bone marrow failure that occurs in ADH5/FANCD2-deficient mice. To do this, I stained foetal liver or adult bone marrow from *Adh5$^{sw/-}$Fancd2$^{-/-}$ Vav1-iCre* mice (and controls) with antibodies against immunophenotypic markers of HSCs and blood progenitor populations and performed flow cytometry analysis to examine their proportions. HSCs first emerge at embryonic day 10.5 (E10.5) from the aorta-gonad-mesonephros (AGM) region, before migrating to the foetal liver at E11 where haematopoiesis persists until migration to the bone marrow at E15.5 – 17.5 (Mahony & Bertrand, 2019) (Fig. 6.2A). Surprisingly, I found that the proportion of foetal liver HSCs at E13.5 was markedly depleted in *Adh5$^{sw/-}$ Fancd2$^{-/-}$ Vav1-Cre* mice, to the same degree as in constitutive double-mutant mice (Fig. 6.2B). These HSCs remained undetected in the adult bone marrow (Fig. 6.2C), though the proportions of downstream haematopoietic progenitors (ST-HSCs, MPPs, CMPs, MEPs, GMPs, CLPs) were significantly rescued in *Adh5$^{sw/-}$Fancd2$^{-/-}$ Vav1-Cre* mice compared to *Adh5$^{sw/-}$Fancd2$^{-/-}$* controls (Fig. 6.2C-D). These progenitors appeared sufficient to maintain multilineage blood production throughout the lifespan of *Adh5$^{sw/-}$Fancd$^{-/-}$ Vav1-Cre* animals (12-57 weeks-old), with only 3 out of 17 mice exhibiting anaemia (as defined by red blood cell count < 5 cells (x10^6) per mm^3) (Fig. 6.2E). This unexpected result provides unique insight into the requirements for formaldehyde detoxification during haematopoiesis. Lineage tracing studies have shown that *Vav1* expression begins at E11.5 of embryogenesis, meaning ADH5 expression will be absent in all *Adh5$^{sw/-}$Fancd2$^{-/-}$ Vav1-Cre* tissues until this point. It is likely that the loss of HSCs observed at E13.5 (Fig. 6.2B) occurs during this period (E10.5 – E11.5), indicating that formaldehyde detoxification is crucial at the point of HSC emergence. Once *Vav1* (and ADH5) expression activates, formaldehyde detoxification would protect the remaining progenitor cells, likely explaining the rescue observed in these populations (Fig. 6.C, F).

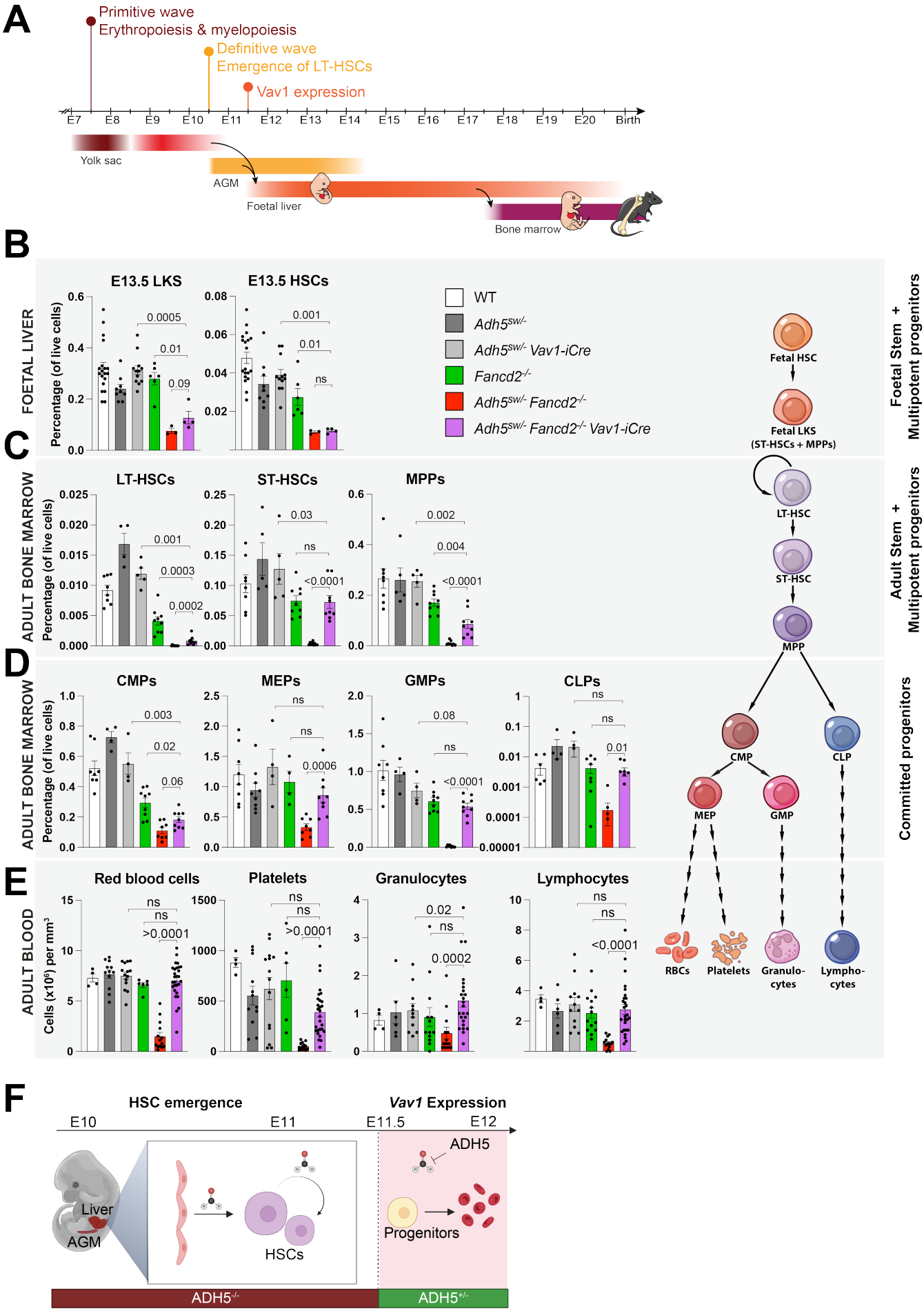
A
Primitive wave
Erythropoiesis & myelopoiesis
Definitive wave
Emergence of LT-HSCs
Vav1 expression
E7 E8 E9 E10 E11 E12 E13 E14 E15 E16 E17 E18 E19 E20 Birth
Yolk sac
AGM
Foetal liver
Bone marrow
B
FOETAL LIVER
E13.5 LKS
E13.5 HSCs
Percentage (of live cells)
WT
Adh5sw/-
Adh5sw/- Vav1-iCre
Fancd2-/-
Adh5sw/- Fancd2-/-
Adh5sw/- Fancd2-/- Vav1-iCre
Fetal HSC
Fetal LKS (ST-HSCs + MPPs)
Foetal Stem + Multipotent progenitors
C
ADULT BONE MARROW
LT-HSCs
ST-HSCs
MPPs
LT-HSC
ST-HSC
MPP
Adult Stem + Multipotent progenitors
D
ADULT BONE MARROW
CMPs
MEPs
GMPs
CLPs
CMP
CLP
MEP
GMP
Committed progenitors
E
ADULT BLOOD
Red blood cells
Platelets
Granulocytes
Lymphocytes
Cells (x10⁶) per mm³
RBCs
Platelets
Granulo-cytes
Lympho-cytes
F
HSC emergence
Vav1 Expression
E10
E11
E11.5
E12
ADH5
Liver
AGM
HSCs
Progenitors
ADH5-/-
ADH5+/-

Figure 6.2 Rescuing haematopoietic ADH5 rescues anaemia but does not prevent embryonic HSC deficiency in ADH5/FANCD2-deficient mice.

A) Schematic of the haematopoietic development in mice. **B – E)** Average proportions of haematopoietic cells in embryonic day 13.5 foetal livers **(B)**, adult mouse bone marrow **(C-D)** or adult mouse blood **(E)**. Adult ADH5/FANCD2-deficient samples were obtained from sick 4- to 6-week-old *Adh5*$^{sw/-}$*Fancd2*$^{-/-}$ mice and from sick 12- to 57-week-old *Adh5*$^{sw/-}$*Fancd2*$^{-/-}$ *Vav1-iCre* mice. Adult controls were age matched (4 – 57 weeks old). Foetal liver and bone marrow cell quantification was done by flow cytometry. Blood cells were quantified using blood counter (Horiba). All flow cytometry populations were first gated for single live cells. LKS = Lineage- c-Kit+ Sca1+ cells, embryonic HSCs = Lineage- c-Kit+ Sca1+ CD150+ CD41- CD48-. All other populations were gated as in Fig. 4.6. Error bars denote standard error of the mean, dots indicate individual mice. P values calculated by Mann-Whitney U test. Ns = P > 0.1. F) Model of HSC depletion in *Adh5*$^{sw/-}$ *Fancd2*$^{-/-}$ *Vav1-iCre* mice. HSCs emerge from the embryonic aorta-gonad-mesonephros (AGM) at E10.5 and migrate to the foetal liver. *Vav1* expression occurs at E11.5, meaning ADH5 expression will not be rescued in *Adh5*$^{sw/-}$ *Fancd2*$^{-/-}$ *Vav1-iCre* haematopoietic cells until this point. Lack of ADH5 and FANCD2 in embryonic HSCs leads to loss of these cells due to formaldehyde damage before E11.5. After E11.5, *Vav1* drives Cre expression and rescues ADH5 in remaining HSCs and haematopoietic progenitors, allowing them to maintain downstream blood production throughout life. Created in BioRender. Russell, H. (2026) https://BioRender.com/x8j92uu

6.3 Systemic clearance of formaldehyde does not prevent liver and kidney deterioration in ADH5/FANCD2-deficient mice

Unlike *Adh5*$^{sw/-}$*Fancd2*$^{-/-}$ mice, *Adh5*$^{sw/-}$*Fancd2*$^{-/-}$ *Vav1-Cre* animals were protected against bone marrow failure (Fig. 6.2E), which allowed us to establish an ageing cohort and study additional phenotypes over time (Fig. 6.3A). Throughout the experiment, weight and body condition were monitored thrice weekly and mice were culled when they reached an endpoint (15% body weight loss, hunching, grimacing or identification of a mass). Post-mortem analysis included identification of masses/gross abnormalities, organ weighing (brain, liver, kidneys, spleen), histological examination of the kidneys, liver and GI tract, complete blood count and measurement of serum markers of liver and kidney damage.

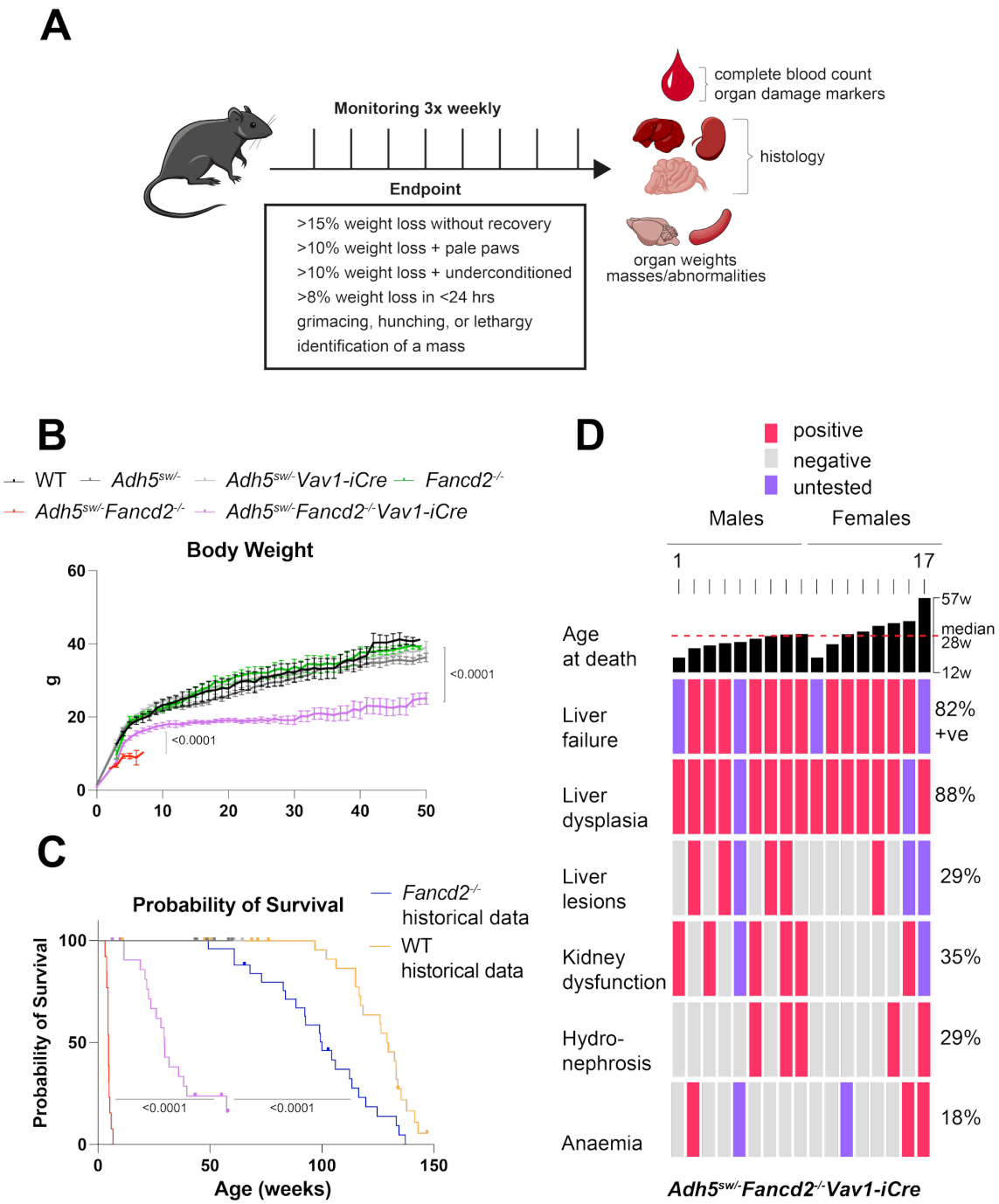

Figure 6.3. *Adh5$^{sw/-}$Fancd2$^{-/-}$ Vav1-iCre* mice survive up to 57 weeks of age and develop liver and kidney defects.

A) Experimental methodology for ageing of *Adh5$^{sw/-}$Fancd2$^{-/-}$ Vav1-iCre* mice and controls which were monitored (weighed and health checked) 3x weekly until endpoint was reached. At endpoint, necropsy was performed where gross abnormalities were noted, organs were harvested and weighed, complete blood count was performed, markers of liver and kidney damage measured in the serum, and the liver, kidney and intestinal tract histologically examined. Partially created in BioRender. Russell, H. (2026) https://BioRender.com/x8j92uu **B)** Average lifetime body weights. Error bars denote standard error of the mean. P value from mixed-effects analysis of *Adh5$^{sw/-}$Fancd2$^{-/-}$* vs *Adh5$^{sw/-}$Fancd2$^{-/-}$ Vav1-iCre* or *Adh5$^{sw/-}$Vav1-iCre* vs *Adh5$^{sw/-}$Fancd2$^{-/-}$ Vav1-iCre*. N = 21 (WT), 20 (*Fancd2$^{-/-}$*), 79 (*Adh5$^{sw/-}$*), 82 (*Adh5$^{sw/-}$ Vav1-iCre*), 21 (*Adh5$^{sw/-}$Fancd2$^{-/-}$*), 34

(*Adh5$^{sw/-}$Fancd2$^{-/-}$ Vav1-iCre*). **C)** Kaplan-Meier survival curve. P value from log-rank test. *Fancd2$^{-/-}$* and WT survival curves are from historical data in the same mouse background (Pontel et al., 2015). N = 29 (WT), 25 (*Fancd2$^{-/-}$*), 7 (*Adh5$^{sw/-}$*), 13 (*Adh5$^{sw/-}$ Vav1-iCre*), 13 (*Adh5$^{sw/-}$ Fancd2$^{-/-}$*) and 22 (*Adh5$^{sw/-}$Fancd2$^{-/-}$ Vav1-iCre*). Squares indicate censored mice. **D)** Oncoplot of phenotypes of *Adh5$^{sw/-}$Fancd2$^{-/-}$ Vav1-iCre* mice at necropsy. Red dotted line = median survival. Each bar = 1 mouse.

Adh5$^{sw/-}$Fancd2$^{-/-}$ Vav1-Cre mice were notably smaller than wild-type controls and survived on average 28-weeks - 6-times longer than *Adh5$^{sw/-}$Fancd2$^{-/-}$* mice (Fig. 6.3B,C). Only three mice (out of fifteen tested) presented with anaemia at necropsy showing that blood production was sustained in majority of mice (Fig. 6.3D). Post-mortem analysis revealed full penetrance of the liver defect phenotype. Indeed, 100% of examined *Adh5$^{sw/-}$Fancd2$^{-/-}$ Vav1-Cre* mice presented with liver dysfunction, as defined by detectable serum bilirubin (>2 U/L) or low serum albumin (< 17 g/L) (Fig. 6.3D, Fig. 6.4A). Liver damage markers - ALT and AST – were also greatly elevated in *Adh5$^{sw/-}$Fancd2$^{-/-}$ Vav1-iCre* serum compared to controls (Fig. 6.4A), confirming that rescuing haematopoietic ADH5 does not reduce liver damage in ADH5/FANCD2-deficient mice.

Importantly, *Adh5$^{sw/-}$Fancd2$^{-/-}$ Vav1-iCre* livers were similar in size compared to controls (Fig,6.4A), suggesting that liver failure was due to cellular defect rather than loss of hepatocellular mass. Both *Adh5$^{sw/-}$Fancd2$^{-/-}$* and *Adh5$^{sw/-}$Fancd2$^{-/-}$ Vav1-Cre* livers showed age-dependent hyperpolyploidisation, with liver nuclei harbouring as many as 32 copies of each chromosome when measured by flow cytometry (Fig. 6.4B-C). *Adh5$^{sw/-}$Fancd2$^{-/-}$ Vav1-Cre* livers had on average 34% of nuclei with >8N, compared to only ~1% of nuclei in controls (Fig. 6.4B). Of note, flow cytometric analysis likely underestimates the proportion of polyploid hepatocytes, as it does not exclude liver stromal cells which are mainly diploid. Indeed, by 22 weeks of age tissue histology showed that almost all *Adh5$^{sw/-}$Fancd2$^{-/-}$ Vav1-Cre* hepatocytes had grossly enlarged nuclei and cytoplasm, leading to a reduction in cell number per field compared to controls (Fig. 6.4C). The decline in *Adh5$^{sw/-}$Fancd2$^{-/-}$ Vav1-Cre* liver function may therefore be due to reduced hepatocyte number, with large hyperpolyploid cells unable to sustain organ function. Intriguingly, several of *Adh5$^{sw/-}$Fancd2$^{-/-}$ Vav1-Cre* livers had clusters of smaller cells (5 out of 14

histologically examined) (Fig. 6.4D). Determining whether these 'lesions' are composed of (pre)neoplastic cells derived from polyploid hepatocytes or are regenerative normal cells which have somehow escaped polyploidisation would require microdissection and sequencing to determine their karyotype. This work is planned and should give insight into whether liver hyperpolyploidy is a cancer-protective or pathological phenomenon.

Aside from liver failure, 35% of aged *Adh5*$^{sw/-}$*Fancd2*$^{-/-}$ *Vav1-iCre* mice developed kidney dysfunction as indicated by high creatinine and urea in terminal serum samples (Fig. 6.3D, 6.4A), indicating that rescuing ADH5 in haematopoietic cells does not prevent kidney deterioration in ADH5/FANCD2-deficient mice. Like the liver, *Adh5*$^{sw/-}$*Fancd2*$^{-/-}$ *Vav1-iCre* kidneys had increased nuclear ploidy, with an average of 40% of nuclei harbouring >2 genomic copies compared to 10% in *Adh5*$^{sw/-}$ *Vav1-iCre* controls (Fig. 6.4B). Some 8N nuclei were also detected, though ploidy did not extend beyond this. Combined with our observations in the liver, these findings indicate that formaldehyde damage promotes polyploidisation which is exacerbated in the absence of Fanconi anaemia repair.

Curiously, 29% of *Adh5*$^{sw/-}$*Fancd2*$^{-/-}$ *Vav1-iCre* mice had unilateral hydronephrosis at necropsy (Fig. 6.3B, 6.4D). Hydronephrosis occurs when urine accumulates in the kidney, causing dilation of the renal pelvis and compression of the parenchyma which can lead to atrophy, as shown in Fig. 6.4D. Known causes of hydronephrosis include urinary tract obstruction (e.g., from tumours or kidney stones), external compression (from neoplasm or inflated sperm vesicles), genetic defects in urine concentration, or congenital glomerular abnormalities. There was no evidence of external or internal urinary tract restriction during necropsy, indicating the hydronephrosis is due to an intrinsic defect in renal function or structure rather than mechanical blockage. Spontaneous hydronephrosis is a common background finding in inbred C567/B6L strains; however, in my study this phenotype was observed exclusively in *Adh5*$^{sw/-}$*Fancd2*$^{-/-}$ *Vav1-iCre* mice and not age-matched littermates (data not shown), suggesting it is specific to FANCD2/ADH5 deficiency.

Together, these findings point to significant multi-organ dysfunction in *Adh5*$^{sw/-}$*Fancd2*$^{-/-}$ *Vav1-iCre* mice, despite the rescue of haematopoietic formaldehyde detoxification, which appears insufficient to prevent deterioration of both the liver and kidneys.

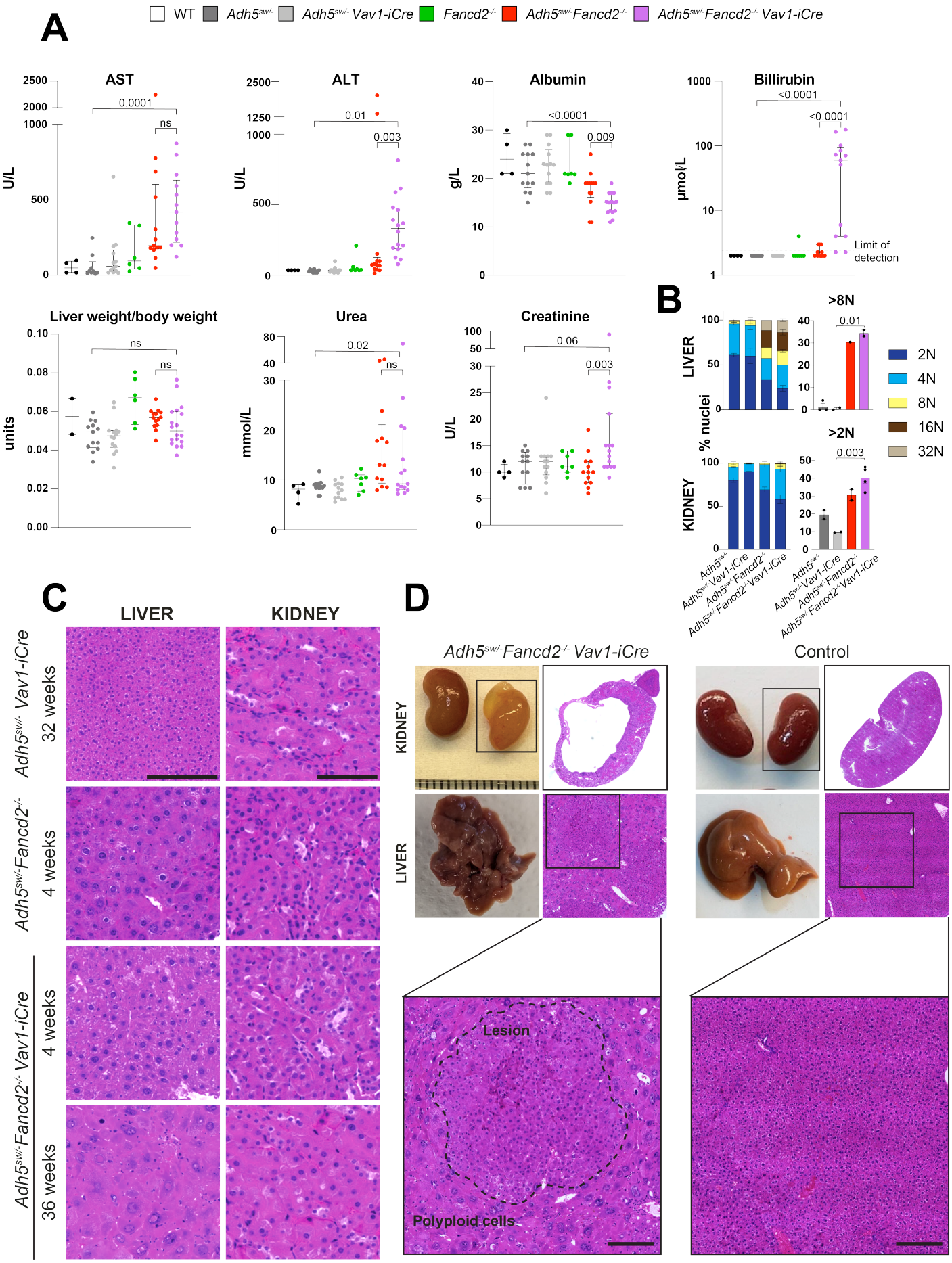
A
WT
Adh5sw/-
Adh5sw/- Vav1-iCre
Fancd2-/-
Adh5sw/-Fancd2-/-
Adh5sw/-Fancd2-/- Vav1-iCre
AST
ALT
Albumin
Billirubin
Liver weight/body weight
Urea
Creatinine
U/L
g/L
µmol/L
units
mmol/L
0.0001
ns
0.01
0.003
<0.0001
0.009
Limit of detection
0.02
0.06
B
>8N
>2N
LIVER
KIDNEY
% nuclei
2N
4N
8N
16N
32N
C
LIVER
KIDNEY
Adh5sw/- Vav1-iCre
32 weeks
Adh5sw/-Fancd2-/-
4 weeks
Adh5sw/-Fancd2-/- Vav1-iCre
4 weeks
36 weeks
D
Adh5sw/-Fancd2-/- Vav1-iCre
Control
KIDNEY
LIVER
Lesion
Polyploid cells

Figure 6.4. *Adh5$^{sw/-}$Fancd2$^{-/-}$ Vav1-iCre* mice develop liver and kidney karyomegaly and dysfunction.

A) Median level of biochemical markers in terminal mouse serum of *Adh5$^{sw/-}$Fancd2$^{-/-}$* and *Adh5$^{sw/-}$Fancd2$^{-/-}$ Vav1-iCre* mice and age-matched controls. Middle line = median. Error bars indicate interquartile range. Dots denote individual mice/N values. P value calculated by Mann-Whitney U. ns = P > 0.1. **B)** Average % of mouse kidney or liver nuclei with 2, 4, 8, 16 or 32 genomic copies per nucleus in 4-6 week old (*Adh5$^{sw/-}$Fancd2$^{-/-}$*) or 10-22 week old (all other genotypes) mice measured by nuclei isolation and flow cytometry for DNA content. Error bars denote standard error of the mean. P values calculated by Welch's t test. **C)** Representative liver and kidney sections stained with haematoxylin and eosin (H&E). Scale bar, 100 μm. **D)** Representative macroscopic pictures and H&E stained sections of hydronephrotic kidney, and liver lesions in *Adh5$^{sw/-}$Fancd2$^{-/-}$ Vav1-iCre* mice with age matched controls. Scale bar, 200 μm.

6.4 ADH5/FANCD2-deficient mice have normal intestinal epithelium

Finally, I examined the intestinal architecture and prevalence of gut stem cells and their progeny in ADH5/FANCD2-deficient mice and genotypic controls to identify if lack of formaldehyde detoxification and FA repair compromises this highly proliferative tissue. To first determine the burden of formaldehyde in this tissue, I extracted DNA from the GI tract of mice with constitutive ADH5 deficiency (*Adh5$^{sw/-}$*) or blood-specific rescue of ADH5 expression (*Adh5$^{sw/-}$ Vav1-iCre*) and used mass spectrometry to quantify the level of formaldehyde-DNA adducts (Fig. 6.5A). Compared to controls, both *Adh5$^{sw/-}$* and *Adh5$^{sw/-}$ Vav1-iCre* mice had significantly increased formaldehyde-DNA adducts in the GI tract, with *Adh5$^{sw/-}$* mice harbouring ~900 (small intestine) to ~1500 (stomach) adducts per genome, compared to 500 – 1000 in *Adh5$^{sw/-}$ Vav1-iCre* mice (Fig. 6.5A). This suggests that the GI tract encounters formaldehyde which can be partially, but not fully, detoxified by systemic ADH5.

I next sought to determine whether damage caused by formaldehyde leads to impairment of the gut in the absence of FA repair. To this end, the proximal small intestine from *Adh5$^{sw/-}$Fancd2$^{-/-}$*, *Adh5$^{sw/-}$Fancd2$^{-/-}$ Vav1-iCre* mice and genotypic controls was dissected from 4-week old animals, fixed and stained (using immunohistochemistry or RNAscope) for markers of intestinal stem cells (OLFM4), paneth cells (lysozyme), goblet cells (alcian blue staining) and apoptotic or proliferative markers (cleaved PARP-1, KI67). The longer lifespan of *Adh5$^{sw/-}$Fancd2$^{-/-}$ Vav1-*

iCre mice compared to constitutive double knockouts also provided an opportunity to examine the guts of older FANCD2/ADH5-deficient mice (and age-matched controls) to determine whether any age-associated phenotype emerged.

Prior studies have shown that DNA damage caused by irradiation or chemotherapy leads to profound loss of OLFM4+ stem cells, as well as reduced proliferation, indicated by a decrease in KI67 expression, and loss of paneth and goblet cells in the rodent intestinal tract (Choi et al., 2019; Jang et al., 2022; Kwak et al., 2021; Zeng et al., 2020). This DNA damage also invokes a substantial amount of apoptosis in the GI tract, which could be measured by the expression of cleaved caspase 3 and Parp1 (Akpolat et al., 2020; S. Jeong et al., 2024). It was reasonable to expect that unrepaired DNA damage induced by formaldehyde and lack of FA repair would lead to a similar effect. However, strikingly, both *Adh5*$^{sw/-}$*Fancd2*$^{-/-}$ and *Adh5*$^{sw/-}$*Fancd2*$^{-/-}$ *Vav1-iCre* mice showed normal intestinal architecture and had similar numbers of stem, paneth or goblet cells compared to controls, even upon ageing of *Adh5*$^{sw/-}$*Fancd2*$^{-/-}$ *Vav1-iCre* mice to 38 weeks (Fig. 6.5B). FANCD2/ADH5-deficient mice also showed no increase in apoptotic or proliferative markers compared to controls, indicating there was no increase in cell death or compensatory proliferation (Fig. 6.6A).

Finally, I sought to examine the prevalence of revival stem cells (RevSc). Whilst OLFM4 is a marker of the proliferative, LGR5-expressing (LGR5+), intestinal stem cell population, studies have identified clusterin as a marker of quiescent gut stem cells which can proliferate and regenerate the gut upon injury (Ayyaz et al., 2019; Shapiro et al., 2015). It has been proposed that these stem cells are more resistant to DNA damage induced by chemo- or radiotherapy, and can repopulate all intestinal epithelial cells, including LGR5+ stem cells, following their ablation (Ayyaz et al., 2019). It is therefore plausible that this backup stem cell population may have escaped formaldehyde-induced replication stress and could be responsible for maintaining gut homeostasis in ADH5/FANCD2-deficient mice. However, *clusterin* staining by RNAscope was minimal in these mice and indistinguishable between the genotypes (Fig. 6.6B). Together, these analyses demonstrate that, remarkably, despite having an increased formaldehyde burden and

lacking the ability to repair formaldehyde damage via FA repair, ADH5/FANCD2-deficient mice have no significant defect in gut epithelium.

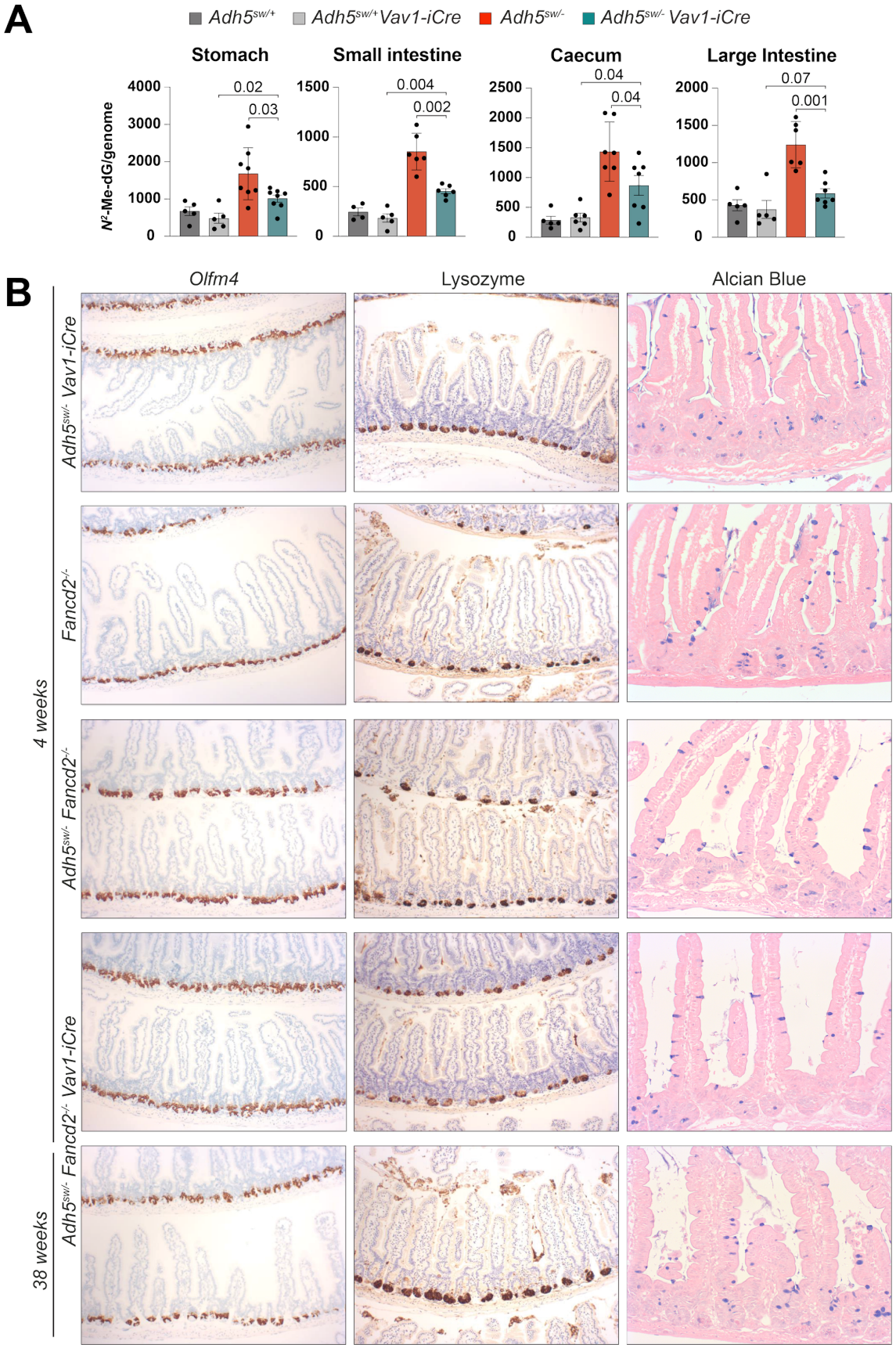
A
Adh5sw/+
Adh5sw/+Vav1-iCre
Adh5sw/-
Adh5sw/-Vav1-iCre
Stomach
Small intestine
Caecum
Large Intestine
N2-Me-dG/genome
0.02
0.03
0.004
0.002
0.04
0.04
0.07
0.001
B
Olfm4
Lysozyme
Alcian Blue
Adh5sw/- Vav1-iCre
Fancd2-/-
Adh5sw/- Fancd2-/-
Adh5sw/- Fancd2-/- Vav1-iCre
4 weeks
38 weeks

Figure 6.5. FANCD2/ADH5-deficient mice do not have reduced intestinal stem, Paneth or goblet cells despite significant formaldehyde burden.

A) Average levels of N^2-methyldeoxyguanine per genome in the gastrointestinal tract of 6-week-old mice. Dots denote individual mice. Error bars indicate standard error of the mean. P value from Mann-Whitney U test. B) Mouse small intestine sections stained with alcian blue (to identify goblet cells), anti-lysozyme antibody (Paneth cells) or RNAscope probes for *Olfm4* mRNA (stem cells) imaged at 20x (*Olfm4*, lysozyme) or 40x (alcian blue) magnification. *Olfm4*-expressing cells, lysozyme expressing cells or alcian blue-positive cells are stained brown, brown or blue (from left to right). Sections were counterstained with haematoxylin (blue) for *Olfm4* and lysozyme-stained sections, or eosin (pink) for alcian blue-stained sections. Images obtained by Rachel Ridgeway (Sansom lab, Glasgow).

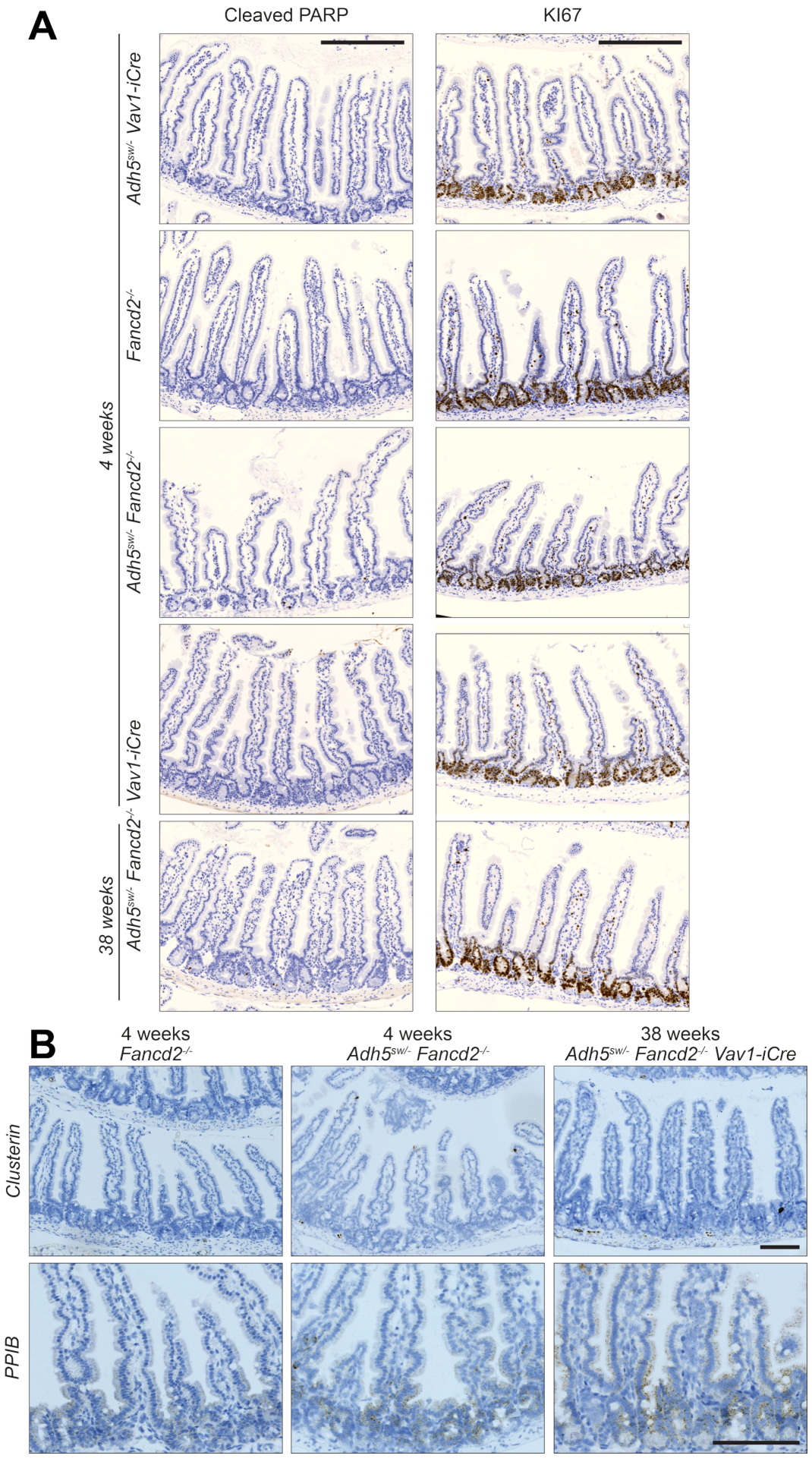
A
Cleaved PARP
KI67
Adh5sw/- Vav1-iCre
Fancd2-/-
Adh5sw/- Fancd2-/-
Vav1-iCre
Adh5sw/- Fancd2-/-
4 weeks
38 weeks
B
4 weeks
Fancd2-/-
4 weeks
Adh5sw/- Fancd2-/-
38 weeks
Adh5sw/- Fancd2-/- Vav1-iCre
Clusterin
PPIB

Figure 6.6 FANCD2/ADH5-deficient mice do not have increased levels of apoptosis, proliferation or revival stem cells in the gut epithelium.

Small intestine sections of indicated genotypes stained with haematoxylin (blue) and A) antibodies against cleaved PARP or KI67 B) RNAscope probes binding *Clusterin* mRNA or *PPIB* mRNA (positive control RNA staining). Scale bar = 200 μm. Brown = cleaved PARP, KI67, *Clusterin* or *PPIB*.

6.5 Discussion

I have generated a novel mouse model which globally lacks both tiers of protection against formaldehyde – detoxification and repair – but retains detoxification capacity in haematopoietic tissues. The use of the Lox-Cre system allows ADH5 re-expression as early as E11.5 in *Vav1*-expressing haematopoietic cells (Bustelo et al., 1993; Ogilvy et al., 1999), providing a clean way to examine the contribution of haematopoietic formaldehyde detoxification to organ protection without the confounding effect of bone marrow transplantation. Rescuing haematopoietic ADH5 alleviated the juvenile bone marrow failure that occurs in ADH5/FANCD2-deficient mice, allowing for the mice to be aged and additional phenotypes of two-tier deficiency explored. This provided a unique opportunity to examine which tissues rely on Fanconi's anaemia pathway to repair formaldehyde damage and raised intriguing insights for further studies.

6.5.1 Cell-intrinsic formaldehyde detoxification is required for HSCs protection from the point of emergence

Previous work from our lab showed that inactivation of both tiers of protection against formaldehyde leads to catastrophic loss of haematopoietic cells in mice (Langevin et al., 2011; Pontel et al., 2015). Indeed, mice lacking FANCD2 and either of the enzymes responsible for formaldehyde breakdown - mitochondrial ALDH2 (*Aldh2*$^{-/-}$*Fancd2*$^{-/-}$) or cytoplasmic ADH5 (*Adh5*$^{-/-}$*Fancd2*$^{-/-}$) - completely lacked functional HSCs. Garaycoechea et al. revealed that this HSC depletion begins in *Aldh2*$^{-/-}$*Fancd2*$^{-/-}$ embryos between E13.5 and E18.5 (Garaycoechea et al., 2018). At E13.5, *Aldh2*$^{-/-}$*Fancd2*$^{-/-}$ foetal liver HSCs were not impaired in number or ability to repopulate the bone marrow of irradiated mice. However, by E18.5, *Aldh2*$^{-/-}$*Fancd2*$^{-/-}$ mice had no detectable HSCs in the bone marrow. This highlighted the importance of formaldehyde

detoxification in HSCs during this developmental window, but also raised the question of why HSCs are not lost earlier. My work helps address this question by showing that ADH5 is the primary formaldehyde detoxifier required during early HSC emergence (Fig. 6.2). Published lineage tracing studies have shown that *Vav1-iCre* expression occurs after E11.5 (de Boer et al., 2003). I found that by E13.5, HSCs in *Adh5*$^{sw/-}$*Fancd2*$^{-/-}$ *Vav1-iCre* foetal livers are significantly depleted (Fig. 6.2B). Therefore, loss of the HSC pool must primarily occur between E10.5, when HSC are formed, and E13.5, likely in the small window of time before expected ADH5 rescue around E11.5 (Fig. 6.2F). My data supports this model, though it would be worth performing additional western blots and flow cytometric analyses of the *Adh5*$^{-/-}$*Fancd2*$^{-/-}$ *Vav1-iCre* foetal liver to confirm that ADH5 is indeed reactivated around E11.5, and that HSC loss truly occurs at this timepoint.

Nonetheless, my data shows that HSCs in *Adh5*$^{-/-}$*Fancd2*$^{-/-}$ *Vav1-iCre* mice are lost by E13.5, almost as soon as they emerge (Fig. 6.3B). So, what makes HSCs so exquisitely sensitive to formaldehyde? It has been speculated that HSCs have reduced tolerance for DNA damage compared to other cell types (Biechonski et al., 2017, 2018). Studies have shown that HSCs have increased P53 expression compared to downstream progenitors (Y. Liu et al., 2009) and exhibit increased apoptosis in response to DNA damaging agents such as ionising radiation (Milyavsky et al., 2010). In *Aldh2*$^{-/-}$*Fancd2*$^{-/-}$ mice, a concomitant knockout of P53 (*Aldh2*$^{-/-}$*Fancd2*$^{-/-}$*Trp53*$^{-/-}$) completely alleviates the HSC loss and restores their functional capacity. This indicates that, at least in *Aldh2*$^{-/-}$*Fancd2*$^{-/-}$ HSCs, P53 mediates cell loss in response to aldehyde damage. Since fboth ADH5 and ALDH2 detoxify formaldehyde, it is likely that ADH5/FANCD2-deficient mice lose HSCs through the same mechanism, but at an earlier developmental stage (E10.5-E11.5). The temporal differences in reliance on ADH5 or ALDH2 in FANCD2-deficiency could be attributed to niche-specific differences in formaldehyde burden at the different stages of HSC development. For instance, the cytoplasmic formaldehyde load may be higher in HSCs in the foetal liver between E10.5 – 15.5, or during migration through the aorta at E15.5 – 17.5, necessitating detoxification by ADH5. Meanwhile, mitochondrial formaldehyde detoxification

through ALDH2 may be more important during development in the foetal bone marrow at 18.5, perhaps owing to a shift in metabolism. Further investigation is ongoing to interrogate these possibilities that my work has informed and validate our model of the depletion of emerging HSCs in response to formaldehyde damage.

6.5.2 Haematopoietic formaldehyde detoxification is insufficient to prevent liver and kidney deterioration in ADH5/FANCD2-deficient mice

Prior work from our lab showed that transplanting WT bone marrow into *Adh5*$^{-/-}$*Fancd2*$^{-/-}$ mice did not ameliorate liver damage (Pontel et al., 2015), however technical limitations of this approach necessitated further validation of this result. Here, using mouse genetics, I confirmed that liver damage associated with ADH5/FANCD2-defiency occurs even if haematopoietic formaldehyde detoxification is restored early during development (Fig. 6.4). This indicates that most formaldehyde in this organ comes from tissue-intrinsic sources and cannot be sufficiently detoxified by blood. As noted earlier, the liver plays a key role in folate metabolism during the one-carbon cycle, which produces formaldehyde as a by-product (Burgos-Barragan et al., 2017; Steinberg, 1984; Steinberg et al., 1979). Additionally, the liver metabolizes exogenous formaldehyde sources, such as methanol, which is converted to formaldehyde in this tissue (Pocker & Li, 1991). Given its central role in metabolism and detoxification, it is likely that the liver produces formaldehyde at concentrations that cannot be mitigated by systemic detoxification alone, as shown by my data.

A more unexpected finding was that ADH5-proficient blood did not prevent kidney deterioration in *Adh5*$^{sw/-}$*Fancd2*$^{-/-}$ *Vav1-iCre* mice, unlike in *Adh5*$^{-/-}$ *Fancd2*$^{-/-}$ mice following transplantation of the WT bone marrow (Pontel et al., 2015). Indeed, *Adh5*$^{sw/-}$*Fancd2*$^{-/-}$ *Vav1-iCre* mice still exhibited kidney damage, increased tubule cell polyploidisation and, in 29% of cases, hydronephrosis (Fig. 6.3B, 6.4). This observation raises two questions: (1) why was the kidney rescued in our previous transplantation study, but not in my *Adh5*$^{sw/-}$*Fancd2*$^{-/-}$ *Vav1-iCre* mice? (2) why did rescuing haematopoietic ADH5 alleviate kidney deterioration in Cockayne syndrome

mice (*Adh5$^{sw/-}$Csb$^{-/-}$ Vav1-iCre*) but not in the Fanconi anaemia model (*Adh5$^{sw/-}$Fancd2$^{-/-}$ Vav1-iCre*)?

The first question could be explained by the duration of the experiment. In Pontel et al.'s transplantation experiment, mice were only aged for 12 weeks following transplantation (15-18 weeks of age) before requiring culling due to leukaemia. In contrast, *Adh5$^{sw/-}$Fancd2$^{-/-}$ Vav1-iCre* mice survived as long as 57-weeks (Fig. 6.3B, C). This significantly extended lifespan allows more time for formaldehyde damage to accumulate, perhaps surpassing a threshold of damage that results in cell death/dysfunction, or exhausting kidney regenerative capacity. To validate this, urea and creatinine should be analysed at additional timepoints in *Adh5$^{sw/-}$Fancd2$^{-/-}$ Vav1-iCre* mice to confirm whether the kidney indeed deteriorates as a function of time.

The second question – why the kidney deterioration was rescued in *Adh5$^{sw/-}$Csb$^{-/-}$ Vav1-iCre* but not in *Adh5$^{sw/-}$Fancd2$^{-/-}$ Vav1-iCre* mice – might be explained by the different cell-types affected in each model. In ADH5/CSB-deficient mice, formaldehyde damage precipitates in the proximal tubule cells, which display interstitial nephritis and unique transcriptional upregulation of injury-associated, inflammatory, and integrated stress response genes (Mulderrig et al., 2021). Conversely, whilst ADH5/FANCD2-deficient mice show some polyploidisation of tubule cells indicative of damage (Fig. 6.4B, C), podocytes - a key population in the kidney glomerulus responsible for blood filtration into the nephron – are also affected in this model (Pontel et al., 2015). As result, mice develop proteinuria (characterised by presence of protein in the urine), an inability to filter out proteins from the urinary space. Thus, TCR is crucial for repairing formaldehyde damage in proximal tubule cells, whilst FA repair is important for formaldehyde-induced damage repair in both tubule cells and podocytes. This damage to both cell types may not be sufficiently ameliorated by blood formaldehyde clearance.

Finally, it is worth considering that some of the kidney deterioration in *Adh5$^{sw/-}$Fancd2$^{-/-}$ Vav1-iCre* mice could be a result of the failing liver, rather than direct formaldehyde damage to this organ. Hepatorenal syndrome occurs in advanced liver disease, when reduced hepatic function

causes vasoconstriction of renal blood vessels and reduces glomerular filtration rate, increasing the level of waste products in the serum such as creatinine and urea (Baraldi et al., 2015; Ranasinghe et al., 2025). Some of the elevation of these waste products in *Adh5$^{sw/-}$Fancd2$^{-/-}$ Vav1-iCre* mice may be a result of this (Fig. 6.4A), as well as the hydronephrosis, which has been associated with liver dysfunction in mice (Nemoto et al., 2024). Determining if this is the case would require decoupling the two organs. Our lab has developed a mouse model which has liver-specific deficiency in FANCD2 and ADH5, whilst other organs remain ADH5-proficient. If these liver-specific ADH5/FANCD2-knockout mice also develop kidney dysfunction, this will indicate that liver deterioration contributes to the kidney decline of ADH5/FANCD2-deficient mice and explain the lack of rescue of kidney deterioration in the *Adh5$^{sw/-}$Fancd2$^{-/-}$ Vav1-iCre* model.

6.5.3 ADH5/FANCD2 deficiency increases nuclear ploidy and causes liver dysfunction

A striking phenotype in *Adh5$^{sw/-}$Fancd2$^{-/-}$ Vav1-iCre* mice was the nuclear hyperpolyploidy which occurred in some kidney tubule cells, but most prominently in the liver, with almost all hepatocytes having enlarged nuclei containing up to 32 copies of each chromosome (Fig. 6.4B, C). Nuclear polyploidy occurs when cells harbour multiple whole genome copies within a single nucleus, and is distinct from cellular polyploidy, in which cells contain multiple nuclei (Fang et al., 2022). The liver is a site of physiological polyploidisation, with 70-90% of rodent hepatocytes becoming polyploid by adulthood, and 30% in humans (Wang et al., 2017). However, the balance between cell division and cell polyploidisation is tightly controlled, with hepatocytes dividing infrequently to retain cellular mass, and nuclear ploidy rarely extending beyond 8N under normal conditions. In my *Adh5$^{sw/-}$Fancd2$^{-/-}$ Vav1-iCre* mice this balance appears to have been tipped towards polyploidisation over cell division, leading to increased cell size at the expense of cell number. What is it about FANCD2/ADH5-deficiency that disrupts this balance? One logical explanation is that cells cannot divide due to persistent DNA damage. FA repair is responsible for both DNA-crosslink repair and resolution of stalled replication forks (Ceccaldi et al., 2016;

Schwab et al., 2015). Defects in this repair pathway cause increased replication fork stalling and replication stress, resulting in cell cycle checkpoint activation and arrest during S/G2 (Okamoto et al., 2021; Peña-Gómez et al., 2022). Prolonged S/G2 arrest has been shown to cause cell cycle exit (Feringa et al., 2018). In most cells, exit from cell cycle with extra genomic copies activates the tetraploid checkpoint which initiates a signalling cascade that converges on cell senescence or apoptosis (Andreassen et al., 2001; Zhao & Guan, 2014). However, in hepatocytes this response seems to be attenuated, allowing polyploid cells to persist and retain their proliferative capacity. In ADH5/FANCD2-deficient livers (Guidotti et al., 2003), hepatic mass is therefore maintained by hepatocytes that undergo multiple rounds of whole-genome duplication events without cytokinesis (Margall-Ducos et al., 2007).

This observation poses several interesting questions. First, how is this drastic level of nuclear ploidy arising? Nuclear polyploidy can arise by two main mechanisms: (1) through mitotic slippage, wherein cells enter the M phase but do not complete chromosome segregation and exit mitosis without karyokinesis or (2) through endoreduplication, in which cells undergo repeated cycles of G1/S/G2 transitions without entering mitosis. The former is believed to be the mechanism of physiological polyploidisation of hepatocytes, alongside cytokinesis failure which leads to emergence of binucleated cells (and therefore contributes to an increased cellular ploidy rather than nuclear ploidy) (Wang et al., 2017). Ploidy induced by replication-stalling DNA damage is more likely to occur via the latter mechanism – endoreduplication – due to checkpoint activation preventing entry into mitosis (Gandarillas et al., 2018; Molinuevo et al., 2024; Zheng et al., 2012). Unpublished results from a related project in the lab support this idea and show that ADH5/FANCD2-deficient mouse hepatocytes frequently skip mitosis. This means that DNA damage-induced polyploidy occurs via distinct mechanism to physiological ploidy.

Crucially, I have shown that *Adh5*$^{sw/-}$*Fancd2*$^{-/-}$ *Vav1-iCre* livers become almost uniformly hyperpolyploid (as shown by histology), show progressive decline in function, and eventually fail (Fig. 6.4A, B, C). *Adh5*$^{sw/-}$*Fancd2*$^{-/-}$ *Vav1-iCre* livers are functionally compromised despite the conservation of liver mass, suggesting that failure is due to hepatocyte dysfunction rather than

loss of tissue (Fig. 6.4A). However, it is unclear whether ploidy is a causative factor in these circumstances, or an adaptive response. In other words, we cannot rule out that ploidy may simply be a side effect of DNA damage rather than the direct cause of liver dysfunction in this model. To decouple these two processes, our lab is developing mouse models to suppress polyploidy in ADH5/FANCD2 deficiency and assess whether this alleviates liver phenotype.

Why might polyploid cells have reduced function? It may be that at this dramatic level of chromosome amplification (16-32N), the amounts of RNA polymerase and transcription factors become limiting, leading to dysregulation of transcription. Additionally, polyploid cells often harbour under-replicated genomic regions, leading to loss of some genes and alterations in gene dosage (Hua & Orr-Weaver, 2017). This dysregulation of gene expression may inhibit essential hepatocyte functions. Indeed, a prior study has indicated that polyploid cells have a reduced maximal metabolic rate, with species with higher ploidy having a lower metabolic scope (Vinogradov et al., 2001). In wild-type animals, which this study examined, on average 10% of hepatocytes were polyploid. In this situation, the reduced metabolic output of these polyploid cells could be easily compensated for by diploid cells. However, aged *Adh5*$^{sw/-}$*Fancd2*$^{-/-}$ *Vav1-iCre* livers were almost uniformly polyploid, and their combined deficiency in metabolic output may culminate in organ failure. Additionally, we are in the process of examining ADH5/FANCD2-deficient livers for markers of senescence – a state which polyploidy has been associated with (Hayashi et al., 2024; Johmura et al., 2014; Takahashi et al., 2006). It could be that the level of genome duplication in *Adh5*$^{sw/-}$*Fancd2*$^{-/-}$ *Vav1-iCre* eventually surpasses a threshold to induce cell senescence; this may be an alternate explanation for the reduced function of *Adh5*$^{sw/-}$*Fancd2*$^{-/-}$ *Vav1-iCre* hepatocytes.

Curiously, some *Adh5*$^{sw/-}$*Fancd2*$^{-/-}$ *Vav1-iCre* livers contained ‘lesions’ of smaller cells, likely with reduced ploidy (Fig. 6.4D). It is possible these lesions are cancerous. Whole genome duplication is associated with many cancers and acts as a negative prognostic marker in liver cancer (Bielski et al., 2018; Bou-Nader et al., 2020). The mechanism of this is thought to be

through induction of genome instability upon mitosis entry (Lau & Poon, 2023). Cells harbouring multiple genomic copies are prone to chromosome breakages and mis-segregations during multipolar mitoses, which can lead to aneuploidy and transformation (Crasta et al., 2012; Hoffelder et al., 2004; Silkworth et al., 2009). It is plausible that attempted mitosis of these grossly polyploid *Adh5*$^{sw/-}$*Fancd2*$^{-/-}$ *Vav1-iCre* hepatocytes may have led to such a transformation.

An alternative explanation for these lesions is that they arise from cells which have somehow escaped DNA-damage induced polyploidisation. In this case, it would be interesting to identify what underpins this adaptation. Another, worrying possibility is that these 'escaped' cells have somehow reactivated ADH5 through *Vav1* expression. Whilst there is no evidence that *Vav1* is expressed in hepatocytes (de Boer et al., 2003), it would still be prudent to eliminate this possibility. To this end, we plan to extract genomic DNA from microdissected tissue and determine the genotype of the lesions using digital droplet PCR. Later, by coupling microdissection with whole genome sequencing we hope to identify whether these lesions originate from cells which have 'escaped' ploidy and/or damage, or from hyperpolyploid cells. Though outside the scope of my doctoral studies, this work should provide insight into the mechanisms of hepatocyte adaptation to chronic DNA damage.

6.5.4 The ADH5/FANCD2-deficient gut is uniquely protected against formaldehyde damage

Despite the highly proliferative nature of the intestinal tract (Reynolds et al., 2014) and the importance of FA repair in repairing formaldehyde damage in other proliferative cells, we found no evidence of any gut defect in ADH5/FANCD2-deficient mice. These mice had comparable staining for stem, paneth, and goblet cells compared to controls, and no indications of increased apoptosis or proliferation (Fig. 6.5B, Fig. 6.6A). This is surprising, especially given that adduct measurements suggest the GI tract harbours a similar formaldehyde burden to the bone marrow (Fig. 6.5A, Fig. 5.1.C).

So, what is it that makes the ADH5/FANCD2-deficient intestinal epithelium uniquely protected from the effects of formaldehyde damage, when other replicating systems fail? One possibility is the existence of a 'backup' mechanism to protect the intestinal epithelium against formaldehyde damage, such as a reserve stem cell population. However, staining for *clusterin*, expressed by these RevSc's (Ayyaz et al., 2019; Shapiro et al., 2015) showed no increase in their activation in ADH5/FANCD2-deficient mice, suggesting that this population does not play a role in gut homeostasis in our models. (Fig. 6.6B) It is possible that a different cell population might regenerate the gut epithelium after formaldehyde damage. Some studies have indeed indicated that a distinct subset of secretory progenitor cells are capable of 'de-differentiating' to replenish LGR5+ ISCs (N. Li et al., 2016; Tetteh et al., 2016; van Es et al., 2012). It would be worth performing additional examinations for markers of such populations in the FANCD2/ADH5-deficient gut to investigate this possibility.

Even if reserve populations regenerate the ADH5/FANCD2-deficient gut, it remains unclear how these cells would resist the toxic effects of replication-stalling formaldehyde damage upon cell cycle re-entry. One possibility is that the intestinal epithelium has an alternate means of repairing replication-stalling formaldehyde damage independent of FA repair. Recent findings by Sheng et al. (2020), have challenged the prevailing theory that RevSc's are DNA damage resistant due to quiescence, instead showing that a population of rapidly cycling LGR5-low/negative cells survive ionising radiation and repopulate the intestinal epithelium. Single cell RNA-sequencing revealed that this population has high expression of DNA damage response and repair genes following IR, including homologous recombination factors such as RAD51, BRCA1/2 and SMC6 (Sheng et al., 2020). Perhaps high DNA repair activity in intestinal stem cells is sufficient to resolve formaldehyde-induced damage in the absence of FA repair. Or, more tantalisingly, there may be an unexplored mechanism to resolve formaldehyde-induced DNA crosslinks in the intestinal epithelium. Further interrogation of the FANCD2/ADH5-deficient gut, for instance through

RNA-sequencing methods to identify genes upregulated in these mice, should provide answers to these questions.

A final possibility is that the level of formaldehyde damage in the intestinal cells is simply not high enough to elicit toxicity. Although formaldehyde adducts in the GI tract of ADH5-deficient mice are comparable to the bone marrow (Fig. 6.5A, Fig. 5.1C), which fails in ADH5/FANCD2-deficient mice, intestinal cells may have a higher tolerance for formaldehyde damage compared to haematopoietic cells. Indeed, other ADH5-deficient tissues, for instance the kidney vs the brain, have a substantially different formaldehyde burden which lead to toxicity in the absence of repair (Fig. 5.5C). Additional examinations, such as immunohistochemical analysis of phosphorylated P53, P21, or H2AX, would help determine if the DNA damage response is evoked in the intestinal cells of ADH5/FANCD2-deficient mice. It would also be prudent to include a positive control for DNA-damage induced intestinal dysregulation in future analyses, such as irradiated or cisplatin-treated mice, to compare the cellular response to formaldehyde vs other DNA-damaging agents and ensure the validity of staining. This work is currently in progress. Like in other tissues of the ADH5 'switch' model, spatial techniques should also be used to confirm that ADH5 is absent in the gut epithelium of *Adh5*$^{sw/-}$*Fancd2*$^{-/-}$*Vav1-iCre* mice and that the lack of phenotype isn't caused by rare recombination events restoring ADH5 expression.

In summary, rescuing haematopoietic ADH5 in ADH5/FANCD2-deficient does not rescue embryonic HSC depletion, but does rescue adult haematopoietic progenitors, preventing anaemia and allowing a 6-times longer lifespan. These mice eventually succumb to kidney and liver dysfunction, and show elevated karyomegaly in these tissues, indicating that systemic formaldehyde detoxification is insufficient to protect these organs from formaldehyde damage. Surprisingly, ADH5/FANCD2 deficient mice did not show an intestinal defect, despite the importance of FA repair in protecting against formaldehyde in other proliferative systems. This surprising result indicates that the gut niche has a distinct mechanism to protect against formaldehyde-induced damage. Determining the nature of this protection will be important for

better understanding of gut pathologies that arise in response to DNA damage, e.g. following chemotherapy or during tumorigenesis.

7 CONCLUDING REMARKS

Formaldehyde is an endogenous DNA damaging agent which promotes cancer and ageing. Production of this genotoxin is substantial in humans, with the inability to detoxify formaldehyde leading to severe outcomes including bone marrow failure, dwarfism and mental retardation (Dingler et al., 2020). Two tiers of protection are essential to mitigate these toxic effects 1) detoxification of formaldehyde (by ADH5 and ALDH2), and 2) DNA repair by the replication coupled FA pathway or by transcription coupled repair (TCR) (Dingler et al., 2020; Langevin et al., 2011; Pontel et al., 2015).

In mice lacking ADH5, deficiencies in these two repair pathways causes distinct pathological outcomes: defects in proliferative hematopoietic stem cells (caused by FA repair deficiency) and degenerative defects in non-dividing tissues such as the brain and kidney (caused by TCR deficiency). While previous work from our lab investigated FA pathway defects in hematopoietic cells, other proliferative systems, such as the gastrointestinal (GI) tract, remained unexplored. Similarly, the phenotype of other non-dividing cell types, such as quiescent adult HSCs, in Cockayne Syndrome mice, was unclear.

Additionally, the source of formaldehyde driving this tissue deterioration, and the contribution of different systems to its detoxification, was unknown. In my PhD studies, I sought to address these gaps in knowledge by investigating the tissue-specific requirements for protection against formaldehyde. I had three aims to achieve this:

Aim 1: Examine the role of TCR in repairing formaldehyde-induced damage in haematopoietic cells.

To address this, I examined the haematopoietic phenotype in *Adh5*$^{-/-}$*Csb*$^{-/-}$ mice. Sequencing of somatic mutations in these mice and genotypic controls revealed that TCR is active in HSPCs and

performs mutagenic repair of formaldehyde damage. Despite this repair activity, the absence of TCR did not compromise HSC proportions or functionality in *Adh5*$^{-/-}$*Csb*$^{-/-}$ mice, suggesting that this repair pathway is dispensable in this context. This could be due to A) tolerance of low levels of unrepaired formaldehyde damage by HSCs (e.g., in ADH5-deficiency but not concomitant ADH5/ALDH2-deficiency) B) Compensation by other repair mechanisms active in quiescence, such as GG-NER or NHEJ, or C) exit of HSCs from quiescence in response to DNA damage, allowing utilisation of FA repair. Future work should aim to resolve these three possibilities.

A surprising finding was that *Adh5*$^{-/-}$*Csb*$^{-/-}$ mice had reduced levels of proerythroblasts and erythroblasts, which likely underlies the anaemia observed in these mice. This indicates a previously unexamined importance for TCR in erythropoiesis. This could be due to a high burden of formaldehyde damage at this stage and/or a particular sensitivity to transcription stress during erythroblast differentiation. Future examination of the dynamics of nascent transcription in TCR-deficient erythroid cells will shed light on this thus far unappreciated role of TCR.

Aim 2: Understand the contribution of systemic detoxification to the protection of peripheral organs from formaldehyde damage.

Using the Lox-Cre system, we generated an ADH5-deficient mouse model in which ADH5 expression was selectively restored in haematopoietic lineages. This rescue reduced the brain and kidney deterioration in ADH5/CSB-deficient mice but did not rescue liver deterioration in ADH5/FANCD2-deficient mice. These findings give insight into the source of formaldehyde in these different tissues. Whilst the liver produces large amounts intrinsically, a significant proportion of formaldehyde in (or disseminating to) the brain and kidney can be detoxified by haematopoietic cells. This observation opens exciting possibilities for future treatments of formaldehyde-driven diseases, such as Cockayne syndrome. The potential to reduce kidney and brain deterioration in this disease through scavenging blood formaldehyde should be explored. As a proof-of-principle, this could be tested by treating *Adh5*$^{-/-}$*Csb*$^{-/-}$ mice with currently available

formaldehyde scavengers to see if organ damage can be ameliorated. Should such drugs prove effective in these mice, it would be worth considering their use to treat human disease.

Aim 3: Study the requirement for FA repair of formaldehyde-induced DNA damage in other proliferative tissues.

To address this question, I examined the GI tract of ADH5/FANCD2-deficient mice, both constitutive knockouts and longer-lived mice with haematopoietic ADH5 rescue. I found that despite the highly proliferative nature of this tissue, there was no overt phenotype in the GI tract. This surprising result indicates the gut epithelium has a unique ability to resist formaldehyde-induced DNA damage. Like in ADH5/CSB-deficient HSCs, this could be due to either compensatory repair pathways, or increased tolerance to DNA damage in these cells. The potential existence of an alternative mechanism to resolve or overcome interstrand crosslinks independent of FA repair is highly intriguing and future work should address this. Assessing whether the DNA damage response (e.g., P53, P21, yH2AX) is activated in the gut epithelium in response to formaldehyde damage will help determine whether this damage is tolerated and repair induced. Additionally, RNA-sequencing methods and genetic screens in gut organoid models would aid in discovering potentially novel factors mediating such tolerance and/or repair.

In summary, addressing these three aims has helped shed light on the origin of endogenous formaldehyde in the body, and the importance of its detoxification by the systemic circulation. My work has also uncovered the unexpected resistance of quiescent HSCs and gut epithelial cells to formaldehyde, establishing a foundation for future investigations into the mechanisms of this resistance.

FUTURE DIRECTIONS

Aside from HSCs and the GI tract, these mouse models provide an opportunity to examine other tissue-specific requirements for DNA repair. For instance, the skin is another highly proliferative tissue which is affected in Fanconi anaemia. FA patients often develop hyper or hypopigmentation of the skin or café au lait spots and have a higher risk of skin cancers (Tischkowitz & Hodgson,

2003). ADH5/FANCD2-deficient mice do show skin hyperpigmentation, but early mortality of constitutively deficient mice prevented development of any other phenotype. The longer lived *Adh5$^{sw/-}$Fancd2$^{-/-}$ Vav1-iCre* mice might provide an opportunity to model the development of skin cancers in the context of FA deficiency and understand how formaldehyde damage can drive skin tumorigenesis.

Additionally, the lungs of two-tier deficient mice remain an unexplored organ with the potential for novel insights. Proliferative AT2 alveolar cells in this organ are responsible for tissue regeneration in homeostasis and after injury (Han et al., 2023), but were shown to be distinctly sensitive to DNA damage. Treatment of mice with DNA-damaging bleomycin or radiation depletes this AT2 population and leads to development of pulmonary fibrosis – a prevalent and poorly understood disease in humans for which effective treatment is limited (S. Zhou et al., 2022, p. 2, 2022). Humans deficient in telomerase also develop lung fibrosis (van Batenburg et al., 2021), indicating that induction of the DNA damage response (e.g., through replicative senescence) can drive this pathology. Given the important role of FA repair in resolving replication stress in other proliferative systems, it is intriguing to ask whether this repair mechanism also protects regenerative AT2 stem cells, and whether deficiency in this pathway contributes to lung pathologies.

Tissue-specific models of two-tier deficiency described in this thesis also provide opportunities to further explore formaldehyde production and detoxification. In this work, I have primarily assessed the impact of restoring systemic formaldehyde detoxification on peripheral tissues. However, it would be equally intriguing to reverse this perspective and investigate how much circulating formaldehyde is produced by individual tissues. My current observations suggest that the liver is a significant site of formaldehyde accumulation. To this end, our lab has generated a liver-specific model of ADH5/FANCD2-deficiency. This model provides a unique opportunity to evaluate the extent to which the absence of ADH5 in the liver alone influences formaldehyde burden in other tissues. Similarly, kidney and brain-specific ADH5 knockout models would provide valuable insights into the extent of intrinsic formaldehyde production in these organs.

Further advancements in screening techniques will hopefully reveal additional cellular sources of formaldehyde, expanding our understanding of both cellular and tissue-specific contributions and potentially revealing new strategies to reduce formaldehyde burden. Through these analyses, we can further narrow down the sources of endogenous formaldehyde, and the detoxification and repair pathways which protect against it.

8 REFERENCES

Ackerman, S. (1992). The Development and Shaping of the Brain. In *Discovering the Brain*. National Academies Press (US). https://www.ncbi.nlm.nih.gov/books/NBK234146/

Akashi, K., Traver, D., Miyamoto, T., & Weissman, I. L. (2000). A clonogenic common myeloid progenitor that gives rise to all myeloid lineages. *Nature*, *404*(6774), 193–197. https://doi.org/10.1038/35004599

Akpolat, M., Oz, Z. S., Gulle, K., Hamamcioglu, A. C., Bakkal, B. H., & Kececi, M. (2020). X irradiation induced colonic mucosal injury and the detection of apoptosis through PARP-1/p53 regulatory pathway. *Biomedicine & Pharmacotherapy*, *127*, 110134. https://doi.org/10.1016/j.biopha.2020.110134

Alamri, Z. Z. (2018). The role of liver in metabolism: An updated review with physiological emphasis. *International Journal of Basic & Clinical Pharmacology*, *7*(11), 2271–2276. https://doi.org/10.18203/2319-2003.ijbcp20184211

Alcón, P., Kaczmarczyk, A. P., Ray, K. K., Liolios, T., Guilbaud, G., Sijacki, T., Shen, Y., McLaughlin, S. H., Sale, J. E., Knipscheer, P., Rueda, D. S., & Passmore, L. A. (2024). FANCD2–FANCI surveys DNA and recognizes double- to single-stranded junctions. *Nature*, *632*(8027), 1165–1173. https://doi.org/10.1038/s41586-024-07770-w

Alcón, P., Shakeel, S., Chen, Z. A., Rappsilber, J., Patel, K. J., & Passmore, L. A. (2020). FANCD2-FANCI is a clamp stabilized on DNA by monoubiquitination of FANCD2 during DNA repair. *Nature Structural & Molecular Biology*, *27*(3), 240–248. https://doi.org/10.1038/s41594-020-0380-1

Alekseenko, L. L., Shilina, M. A., Lyublinskaya, O. G., Kornienko, J. S., Anatskaya, O. V., Vinogradov, A. E., Grinchuk, T. M., Fridlyanskaya, I. I., & Nikolsky, N. N. (2018).

Quiescent Human Mesenchymal Stem Cells Are More Resistant to Heat Stress than Cycling Cells. *Stem Cells International*, *2018*(1), 3753547. https://doi.org/10.1155/2018/3753547

Alexandrov, L. B., Kim, J., Haradhvala, N. J., Huang, M. N., Tian Ng, A. W., Wu, Y., Boot, A., Covington, K. R., Gordenin, D. A., Bergstrom, E. N., Islam, S. M. A., Lopez-Bigas, N., Klimczak, L. J., McPherson, J. R., Morganella, S., Sabarinathan, R., Wheeler, D. A., Mustonen, V., Getz, G., … Stratton, M. R. (2020). The repertoire of mutational signatures in human cancer. *Nature*, *578*(7793), 94–101. https://doi.org/10.1038/s41586-020-1943-3

Alexandrov, L. B., Nik-Zainal, S., Wedge, D. C., Aparicio, S. A. J. R., Behjati, S., Biankin, A. V., Bignell, G. R., Bolli, N., Borg, A., Børresen-Dale, A.-L., Boyault, S., Burkhardt, B., Butler, A. P., Caldas, C., Davies, H. R., Desmedt, C., Eils, R., Eyfjörd, J. E., Foekens, J. A., … Stratton, M. R. (2013). Signatures of mutational processes in human cancer. *Nature*, *500*(7463), 415–421. https://doi.org/10.1038/nature12477

Alter, B. P., Rosenberg, P. S., & Brody, L. C. (2007). Clinical and molecular features associated with biallelic mutations in FANCD1/BRCA2. *Journal of Medical Genetics*, *44*(1), 1–9. https://doi.org/10.1136/jmg.2006.043257

Anandarajan, V., Noguchi, C., Oleksak, J., Grothusen, G., Terlecky, D., & Noguchi, E. (2020). Genetic investigation of formaldehyde-induced DNA damage response in Schizosaccharomyces pombe. *Current Genetics*, *66*(3), 593–605. https://doi.org/10.1007/s00294-020-01057-z

Anda, F. C. de, Madabhushi, R., Rei, D., Meng, J., Gräff, J., Durak, O., Meletis, K., Richter, M., Schwanke, B., Mungenast, A., & Tsai, L.-H. (2016). Cortical neurons gradually attain a post-mitotic state. *Cell Research*, *26*(9), 1033–1047. https://doi.org/10.1038/cr.2016.76

Anderson, C. J., Talmane, L., Luft, J., Connelly, J., Nicholson, M. D., Verburg, J. C., Pich, O., Campbell, S., Giaisi, M., Wei, P.-C., Sundaram, V., Connor, F., Ginno, P. A., Sasaki, T.,

Gilbert, D. M., López-Bigas, N., Semple, C. A., Odom, D. T., Aitken, S. J., & Taylor, M. S. (2024). Strand-resolved mutagenicity of DNA damage and repair. *Nature*, *630*(8017), 744–751. https://doi.org/10.1038/s41586-024-07490-1

Andreassen, P. R., Lohez, O. D., Lacroix, F. B., & Margolis, R. L. (2001). Tetraploid State Induces p53-dependent Arrest of Nontransformed Mammalian Cells in G1. *Molecular Biology of the Cell*, *12*(5), 1315–1328.

Antoniou, A., Pharoah, P. D. P., Narod, S., Risch, H. A., Eyfjord, J. E., Hopper, J. L., Loman, N., Olsson, H., Johannsson, O., Borg, Å., Pasini, B., Radice, P., Manoukian, S., Eccles, D. M., Tang, N., Olah, E., Anton-Culver, H., Warner, E., Lubinski, J., … Easton, D. F. (2003). Average Risks of Breast and Ovarian Cancer Associated with BRCA1 or BRCA2 Mutations Detected in Case Series Unselected for Family History: A Combined Analysis of 22 Studies. *American Journal of Human Genetics*, *72*(5), 1117–1130.

Auvray, F., Perrat, A., Arimizu, Y., Chagneau, C. V., Bossuet-Greif, N., Massip, C., Brugère, H., Nougayrède, J.-P., Hayashi, T., Branchu, P., Ogura, Y., & Oswald, E. (2021). Insights into the acquisition of the pks island and production of colibactin in the Escherichia coli population. *Microbial Genomics*, *7*(5), 000579. https://doi.org/10.1099/mgen.0.000579

Ayyaz, A., Kumar, S., Sangiorgi, B., Ghoshal, B., Gosio, J., Ouladan, S., Fink, M., Barutcu, S., Trcka, D., Shen, J., Chan, K., Wrana, J. L., & Gregorieff, A. (2019). Single-cell transcriptomes of the regenerating intestine reveal a revival stem cell. *Nature*, *569*(7754), 121–125. https://doi.org/10.1038/s41586-019-1154-y

Bakker, S. T., van de Vrugt, H. J., Rooimans, M. A., Oostra, A. B., Steltenpool, J., Delzenne-Goette, E., van der Wal, A., van der Valk, M., Joenje, H., te Riele, H., & de Winter, J. P. (2009). Fancm-deficient mice reveal unique features of Fanconi anemia complementation group M. *Human Molecular Genetics*, *18*(18), 3484–3495. https://doi.org/10.1093/hmg/ddp297

Bakker, S. T., van de Vrugt, H. J., Visser, J. A., Delzenne-Goette, E., van der Wal, A., Berns, M. A. D., van de Ven, M., Oostra, A. B., de Vries, S., Kramer, P., Arwert, F., van der Valk, M., de Winter, J. P., & te Riele, H. (2012). Fancf-deficient mice are prone to develop ovarian tumours. *The Journal of Pathology*, *226*(1), 28–39. https://doi.org/10.1002/path.2992

Balajee, A. S., May, A., Dianov, G. L., Friedberg, E. C., & Bohr, V. A. (1997). Reduced RNA polymerase II transcription in intact and permeabilized Cockayne syndrome group B cells. *Proceedings of the National Academy of Sciences*, *94*(9), 4306–4311. https://doi.org/10.1073/pnas.94.9.4306

Baraldi, O., Valentini, C., Donati, G., Comai, G., Cuna, V., Capelli, I., Angelini, M. L., Moretti, M. I., Angeletti, A., Piscaglia, F., & La Manna, G. (2015). Hepatorenal syndrome: Update on diagnosis and treatment. *World Journal of Nephrology*, *4*(5), 511–520. https://doi.org/10.5527/wjn.v4.i5.511

Barker, N. (2014). Adult intestinal stem cells: Critical drivers of epithelial homeostasis and regeneration. *Nature Reviews. Molecular Cell Biology*, *15*(1), 19–33. https://doi.org/10.1038/nrm3721

Becker, F., Ouzin, M., Liedtke, S., Raba, K., & Kogler, G. (2024). DNA Damage Response After Treatment of Cycling and Quiescent Cord Blood Hematopoietic Stem Cells With Distinct Genotoxic Noxae. *Stem Cells*, *42*(2), 158–171. https://doi.org/10.1093/stmcls/sxad085

Beerman, I. (2017). Accumulation of DNA damage in the aged hematopoietic stem cell compartment. *Seminars in Hematology*, *54*(1), 12–18. https://doi.org/10.1053/j.seminhematol.2016.11.001

Beerman, I., Seita, J., Inlay, M. A., Weissman, I. L., & Rossi, D. J. (2014a). Quiescent Hematopoietic Stem Cells Accumulate DNA Damage during Aging that Is Repaired upon Entry into Cell Cycle. *Cell Stem Cell*, *15*(1), 37–50. https://doi.org/10.1016/j.stem.2014.04.016

Beerman, I., Seita, J., Inlay, M. A., Weissman, I. L., & Rossi, D. J. (2014b). Quiescent hematopoietic stem cells accumulate DNA damage during aging that is repaired upon entry into cell cycle. *Cell Stem Cell*, *15*(1), 37–50. https://doi.org/10.1016/j.stem.2014.04.016

Biechonski, S., Olender, L., Zipin-Roitman, A., Yassin, M., Aqaqe, N., Marcu-Malina, V., Rall-Scharpf, M., Trottier, M., Meyn, M. S., Wiesmüller, L., Beider, K., Raz, Y., Grisaru, D., Nagler, A., & Milyavsky, M. (2018). Attenuated DNA damage responses and increased apoptosis characterize human hematopoietic stem cells exposed to irradiation. *Scientific Reports*, *8*(1), 6071. https://doi.org/10.1038/s41598-018-24440-w

Biechonski, S., Yassin, M., & Milyavsky, M. (2017). DNA-damage response in hematopoietic stem cells: An evolutionary trade-off between blood regeneration and leukemia suppression. *Carcinogenesis*, *38*(4), 367–377. https://doi.org/10.1093/carcin/bgx002

Bielski, C. M., Zehir, A., Penson, A. V., Donoghue, M. T. A., Chatila, W., Armenia, J., Chang, M. T., Schram, A. M., Jonsson, P., Bandlamudi, C., Razavi, P., Iyer, G., Robson, M. E., Stadler, Z. K., Schultz, N., Baselga, J., Solit, D. B., Hyman, D. M., Berger, M. F., & Taylor, B. S. (2018). Genome doubling shapes the evolution and prognosis of advanced cancers. *Nature Genetics*, *50*(8), 1189–1195. https://doi.org/10.1038/s41588-018-0165-1

Bjørkøy, G., Lamark, T., Pankiv, S., Øvervatn, A., Brech, A., & Johansen, T. (2009). Monitoring autophagic degradation of p62/SQSTM1. *Methods in Enzymology*, *452*, 181–197. https://doi.org/10.1016/S0076-6879(08)03612-4

Black, J. O. (2016). Xeroderma Pigmentosum. *Head and Neck Pathology*, *10*(2), 139–144. https://doi.org/10.1007/s12105-016-0707-8

Blackford, A. N., & Jackson, S. P. (2017). ATM, ATR, and DNA-PK: The Trinity at the Heart of the DNA Damage Response. *Molecular Cell*, *66*(6), 801–817. https://doi.org/10.1016/j.molcel.2017.05.015

Blokzijl, F., de Ligt, J., Jager, M., Sasselli, V., Roerink, S., Sasaki, N., Huch, M., Boymans, S., Kuijk, E., Prins, P., Nijman, I. J., Martincorena, I., Mokry, M., Wiegerinck, C. L., Middendorp, S., Sato, T., Schwank, G., Nieuwenhuis, E. E. S., Verstegen, M. M. A., … van Boxtel, R. (2016). Tissue-specific mutation accumulation in human adult stem cells during life. *Nature*, *538*(7624), 260–264. https://doi.org/10.1038/nature19768

Boltong, A., & Keast, R. (2012). The influence of chemotherapy on taste perception and food hedonics: A systematic review. *Cancer Treatment Reviews*, *38*(2), 152–163. https://doi.org/10.1016/j.ctrv.2011.04.008

Bonadona, V., Bonaïti, B., Olschwang, S., Grandjouan, S., Huiart, L., Longy, M., Guimbaud, R., Buecher, B., Bignon, Y.-J., Caron, O., Colas, C., Noguès, C., Lejeune-Dumoulin, S., Olivier-Faivre, L., Polycarpe-Osaer, F., Nguyen, T. D., Desseigne, F., Saurin, J.-C., Berthet, P., … French Cancer Genetics Network, for the. (2011). Cancer Risks Associated With Germline Mutations in MLH1, MSH2, and MSH6 Genes in Lynch Syndrome. *JAMA*, *305*(22), 2304–2310. https://doi.org/10.1001/jama.2011.743

Bou-Nader, M., Caruso, S., Donne, R., Celton-Morizur, S., Calderaro, J., Gentric, G., Cadoux, M., L'Hermitte, A., Klein, C., Guilbert, T., Albuquerque, M., Couchy, G., Paradis, V., Couty, J.-P., Zucman-Rossi, J., & Desdouets, C. (2020). Polyploidy spectrum: A new marker in HCC classification. *Gut*, *69*(2), 355–364. https://doi.org/10.1136/gutjnl-2018-318021

Boyle, C., Lansdorp, P. M., & Edelstein-Keshet, L. (2023). Predicting the number of lifetime divisions for hematopoietic stem cells from telomere length measurements. *iScience*, *26*(7), 107053. https://doi.org/10.1016/j.isci.2023.107053

Bray, F., Laversanne, M., Sung, H., Ferlay, J., Siegel, R. L., Soerjomataram, I., & Jemal, A. (2024). Global cancer statistics 2022: GLOBOCAN estimates of incidence and mortality worldwide for 36 cancers in 185 countries. *CA: A Cancer Journal for Clinicians*, *74*(3), 229–263. https://doi.org/10.3322/caac.21834

Breton, C. L., Hennion, M., Arimondo, P. B., & Hyrien, O. (2011). Replication-Fork Stalling and Processing at a Single Psoralen Interstrand Crosslink in Xenopus Egg Extracts. *PLOS ONE*, *6*(4), e18554. https://doi.org/10.1371/journal.pone.0018554

Brueckner, F., Hennecke, U., Carell, T., & Cramer, P. (2007). CPD Damage Recognition by Transcribing RNA Polymerase II. *Science*, *315*(5813), 859–862. https://doi.org/10.1126/science.1135400

Bryder, D., Rossi, D. J., & Weissman, I. L. (2006). Hematopoietic Stem Cells: The Paradigmatic Tissue-Specific Stem Cell. *The American Journal of Pathology*, *169*(2), 338–346. https://doi.org/10.2353/ajpath.2006.060312

Burgos-Barragan, G. (2017). *Molecular dissection of the genotoxicity, origin and metabolism of endogenous formaldehyde*. University of Cambridge.

Burgos-Barragan, G., Wit, N., Meiser, J., Dingler, F. A., Pietzke, M., Mulderrig, L., Pontel, L. B., Rosado, I. V., Brewer, T. F., Cordell, R. L., Monks, P. S., Chang, C. J., Vazquez, A., & Patel, K. J. (2017). Mammals divert endogenous genotoxic formaldehyde into one-carbon metabolism. *Nature*, *548*(7669), 549–554. https://doi.org/10.1038/nature23481

Burns, M. B., Lackey, L., Carpenter, M. A., Rathore, A., Land, A. M., Leonard, B., Refsland, E. W., Kotandeniya, D., Tretyakova, N., Nikas, J. B., Yee, D., Temiz, N. A., Donohue, D. E., McDougle, R. M., Brown, W. L., Law, E. K., & Harris, R. S. (2013). APOBEC3B is an enzymatic source of mutation in breast cancer. *Nature*, *494*(7437), 366–370. https://doi.org/10.1038/nature11881

Bustelo, X. R., Rubin, S. D., Suen, K. L., Carrasco, D., & Barbacid, M. (1993). Developmental expression of the vav protooncogene. *Cell Growth & Differentiation: The Molecular Biology Journal of the American Association for Cancer Research*, *4*(4), 297–308.

Cao, Y., Oh, J., Xue, M., Huh, W. J., Wang, J., Gonzalez-Hernandez, J. A., Rice, T. A., Martin, A. L., Song, D., Crawford, J. M., Herzon, S. B., & Palm, N. W. (2022). Commensal microbiota from patients with inflammatory bowel disease produce genotoxic

metabolites. *Science (New York, N.Y.)*, *378*(6618), eabm3233. https://doi.org/10.1126/science.abm3233

Carnie, C. J., Acampora, A. C., Bader, A. S., Erdenebat, C., Zhao, S., Bitensky, E., van den Heuvel, D., Parnas, A., Gupta, V., D'Alessandro, G., Sczaniecka-Clift, M., Weickert, P., Aygenli, F., Götz, M. J., Cordes, J., Esain-Garcia, I., Melidis, L., Wondergem, A. P., Lam, S., … Stingele, J. (2024). Transcription-coupled repair of DNA–protein cross-links depends on CSA and CSB. *Nature Cell Biology*, *26*(5), 797–810. https://doi.org/10.1038/s41556-024-01391-1

Carvajal-Garcia, J., Samadpour, A. N., Hernandez Viera, A. J., & Merrikh, H. (n.d.). Oxidative stress drives mutagenesis through transcription-coupled repair in bacteria. *Proceedings of the National Academy of Sciences of the United States of America*, *120*(27), e2300761120. https://doi.org/10.1073/pnas.2300761120

Ceccaldi, R., Sarangi, P., & D'Andrea, A. D. (2016). The Fanconi anaemia pathway: New players and new functions. *Nature Reviews Molecular Cell Biology*, *17*(6), 337–349. https://doi.org/10.1038/nrm.2016.48

Chen, M., Tomkins, D. J., Auerbach, W., McKerlie, C., Youssoufian, H., Liu, L., Gan, O., Carreau, M., Auerbach, A., Groves, T., Guidos, C. J., Freedman, M. H., Cross, J., Percy, D. H., Dick, J. E., Joyner, A. L., & Buchwald, M. (1996). Inactivation of Fac in mice produces inducible chromosomal instability and reduced fertility reminiscent of Fanconi anaemia. *Nature Genetics*, *12*(4), 448–451. https://doi.org/10.1038/ng0496-448

Cheng, G., Shi, Y., Sturla, S. J., Jalas, J. R., McIntee, E. J., Villalta, P. W., Wang, M., & Hecht, S. S. (2003). Reactions of Formaldehyde Plus Acetaldehyde with Deoxyguanosine and DNA: Formation of Cyclic Deoxyguanosine Adducts and Formaldehyde Cross-Links. *Chemical Research in Toxicology*, *16*(2), 145–152. https://doi.org/10.1021/tx025614r

Cheng, K. C., Cahill, D. S., Kasai, H., Nishimura, S., & Loeb, L. A. (1992). 8-Hydroxyguanine, an abundant form of oxidative DNA damage, causes G----T and A----C substitutions. *The Journal of Biological Chemistry*, *267*(1), 166–172.

Chiu, S.-C., Liu, H.-H., Chen, C.-L., Chen, P.-R., Liu, M.-C., Lin, S.-Z., & Chang, K.-T. (2015). Extramedullary Hematopoiesis (EMH) in Laboratory Animals: Offering an Insight into Stem Cell Research. *Cell Transplantation*, *24*(3), 349–366. https://doi.org/10.3727/096368915X686850

Choi, C., Lee, C., Shin, S.-W., Kim, S.-Y., Hong, S. N., & Park, H. C. (2019). Comparison of Proton and Photon Beam Irradiation in Radiation-Induced Intestinal Injury Using a Mouse Model. *International Journal of Molecular Sciences*, *20*(8), Article 8. https://doi.org/10.3390/ijms20081894

Clarke, D., & Sokoloff, L. (1999). *Circulation and Energy Metabolism of the Brain*. https://www.semanticscholar.org/paper/Circulation-and-Energy-Metabolism-of-the-Brain-Clarke-Sokoloff/935433f7d90a1dbb53af13e6e51e3ddb1d1369b7

Clarke, T. L., & Mostoslavsky, R. (2022). DNA repair as a shared hallmark in cancer and ageing. *Molecular Oncology*, *16*(18), 3352–3379. https://doi.org/10.1002/1878-0261.13285

Cleary, S. P., Cotterchio, M., Jenkins, M. A., Kim, H., Bristow, R., Green, R., Haile, R., Hopper, J. L., LeMarchand, L., Lindor, N., Parfrey, P., Potter, J., Younghusband, B., & Gallinger, S. (2009). Germline MutY human homologue mutations and colorectal cancer: A multisite case-control study. *Gastroenterology*, *136*(4), 1251–1260. https://doi.org/10.1053/j.gastro.2008.12.050

Corces-Zimmerman, M. R., Hong, W.-J., Weissman, I. L., Medeiros, B. C., & Majeti, R. (2014). Preleukemic mutations in human acute myeloid leukemia affect epigenetic regulators and persist in remission. *Proceedings of the National Academy of Sciences*, *111*(7), 2548–2553. https://doi.org/10.1073/pnas.1324297111

Crasta, K., Ganem, N. J., Dagher, R., Lantermann, A. B., Ivanova, E. V., Pan, Y., Nezi, L., Protopopov, A., Chowdhury, D., & Pellman, D. (2012). DNA breaks and chromosome pulverization from errors in mitosis. *Nature*, *482*(7383), 53–58. https://doi.org/10.1038/nature10802

Damsma, G. E., Alt, A., Brueckner, F., Carell, T., & Cramer, P. (2007). Mechanism of transcriptional stalling at cisplatin-damaged DNA. *Nature Structural & Molecular Biology*, *14*(12), 1127–1133. https://doi.org/10.1038/nsmb1314

de Almeida, A. J. P. O., de Oliveira, J. C. P. L., da Silva Pontes, L. V., de Souza Júnior, J. F., Gonçalves, T. A. F., Dantas, S. H., de Almeida Feitosa, M. S., Silva, A. O., & de Medeiros, I. A. (2022). ROS: Basic Concepts, Sources, Cellular Signaling, and its Implications in Aging Pathways. *Oxidative Medicine and Cellular Longevity*, *2022*, 1225578. https://doi.org/10.1155/2022/1225578

de Boer, J., Williams, A., Skavdis, G., Harker, N., Coles, M., Tolaini, M., Norton, T., Williams, K., Roderick, K., Potocnik, A. J., & Kioussis, D. (2003). Transgenic mice with hematopoietic and lymphoid specific expression of Cre. *European Journal of Immunology*, *33*(2), 314–325. https://doi.org/10.1002/immu.200310005

de Laat, W. L., Appeldoorn, E., Sugasawa, K., Weterings, E., Jaspers, N. G. J., & Hoeijmakers, J. H. J. (1998). DNA-binding polarity of human replication protein A positions nucleases in nucleotide excision repair. *Genes & Development*, *12*(16), 2598–2609.

DeBerardinis, R. J., Coughlin, C. R., & Kaplan, P. (2008). Penicillamine therapy in pediatric cystinuria: Experience from a cohort of American children. *The Journal of Urology*, *180*(6), 2620–2623. https://doi.org/10.1016/j.juro.2008.08.057

Debili, N., Coulombel, L., Croisille, L., Katz, A., Guichard, J., Breton-Gorius, J., & Vainchenker, W. (1996). Characterization of a bipotent erythro-megakaryocytic progenitor in human bone marrow. *Blood*, *88*(4), 1284–1296.

Dejea, C. M., Fathi, P., Craig, J. M., Boleij, A., Taddese, R., Geis, A. L., Wu, X., DeStefano Shields, C. E., Hechenbleikner, E. M., Huso, D. L., Anders, R. A., Giardiello, F. M., Wick, E. C., Wang, H., Wu, S., Pardoll, D. M., Housseau, F., & Sears, C. L. (2018a). Patients with familial adenomatous polyposis harbor colonic biofilms containing tumorigenic bacteria. *Science (New York, N.Y.)*, *359*(6375), 592–597. https://doi.org/10.1126/science.aah3648

Dejea, C. M., Fathi, P., Craig, J. M., Boleij, A., Taddese, R., Geis, A. L., Wu, X., DeStefano Shields, C. E., Hechenbleikner, E. M., Huso, D. L., Anders, R. A., Giardiello, F. M., Wick, E. C., Wang, H., Wu, S., Pardoll, D. M., Housseau, F., & Sears, C. L. (2018b). Patients with familial adenomatous polyposis harbor colonic biofilms containing tumorigenic bacteria. *Science (New York, N.Y.)*, *359*(6375), 592–597. https://doi.org/10.1126/science.aah3648

Di Pastena, F., Pond, G., Tsakiridis, E. E., Gouveia, A., Ahmadi, E., Biziotis, O.-D., Ali, A., Swaminath, A., Okawara, G., Ellis, P. M., Abdulkarim, B., Ahmed, N., Robinson, A., Roa, W., Valdes, M., Kavsak, P., Wierzbicki, M., Wright, J., Steinberg, G., & Tsakiridis, T. (2024). Growth differentiation factor 15 (GDF15) predicts relapse free and overall survival in unresected locally advanced non-small cell lung cancer treated with chemoradiotherapy. *Radiation Oncology (London, England)*, *19*, 155. https://doi.org/10.1186/s13014-024-02546-y

Dianov, G. L., Houle, J. F., Iyer, N., Bohr, V. A., & Friedberg, E. C. (1997). Reduced RNA polymerase II transcription in extracts of cockayne syndrome and xeroderma pigmentosum/Cockayne syndrome cells. *Nucleic Acids Research*, *25*(18), 3636–3642. https://doi.org/10.1093/nar/25.18.3636

Dingler, F. A., Wang, M., Mu, A., Millington, C. L., Oberbeck, N., Watcham, S., Pontel, L. B., Kamimae-Lanning, A. N., Langevin, F., Nadler, C., Cordell, R. L., Monks, P. S., Yu, R., Wilson, N. K., Hira, A., Yoshida, K., Mori, M., Okamoto, Y., Okuno, Y., … Patel, K. J.

(2020). Two Aldehyde Clearance Systems Are Essential to Prevent Lethal Formaldehyde Accumulation in Mice and Humans. *Molecular Cell*, *80*(6), 996-1012.e9. https://doi.org/10.1016/j.molcel.2020.10.012

Domenech, C., Maillard, L., Rousseau, A., Guidez, F., Petit, L., Pla, M., Clay, D., Guimiot, F., Sanfilippo, S., Jacques, S., Grange, P. de la, Robil, N., Soulier, J., & Souyri, M. (2018). Studies in an Early Development Window Unveils a Severe HSC Defect in both Murine and Human Fanconi Anemia. *Stem Cell Reports*, *11*(5), 1075–1091. https://doi.org/10.1016/j.stemcr.2018.10.001

Donne, R., Sangouard, F., Celton-Morizur, S., & Desdouets, C. (2021). Hepatocyte Polyploidy: Driver or Gatekeeper of Chronic Liver Diseases. *Cancers*, *13*(20), 5151. https://doi.org/10.3390/cancers13205151

Dorokhov, Y. L., Shindyapina, A. V., Sheshukova, E. V., & Komarova, T. V. (2015). Metabolic Methanol: Molecular Pathways and Physiological Roles. *Physiological Reviews*, *95*(2), 603–644. https://doi.org/10.1152/physrev.00034.2014

Duncan, A. W., Taylor, M. H., Hickey, R. D., Hanlon Newell, A. E., Lenzi, M. L., Olson, S. B., Finegold, M. J., & Grompe, M. (2010). The ploidy conveyor of mature hepatocytes as a source of genetic variation. *Nature*, *467*(7316), 707–710. https://doi.org/10.1038/nature09414

Eng, M. Y., Luczak, S. E., & Wall, T. L. (2007). ALDH2, ADH1B, and ADH1C Genotypes in Asians: A Literature Review. *Alcohol Research & Health*, *30*(1), 22–27.

Enocksson, A., Lundberg, J., Weitzberg, E., Norrby-Teglund, A., & Svenungsson, B. (2004). Rectal nitric oxide gas and stool cytokine levels during the course of infectious gastroenteritis. *Clinical and Diagnostic Laboratory Immunology*, *11*(2), 250–254. https://doi.org/10.1128/cdli.11.2.250-254.2004

Enoiu, M., Jiricny, J., & Schärer, O. D. (2012). Repair of cisplatin-induced DNA interstrand crosslinks by a replication-independent pathway involving transcription-coupled repair

and translesion synthesis. *Nucleic Acids Research*, *40*(18), 8953–8964. https://doi.org/10.1093/nar/gks670

Falnes, P. Ø., Johansen, R. F., & Seeberg, E. (2002). AlkB-mediated oxidative demethylation reverses DNA damage in Escherichia coli. *Nature*, *419*(6903), 178–182. https://doi.org/10.1038/nature01048

Fanconi Cancer Foundation. (2023). Clinical Care of Fanconi Anemia Gastrointestinal Issues. *Fanconi Cancer Foundation*. https://fanconi.org/clinical-care-guidelines/clinical-care-of-fanconi-anemia-gastrointestinal-issues/

Fang, J., de Bruin, A., Villunger, A., Schiffelers, R., Lei, Z., & Sluijter, J. P. G. (2022). Cellular polyploidy in organ homeostasis and regeneration. *Protein & Cell*, *14*(8), 560–578. https://doi.org/10.1093/procel/pwac064

Fehrenbach, M. K., Tjwa, M., Bechmann, I., & Krueger, M. (2018). Decreased microglial numbers in Vav1-Cre+:dicer knock-out mice suggest a second source of microglia beyond yolk sac macrophages. *Annals of Anatomy = Anatomischer Anzeiger: Official Organ of the Anatomische Gesellschaft*, *218*, 190–198. https://doi.org/10.1016/j.aanat.2018.03.004

Fejzo, M., Rocha, N., Cimino, I., Lockhart, S. M., Petry, C. J., Kay, R. G., Burling, K., Barker, P., George, A. L., Yasara, N., Premawardhena, A., Gong, S., Cook, E., Rimmington, D., Rainbow, K., Withers, D. J., Cortessis, V., Mullin, P. M., MacGibbon, K. W., … O'Rahilly, S. (2024). GDF15 linked to maternal risk of nausea and vomiting during pregnancy. *Nature*, *625*(7996), 760–767. https://doi.org/10.1038/s41586-023-06921-9

Feringa, F. M., Raaijmakers, J. A., Hadders, M. A., Vaarting, C., Macurek, L., Heitink, L., Krenning, L., & Medema, R. H. (2018). Persistent repair intermediates induce senescence. *Nature Communications*, *9*(1), 3923. https://doi.org/10.1038/s41467-018-06308-9

Flach, J., Bakker, S. T., Mohrin, M., Conroy, P. C., Pietras, E. M., Reynaud, D., Alvarez, S., Diolaiti, M. E., Ugarte, F., Forsberg, E. C., Le Beau, M. M., Stohr, B. A., Méndez, J., Morrison, C. G., & Passegué, E. (2014). Replication stress is a potent driver of functional decline in ageing haematopoietic stem cells. *Nature*, *512*(7513), 198–202. https://doi.org/10.1038/nature13619

Fujimaki, K., Li, R., Chen, H., Della Croce, K., Zhang, H. H., Xing, J., Bai, F., & Yao, G. (2019). Graded regulation of cellular quiescence depth between proliferation and senescence by a lysosomal dimmer switch. *Proceedings of the National Academy of Sciences of the United States of America*, *116*(45), 22624–22634. https://doi.org/10.1073/pnas.1915905116

Gandarillas, A., Molinuevo, R., & Sanz-Gómez, N. (2018). Mammalian endoreplication emerges to reveal a potential developmental timer. *Cell Death & Differentiation*, *25*(3), 471–476. https://doi.org/10.1038/s41418-017-0040-0

Garaycoechea, J. I. (2014). *Aldehyde genotoxicity underlies haematopoietic stem cell depletion in Fanconi Anemia*. University of Cambridge.

Garaycoechea, J. I., Crossan, G. P., Langevin, F., Mulderrig, L., Louzada, S., Yang, F., Guilbaud, G., Park, N., Roerink, S., Nik-Zainal, S., Stratton, M. R., & Patel, K. J. (2018). Alcohol and endogenous aldehydes damage chromosomes and mutate stem cells. *Nature*, *553*(7687), 171–177. https://doi.org/10.1038/nature25154

García-Rubio, M. L., Pérez-Calero, C., Barroso, S. I., Tumini, E., Herrera-Moyano, E., Rosado, I. V., & Aguilera, A. (2015). The Fanconi Anemia Pathway Protects Genome Integrity from R-loops. *PLoS Genetics*, *11*(11), e1005674. https://doi.org/10.1371/journal.pgen.1005674

GBD 2016 DALYs and HALE Collaborators. (2017). Global, regional, and national disability-adjusted life-years (DALYs) for 333 diseases and injuries and healthy life expectancy (HALE) for 195 countries and territories, 1990–2016: A systematic analysis for the

Global Burden of Disease Study 2016. *Lancet (London, England)*, *390*(10100), 1260–1344. https://doi.org/10.1016/S0140-6736(17)32130-X

Geijer, M. E., Zhou, D., Selvam, K., Steurer, B., Mukherjee, C., Evers, B., Cugusi, S., van Toorn, M., van der Woude, M., Janssens, R. C., Kok, Y. P., Gong, W., Raams, A., Lo, C. S. Y., Lebbink, J. H. G., Geverts, B., Plummer, D. A., Bezstarosti, K., Theil, A. F., … Marteijn, J. A. (2021). Elongation factor ELOF1 drives transcription-coupled repair and prevents genome instability. *Nature Cell Biology*, *23*(6), 608–619. https://doi.org/10.1038/s41556-021-00692-z

Genovese, G., Kähler, A. K., Handsaker, R. E., Lindberg, J., Rose, S. A., Bakhoum, S. F., Chambert, K., Mick, E., Neale, B. M., Fromer, M., Purcell, S. M., Svantesson, O., Landén, M., Höglund, M., Lehmann, S., Gabriel, S. B., Moran, J. L., Lander, E. S., Sullivan, P. F., … McCarroll, S. A. (2014). Clonal hematopoiesis and blood-cancer risk inferred from blood DNA sequence. *The New England Journal of Medicine*, *371*(26), 2477–2487. https://doi.org/10.1056/NEJMoa1409405

Gentric, G., Maillet, V., Paradis, V., Couton, D., L'Hermitte, A., Panasyuk, G., Fromenty, B., Celton-Morizur, S., & Desdouets, C. (2015). Oxidative stress promotes pathologic polyploidization in nonalcoholic fatty liver disease. *The Journal of Clinical Investigation*, *125*(3), 981–992. https://doi.org/10.1172/JCI73957

Gerdes, J., Lemke, H., Baisch, H., Wacker, H. H., Schwab, U., & Stein, H. (1984). Cell cycle analysis of a cell proliferation-associated human nuclear antigen defined by the monoclonal antibody Ki-67. *Journal of Immunology (Baltimore, Md.: 1950)*, *133*(4), 1710–1715.

Ghosh, R., Gilda, J. E., & Gomes, A. V. (2014). The necessity of and strategies for improving confidence in the accuracy of western blots. *Expert Review of Proteomics*, *11*(5), 549–560. https://doi.org/10.1586/14789450.2014.939635

Giusti, S. A., Vercelli, C. A., Vogl, A. M., Kolarz, A. W., Pino, N. S., Deussing, J. M., & Refojo, D. (2014). Behavioral phenotyping of Nestin-Cre mice: Implications for genetic mouse models of psychiatric disorders. *Journal of Psychiatric Research*, *55*, 87–95. https://doi.org/10.1016/j.jpsychires.2014.04.002

Greaves, M., & Maley, C. C. (2012). Clonal evolution in cancer. *Nature*, *481*(7381), 306–313. https://doi.org/10.1038/nature10762

Gregersen, L. H., Mitter, R., & Svejstrup, J. Q. (2020). Using TTchem-seq for profiling nascent transcription and measuring transcript elongation. *Nature Protocols*, *15*(2), 604–627. https://doi.org/10.1038/s41596-019-0262-3

Gregersen, L. H., & Svejstrup, J. Q. (2018). The Cellular Response to Transcription-Blocking DNA Damage. *Trends in Biochemical Sciences*, *43*(5), 327–341. https://doi.org/10.1016/j.tibs.2018.02.010

Guidotti, J.-E., Brégerie, O., Robert, A., Debey, P., Brechot, C., & Desdouets, C. (2003). Liver Cell Polyploidization: A Pivotal Role for Binuclear Hepatocytes*. *Journal of Biological Chemistry*, *278*(21), 19095–19101. https://doi.org/10.1074/jbc.M300982200

Guyenet, S. J., Furrer, S. A., Damian, V. M., Baughan, T. D., La Spada, A. R., & Garden, G. A. (2010). A Simple Composite Phenotype Scoring System for Evaluating Mouse Models of Cerebellar Ataxia. *Journal of Visualized Experiments : JoVE*, *39*, 1787. https://doi.org/10.3791/1787

Hadjur, S., Ung, K., Wadsworth, L., Dimmick, J., Rajcan-Separovic, E., Scott, R. W., Buchwald, M., & Jirik, F. R. (2001). Defective hematopoiesis and hepatic steatosis in mice with combined deficiencies of the genes encoding Fancc and Cu/Zn superoxide dismutase. *Blood*, *98*(4), 1003–1011. https://doi.org/10.1182/blood.V98.4.1003

Hahm, J. Y., Park, J., Jang, E.-S., & Chi, S. W. (2022). 8-Oxoguanine: From oxidative damage to epigenetic and epitranscriptional modification. *Experimental & Molecular Medicine*, *54*(10), 1626–1642. https://doi.org/10.1038/s12276-022-00822-z

Han, S., Budinger, G. R. S., & Gottardi, C. J. (2023). Alveolar epithelial regeneration in the aging lung. *The Journal of Clinical Investigation*, *133*(20). https://doi.org/10.1172/JCI170504

Harada, S., Agarwal, D. P., & Goedde, H. W. (1981). Aldehyde dehydrogenase deficiency as cause of facial flushing reaction to alcohol in Japanese. *Lancet (London, England)*, *2*(8253), 982. https://doi.org/10.1016/s0140-6736(81)91172-7

Hayashi, K., Horisaka, K., Harada, Y., Ogawa, Y., Yamashita, T., Kitano, T., Wakita, M., Fukusumi, T., Inohara, H., Hara, E., & Matsumoto, T. (2024). Polyploidy mitigates the impact of DNA damage while simultaneously bearing its burden. *Cell Death Discovery*, *10*(1), 1–13. https://doi.org/10.1038/s41420-024-02206-w

He, Z., Gharaibeh, R. Z., Newsome, R. C., Pope, J. L., Dougherty, M. W., Tomkovich, S., Pons, B., Mirey, G., Vignard, J., Hendrixson, D. R., & Jobin, C. (2019). Campylobacter jejuni promotes colorectal tumorigenesis through the action of cytolethal distending toxin. *Gut*, *68*(2), 289–300. https://doi.org/10.1136/gutjnl-2018-317200

HECK, H. d'A., CASANOVA-SCHM1TZ, M., DODD, P. B., SCHACHTER, E. N., WITEK, T. J., & TOSUN, T. (1985). Formaldehyde (CH2O) Concentrations in the Blood of Humans and Fischer-344 Rats Exposed to CH2O Under Controlled Conditions. *American Industrial Hygiene Association Journal*, *46*(1), 1–3. https://doi.org/10.1080/15298668591394275

Henning, K. A., Li, L., Iyer, N., McDaniel, L. D., Reagan, M. S., Legerski, R., Schultz, R. A., Stefanini, M., Lehmann, A. R., Mayne, L. V., & Friedberg, E. C. (1995). The Cockayne syndrome group A gene encodes a WD repeat protein that interacts with CSB protein and a subunit of RNA polymerase II TFIIH. *Cell*, *82*(4), 555–564. https://doi.org/10.1016/0092-8674(95)90028-4

Heuvel, D. van den, Rodríguez-Martínez, M., Meer, P. J. van der, Moreno, N. N., Park, J., Kim, H.-S., Schie, J. J. M. van, Wondergem, A. P., D'Souza, A., Yakoub, G., Herlihy, A. E., Kashyap, K., Boissière, T., Walker, J., Mitter, R., Apelt, K., Lint, K. de, Kirdök, I.,

Ljungman, M., … Luijsterburg, M. S. (2024). STK19 facilitates the clearance of lesion-stalled RNAPII during transcription-coupled DNA repair. *Cell*, *187*(25), 7107-7125.e25. https://doi.org/10.1016/j.cell.2024.10.018

Hewlett, B. R. (2002). Penetration Rates of Formaldehyde. *Microscopy Today*, *10*(6), 30–31. https://doi.org/10.1017/S1551929500058491

Hodskinson, M. R., Bolner, A., Sato, K., Kamimae-Lanning, A. N., Rooijers, K., Witte, M., Mahesh, M., Silhan, J., Petek, M., Williams, D. M., Kind, J., Chin, J. W., Patel, K. J., & Knipscheer, P. (2020). Alcohol-derived DNA crosslinks are repaired by two distinct mechanisms. *Nature*, *579*(7800), 603–608. https://doi.org/10.1038/s41586-020-2059-5

Hoffelder, D. R., Luo, L., Burke, N. A., Watkins, S. C., Gollin, S. M., & Saunders, W. S. (2004). Resolution of anaphase bridges in cancer cells. *Chromosoma*, *112*(8), 389–397. https://doi.org/10.1007/s00412-004-0284-6

Hoffman, E. A., Frey, B. L., Smith, L. M., & Auble, D. T. (2015). Formaldehyde Crosslinking: A Tool for the Study of Chromatin Complexes. *The Journal of Biological Chemistry*, *290*(44), 26404–26411. https://doi.org/10.1074/jbc.R115.651679

Hopkinson, R. J., Hamed, R. B., Rose, N. R., Claridge, T. D. W., & Schofield, C. J. (2010). Monitoring the Activity of 2-Oxoglutarate Dependent Histone Demethylases by NMR Spectroscopy: Direct Observation of Formaldehyde. *ChemBioChem*, *11*(4), 506–510. https://doi.org/10.1002/cbic.200900713

Horst, G. T. J. van der, Steeg, H. van, Berg, R. J. W., Gool, A. J. van, Wit, J. de, Weeda, G., Morreau, H., Beems, R. B., Kreijl, C. F. van, Gruijl, F. R. de, Bootsma, D., & Hoeijmakers, J. H. J. (1997). Defective Transcription-Coupled Repair in Cockayne Syndrome B Mice Is Associated with Skin Cancer Predisposition. *Cell*, *89*(3), 425–435. https://doi.org/10.1016/S0092-8674(00)80223-8

Houghtaling, S., Timmers, C., Noll, M., Finegold, M. J., Jones, S. N., Meyn, M. S., & Grompe, M. (2003). Epithelial cancer in Fanconi anemia complementation group D2 (Fancd2)

knockout mice. *Genes & Development*, *17*(16), 2021–2035. https://doi.org/10.1101/gad.1103403

Hsu, P., Hanawalt, P. C., & Nouspikel, T. (2007). Nucleotide excision repair phenotype of human acute myeloid leukemia cell lines at various stages of differentiation. *Mutation Research/Fundamental and Molecular Mechanisms of Mutagenesis*, *614*(1), 3–15. https://doi.org/10.1016/j.mrfmmm.2006.06.008

Hua, B. L., & Orr-Weaver, T. L. (2017). DNA Replication Control During Drosophila Development: Insights into the Onset of S Phase, Replication Initiation, and Fork Progression. *Genetics*, *207*(1), 29–47. https://doi.org/10.1534/genetics.115.186627

Huang, C., Chambers, D., & Matthews, G. (Eds.). (2019). Systemic Circulation. In *Basic Physiology for Anaesthetists* (2nd ed., pp. 145–147). Cambridge University Press. https://doi.org/10.1017/9781108565011.036

Imlay, J. A., Chin, S. M., & Linn, S. (1988). Toxic DNA Damage by Hydrogen Peroxide Through the Fenton Reaction in Vivo and in Vitro. *Science*, *240*(4852), 640–642. https://doi.org/10.1126/science.2834821

Institute for Health Metrics and Evaluation. (2024). *Global Burden of Disease 2021: Findings from the GBD 2021 Study*. https://www.healthdata.org/research-analysis/library/global-burden-disease-2021-findings-gbd-2021-study

Jackson, K. L., Lin, W.-L., Miriyala, S., Dayton, R. D., Panchatcharam, M., McCarthy, K. J., Castanedes-Casey, M., Dickson, D. W., & Klein, R. L. (2017). P62 Pathology Model in the Rat Substantia Nigra with Filamentous Inclusions and Progressive Neurodegeneration. *PLOS ONE*, *12*(1), e0169291. https://doi.org/10.1371/journal.pone.0169291

Jacob, K. D., Noren Hooten, N., Tadokoro, T., Lohani, A., Barnes, J., & Evans, M. K. (2013). Alzheimer's disease-associated polymorphisms in human OGG1 alter catalytic activity

and sensitize cells to DNA damage. *Free Radical Biology & Medicine*, *63*, 115–125. https://doi.org/10.1016/j.freeradbiomed.2013.05.010

Jacobson, M. K., & Bernofsky, C. (1974). Mitochondrial acetaldehyde dehydrogenase from Saccharomyces cerevisiae. *Biochimica Et Biophysica Acta*, *350*(2), 277–291. https://doi.org/10.1016/0005-2744(74)90502-6

Jaiswal, S., Fontanillas, P., Flannick, J., Manning, A., Grauman, P. V., Mar, B. G., Lindsley, R. C., Mermel, C. H., Burtt, N., Chavez, A., Higgins, J. M., Moltchanov, V., Kuo, F. C., Kluk, M. J., Henderson, B., Kinnunen, L., Koistinen, H. A., Ladenvall, C., Getz, G., … Ebert, B. L. (2014). Age-related clonal hematopoiesis associated with adverse outcomes. *The New England Journal of Medicine*, *371*(26), 2488–2498. https://doi.org/10.1056/NEJMoa1408617

Jamieson, C. H. M., Ailles, L. E., Dylla, S. J., Muijtjens, M., Jones, C., Zehnder, J. L., Gotlib, J., Li, K., Manz, M. G., Keating, A., Sawyers, C. L., & Weissman, I. L. (2004). Granulocyte–Macrophage Progenitors as Candidate Leukemic Stem Cells in Blast-Crisis CML. *New England Journal of Medicine*, *351*(7), 657–667. https://doi.org/10.1056/NEJMoa040258

Jan, M., Snyder, T. M., Corces-Zimmerman, M. R., Vyas, P., Weissman, I. L., Quake, S. R., & Majeti, R. (2012). Clonal Evolution of Pre-Leukemic Hematopoietic Stem Cells Precedes Human Acute Myeloid Leukemia. *Science Translational Medicine*, *4*(149), 149ra118. https://doi.org/10.1126/scitranslmed.3004315

Jang, H., Kim, S., Kim, H., Oh, S. H., Kwak, S. Y., Joo, H.-W., Lee, S. B., Jang, W. I., Park, S., & Shim, S. (2022). Metformin Protects the Intestinal Barrier by Activating Goblet Cell Maturation and Epithelial Proliferation in Radiation-Induced Enteropathy. *International Journal of Molecular Sciences*, *23*(11), Article 11. https://doi.org/10.3390/ijms23115929

Jeggo, P. A., Pearl, L. H., & Carr, A. M. (2016). DNA repair, genome stability and cancer: A historical perspective. *Nature Reviews Cancer*, *16*(1), 35–42. https://doi.org/10.1038/nrc.2015.4

Jeong, S., Lee, J., Park, J. H., Son, Y., Lee, H.-J., Moon, C., Shin, I. S., Kim, J. S., & Kang, S. (2024). Olaparib synergically exacerbates the radiation-induced intestinal apoptosis in mice. *Molecular & Cellular Toxicology*, *20*(4), 979–987. https://doi.org/10.1007/s13273-023-00421-7

Jeong, S.-Y., Kim, J.-A., & Oh, I.-H. (2015). 5-Fluorouracil Treatment Leads to Activation of Stem Cell Niche By Reconstructing Mesenchymal Stromal Cells and Exert a Distinct Microenvironmental Impact on Normal and Leukemic Cells. *Blood*, *126*(23), 1197. https://doi.org/10.1182/blood.V126.23.1197.1197

Jeziorska, D. M., Tunnacliffe, E. A. J., Brown, J. M., Ayyub, H., Sloane-Stanley, J., Sharpe, J. A., Lagerholm, B. C., Babbs, C., Smith, A. J. H., Buckle, V. J., & Higgs, D. R. (2022). On-microscope staging of live cells reveals changes in the dynamics of transcriptional bursting during differentiation. *Nature Communications*, *13*, 6641. https://doi.org/10.1038/s41467-022-33977-4

Joenje, H., Arwert, F., Eriksson, A. W., de Koning, H., & Oostra, A. B. (1981). Oxygen-dependence of chromosomal aberrations in Fanconi's anaemia. *Nature*, *290*(5802), 142–143. https://doi.org/10.1038/290142a0

Johmura, Y., Shimada, M., Misaki, T., Naiki-Ito, A., Miyoshi, H., Motoyama, N., Ohtani, N., Hara, E., Nakamura, M., Morita, A., Takahashi, S., & Nakanishi, M. (2014). Necessary and sufficient role for a mitosis skip in senescence induction. *Molecular Cell*, *55*(1), 73–84. https://doi.org/10.1016/j.molcel.2014.05.003

Jones, S., Emmerson, P., Maynard, J., Best, J. M., Jordan, S., Williams, G. T., Sampson, J. R., & Cheadle, J. P. (2002). Biallelic germline mutations in MYH predispose to multiple colorectal adenoma and somatic G:C-->T:A mutations. *Human Molecular Genetics*, *11*(23), 2961–2967. https://doi.org/10.1093/hmg/11.23.2961

Joseph, C., Quach, J. M., Walkley, C. R., Lane, S. W., Lo Celso, C., & Purton, L. E. (2013). Deciphering hematopoietic stem cells in their niches: A critical appraisal of genetic

models, lineage tracing, and imaging strategies. *Cell Stem Cell*, *13*(5), 520–533. https://doi.org/10.1016/j.stem.2013.10.010

Kamimae-Lanning, A. N., Goloviznina, N. A., & Kurre, P. (2013). Fetal origins of hematopoietic failure in a murine model of Fanconi anemia. *Blood*, *121*(11), 2008–2012. https://doi.org/10.1182/blood-2012-06-439679

Kan, Z., & Madoff, D. C. (2008). Liver Anatomy: Microcirculation of the Liver. *Seminars in Interventional Radiology*, *25*(2), 77–85. https://doi.org/10.1055/s-2008-1076685

Karikkineth, A. C., Scheibye-Knudsen, M., Fivenson, E., Croteau, D. L., & Bohr, V. A. (2017). Cockayne syndrome: Clinical features, model systems and pathways. *Ageing Research Reviews*, *33*, 3–17. https://doi.org/10.1016/j.arr.2016.08.002

Kerzendorfer, C., Colnaghi, R., Abramowicz, I., Carpenter, G., & O'Driscoll, M. (2013). Meier–Gorlin syndrome and Wolf–Hirschhorn syndrome: Two developmental disorders highlighting the importance of efficient DNA replication for normal development and neurogenesis. *DNA Repair*, *12*(8), 637–644. https://doi.org/10.1016/j.dnarep.2013.04.016

Keyes, W. M., Wu, Y., Vogel, H., Guo, X., Lowe, S. W., & Mills, A. A. (2005). P63 deficiency activates a program of cellular senescence and leads to accelerated aging. *Genes & Development*, *19*(17), 1986–1999. https://doi.org/10.1101/gad.342305

Kinzler, K. W., & Vogelstein, B. (1998). Landscaping the Cancer Terrain. *Science*, *280*(5366), 1036–1037. https://doi.org/10.1126/science.280.5366.1036

Kleta, R., Bernardini, I., Ueda, M., Varade, W. S., Phornphutkul, C., Krasnewich, D., & Gahl, W. A. (2004). Long-term follow-up of well-treated nephropathic cystinosis patients. *The Journal of Pediatrics*, *145*(4), 555–560. https://doi.org/10.1016/j.jpeds.2004.03.056

Knudson, A. G. (1971). Mutation and cancer: Statistical study of retinoblastoma. *Proceedings of the National Academy of Sciences of the United States of America*, *68*(4), 820–823. https://doi.org/10.1073/pnas.68.4.820

Kobayashi, H., & Takubo, K. (2020). Protocol for the Maintenance of Quiescent Murine Hematopoietic Stem Cells. *STAR Protocols*, *1*(2), 100078. https://doi.org/10.1016/j.xpro.2020.100078

Kokic, G., Yakoub, G., van den Heuvel, D., Wondergem, A. P., van der Meer, P. J., van der Weegen, Y., Chernev, A., Fianu, I., Fokkens, T. J., Lorenz, S., Urlaub, H., Cramer, P., & Luijsterburg, M. S. (2024). Structural basis for RNA polymerase II ubiquitylation and inactivation in transcription-coupled repair. *Nature Structural & Molecular Biology*, *31*(3), 536–547. https://doi.org/10.1038/s41594-023-01207-0

Kondo, M., Weissman, I. L., & Akashi, K. (1997). Identification of clonogenic common lymphoid progenitors in mouse bone marrow. *Cell*, *91*(5), 661–672. https://doi.org/10.1016/s0092-8674(00)80453-5

Koomen, M., Cheng, N. C., van de Vrugt, H. J., Godthelp, B. C., van der Valk, M. A., Oostra, A. B., Zdzienicka, M. Z., Joenje, H., & Arwert, F. (2002). Reduced fertility and hypersensitivity to mitomycin C characterize Fancg/Xrcc9 null mice. *Human Molecular Genetics*, *11*(3), 273–281. https://doi.org/10.1093/hmg/11.3.273

Koulnis, M., Pop, R., Porpiglia, E., Shearstone, J. R., Hidalgo, D., & Socolovsky, M. (2011). Identification and Analysis of Mouse Erythroid Progenitors using the CD71/TER119 Flow-cytometric Assay. *Journal of Visualized Experiments : JoVE*, *54*, 2809. https://doi.org/10.3791/2809

Kovuru, N., Mochizuki-Kashio, M., Menna, T., Jeffrey, G., Hong, Y., me Yoon, Y., Zhang, Z., & Kurre, P. (2024). Deregulated protein homeostasis constrains fetal hematopoietic stem cell pool expansion in Fanconi anemia. *Nature Communications*, *15*(1), 1852. https://doi.org/10.1038/s41467-024-46159-1

Kozmin, S. G., & Jinks-Robertson, S. (2013). The Mechanism of Nucleotide Excision Repair-Mediated UV-Induced Mutagenesis in Nonproliferating Cells. *Genetics*, *193*(3), 803–817. https://doi.org/10.1534/genetics.112.147421

Kubota, M., Ohta, S., Ando, A., Koyama, A., Terashima, H., Kashii, H., Hoshino, H., Sugita, K., & Hayashi, M. (2015). Nationwide survey of Cockayne syndrome in Japan: Incidence, clinical course and prognosis. *Pediatrics International*, *57*(3), 339–347. https://doi.org/10.1111/ped.12635

Kudryavtsev, B. N., Kudryavtseva, M. V., Sakuta, G. A., & Stein, G. I. (1993). Human hepatocyte polyploidization kinetics in the course of life cycle. *Virchows Archiv B*, *64*(1), 387–393. https://doi.org/10.1007/BF02915139

Kunkel, T. A. (2009). Evolving views of DNA replication (in)fidelity. *Cold Spring Harbor Symposia on Quantitative Biology*, *74*, 91–101. https://doi.org/10.1101/sqb.2009.74.027

Kupculak, M., Bai, F., Luo, Q., Yoshikawa, Y., Lopez-Martinez, D., Xu, H., Uphoff, S., & Cohn, M. A. (2023). Phosphorylation by ATR triggers FANCD2 chromatin loading and activates the Fanconi anemia pathway. *Cell Reports*, *42*(7), 112721. https://doi.org/10.1016/j.celrep.2023.112721

Kurita, R., Suda, N., Sudo, K., Miharada, K., Hiroyama, T., Miyoshi, H., Tani, K., & Nakamura, Y. (2013). Establishment of Immortalized Human Erythroid Progenitor Cell Lines Able to Produce Enucleated Red Blood Cells. *PLOS ONE*, *8*(3), e59890. https://doi.org/10.1371/journal.pone.0059890

Kwak, S.-Y., Shim, S., Park, S., Kim, H., Lee, S.-J., Kim, M.-J., Jang, W.-S., Kim, Y., & Jang, H. (2021). Ghrelin reverts intestinal stem cell loss associated with radiation-induced enteropathy by activating Notch signaling. *Phytomedicine*, *81*, 153424. https://doi.org/10.1016/j.phymed.2020.153424

Laconi, E., Marongiu, F., & DeGregori, J. (2020). Cancer as a disease of old age: Changing mutational and microenvironmental landscapes. *British Journal of Cancer*, *122*(7), 943–952. https://doi.org/10.1038/s41416-019-0721-1

Langevin, F., Crossan, G. P., Rosado, I. V., Arends, M. J., & Patel, K. J. (2011). Fancd2 counteracts the toxic effects of naturally produced aldehydes in mice. *Nature*, *475*(7354), 53–58. https://doi.org/10.1038/nature10192

Lasaga, M., Río, P., Vilas-Zornoza, A., Planell, N., Navarro, S., Alignani, D., Fernández-Varas, B., Mouzo, D., Zubicaray, J., Pujol, R. M., Nicoletti, E., Schwartz, J. D., Sevilla, J., Ainciburi, M., Ullate-Agote, A., Surrallés, J., Perona, R., Sastre, L., Prosper, F., … Bueren, J. A. (2023). Gene therapy restores the transcriptional program of hematopoietic stem cells in Fanconi anemia. *Haematologica*, *108*(10), Article 10. https://doi.org/10.3324/haematol.2022.282418

Lau, T. Y., & Poon, R. Y. C. (2023). Whole-Genome Duplication and Genome Instability in Cancer Cells: Double the Trouble. *International Journal of Molecular Sciences*, *24*(4), 3733. https://doi.org/10.3390/ijms24043733

Laugel, V. (1993). Cockayne Syndrome. In M. P. Adam, J. Feldman, G. M. Mirzaa, R. A. Pagon, S. E. Wallace, & A. Amemiya (Eds.), *GeneReviews®*. University of Washington, Seattle. http://www.ncbi.nlm.nih.gov/books/NBK1342/

Leavy, O. (2010). Microglial cell origins. *Nature Reviews Immunology*, *10*(12), 809–809. https://doi.org/10.1038/nri2896

Lee-Six, H., Øbro, N. F., Shepherd, M. S., Grossmann, S., Dawson, K., Belmonte, M., Osborne, R. J., Huntly, B. J. P., Martincorena, I., Anderson, E., O'Neill, L., Stratton, M. R., Laurenti, E., Green, A. R., Kent, D. G., & Campbell, P. J. (2018). Population dynamics of normal human blood inferred from somatic mutations. *Nature*, *561*(7724), 473–478. https://doi.org/10.1038/s41586-018-0497-0

Leonardo, A. D., Linke, S. P., Clarkin, K., & Wahl, G. M. (1994). DNA damage triggers a prolonged p53-dependent G1 arrest and long-term induction of Cip1 in normal human fibroblasts. *Genes & Development*, *8*(21), 2540–2551. https://doi.org/10.1101/gad.8.21.2540

Li, N., Nakauka-Ddamba, A., Tobias, J., Jensen, S. T., & Lengner, C. J. (2016). Mouse Label-Retaining Cells Are Molecularly And Functionally Distinct From Reserve Intestinal Stem Cells. *Gastroenterology*, *151*(2), 298-310.e7. https://doi.org/10.1053/j.gastro.2016.04.049

Li, X., Le Beau, M. M., Ciccone, S., Yang, F.-C., Freie, B., Chen, S., Yuan, J., Hong, P., Orazi, A., Haneline, L. S., & Clapp, D. W. (2005). Ex vivo culture of Fancc-/- stem/progenitor cells predisposes cells to undergo apoptosis, and surviving stem/progenitor cells display cytogenetic abnormalities and an increased risk of malignancy. *Blood*, *105*(9), 3465–3471. https://doi.org/10.1182/blood-2004-06-2483

Liddelow, S. A., & Barres, B. A. (2017). Reactive Astrocytes: Production, Function, and Therapeutic Potential. *Immunity*, *46*(6), 957–967. https://doi.org/10.1016/j.immuni.2017.06.006

Lillenes, M. S., Rabano, A., Støen, M., Riaz, T., Misaghian, D., Møllersen, L., Esbensen, Y., Günther, C.-C., Selnes, P., Stenset, V. T. V., Fladby, T., & Tønjum, T. (2016). Altered DNA base excision repair profile in brain tissue and blood in Alzheimer's disease. *Molecular Brain*, *9*(1), 61. https://doi.org/10.1186/s13041-016-0237-z

Lindahl, T. (1993). Instability and decay of the primary structure of DNA. *Nature*, *362*(6422), 709–715. https://doi.org/10.1038/362709a0

Liu, L., Yan, Y., Zeng, M., Zhang, J., Hanes, M. A., Ahearn, G., McMahon, T. J., Dickfeld, T., Marshall, H. E., Que, L. G., & Stamler, J. S. (2004). Essential Roles of *S*-Nitrosothiols in Vascular Homeostasis and Endotoxic Shock. *Cell*, *116*(4), 617–628. https://doi.org/10.1016/S0092-8674(04)00131-X

Liu, Y., Elf, S. E., Miyata, Y., Sashida, G., Liu, Y., Huang, G., Giandomenico, S. D., Lee, J. M., Deblasio, A., Menendez, S., Antipin, J., Reva, B., Koff, A., & Nimer, S. D. (2009). P53 Regulates Hematopoietic Stem Cell Quiescence. *Cell Stem Cell*, *4*(1), 37–48. https://doi.org/10.1016/j.stem.2008.11.006

Loenarz, C., & Schofield, C. J. (2008). Expanding chemical biology of 2-oxoglutarate oxygenases. *Nature Chemical Biology*, *4*(3), 152–156. https://doi.org/10.1038/nchembio0308-152

Lopez Chiloeches, M., Bergonzini, A., Martin, O. C. B., Bergstein, N., Erttmann, S. F., Aung, K. M., Gekara, N. O., Avila Cariño, J. F., Pateras, I. S., & Frisan, T. (2024). Genotoxin-producing Salmonella enterica induces tissue-specific types of DNA damage and DNA damage response outcomes. *Frontiers in Immunology*, *14*. https://doi.org/10.3389/fimmu.2023.1270449

López-Otín, C., Blasco, M. A., Partridge, L., Serrano, M., & Kroemer, G. (2013). The Hallmarks of Aging. *Cell*, *153*(6), 1194–1217. https://doi.org/10.1016/j.cell.2013.05.039

Lu, T., Pan, Y., Kao, S.-Y., Li, C., Kohane, I., Chan, J., & Yankner, B. A. (2004). Gene regulation and DNA damage in the ageing human brain. *Nature*, *429*(6994), 883–891. https://doi.org/10.1038/nature02661

Lu, Y., Lian, H., Sharma, P., Schreiber-Agus, N., Russell, R. G., Chin, L., van der Horst, G. T. J., & Bregman, D. B. (2001). Disruption of the Cockayne Syndrome B Gene Impairs Spontaneous Tumorigenesis in Cancer-Predisposed Ink4a/ARF Knockout Mice. *Molecular and Cellular Biology*, *21*(5), 1810–1818. https://doi.org/10.1128/MCB.21.5.1810-1818.2001

Luo, W., Li, H., Zhang, Y., & Ang, C. Y. W. (2001). Determination of formaldehyde in blood plasma by high-performance liquid chromatography with fluorescence detection. *Journal of Chromatography B: Biomedical Sciences and Applications*, *753*(2), 253–257. https://doi.org/10.1016/S0378-4347(00)00552-1

Lyons, A. B., & Parish, C. R. (1994). Determination of lymphocyte division by flow cytometry. *Journal of Immunological Methods*, *171*(1), 131–137. https://doi.org/10.1016/0022-1759(94)90236-4

Mahony, C. B., & Bertrand, J. Y. (2019). How HSCs Colonize and Expand in the Fetal Niche of the Vertebrate Embryo: An Evolutionary Perspective. *Frontiers in Cell and Developmental Biology*, *7*, 34. https://doi.org/10.3389/fcell.2019.00034

Marescal, O., & Cheeseman, I. M. (2020). Cellular Mechanisms and Regulation of Quiescence. *Developmental Cell*, *55*(3), 259–271. https://doi.org/10.1016/j.devcel.2020.09.029

Margall-Ducos, G., Celton-Morizur, S., Couton, D., Brégerie, O., & Desdouets, C. (2007). Liver tetraploidization is controlled by a new process of incomplete cytokinesis. *Journal of Cell Science*, *120*(20), 3633–3639. https://doi.org/10.1242/jcs.016907

Martos, P. A., & Pawliszyn, J. (1998). Sampling and Determination of Formaldehyde Using Solid-Phase Microextraction with On-Fiber Derivatization. *Analytical Chemistry*, *70*(11), 2311–2320. https://doi.org/10.1021/ac9711394

Mathieu, N., Kaczmarek, N., Rüthemann, P., Luch, A., & Naegeli, H. (2013). DNA Quality Control by a Lesion Sensor Pocket of the Xeroderma Pigmentosum Group D Helicase Subunit of TFIIH. *Current Biology*, *23*(3), 204–212. https://doi.org/10.1016/j.cub.2012.12.032

Mayle, A., Luo, M., Jeong, M., & Goodell, M. A. (2013). Mouse Hematopoietic Stem Cell Identification And Analysis. *Cytometry. Part A : The Journal of the International Society for Analytical Cytology*, *83*(1), 27–37. https://doi.org/10.1002/cyto.a.22093

McCulloch, S. D., & Kunkel, T. A. (2008). The fidelity of DNA synthesis by eukaryotic replicative and translesion synthesis polymerases. *Cell Research*, *18*(1), 148–161. https://doi.org/10.1038/cr.2008.4

Meer, P. J. van der, Yakoub, G., Nakazawa, Y., Ogi, T., & Luijsterburg, M. S. (2024). *Clearance of DNA damage-arrested RNAPII is selectively impaired in Cockayne syndrome cells* (p. 2024.05.17.594644). bioRxiv. https://doi.org/10.1101/2024.05.17.594644

Mellon, I., Spivak, G., & Hanawalt, P. C. (1987). Selective removal of transcription-blocking DNA damage from the transcribed strand of the mammalian DHFR gene. *Cell*, *51*(2), 241–249. https://doi.org/10.1016/0092-8674(87)90151-6

Mevissen, T. E. T., Kümmecke, M., Schmid, E. W., Farnung, L., & Walter, J. C. (2024). STK19 positions TFIIH for cell-free transcription-coupled DNA repair. *Cell*, *187*(25), 7091-7106.e24. https://doi.org/10.1016/j.cell.2024.10.020

Mikkola, H. K. A., & Orkin, S. H. (2006). The journey of developing hematopoietic stem cells. *Development*, *133*(19), 3733–3744. https://doi.org/10.1242/dev.02568

Milyavsky, M., Gan, O. I., Trottier, M., Komosa, M., Tabach, O., Notta, F., Lechman, E., Hermans, K. G., Eppert, K., Konovalova, Z., Ornatsky, O., Domany, E., Meyn, M. S., & Dick, J. E. (2010). A distinctive DNA damage response in human hematopoietic stem cells reveals an apoptosis-independent role for p53 in self-renewal. *Cell Stem Cell*, *7*(2), 186–197. https://doi.org/10.1016/j.stem.2010.05.016

Mohrin, M., Bourke, E., Alexander, D., Warr, M. R., Barry-Holson, K., Le Beau, M. M., Morrison, C. G., & Passegué, E. (2010). Hematopoietic stem cell quiescence promotes error prone DNA repair and mutagenesis. *Cell Stem Cell*, *7*(2), 174–185. https://doi.org/10.1016/j.stem.2010.06.014

Moldovan, G.-L., & D'Andrea, A. D. (2009). How the Fanconi Anemia pathway guards the genome. *Annual Review of Genetics*, *43*, 223–249. https://doi.org/10.1146/annurev-genet-102108-134222

Molinuevo, R., Menendez, J., Cadle, K., Ariqat, N., Choy, M. K., Lagousis, C., Thomas, G., Strietzel, C., Bubolz, J. W., & Hinck, L. (2024). Physiological DNA damage promotes

functional endoreplication of mammary gland alveolar cells during lactation. *Nature Communications*, *15*(1), 3288. https://doi.org/10.1038/s41467-024-47668-9

Møller, P., Seppälä, T., Bernstein, I., Holinski-Feder, E., Sala, P., Evans, D. G., Lindblom, A., Macrae, F., Blanco, I., Sijmons, R., Jeffries, J., Vasen, H., Burn, J., Nakken, S., Hovig, E., Rødland, E. A., Tharmaratnam, K., de Vos tot Nederveen Cappel, W. H., Hill, J., … Möslein, G. (2017). Cancer incidence and survival in Lynch syndrome patients receiving colonoscopic and gynaecological surveillance: First report from the prospective Lynch syndrome database. *Gut*, *66*(3), 464–472. https://doi.org/10.1136/gutjnl-2015-309675

Mulderrig, L., Garaycoechea, J. I., Tuong, Z. K., Millington, C. L., Dingler, F. A., Ferdinand, J. R., Gaul, L., Tadross, J. A., Arends, M. J., O'Rahilly, S., Crossan, G. P., Clatworthy, M. R., & Patel, K. J. (2021). Aldehyde-driven transcriptional stress triggers an anorexic DNA damage response. *Nature*, *600*(7887), 158–163. https://doi.org/10.1038/s41586-021-04133-7

Mullican, S. E., Lin-Schmidt, X., Chin, C.-N., Chavez, J. A., Furman, J. L., Armstrong, A. A., Beck, S. C., South, V. J., Dinh, T. Q., Cash-Mason, T. D., Cavanaugh, C. R., Nelson, S., Huang, C., Hunter, M. J., & Rangwala, S. M. (2017). GFRAL is the receptor for GDF15 and the ligand promotes weight loss in mice and nonhuman primates. *Nature Medicine*, *23*(10), 1150–1157. https://doi.org/10.1038/nm.4392

Naim, V., & Rosselli, F. (2009). The FANC pathway and BLM collaborate during mitosis to prevent micro-nucleation and chromosome abnormalities. *Nature Cell Biology*, *11*(6), 761–768. https://doi.org/10.1038/ncb1883

Nakazawa, Y., Hara, Y., Oka, Y., Komine, O., Van Den Heuvel, D., Guo, C., Daigaku, Y., Isono, M., He, Y., Shimada, M., Kato, K., Jia, N., Hashimoto, S., Kotani, Y., Miyoshi, Y., Tanaka, M., Sobue, A., Mitsutake, N., Suganami, T., … Ogi, T. (2020). Ubiquitination of DNA Damage-Stalled RNAPII Promotes Transcription-Coupled Repair. *Cell*, *180*(6), 1228-1244.e24. https://doi.org/10.1016/j.cell.2020.02.010

Nakazawa, Y., Sasaki, K., Mitsutake, N., Matsuse, M., Shimada, M., Nardo, T., Takahashi, Y., Ohyama, K., Ito, K., Mishima, H., Nomura, M., Kinoshita, A., Ono, S., Takenaka, K., Masuyama, R., Kudo, T., Slor, H., Utani, A., Tateishi, S., … Ogi, T. (2012). Mutations in UVSSA cause UV-sensitive syndrome and impair RNA polymerase IIo processing in transcription-coupled nucleotide-excision repair. *Nature Genetics*, *44*(5), 586–592. https://doi.org/10.1038/ng.2229

Nance, M. A., & Berry, S. A. (1992). Cockayne syndrome: Review of 140 cases. *American Journal of Medical Genetics*, *42*(1), 68–84. https://doi.org/10.1002/ajmg.1320420115

Natale, V. (2011). A comprehensive description of the severity groups in Cockayne syndrome. *American Journal of Medical Genetics Part A*, *155*(5), 1081–1095. https://doi.org/10.1002/ajmg.a.33933

Nath, A., Chakrabarti, P., Sen, S., & Barui, A. (2022). Reactive Oxygen Species in Modulating Intestinal Stem Cell Dynamics and Function. *Stem Cell Reviews and Reports*, *18*(7), 2328–2350. https://doi.org/10.1007/s12015-022-10377-1

National Cancer Institute. (2007, September 17). *What Is Cancer? - NCI* (nciglobal,ncienterprise) [cgvArticle]. https://www.cancer.gov/about-cancer/understanding/what-is-cancer

Nemoto, S., Uchida, K., & Ohno, H. (2024). Implications of Genetic Factors Underlying Mouse Hydronephrosis: Cautionary Considerations on Phenotypic Interpretation in Genetically Engineered Mice. *International Journal of Molecular Sciences*, *25*(13), 7203. https://doi.org/10.3390/ijms25137203

Nieto Moreno, N., Olthof, A. M., & Svejstrup, J. Q. (2023). Transcription-Coupled Nucleotide Excision Repair and the Transcriptional Response to UV-Induced DNA Damage. *Annual Review of Biochemistry*, *92*(1), 81–113. https://doi.org/10.1146/annurev-biochem-052621-091205

Nik-Zainal, S., Alexandrov, L. B., Wedge, D. C., Van Loo, P., Greenman, C. D., Raine, K., Jones, D., Hinton, J., Marshall, J., Stebbings, L. A., Menzies, A., Martin, S., Leung, K., Chen,

L., Leroy, C., Ramakrishna, M., Rance, R., Lau, K. W., Mudie, L. J., … Stratton, M. R. (2012). Mutational Processes Molding the Genomes of 21 Breast Cancers. *Cell*, *149*(5), 979–993. https://doi.org/10.1016/j.cell.2012.04.024

Noll, M., Battaile, K. P., Bateman, R., Lax, T. P., Rathbun, K., Reifsteck, C., Bagby, G., Finegold, M., Olson, S., & Grompe, M. (2002). Fanconi anemia group A and C double-mutant mice: Functional evidence for a multi-protein Fanconi anemia complex. *Experimental Hematology*, *30*(7), 679–688. https://doi.org/10.1016/s0301-472x(02)00838-x

Nouspikel, T., & Hanawalt, P. C. (2000). Terminally differentiated human neurons repair transcribed genes but display attenuated global DNA repair and modulation of repair gene expression. *Molecular and Cellular Biology*, *20*(5), 1562–1570. https://doi.org/10.1128/MCB.20.5.1562-1570.2000

Ogi, T., Limsirichaikul, S., Overmeer, R. M., Volker, M., Takenaka, K., Cloney, R., Nakazawa, Y., Niimi, A., Miki, Y., Jaspers, N. G., Mullenders, L. H. F., Yamashita, S., Fousteri, M. I., & Lehmann, A. R. (2010). Three DNA polymerases, recruited by different mechanisms, carry out NER repair synthesis in human cells. *Molecular Cell*, *37*(5), 714–727. https://doi.org/10.1016/j.molcel.2010.02.009

Ogilvy, S., Elefanty, A. G., Visvader, J., Bath, M. L., Harris, A. W., & Adams, J. M. (1998). Transcriptional regulation of vav, a gene expressed throughout the hematopoietic compartment. *Blood*, *91*(2), 419–430.

Ogilvy, S., Metcalf, D., Gibson, L., Bath, M. L., Harris, A. W., & Adams, J. M. (1999). Promoter elements of vav drive transgene expression in vivo throughout the hematopoietic compartment. *Blood*, *94*(6), 1855–1863.

Oka, Y., Hamada, M., Nakazawa, Y., Muramatsu, H., Okuno, Y., Higasa, K., Shimada, M., Takeshima, H., Hanada, K., Hirano, T., Kawakita, T., Sakaguchi, H., Ichimura, T., Ozono, S., Yuge, K., Watanabe, Y., Kotani, Y., Yamane, M., Kasugai, Y., … Ogi, T. (2020). Digenic mutations in ALDH2 and ADH5 impair formaldehyde clearance and

cause a multisystem disorder, AMeD syndrome. *Science Advances*, *6*(51), eabd7197. https://doi.org/10.1126/sciadv.abd7197

Oka, Y., Nakazawa, Y., Shimada, M., & Ogi, T. (2024). Endogenous aldehyde-induced DNA–protein crosslinks are resolved by transcription-coupled repair. *Nature Cell Biology*, *26*(5), 784–796. https://doi.org/10.1038/s41556-024-01401-2

Okamoto, Y., Abe, M., Mu, A., Tempaku, Y., Rogers, C. B., Mochizuki, A. L., Katsuki, Y., Kanemaki, M. T., Takaori-Kondo, A., Sobeck, A., Bielinsky, A.-K., & Takata, M. (2021). SLFN11 promotes stalled fork degradation that underlies the phenotype in Fanconi anemia cells. *Blood*, *137*(3), 336–348. https://doi.org/10.1182/blood.2019003782

Oshima, J., Sidorova, J. M., & Monnat, R. J. (2017). Werner syndrome: Clinical features, pathogenesis and potential therapeutic interventions. *Ageing Research Reviews*, *33*, 105–114. https://doi.org/10.1016/j.arr.2016.03.002

Osorio, F. G., Rosendahl Huber, A., Oka, R., Verheul, M., Patel, S. H., Hasaart, K., de la Fonteijne, L., Varela, I., Camargo, F. D., & van Boxtel, R. (2018). Somatic Mutations Reveal Lineage Relationships and Age-Related Mutagenesis in Human Hematopoiesis. *Cell Reports*, *25*(9), 2308-2316.e4. https://doi.org/10.1016/j.celrep.2018.11.014

Parmar, K., Kim, J., Sykes, S. M., Shimamura, A., Stuckert, P., Zhu, K., Hamilton, A., Deloach, M. K., Kutok, J. L., Akashi, K., Gilliland, D. G., & D'andrea, A. (2010). Hematopoietic stem cell defects in mice with deficiency of Fancd2 or Usp1. *Stem Cells (Dayton, Ohio)*, *28*(7), 1186–1195. https://doi.org/10.1002/stem.437

Paul-Konietzko, K., Thomale, J., Arakawa, H., & Iliakis, G. (2015). DNA Ligases I and III Support Nucleotide Excision Repair in DT40 Cells with Similar Efficiency. *Photochemistry and Photobiology*, *91*(5), 1173–1180. https://doi.org/10.1111/php.12487

Peña-Gómez, M. J., Moreno-Gordillo, P., Narmontė, M., García-Calderón, C. B., Rukšėnaitė, A., Klimašauskas, S., & Rosado, I. V. (2022). FANCD2 maintains replication fork stability during misincorporation of the DNA demethylation products 5-hydroxymethyl-2'-

deoxycytidine and 5-hydroxymethyl-2'-deoxyuridine. *Cell Death & Disease*, *13*(5), 1–11. https://doi.org/10.1038/s41419-022-04952-0

Pietzke, M., Burgos-Barragan, G., Wit, N., Tait-Mulder, J., Sumpton, D., Mackay, G. M., Patel, K. J., & Vazquez, A. (2020). Amino acid dependent formaldehyde metabolism in mammals. *Communications Chemistry*, *3*, 78. https://doi.org/10.1038/s42004-020-0324-z

Pocker, Y., & Li, H. (1991). Kinetics and Mechanism of Methanol and Formaldehyde Interconversion and Formaldehyde Oxidation Catalyzed by Liver Alcohol Dehydrogenase. In H. Weiner, B. Wermuth, & D. W. Crabb (Eds.), *Enzymology and Molecular Biology of Carbonyl Metabolism 3* (pp. 315–325). Springer US. https://doi.org/10.1007/978-1-4684-5901-2_34

Pontel, L. B., Rosado, I. V., Burgos-Barragan, G., Garaycoechea, J. I., Yu, R., Arends, M. J., Chandrasekaran, G., Broecker, V., Wei, W., Liu, L., Swenberg, J. A., Crossan, G. P., & Patel, K. J. (2015). Endogenous Formaldehyde Is a Hematopoietic Stem Cell Genotoxin and Metabolic Carcinogen. *Molecular Cell*, *60*(1), 177–188. https://doi.org/10.1016/j.molcel.2015.08.020

Preston, B. D., Albertson, T. M., & Herr, A. J. (2010). DNA Replication Fidelity and Cancer. *Seminars in Cancer Biology*, *20*(5), 281–293. https://doi.org/10.1016/j.semcancer.2010.10.009

Putze, J., Hennequin, C., Nougayrède, J.-P., Zhang, W., Homburg, S., Karch, H., Bringer, M.-A., Fayolle, C., Carniel, E., Rabsch, W., Oelschlaeger, T. A., Oswald, E., Forestier, C., Hacker, J., & Dobrindt, U. (2009). Genetic Structure and Distribution of the Colibactin Genomic Island among Members of the Family Enterobacteriaceae. *Infection and Immunity*, *77*(11), 4696–4703. https://doi.org/10.1128/iai.00522-09

Ranasinghe, I. R., Sharma, B., & Bashir, K. (2025). Hepatorenal Syndrome. In *StatPearls*. StatPearls Publishing. http://www.ncbi.nlm.nih.gov/books/NBK430856/

Randall, T. D., & Weissman, I. L. (1997). Phenotypic and Functional Changes Induced at the Clonal Level in Hematopoietic Stem Cells After 5-Fluorouracil Treatment. *Blood*, *89*(10), 3596–3606. https://doi.org/10.1182/blood.V89.10.3596

Ranes, M., Boeing, S., Wang, Y., Wienholz, F., Menoni, H., Walker, J., Encheva, V., Chakravarty, P., Mari, P.-O., Stewart, A., Giglia-Mari, G., Snijders, A. P., Vermeulen, W., & Svejstrup, J. Q. (2016). A ubiquitylation site in Cockayne syndrome B required for repair of oxidative DNA damage, but not for transcription-coupled nucleotide excision repair. *Nucleic Acids Research*, *44*(11), 5246–5255. https://doi.org/10.1093/nar/gkw216

Rath, E., & Haller, D. (2022). Intestinal epithelial cell metabolism at the interface of microbial dysbiosis and tissue injury. *Mucosal Immunology*, *15*(4), 595–604. https://doi.org/10.1038/s41385-022-00514-x

Reid-Bayliss, K. S., Arron, S. T., Loeb, L. A., Bezrookove, V., & Cleaver, J. E. (2016). Why Cockayne syndrome patients do not get cancer despite their DNA repair deficiency. *Proceedings of the National Academy of Sciences*, *113*(36), 10151–10156. https://doi.org/10.1073/pnas.1610020113

Reingruber, H., & Pontel, L. B. (2018). Formaldehyde metabolism and its impact on human health. *Current Opinion in Toxicology*, *9*, 28–34. https://doi.org/10.1016/j.cotox.2018.07.001

Reynolds, A., Wharton, N., Parris, A., Mitchell, E., Sobolewski, A., Kam, C., Bigwood, L., El Hadi, A., Münsterberg, A., Lewis, M., Speakman, C., Stebbings, W., Wharton, R., Sargen, K., Tighe, R., Jamieson, C., Hernon, J., Kapur, S., Oue, N., … Williams, M. R. (2014). Canonical Wnt signals combined with suppressed TGFβ/BMP pathways promote renewal of the native human colonic epithelium. *Gut*, *63*(4), 610–621. https://doi.org/10.1136/gutjnl-2012-304067

Rivera-Torruco, G., Muench, M. O., & Valle-Rios, R. (2024). Exploring extramedullary hematopoiesis: Unraveling the hematopoietic microenvironments. *Frontiers in Hematology*, *3*. https://doi.org/10.3389/frhem.2024.1371823

Rix, B., Maduro, A. H., Bridge, K. S., & Grey, W. (2022). Markers for human haematopoietic stem cells: The disconnect between an identification marker and its function. *Frontiers in Physiology*, *13*, 1009160. https://doi.org/10.3389/fphys.2022.1009160

Rosenberg, P. S., Greene, M. H., & Alter, B. P. (2003). Cancer incidence in persons with Fanconi anemia. *Blood*, *101*(3), 822–826. https://doi.org/10.1182/blood-2002-05-1498

Rossi, D. J., Bryder, D., Seita, J., Nussenzweig, A., Hoeijmakers, J., & Weissman, I. L. (2007). Deficiencies in DNA damage repair limit the function of haematopoietic stem cells with age. *Nature*, *447*(7145), 725–729. https://doi.org/10.1038/nature05862

Rozelle, A. L., Cheun, Y., Vilas, C. K., Koag, M.-C., & Lee, S. (2021). DNA interstrand cross-links induced by the major oxidative adenine lesion 7,8-dihydro-8-oxoadenine. *Nature Communications*, *12*(1), 1897. https://doi.org/10.1038/s41467-021-22273-2

Rübe, C. E., Fricke, A., Widmann, T. A., Fürst, T., Madry, H., Pfreundschuh, M., & Rübe, C. (2011). Accumulation of DNA Damage in Hematopoietic Stem and Progenitor Cells during Human Aging. *PLOS ONE*, *6*(3), e17487. https://doi.org/10.1371/journal.pone.0017487

Sah, E., Krishnamurthy, S., Ahmidouch, M. Y., Gillispie, G. J., Milligan, C., & Orr, M. E. (2021). The Cellular Senescence Stress Response in Post-Mitotic Brain Cells: Cell Survival at the Expense of Tissue Degeneration. *Life*, *11*(3), 229. https://doi.org/10.3390/life11030229

Sandoval, A., Consoli, U., & Plunkett, W. (1996). Fludarabine-mediated inhibition of nucleotide excision repair induces apoptosis in quiescent human lymphocytes. *Clinical Cancer Research*, *2*(10), 1731–1741.

Sanghani, P. C., Stone, C. L., Ray, B. D., Pindel, E. V., Hurley, T. D., & Bosron, W. F. (2000). Kinetic mechanism of human glutathione-dependent formaldehyde dehydrogenase. *Biochemistry*, *39*(35), 10720–10729. https://doi.org/10.1021/bi9929711

Schindler, D., & Hoehn, H. (1988). Fanconi anemia mutation causes cellular susceptibility to ambient oxygen. *American Journal of Human Genetics*, *43*(4), 429–435.

Schöneich, C. (2005). Methionine oxidation by reactive oxygen species: Reaction mechanisms and relevance to Alzheimer's disease. *Biochimica et Biophysica Acta (BBA) - Proteins and Proteomics*, *1703*(2), 111–119. https://doi.org/10.1016/j.bbapap.2004.09.009

Schwab, R. A., Nieminuszczy, J., Shah, F., Langton, J., Lopez Martinez, D., Liang, C.-C., Cohn, M. A., Gibbons, R. J., Deans, A. J., & Niedzwiedz, W. (2015). The Fanconi Anemia Pathway Maintains Genome Stability by Coordinating Replication and Transcription. *Molecular Cell*, *60*(3), 351–361. https://doi.org/10.1016/j.molcel.2015.09.012

Selby, C. P., Lindsey-Boltz, L. A., Li, W., & Sancar, A. (2023). Molecular Mechanisms of Transcription-Coupled Repair. *Annual Review of Biochemistry*, *92*(1), 115–144. https://doi.org/10.1146/annurev-biochem-041522-034232

Shao, C., Xiong, S., Li, G.-M., Gu, L., Mao, G., Markesbery, W. R., & Lovell, M. A. (2008). Altered 8-oxoguanine glycosylase in mild cognitive impairment and late-stage Alzheimer's disease brain. *Free Radical Biology & Medicine*, *45*(6), 813–819. https://doi.org/10.1016/j.freeradbiomed.2008.06.003

Shao, X., Somlo, S., & Igarashi, P. (2002). Epithelial-specific Cre/lox recombination in the developing kidney and genitourinary tract. *Journal of the American Society of Nephrology: JASN*, *13*(7), 1837–1846. https://doi.org/10.1097/01.asn.0000016444.90348.50

Shapiro, B., Tocci, P., Haase, G., Gavert, N., & Ben-Ze'ev, A. (2015). Clusterin, a gene enriched in intestinal stem cells, is required for L1-mediated colon cancer metastasis. *Oncotarget*, *6*(33), 34389–34401.

Shearstone, J. R., Pop, R., Bock, C., Boyle, P., Meissner, A., & Socolovsky, M. (2011). Global DNA Demethylation During Erythropoiesis in vivo. *Science (New York, N.Y.)*, *334*(6057), 799. https://doi.org/10.1126/science.1207306

Sheng, X., Lin, Z., Lv, C., Shao, C., Bi, X., Deng, M., Xu, J., Guerrero-Juarez, C. F., Li, M., Wu, X., Zhao, R., Yang, X., Li, G., Liu, X., Wang, Q., Nie, Q., Cui, W., Gao, S., Zhang, H., … Yu, Z. (2020). Cycling Stem Cells Are Radioresistant and Regenerate the Intestine. *Cell Reports*, *32*(4), 107952. https://doi.org/10.1016/j.celrep.2020.107952

Sherman, M. H., Bassing, C. H., & Teitell, M. A. (2011). DNA damage response regulates cell differentiation. *Trends in Cell Biology*, *21*(5), 312–319. https://doi.org/10.1016/j.tcb.2011.01.004

Shi, Y., Lan, F., Matson, C., Mulligan, P., Whetstine, J. R., Cole, P. A., Casero, R. A., & Shi, Y. (2004a). Histone demethylation mediated by the nuclear amine oxidase homolog LSD1. *Cell*, *119*(7), 941–953. https://doi.org/10.1016/j.cell.2004.12.012

Shi, Y., Lan, F., Matson, C., Mulligan, P., Whetstine, J. R., Cole, P. A., Casero, R. A., & Shi, Y. (2004b). Histone Demethylation Mediated by the Nuclear Amine Oxidase Homolog LSD1. *Cell*, *119*(7), 941–953. https://doi.org/10.1016/j.cell.2004.12.012

Shibutani, S., Takeshita, M., & Grollman, A. P. (1991). Insertion of specific bases during DNA synthesis past the oxidation-damaged base 8-oxodG. *Nature*, *349*(6308), 431–434. https://doi.org/10.1038/349431a0

Shih, H.-M., Wu, C.-J., & Lin, S.-L. (2018). Physiology and pathophysiology of renal erythropoietin-producing cells. *Journal of the Formosan Medical Association*, *117*(11), 955–963. https://doi.org/10.1016/j.jfma.2018.03.017

Shimamura, A., & Alter, B. P. (2010). Pathophysiology and Management of Inherited Bone Marrow Failure Syndromes. *Blood Reviews*, *24*(3), 101–122. https://doi.org/10.1016/j.blre.2010.03.002

Shimshek, D. R., Kim, J., Hübner, M. R., Spergel, D. J., Buchholz, F., Casanova, E., Stewart, A. F., Seeburg, P. H., & Sprengel, R. (2002). Codon-improved Cre recombinase (iCre) expression in the mouse. *Genesis (New York, N.Y.: 2000)*, *32*(1), 19–26. https://doi.org/10.1002/gene.10023

Shlush, L. I., Zandi, S., Mitchell, A., Chen, W. C., Brandwein, J. M., Gupta, V., Kennedy, J. A., Schimmer, A. D., Schuh, A. C., Yee, K. W., McLeod, J. L., Doedens, M., Medeiros, J. J. F., Marke, R., Kim, H. J., Lee, K., McPherson, J. D., Hudson, T. J., Brown, A. M. K., … Dick, J. E. (2014). Identification of pre-leukemic hematopoietic stem cells in acute leukemia. *Nature*, *506*(7488), 328–333. https://doi.org/10.1038/nature13038

Silkworth, W. T., Nardi, I. K., Scholl, L. M., & Cimini, D. (2009). Multipolar spindle pole coalescence is a major source of kinetochore mis-attachment and chromosome mis-segregation in cancer cells. *PloS One*, *4*(8), e6564. https://doi.org/10.1371/journal.pone.0006564

Singer, I. I., Kawka, D. W., Scott, S., Weidner, J. R., Mumford, R. A., Riehl, T. E., & Stenson, W. F. (1996). Expression of inducible nitric oxide synthase and nitrotyrosine in colonic epithelium in inflammatory bowel disease. *Gastroenterology*, *111*(4), 871–885. https://doi.org/10.1016/s0016-5085(96)70055-0

Singh, S., Jakubison, B., & Keller, J. R. (2020). Protection of hematopoietic stem cells from stress-induced exhaustion and aging. *Current Opinion in Hematology*, *27*(4), 225. https://doi.org/10.1097/MOH.0000000000000586

Soares, J. P., Cortinhas, A., Bento, T., Leitão, J. C., Collins, A. R., Gaivã, I., & Mota, M. P. (2014). Aging and DNA damage in humans: A meta-analysis study. *Aging*, *6*(6), 432–439. https://doi.org/10.18632/aging.100667

Spisak, N., de Manuel, M., Milligan, W., Sella, G., & Przeworski, M. (2024). The clock-like accumulation of germline and somatic mutations can arise from the interplay of DNA

damage and repair. *PLOS Biology*, *22*(6), e3002678. https://doi.org/10.1371/journal.pbio.3002678

Steinberg, S. E. (1984). Mechanisms of folate homeostasis. *American Journal of Physiology-Gastrointestinal and Liver Physiology*, *246*(4), G319–G324. https://doi.org/10.1152/ajpgi.1984.246.4.G319

Steinberg, S. E., Campbell, C. L., & Hillman, R. S. (1979). Kinetics of the Normal Folate Enterohepatic Cycle. *Journal of Clinical Investigation*, *64*(1), 83–88.

Suzuki, S., Racine, R. R., Manalo, N. A., Cantor, S. B., & Raffel, G. D. (2017). Impairment of fetal hematopoietic stem cell function in the absence of Fancd2. *Experimental Hematology*, *48*, 79–86. https://doi.org/10.1016/j.exphem.2016.11.006

Svejstrup, J. Q. (2002). Mechanisms of transcription-coupled DNA repair. *Nature Reviews Molecular Cell Biology*, *3*(1), 21–29. https://doi.org/10.1038/nrm703

Swanton, C., McGranahan, N., Starrett, G. J., & Harris, R. S. (2015). APOBEC enzymes: Mutagenic fuel for cancer evolution and heterogeneity. *Cancer Discovery*, *5*(7), 704–712. https://doi.org/10.1158/2159-8290.CD-15-0344

Swinnen, N., Smolders, S., Avila, A., Notelaers, K., Paesen, R., Ameloot, M., Brône, B., Legendre, P., & Rigo, J.-M. (2013). Complex invasion pattern of the cerebral cortex bymicroglial cells during development of the mouse embryo. *Glia*, *61*(2), 150–163. https://doi.org/10.1002/glia.22421

Szilvassy, S. J., Humphries, R. K., Lansdorp, P. M., Eaves, A. C., & Eaves, C. J. (1990). Quantitative assay for totipotent reconstituting hematopoietic stem cells by a competitive repopulation strategy. *Proceedings of the National Academy of Sciences of the United States of America*, *87*(22), 8736–8740. https://doi.org/10.1073/pnas.87.22.8736

Takahashi, A., Ohtani, N., Yamakoshi, K., Iida, S., Tahara, H., Nakayama, K., Nakayama, K. I., Ide, T., Saya, H., & Hara, E. (2006). Mitogenic signalling and the p16INK4a-Rb pathway

cooperate to enforce irreversible cellular senescence. *Nature Cell Biology*, *8*(11), 1291–1297. https://doi.org/10.1038/ncb1491

Tayri-Wilk, T., Slavin, M., Zamel, J., Blass, A., Cohen, S., Motzik, A., Sun, X., Shalev, D. E., Ram, O., & Kalisman, N. (2020). Mass spectrometry reveals the chemistry of formaldehyde cross-linking in structured proteins. *Nature Communications*, *11*(1), 3128. https://doi.org/10.1038/s41467-020-16935-w

Tetteh, P. W., Basak, O., Farin, H. F., Wiebrands, K., Kretzschmar, K., Begthel, H., van den Born, M., Korving, J., de Sauvage, F., van Es, J. H., van Oudenaarden, A., & Clevers, H. (2016). Replacement of Lost Lgr5-Positive Stem Cells through Plasticity of Their Enterocyte-Lineage Daughters. *Cell Stem Cell*, *18*(2), 203–213. https://doi.org/10.1016/j.stem.2016.01.001

Thakur, B. K., Malaisé, Y., & Martin, A. (2019). Unveiling the Mutational Mechanism of the Bacterial Genotoxin Colibactin in Colorectal Cancer. *Molecular Cell*, *74*(2), 227–229. https://doi.org/10.1016/j.molcel.2019.04.007

Tischkowitz, M., & Hodgson, S. (2003). Fanconi anaemia. *Journal of Medical Genetics*, *40*(1), 1–10. https://doi.org/10.1136/jmg.40.1.1

Trapp, C., Reite, K., Klungland, A., & Epe, B. (2007). Deficiency of the Cockayne syndrome B (CSB) gene aggravates the genomic instability caused by endogenous oxidative DNA base damage in mice. *Oncogene*, *26*(27), 4044–4048. https://doi.org/10.1038/sj.onc.1210167

Trewick, S. C., Henshaw, T. F., Hausinger, R. P., Lindahl, T., & Sedgwick, B. (2002). Oxidative demethylation by Escherichia coli AlkB directly reverts DNA base damage. *Nature*, *419*(6903), 174–178. https://doi.org/10.1038/nature00908

Tsukada, Y., Fang, J., Erdjument-Bromage, H., Warren, M. E., Borchers, C. H., Tempst, P., & Zhang, Y. (2006). Histone demethylation by a family of JmjC domain-containing proteins. *Nature*, *439*(7078), 811–816. https://doi.org/10.1038/nature04433

Tubbs, A., & Nussenzweig, A. (2017). Endogenous DNA Damage as a Source of Genomic Instability in Cancer. *Cell*, *168*(4), 644–656. https://doi.org/10.1016/j.cell.2017.01.002

Tufegdžić Vidaković, A., Mitter, R., Kelly, G. P., Neumann, M., Harreman, M., Rodríguez-Martínez, M., Herlihy, A., Weems, J. C., Boeing, S., Encheva, V., Gaul, L., Milligan, L., Tollervey, D., Conaway, R. C., Conaway, J. W., Snijders, A. P., Stewart, A., & Svejstrup, J. Q. (2020). Regulation of the RNAPII Pool Is Integral to the DNA Damage Response. *Cell*, *180*(6), 1245-1261.e21. https://doi.org/10.1016/j.cell.2020.02.009

Tulpule, A., Lensch, M. W., Miller, J. D., Austin, K., D'Andrea, A., Schlaeger, T. M., Shimamura, A., & Daley, G. Q. (2010). Knockdown of Fanconi anemia genes in human embryonic stem cells reveals early developmental defects in the hematopoietic lineage. *Blood*, *115*(17), 3453–3462. https://doi.org/10.1182/blood-2009-10-246694

Ullman-Culleré, M. H., & Foltz, C. J. (1999). Body Condition Scoring: A Rapid and Accurate Method for Assessing Health Status in Mice. *Laboratory Animal Science*, *49*(3).

Uotila, L., & Koivusalo, M. (1974). Formaldehyde dehydrogenase from human liver. Purification, properties, and evidence for the formation of glutathione thiol esters by the enzyme. *The Journal of Biological Chemistry*, *249*(23), 7653–7663.

Valverde, M., Lozano-Salgado, J., Fortini, P., Rodriguez-Sastre, M. A., Rojas, E., & Dogliotti, E. (2018). Hydrogen Peroxide-Induced DNA Damage and Repair through the Differentiation of Human Adipose-Derived Mesenchymal Stem Cells. *Stem Cells International*, *2018*, 1615497. https://doi.org/10.1155/2018/1615497

van Batenburg, A. A., Kazemier, K. M., van Oosterhout, M. F. M., van der Vis, J. J., Grutters, J. C., Goldschmeding, R., & van Moorsel, C. H. M. (2021). Telomere shortening and DNA damage in culprit cells of different types of progressive fibrosing interstitial lung disease. *ERJ Open Research*, *7*(2), 00691–02020. https://doi.org/10.1183/23120541.00691-2020

van de Vrugt, H. J., Eaton, L., Newell, A. H., Al-Dhalimy, M., Liskay, R. M., Olson, S. B., & Grompe, M. (2009). Embryonic lethality after combined inactivation of Fancd2 and Mlh1

in mice. *Cancer Research*, *69*(24), 9431–9438. https://doi.org/10.1158/0008-5472.CAN-09-2452

Van der Auwera, G. A., Carneiro, M. O., Hartl, C., Poplin, R., del Angel, G., Levy-Moonshine, A., Jordan, T., Shakir, K., Roazen, D., Thibault, J., Banks, E., Garimella, K. V., Altshuler, D., Gabriel, S., & DePristo, M. A. (2013). From FastQ data to high confidence variant calls: The Genome Analysis Toolkit best practices pipeline. *Current Protocols in Bioinformatics / Editoral Board, Andreas D. Baxevanis ... [et Al.]*, *11*(1110), 11.10.1-11.10.33. https://doi.org/10.1002/0471250953.bi1110s43

Van Der Horst, G. T. J., Meira, L., Gorgels, T. G. M. F., De Wit, J., Velasco-Miguel, S., Richardson, J. A., Kamp, Y., Vreeswijk, M. P. G., Smit, B., Bootsma, D., Hoeijmakers, J. H. J., & Friedberg, E. C. (2002). UVB radiation-induced cancer predisposition in Cockayne syndrome group A (Csa) mutant mice. *DNA Repair*, *1*(2), 143–157. https://doi.org/10.1016/S1568-7864(01)00010-6

van der Horst, G. T., van Steeg, H., Berg, R. J., van Gool, A. J., de Wit, J., Weeda, G., Morreau, H., Beems, R. B., van Kreijl, C. F., de Gruijl, F. R., Bootsma, D., & Hoeijmakers, J. H. (1997). Defective transcription-coupled repair in Cockayne syndrome B mice is associated with skin cancer predisposition. *Cell*, *89*(3), 425–435. https://doi.org/10.1016/s0092-8674(00)80223-8

van der Weegen, Y., de Lint, K., van den Heuvel, D., Nakazawa, Y., Mevissen, T. E. T., van Schie, J. J. M., San Martin Alonso, M., Boer, D. E. C., González-Prieto, R., Narayanan, I. V., Klaassen, N. H. M., Wondergem, A. P., Roohollahi, K., Dorsman, J. C., Hara, Y., Vertegaal, A. C. O., de Lange, J., Walter, J. C., Noordermeer, S. M., … Luijsterburg, M. S. (2021). ELOF1 is a transcription-coupled DNA repair factor that directs RNA polymerase II ubiquitylation. *Nature Cell Biology*, *23*(6), 595–607. https://doi.org/10.1038/s41556-021-00688-9

van Es, J. H., Sato, T., van de Wetering, M., Lyubimova, A., Yee Nee, A. N., Gregorieff, A., Sasaki, N., Zeinstra, L., van den Born, M., Korving, J., Martens, A. C. M., Barker, N., van Oudenaarden, A., & Clevers, H. (2012). Dll1+ secretory progenitor cells revert to stem cells upon crypt damage. *Nature Cell Biology*, *14*(10), 1099–1104. https://doi.org/10.1038/ncb2581

van Sluis, M., Yu, Q., van der Woude, M., Gonzalo-Hansen, C., Dealy, S. C., Janssens, R. C., Somsen, H. B., Ramadhin, A. R., Dekkers, D. H. W., Wienecke, H. L., Demmers, J. J. P. G., Raams, A., Davó-Martínez, C., Llerena Schiffmacher, D. A., van Toorn, M., Häckes, D., Thijssen, K. L., Zhou, D., Lammers, J. G., … Marteijn, J. A. (2024). Transcription-coupled DNA–protein crosslink repair by CSB and CRL4CSA-mediated degradation. *Nature Cell Biology*, *26*(5), 770–783. https://doi.org/10.1038/s41556-024-01394-y

van Steeg, H., & Kraemer, K. H. (1999). Xeroderma pigmentosum and the role of UV-induced DNA damage in skin cancer. *Molecular Medicine Today*, *5*(2), 86–94. https://doi.org/10.1016/S1357-4310(98)01394-X

Vare, D., Groth, P., Carlsson, R., Johansson, F., Erixon, K., & Jenssen, D. (2012). DNA interstrand crosslinks induce a potent replication block followed by formation and repair of double strand breaks in intact mammalian cells. *DNA Repair*, *11*(12), 976–985. https://doi.org/10.1016/j.dnarep.2012.09.010

Vélez-Cruz, R., Zadorin, A. S., Coin, F., & Egly, J.-M. (2013). Sirt1 suppresses RNA synthesis after UV irradiation in combined xeroderma pigmentosum group D/Cockayne syndrome (XP-D/CS) cells. *Proceedings of the National Academy of Sciences of the United States of America*, *110*(3), E212-220. https://doi.org/10.1073/pnas.1213076110

Vijg, J. (2014). Somatic mutations, genome mosaicism, cancer and aging. *Current Opinion in Genetics & Development*, *26*, 141–149. https://doi.org/10.1016/j.gde.2014.04.002

Vinogradov, A. E., Anatskaya, O. V., & Kudryavtsev, B. N. (2001). Relationship of hepatocyte ploidy levels with body size and growth rate in mammals. *Genome*, *44*(3), 350–360. https://doi.org/10.1139/g01-015

Vlachogiannis, N. I., Ntouros, P. A., Pappa, M., Kravvariti, E., Kostaki, E. G., Fragoulis, G. E., Papanikolaou, C., Mavroeidi, D., Bournia, V.-K., Panopoulos, S., Laskari, K., Arida, A., Gorgoulis, V. G., Tektonidou, M. G., Paraskevis, D., Sfikakis, P. P., & Souliotis, V. L. (2023). Chronological Age and DNA Damage Accumulation in Blood Mononuclear Cells: A Linear Association in Healthy Humans after 50 Years of Age. *International Journal of Molecular Sciences*, *24*(8), Article 8. https://doi.org/10.3390/ijms24087148

Walport, L. J., Hopkinson, R. J., & Schofield, C. J. (2012). Mechanisms of human histone and nucleic acid demethylases. *Current Opinion in Chemical Biology*, *16*(5–6), 525–534. https://doi.org/10.1016/j.cbpa.2012.09.015

Wang, A. T., Sengerová, B., Cattell, E., Inagawa, T., Hartley, J. M., Kiakos, K., Burgess-Brown, N. A., Swift, L. P., Enzlin, J. H., Schofield, C. J., Gileadi, O., Hartley, J. A., & McHugh, P. J. (2011). Human SNM1A and XPF–ERCC1 collaborate to initiate DNA interstrand cross-link repair. *Genes & Development*, *25*(17), 1859–1870. https://doi.org/10.1101/gad.15699211

Wang, M., McIntee, E. J., Cheng, G., Shi, Y., Villalta, P. W., & Hecht, S. S. (2000). Identification of DNA Adducts of Acetaldehyde. *Chemical Research in Toxicology*, *13*(11), 1149–1157. https://doi.org/10.1021/tx000118t

Wang, M.-J., Chen, F., Lau, J. T. Y., & Hu, Y.-P. (2017). Hepatocyte polyploidization and its association with pathophysiological processes. *Cell Death & Disease*, *8*(5), e2805–e2805. https://doi.org/10.1038/cddis.2017.167

Wang, Y., Chakravarty, P., Ranes, M., Kelly, G., Brooks, P. J., Neilan, E., Stewart, A., Schiavo, G., & Svejstrup, J. Q. (2014). Dysregulation of gene expression as a cause of Cockayne

syndrome neurological disease. *Proceedings of the National Academy of Sciences*, *111*(40), 14454–14459. https://doi.org/10.1073/pnas.1412569111

Weissman, L., Jo, D.-G., Sørensen, M. M., de Souza-Pinto, N. C., Markesbery, W. R., Mattson, M. P., & Bohr, V. A. (2007). Defective DNA base excision repair in brain from individuals with Alzheimer's disease and amnestic mild cognitive impairment. *Nucleic Acids Research*, *35*(16), 5545–5555. https://doi.org/10.1093/nar/gkm605

Whitney, M. A., Royle, G., Low, M. J., Kelly, M. A., Axthelm, M. K., Reifsteck, C., Olson, S., Braun, R. E., Heinrich, M. C., Rathbun, R. K., Bagby, G. C., & Grompe, M. (1996). Germ cell defects and hematopoietic hypersensitivity to gamma-interferon in mice with a targeted disruption of the Fanconi anemia C gene. *Blood*, *88*(1), 49–58.

Wilkinson, A. C., Ishida, R., Kikuchi, M., Sudo, K., Morita, M., Crisostomo, R. V., Yamamoto, R., Loh, K. M., Nakamura, Y., Watanabe, M., Nakauchi, H., & Yamazaki, S. (2019). Long-term ex vivo haematopoietic-stem-cell expansion allows nonconditioned transplantation. *Nature*, *571*(7763), Article 7763. https://doi.org/10.1038/s41586-019-1244-x

Wilkinson, A. C., Ishida, R., Nakauchi, H., & Yamazaki, S. (2020). Long-term ex vivo expansion of mouse hematopoietic stem cells. *Nature Protocols*, *15*(2), 628–648. https://doi.org/10.1038/s41596-019-0263-2

Williams, H. L., Gottesman, M. E., & Gautier, J. (2012). Replication-independent repair of DNA interstrand crosslinks. *Molecular Cell*, *47*(1), 140–147. https://doi.org/10.1016/j.molcel.2012.05.001

Williams, H. L., Gottesman, M. E., & Gautier, J. (2013). The differences between ICL repair during and outside of S-Phase. *Trends in Biochemical Sciences*, *38*(8), 386–393. https://doi.org/10.1016/j.tibs.2013.05.004

Wilson, A., Laurenti, E., Oser, G., van der Wath, R. C., Blanco-Bose, W., Jaworski, M., Offner, S., Dunant, C. F., Eshkind, L., Bockamp, E., Lió, P., MacDonald, H. R., & Trumpp, A.

(2008). Hematopoietic Stem Cells Reversibly Switch from Dormancy to Self-Renewal during Homeostasis and Repair. *Cell*, *135*(6), 1118–1129. https://doi.org/10.1016/j.cell.2008.10.048

Wilson, M. R., Jiang, Y., Villalta, P. W., Stornetta, A., Boudreau, P. D., Carrá, A., Brennan, C. A., Chun, E., Ngo, L., Samson, L. D., Engelward, B. P., Garrett, W. S., Balbo, S., & Balskus, E. P. (2019). The human gut bacterial genotoxin colibactin alkylates DNA. *Science (New York, N.Y.)*, *363*(6428), eaar7785. https://doi.org/10.1126/science.aar7785

Wit, N., Gogola, E., West, J. A., Vornbäumen, T., Seear, R. V., Bailey, P. S. J., Burgos-Barragan, G., Wang, M., Krawczyk, P., Huberts, D. H. E. W., Gergely, F., Matheson, N. J., Kaser, A., Nathan, J. A., & Patel, K. J. (2023). A histone deacetylase 3 and mitochondrial complex I axis regulates toxic formaldehyde production. *Science Advances*, *9*(20), eadg2235. https://doi.org/10.1126/sciadv.adg2235

Wong, J. C. Y., Alon, N., Mckerlie, C., Huang, J. R., Meyn, M. S., & Buchwald, M. (2003). Targeted disruption of exons 1 to 6 of the Fanconi Anemia group A gene leads to growth retardation, strain-specific microphthalmia, meiotic defects and primordial germ cell hypoplasia. *Human Molecular Genetics*, *12*(16), 2063–2076. https://doi.org/10.1093/hmg/ddg219

World Health Organisation. (2024). *Global health estimates Life expectancy and healthy life expectancy*. https://www.who.int/data/gho/data/themes/mortality-and-global-health-estimates/ghe-life-expectancy-and-healthy-life-expectancy

Xiang, Y., Zheng, Y., Liu, S., Liu, G., Li, Z., & Dong, W. (2021). Comparison of the sensitivity of Western blotting between PVDF and NC membranes. *Scientific Reports*, *11*(1), 12022. https://doi.org/10.1038/s41598-021-91521-8

Xie, M., Lu, C., Wang, J., McLellan, M. D., Johnson, K. J., Wendl, M. C., McMichael, J. F., Schmidt, H. K., Yellapantula, V., Miller, C. A., Ozenberger, B. A., Welch, J. S., Link, D. C., Walter, M. J., Mardis, E. R., Dipersio, J. F., Chen, F., Wilson, R. K., Ley, T. J., &

Ding, L. (2014). Age-related mutations associated with clonal hematopoietic expansion and malignancies. *Nature Medicine*, *20*(12), 1472–1478. https://doi.org/10.1038/nm.3733

Xu, J., Lahiri, I., Wang, W., Wier, A., Cianfrocco, M. A., Chong, J., Hare, A. A., Dervan, P. B., DiMaio, F., Leschziner, A. E., & Wang, D. (2017). Structural Basis for Eukaryotic Transcription-Coupled DNA Repair Initiation. *Nature*, *551*(7682), 653–657. https://doi.org/10.1038/nature24658

Xu, J., Zhu, L., He, S., Wu, Y., Jin, W., Yu, T., Qu, J. Y., & Wen, Z. (2015). Temporal-Spatial Resolution Fate Mapping Reveals Distinct Origins for Embryonic and Adult Microglia in Zebrafish. *Developmental Cell*, *34*(6), 632–641. https://doi.org/10.1016/j.devcel.2015.08.018

Yang, L., Bryder, D., Adolfsson, J., Nygren, J., Månsson, R., Sigvardsson, M., & Jacobsen, S. E. W. (2005). Identification of Lin–Sca1+kit+CD34+Flt3– short-term hematopoietic stem cells capable of rapidly reconstituting and rescuing myeloablated transplant recipients. *Blood*, *105*(7), 2717–2723. https://doi.org/10.1182/blood-2004-06-2159

Yang, Y., Kuang, Y., Montes De Oca, R., Hays, T., Moreau, L., Lu, N., Seed, B., & D'Andrea, A. D. (2001). Targeted disruption of the murine Fanconi anemia gene, Fancg/Xrcc9. *Blood*, *98*(12), 3435–3440. https://doi.org/10.1182/blood.v98.12.3435

Ye, C. J., Stevens, J. B., Liu, G., Bremer, S. W., Jaiswal, A. S., Ye, K. J., Lin, M.-F., Lawrenson, L., Lancaster, W. D., Kurkinen, M., Liao, J. D., Gairola, C. G., Shekhar, M. P. V., Narayan, S., Miller, F. R., & Heng, H. H. Q. (2009). Genome Based Cell Population Heterogeneity Promotes Tumorigenicity: The Evolutionary Mechanism of Cancer. *Journal of Cellular Physiology*, *219*(2), 288–300. https://doi.org/10.1002/jcp.21663

Yoon, Y. me, Storm, K. J., Kamimae-Lanning, A. N., Goloviznina, N. A., & Kurre, P. (2016). Endogenous DNA Damage Leads to p53-Independent Deficits in Replicative Fitness in

Fetal Murine Fancd2−/− Hematopoietic Stem and Progenitor Cells. *Stem Cell Reports*, *7*(5), 840–853. https://doi.org/10.1016/j.stemcr.2016.09.005

Yousefzadeh, M., Henpita, C., Vyas, R., Soto-Palma, C., Robbins, P., & Niedernhofer, L. (2021). DNA damage—How and why we age? *eLife*, *10*, e62852. https://doi.org/10.7554/eLife.62852

Zakhari, S. (2006). Overview: How Is Alcohol Metabolized by the Body? *Alcohol Research & Health*, *29*(4), 245–254.

Zayoud, K., Chikhaoui, A., Kraoua, I., Tebourbi, A., Najjar, D., Ayari, S., Safra, I., Kraiem, I., Turki, I., Menif, S., & Yacoub-Youssef, H. (2024). Immunity in the Progeroid Model of Cockayne Syndrome: Biomarkers of Pathological Aging. *Cells*, *13*(5), Article 5. https://doi.org/10.3390/cells13050402

Zeman, M. K., & Cimprich, K. A. (2014). Causes and consequences of replication stress. *Nature Cell Biology*, *16*(1), 2–9. https://doi.org/10.1038/ncb2897

Zeng, H., Li, H., Yue, M., Fan, Y., Cheng, J., Wu, X., Xu, R., Yang, W., Li, M., Tang, J., Chen, H., Kuang, B., Fan, G., Zhu, Q., & Shao, L. (2020). Isoprenaline protects intestinal stem cells from chemotherapy-induced damage. *British Journal of Pharmacology*, *177*(3), 687–700. https://doi.org/10.1111/bph.14883

Zhang, Z., & Lutz, B. (2002). Cre recombinase-mediated inversion using lox66 and lox71: Method to introduce conditional point mutations into the CREB-binding protein. *Nucleic Acids Research*, *30*(17), e90.

Zhao, B., & Guan, K.-L. (2014). Hippo pathway key to ploidy checkpoint. *Cell*, *158*(4), 695–696. https://doi.org/10.1016/j.cell.2014.07.041

Zheng, L., Dai, H., Zhou, M., Li, X., Liu, C., Guo, Z., Wu, X., Wu, J., Wang, C., Zhong, J., Huang, Q., Garcia-Aguilar, J., Pfeifer, G. P., & Shen, B. (2012). Polyploid cells rewire DNA damage response networks to overcome replication stress-induced barriers for

tumour progression. *Nature Communications*, *3*, 815. https://doi.org/10.1038/ncomms1825

Zhou, J., Zhou, X. A., Zhang, N., & Wang, J. (2020). Evolving insights: How DNA repair pathways impact cancer evolution. *Cancer Biology & Medicine*, *17*(4), 805–827. https://doi.org/10.20892/j.issn.2095-3941.2020.0177

Zhou, S., Zhu, J., Zhou, P.-K., & Gu, Y. (2022). Alveolar type 2 epithelial cell senescence and radiation-induced pulmonary fibrosis. *Frontiers in Cell and Developmental Biology*, *10*. https://doi.org/10.3389/fcell.2022.999600

Zulu, S., & Kenyon, M. (2018). Principles of Conditioning Therapy and Cell Infusion. In M. Kenyon & A. Babic (Eds.), *The European Blood and Marrow Transplantation Textbook for Nurses: Under the Auspices of EBMT*. Springer. http://www.ncbi.nlm.nih.gov/books/NBK543663/